On Master Equations and Rate Equations in Molecular Electronics: There and Back Again

Im Fachbereich Physik der
Freien Universität Berlin
eingereichte

Dissertation

von

Maximilian Gregory Schultz

aus München

Berlin, im März 2009

Erstgutachter: Prof. Felix von Oppen, PhD
Zweitgutachter: Prof. Dr. Tobias Brandes
Datum der mündlichen Prüfung: 15. Juni 2009

From a Son To a Father

Contents

Chapter 1

Introduction

> Cabalgaron tres días, y le dijo: "¡Oh, rey del tiempo y substancia y cifra del siglo!, en Babilonia me quisiste perder en un laberinto de bronce con muchas escaleras, puertas y muros; ahora el Poderoso ha tenido a bien que te muestre el mío, donde no hay escaleras que subir, ni puertas que forzar, ni fatigosas galerías que recorrer, ni muros que veden el paso."
> Luego le desató las ligaduras y lo abandonó en la mitad del desierto, donde murió de hambre y de sed.
>
> Borges, *Una Leyenda Arábiga (Historia de los dos Reyes y los dos Laberintos, como Nota de Burton)*

In Borges's narrative of the two kings and their two labyrinths, the king of Babylonia seeks to humiliate the king of Arabs and bids him into a labyrinth built so confusing and subtle that no man would venture to enter it. Despite the many walls, stairways, and doors, the king of Arabs finds the door out of the labyrinth and invites his host to see his own labyrinth in turn. Back in his own country, the king of Arabs gathers his army and returns to Babylonia, where he takes its king captive. He binds him to a camel and both ride for three days, when he finally takes revenge on the king of Babylonia and shows him a labyrinth, which has no doors, no galleries, and no walls. It is the plain of the desert where he leaves the king of Babylonia alone, who dies of hunger and thirst.

Embarking on a scientific research project in the theory of condensed matter one naturally finds oneself being trapped in a labyrinth constructed of diverging integrals, inapplicable or uncontrolled approximations, equations which either too few or too many terms, and eventually the bottomless task of numerical implementation and interpretation of the obtained data. The full Schrödinger equation for the quantum mechanical many-body problem features a complexity and subtlety hardly anybody would venture to solve exactly. First-principle methods and *ab-initio* calculations using density-functional theory yield reliable results for static problems but hold severe methodological problems as the precise form of the equation that has to be solved is still unknown.

Instead, physicist have been working hard during in the past one hundred years and have invented an abundance of prototype models and approximation methods to overcome walls and open closed doors. Some of these have led to hitherto unknown fields of study, some of them have even become of enormous technological importance. These methods and ideas, being restricted to our field of interest, which is

non-equilibrium quantum transport theory, can be classified into a handful categories or paradigms. These are certainly mutually non-exclusive; they are by no means complete but only meant to give a rough sketch of the global picture.

Some simple, most often non-interacting problems can be solved exactly and serve as a reference for perturbation theory with which corrections due to weak interactions, small couplings, or dilute contamination of clean samples by impurity-doping can be obtained. On the formal level of the actual theory, the discussion of such limiting cases comprises the linearisation of equations, the negligence of memory effects by choosing appropriate asymptotic time scales on which the dynamics turns out to be Markovian, or to eliminate any time-dependent dynamics by only considering a system's stationary state. The use of perturbation theory as a means to extend knowledge by studying small modifications of an already solved problem is one of the methodological pillars of theoretical physics. The application of diagrammatic expansions, partial summations of series, or the theory of Green functions have become invaluable tools for theorists in many-body physics and have also fostered research and investigation of the formal methods themselves.

Without suitably refined computational techniques and no understanding of fundamental physical mechanisms, which is often encountered in science, especially when qualitatively new physics are discovered, a consistent macroscopic description of a physical system provides first theoretical insight. Without reverting to a microscopic derivation, phenomenological theories evade the many-body problem at the expense of obtaining only a description of observable physics. The historical examples of this approach to condensed matter theory include the famous Drude and Sommerfeld theories of electrical conductance, where the material's parameters are not substantiated microscopically but kept as phenomenological constants in the equations. Corroborating the macroscopic theory by a microscopic one is a difficult task. In some cases, this has been achieved, as for example the phenomenological theory of superconductivity due to London has been replaced by the microscopic theory of Bardeen, Schrieffer, and Cooper. In general, however, the understanding of electrical conductance of bulk materials and its fundamental physical mechanisms has led to the discovery and research of a plethora of materials, parameter regimes, and exotic phenomenology, which still constitutes the basis of today's research in condensed matter theory.

As an intermediate step between only describing the phenomenology of a physical system and being drowned in the details of exact microscopic modelling, one often employs the strategy of replacing complicated physics by simple effective models. The Anderson model, where the effect of magnetic impurities in bulk materials is described by the influence of this very impurity *per se* instead of the detailed quantum mechanical structure of an atomistic model, is one example for such a treatment. Even large systems of interacting particles can be submitted to such an approach. The Fermi-liquid paradigm subsumes the effect of electron–electron interactions of a large Fermi system in the formation of particle-like entities, which can be treated by an effective theory of weakly interacting quasi-particles.

Probably the most drastic and radical way of simplifying the many-body problem is the reduction of the number of interacting particles. This approach goes beyond the mere exploitation of self-similar structures on different scales as the many flavours of renormalisation-group methods do or the restriction to the physics of low-dimensional systems. It leads to the emergence of a mesoscopic world on a nanometre scale that is interfacing the microscopic and the mesoscopic level and thereby allows us to study the cross-over from single-particle physics to collective phenomena. Pursuing this reductionistic idea consistently to the absolute minimum eventually leads to the notion of quantum nanostructures, artificial atoms, and single-molecule devices, whose study has been fostered by the enormous advance in experimental technology in

the past decades. The paradigm of simplification by reduction and the study of the quantum transport theory of quantum nanostructures and single-molecule devices constitutes the physical foundation of this thesis.

In the high-temperature, sequential-tunnelling regime of molecular electronics for the Anderson–Holstein model, there are no obstructing walls of analytic magic; there are no misleading doors of cryptic approximations. Both rate equations and master equations are linear equations whose precise matrix structure can be derived from general expressions, and due to their linearity, the numerical implementation is straightforward. Being stripped of obvious obfuscating features, without the need to model a single-molecule junction with all its details, and relying on the power of bare and simple models to which complexity and structure can be added step by step, the problem still constitutes a labyrinth, although rather in the sense of Borges. It asks for the mere survival, for understanding the equations' and their solutions' structure from a fundamental point of view. In this sense, the task we have taken in this thesis is to do better than the king of Babylonia and to survive in the Borgesian desert of molecular electronics.

1.1 Quantum Nanostructures

Quantum nanostructures are confined quantum mechanical systems of spatial extension on a nanometre scale. They are realisations of textbook examples of simple quantum systems like a potential well, whose semiconductor realisation is termed "quantum dot" for it resembles a zero-dimensional system.[1] A quantum nanostructure allows fundamental quantum mechanics to be monitored and investigated experimentally. Of course, this is not the only possibility to study quantum mechanics on the single-particle level. Single ions stored in Paul traps (Leibfried *et al.*, 2003), for instance, are much better isolated from the environment than quantum dots are and admit a precise control of their physics using frequency-stabilised laser beams. The physical parameters like the energy spectrum and oscillator strengths, however, are inherent to the atomic species being used and cannot be tailored like in artificially created semiconductor structures.

The interaction of the quantum nanostructure with the macroscopic world is in general achieved by measuring absorption and transmission properties of either photons, where the coherent quantum optical properties of the nanostructure are observed, or electrons, where it is the electrical transport properties that are investigated. In both cases, the nanostructure is interacting with infinitely large reservoirs, either due to spontaneous emission of photons into the surrounding radiation field or by the coupling to metallic electrodes via tunnel junctions. The theoretical description is that of an open quantum system, namely system–bath interactions. The abstract Hamiltonian used to describe these is

$$H = H_{\mathrm{S}} + H_{\mathrm{E}} + H_{\mathrm{S-E}},$$

with a free system H_{S}, a free particle reservoir, that is the metallic electrodes, which act as the environment H_{E}, and a system–bath interaction $H_{\mathrm{S-E}}$, which in our case will be an Anderson-type tunnel coupling. In the context of this work, we assume the tunnel coupling to both electrodes to be weak such that the non-equilibrium dynamics can be treated by perturbation theory in $H_{\mathrm{S-E}}$. The main difference between optical and electrical investigation of nanostructures lies in the type of the bath. Due to the conservation of particle number in fermionic reservoirs, the quantum mechanics of the interacting nanostructure is severely restricted, as for instance linear superpositions of neutral and charged states, which in quantum

[1] For a review on the physics of quantum dots, see Kouwenhove & Marcus (1998) or Kouwenhoven *et al.* (2001).

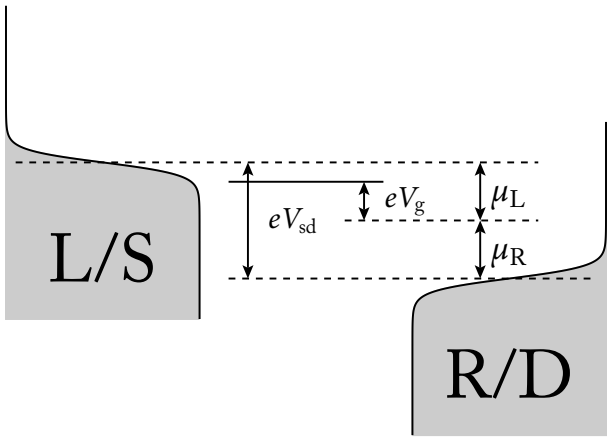

Figure 1.1: Abstract model of a quantum nanostructure: one or more localised electronic levels indicated by the solid line, coupled to both a source (left) and a drain (right) electrode held at temperature $k_B T$. The bias or source–drain voltage is the difference of the leads' chemical potentials μ_α, which are assumed to be of the same modulus $\mu_L = -\mu_R = \frac{1}{2} eV_{sd}$, such that the potential drop is symmetric at both tunnel junctions. The gate voltage is the distance of the localised system from the energetic zero.

optics give rise to Rabi oscillations, cannot be formed. Yet, the conservation of particle number allows to measure particle currents through the nanostructure by using two reservoirs instead of only one, a source and a drain electrode, which inject and extract charges by tunnelling. In Figure 1.1, we show the abstract model of such a quantum nanostructure. The two electrodes are labelled by their geometric position as left (L) and right (R). Their difference in chemical potential $\mu_L - \mu_R$ gives rise to a source–drain voltage, also known as bias $eV_{sd} := \mu_L - \mu_R$. We assume the voltage drop from each electrode to be symmetric with respect to the localised system, $\mu_L = -\mu_R = \frac{1}{2} eV_{sd}$. Since the general direction of particle transport through the nanostructure is from higher to lower chemical potential, we commonly use the notion of source (S) and drain (D) electrode instead of left and right. The source electrode is hereby defined as the one with higher, that is positive, chemical potential, which for example for positive bias voltage is the left electrode. Some experimental set-ups allow for attaching an additional electrode, a gate electrode, with which the energetic position of the nanostructure inside the bias window can be freely adjusted, and the nanostructure can be tuned through resonances or the Coulomb-blockade diamonds. Experiments with a scanning tunnelling microscope for example do not fall in this category (Qiu *et al.*, 2003). Since there the quantum nanostructure, which most often is a complex molecule, is located between the tip of the microscope and an underlying substrate, such systems cannot be gated by construction.

In the absence of Coulomb repulsion, the model of a single electronic level being confined between two metallic electrodes can be solved in closed form. This "resonant tunnelling" model, whose transmission function is a Lorentzian with its width Γ being given by the Golden-Rule expressions due to the tunnel couplings, is the simplest model for a quantum nanostructure. With more than one level or Coulomb repulsion between the electrons in two spin-degenerate levels, the system becomes highly non-trivial, the most obvious effect being the emergence of Coulomb blockade physics.[2] Theoretical approaches to solve the problem in certain limits include renormalisation group calculations (Karrasch *et al.*, 2006) or effective low-temperature theories (Schrieffer & Wolff, 1966) that show the emergence of Kondo physics (Pustilnik & Glazman, 2005), which can be studied experimentally (Goldhaber-Gordon *et al.*, 1998). The electronic spin being not only a degree of freedom of the nanostructure but also of the metallic electrodes inspires the study of transport properties with ferromagnetic leads. The alignment of the quantum dot's spin with respect to the electrodes' magnetisation significantly influences the electronic transparency of the

[2] See Grabert & Devoret (1992) as a general reference on single-charge tunnelling in quantum nanostructures.

nanostructure (Braig & Brouwer, 2005; Braun *et al.*, 2004). In our study of suspended carbon nanotubes, we shall recover systems of similar abstract structure.

The quantum-dot paradigm allows us to build models for more complicated nanostructures. Sequential arrays of two or more quantum dots are being studied intensively in the literature (Gurvitz, 1998; Wegewijs & Nazarov, 1999). In such systems, one can observe coherent and quantum optical effects in the two-level system defined by the localised two-dot system (Brandes, 2005). There, coherent superpositions between different charge states are allowed. An electron occupying the nanostructure can be in either of the two quantum dots: it can also occupy both of them simultaneously being in a linear superposition of the respective wave functions. As we shall see in this thesis, a parallel array of electronic levels, which models a multi-orbital nanostructure, also allows for coherent dynamics, although different from the sequential systems' dynamics.

1.2 Single-Molecule Junctions

Quantum dots are characterised by their electronic properties and thus resemble an artificial atom: a molecule can also sustain internal vibrations of the individual nuclei against each other. The transport properties of single-molecule junctions are therefore expected to show traces of the molecular vibrations in the current–voltage or noise characteristics.[3] In the fabrication and experimental set-ups of these junctions, which forms a research field of its own (Cuniberti *et al.*, 2005), one also has to rely on less controllable chemical methods instead of purely lithographic ones as they are used for semiconductor devices. Many of today's experiments thus focus on the qualitative detection of transport properties (Park *et al.*, 2000). The study of carbon nanotubes and their quantitative conductance properties has attracted significant interest in molecular electronics not only because of their relation to graphene physics but also due to the good control of the fabrication process of nanotube based devices (Leturcq *et al.*, 2009; Sapmaz *et al.*, 2006).

The primitive model of a single-molecule junction is defined by the presence of a few vibronic modes that are coupled to the electronic levels. In molecular physic, one commonly employs the Born–Oppenheimer approximation to separate the apparently slow vibronic motion from the fast electronic motion and obtains an adiabatic potential of the vibronic dynamics for each electronic state of the molecule. In this picture, the main effect of having a different number of charges on the molecule consists of a shift of the oscillator's equilibrium position and a change of the vibrational frequency. The resonant tunnelling model of a quantum nanostructure, which deals with discrete charges, is thus easily extended to the simplest model of a single-molecule junction by linearly coupling the system's total charge to the oscillator coordinate. This model, which is known as the Anderson–Holstein model, for it combines the Anderson impurity model and the Holstein polaron, is described by the system Hamiltonian[4]

$$H_{\mathrm{S}} = \sum_{\sigma} \varepsilon_{\mathrm{d}} d_{\sigma}^{\dagger} d_{\sigma} + \hbar\omega b^{\dagger} b + \sum_{\sigma} \lambda \hbar\omega d_{\sigma}^{\dagger} d_{\sigma} (b^{\dagger} + b), \tag{1.2.1}$$

where we have only included the charging effect on the oscillator's equilibrium position. Models with charge-dependent frequencies are discussed for instance by Wegewijs & Nowack (2005a) and Koch &

[3] See for instance Koch (2006) or Galperin *et al.* (2007) for a review.

[4] The notation is d_{σ} for the localised system's electronic operators with electronic spin σ and b for the annihilation operator of the harmonic oscillator with frequency ω. The electron–phonon coupling constant is denoted by λ. In this thesis, we conveniently use natural units by setting $\hbar = 1$ and $e = 1$. We only keep the explicit reference to these constants in the Golden-Rule rates Γ, the oscillator quantum $\hbar\omega$, and the applied voltages eV to comply with the common use of language.

von Oppen (2005a). In this thesis, we shall be concerned with the generic Anderson–Holstein model and, as symmetry-induced degeneracies of electronic orbitals are a second property that, in addition to the vibronic structure, distinguishes single-molecule junctions from quantum-dot systems, in particular its generalisation to degenerate and near-degenerate multi-orbital molecules.

Coulomb repulsion between the electrons in two spin-degenerate levels is usually modelled by adding the term $Un_\uparrow n_\downarrow$ to the system Hamiltonian. Such a term being quartic in the electronic operators renders the system Hamiltonian non-diagonal in the product space of the spin-degenerate electronic levels. In second-order perturbation theory, this is, however, irrelevant, as Wick's theorem need not be applied. One can simplify the problem by either setting $U = 0$, and deal with non-interacting on-site physics, or by letting $U \to \infty$, which allows at most one excess charge on the molecule. Only in the sequential-tunnelling approximation, the assumption of strong Coulomb blockade, $U \to \infty$, is up to combinatorial factors in the Golden-Rule rates, equivalent to completely ignoring electronic spin. To state the full model concretely, we define the free electronic reservoirs as non-interacting Fermi-gas electrodes in the wide-band limit with constant and unit density of states ν,

$$H_\mathrm{E} = \sum_{\boldsymbol{k}\sigma\alpha} \varepsilon_{\boldsymbol{k}\sigma} c^\dagger_{\boldsymbol{k}\sigma\alpha} c_{\boldsymbol{k}\sigma\alpha},$$

where the index $\alpha \in \{\mathrm{L},\mathrm{R}\}$ labels the respective reservoir. Instead of the geometric indices left and right we also use the indices S and D for source and drain, respectively. The system–bath interaction is given by a bi-linear tunnel coupling of the common form[5]

$$H_\mathrm{S\text{–}E} = H_\mathrm{T} = \sum_{\boldsymbol{k}\sigma\alpha} t_{\boldsymbol{k}\sigma\alpha} d^\dagger_\sigma c_{\boldsymbol{k}\sigma\alpha} + \mathrm{h.c.}.$$

In concrete applications, we shall assume the tunnel amplitudes $t_{\boldsymbol{k}\sigma\alpha}$ to depend only on the reservoir and spin indices, be the same for all wave vectors $\boldsymbol{k}$, that is $t_{\boldsymbol{k}\sigma\alpha} = t_{\sigma\alpha}$, and be real $t_{\alpha\sigma} = t^*_{\alpha\sigma}$. The tunnel amplitudes define the Golden-Rule rates $\Gamma^\sigma_\alpha = \frac{2\pi}{\hbar}\nu|t_{\sigma\alpha}|^2$, which in the resonant tunnelling model determine the width of the Lorentzian-shaped transmission function.

A linear electron–phonon coupling like the one used in the Anderson–Holstein model can easily be eliminated by means of a canonical transformation. This transformation, called the polaron transformation,[6] essentially applies the shift operator to the charged sector of the molecular Hilbert space. Both the on-site energy ε_d and the charging energy U are renormalised, and the transformation of the electronic on-site operators can be subsumed in imprinting a matrix structure on the bare tunnel amplitudes $t_{\sigma\alpha}$. The matrix elements of the renormalised tunnel amplitudes define the Franck–Condon matrix, which weighs the electronic transitions of the molecule due to tunnelling by the wave-function overlap of the respective vibronic states and thus incorporates the Franck–Condon principle of molecular physics. For the Anderson–Holstein model, the resulting expressions are known in closed form. For more complicated molecular systems, like the $E\otimes e$ Jahn–Teller Hamiltonian of chapter 3.5, the system Hamiltonian has to be diagonalised numerically. The representation of the original operators in terms of the diagonal basis then defines the matrix-valued renormalisation of the tunnel amplitudes, which is explicated in more detail in appendix E.

[5] Since in this context they are the same, we use the notations $H_\mathrm{S\text{–}E}$ for the system–bath interaction and H_T for the Anderson-type tunnelling Hamiltonian synonymously.

[6] For a full discussion of the polaron transformation for the single-mode model, see Mahan (2000, chap 4.2), Koch (2006, app. A), or appendix E.3 of this thesis. The generalisation to the two-level Anderson–Holstein model is given in chapter 5.1.

The application of the polaron transformation to solve the electron–phonon coupling requires the tunnelling to the electrodes to be sufficiently weak to treat the matrix-valued tunnelling by perturbation theory. The lowest-order perturbative regime of molecular electronics, sequential tunnelling of single charges, gives rise to two different descriptions, rate equations and master equations. The study of these equations and their mutual relation is the central topic of this thesis.

The opposite of the weak-coupling limit is the perturbative quantum limit (Mitra *et al.*, 2004): the resonant tunnelling problem is solved exactly and, using the non-equilibrium Keldysh technique, the electron–phonon coupling is treated as a perturbation. Using single-particle S-matrix methods only, Wingreen *et al.* (1988) succeed to obtain an exact solution of the transport problem in a very restricted regime. The many-body properties of the electronic reservoirs do, however, lead to a significant modification of the differential conductance peaks as it is shown by Flensberg (2003).

A completely different form of coupling a molecule's vibrational modes to its electronic degrees of freedom is due to the interaction of a suspended carbon nanotube's bending mode with an externally applied magnetic field (Shekhter *et al.*, 2006). The minimal coupling in the molecular Hamiltonian intertwines the charge and the electronic and thus also the oscillator's momentum via the vector potential $\vec{A}(\vec{r})$. The equivalent of the polaron transformation is not defined by the displacement operator, being the exponential of the momentum, but by the exponential of the coordinate $\hat{x}$, thereby reversing the role of coordinate and momentum in this type of single-molecule junction. The additional phase-factor in the renormalised tunnel amplitudes then allows for Aharonov–Bohm physics due to the delocalised vibrational wave function of the oscillating carbon nanotube.

Nanoelectromechanical devices and in particular shuttle devices (Donarini, 2005) are very similar to the concept of Anderson–Holstein molecules. In contrast to an internal, on-site harmonic oscillator mode, it is the harmonic coupling of the nanostructure to the metallic electrodes, which gives rise to oscillations of the nanostructure as a whole. Abstractly, such systems are modelled by using position-dependent tunnel amplitudes $t_\alpha = t_\alpha(\hat{x})$. The general purpose of shuttle mechanisms is not so much the implementation of molecular physics on the nanometre scale but rather the interaction of mesoscopic oscillators with single-charge tunnelling, for example pumping single electrons through a quantum nanostructure on the time scale of the shuttle's oscillation frequency.

Besides the vibronic degrees of freedom there are other molecule-specific properties that do influence the transport properties of single-molecule junctions and which are being studied in the literature. The orientation of the magnetisation of magnetic molecules, caged in a C_{60}-fullerene, can be changed under the influence of tunnelling electrons. Sophisticated technological set-ups would thus allow an experimentalist to store and read magnetic information by applying electric currents (Elste & Timm, 2005; Timm & Elste, 2006). Using larger molecules with geometries more complicated than the cylindrical structure of carbon nanotubes or the spherical symmetry of fullerenes, one can access and study the transport properties due to the molecule's different conformational configurations (Thijssen *et al.*, 2006), for example the current-induced switching behaviour of meta- and bistable molecules (Elste *et al.*, 2008).

Outline of the Thesis

After having introduced the general types of quantum nanostructures and single-molecule junctions that we consider in this thesis, chapter 2 will lay out the theoretical framework of master equations and rate equations. We present a discussion of Markovian master equations from a formal point of view stressing the

implications of the Lindblad–Kossakowski representation theorem for the formal structure of the equation and its physical restrictions. A derivation of these equations from the von Neumann equation is given first by a brute-force expansion of the propagators in terms of the tunnelling Hamiltonian to introduce the most common approximations used in the literature. Using a more rigorous approach due to Davies and others, we re-derive the equations in a different manner thus evading the use of many of the aforementioned approximations. Instead, the same results will be obtained by a careful choice of initial conditions and asymptotic time scales. The rigorous approach results in a natural distinction of the weak-coupling limit in master equations for the full reduced density matrix and rate equations for the electronic and vibronic populations only depending on the spectral structure of the system Hamiltonian.

These two types of Markovian kinetic equations for the quantum transport problem of molecular electronics have been used and are used by a number of research groups in applications involving simple prototype models as well as complicated and very detailed modelled systems. These two equations have defined two different, hardly overlapping strands of the theory; their distinction, their interplay, and their mutual relation have inspired and motivated this thesis. The main influences and stimuli of the discussions on the following one hundred and fifty pages are mostly due to the works of Koch, von Oppen, and Timm[7] as well as Wegewijs,[8] who specialise on the rate-equation part of the weak-coupling theory. Besides the master-equation formulation of quantum transport through spin-degenerate quantum dots due to Braun *et al.* (2004), master equations are applied to single-molecule junctions in the works of Richter and Grifoni,[9] who model complex molecules like carbon nanotubes and benzene rings. Common to many of these discussions especially on the master-equation side is a focus on the numerical treatment, which unfortunately tends to neglect the principal investigation of the fundamental transport properties due to the presence of electronic degeneracies. As also both of the descriptive strands, master equations and rate equations, are developed in separate groups and applications, this thesis strives to provide a unifying picture and conceptual framework of the weak-coupling limit of molecular electronics. The scientific results are therefore not presented in the order of publication but rather in a conceptually consistent way. Parts of this thesis have already been published in Schultz *et al.* (2008) (chapter 3.5) and Schultz & von Oppen (2008) (chapter 6), as well as a collaboration with an experimental group in Leturcq *et al.* (2009) (chapters 3.3.2 and 3.4). A publication of the results of chapter 5 is in preparation.

The treatment of quantum transport theory by rate equations is an intuitive approach to the problem by the use of Fermi's Golden Rule, and we focus on this type of transport equations in chapter 3 first. Motivated by recent experiments on suspended carbon nanotubes, we discuss several generic phenomena of the equations when being applied to molecular electronics. Especially the Franck–Condon blockaded regime is discussed, as there the experiments show both signatures that can be explained by single-level rate-equation models and signatures that cannot be grasped by such a simplified description. The detailed treatment of the rate equation pursued in this chapter is particularly important in the application to experiments as one can thus understand which part of the observed phenomenology is already due to the qualitative properties of the rate-equation dynamics between states of different energy and which part of the phenomenology explicitly relies on the coherent dynamics inside degenerate or near-degenerate subspaces of the electronic Hamiltonian. The chapter will be concluded by a discussion of the transport properties of an $E\otimes e$ Jahn–Teller molecule, which exhibits a strong current suppression due to a complicated interplay

[7] See for instance Koch (2006) and Timm (2008).

[8] See for instance Wegewijs & Nowack (2005a,b) and Reckermann *et al.* (2008).

[9] See for instance Donarini *et al.* (2006), Begemann *et al.* (2008), and Darau *et al.* (2008).

of spectral distortions and a Berry-phase induced selection rule in the Franck–Condon matrix elements.

As a preparation for the discussion of the master-equation dynamics of the reduced density matrix, we use chapter 4 to discuss single- and two-level resonant tunnelling without interactions be it electron–electron repulsion or electron–phonon interaction. The discussion approaches the steady-state dynamics from two different points of view. First we derive an exact solution using the Keldysh formalism and then obtain the weak-coupling limit by letting the tunnelling-induced broadening Γ of the electronic levels tend to zero. We then contrast these results with the ones obtained from a full master-equation treatment of the reduced density matrix.

The extension of the results of chapter 4 to molecular electronics and the transport theory of single-molecule junctions is the topic of chapter 5. We discuss the generic properties of multi-orbital single-molecule junctions from the Hamiltonian point of view thus deriving first results for the application of the master equation itself. We develop an intuitive understanding of the stationary dynamics of the master equation by first considering only the dynamics of the bare electronic levels and then adding complexity step by step. By doing so, we see how the basic results are modified by the introduction of vibronic levels and the interaction of the localised system with the continuum of reservoir levels. This approach to complicated dynamics guarantees an intuitive understanding of the equations' results, which will come in handy in the last part of this chapter. Throughout this chapter, we specialise on two fundamental models for two-level single-molecule junctions, which only differ in their symmetry properties under rotations in the electronic Hilbert space. We discuss the dependence of the models' behaviour in the parameter space on the degree of symmetry and examine several phenomena and regimes in detail. The chapter will be closed by a generalisation of the model to multi-mode reservoirs, which provides a first extension of the basic theory to systems such as carbon nanotubes.

The last chapter of this thesis is concerned with a two-fold problem. The purely academic problem consists in recombining both master equations and rate equations in a single conceptual framework that allows for a continuous interpolation between the regime where either equation is applicable. Such an endeavour is complicated by the fact that any expansion of the von Neumann equation has to ensure conditions on the positivity of the density matrix. We use the notion of the "singular-coupling limit", which is an extension of the commonly employed weak-coupling limit, to achieve this result. The interplay between the two types of equations is, however, also the purpose of a discussion that wants to treat small external perturbations that break symmetry-induced degeneracies or system-immanent near-degeneracies on a conceptually consistent level. Using the singular-coupling limit, we derive a suitable master equation for such situations and discuss its properties in the spirit of the previous chapters. We thus also obtain an intuitive understanding of the influence of near-degeneracies on the steady-state properties of single-molecule junctions. A discussion of the two models of single-molecule junctions from chapter 5 and their generalisation to arbitrary linear electron–phonon couplings concludes this final chapter.

Chapter 2

The Weak-Coupling Limit

Also zuerst: Was hat man unter $\int_a^b f(x)\,dx$ zu verstehen?

Riemann, *Ueber die Darstellbarkeit einer Function durch eine trigonometrische Reihe.*

Except for very few and mostly physically unspectacular cases, the transport problem through a quantum nanostructure cannot be solved in closed form. The paradigm model that admits an analytic solution, which is used both as a reference for more complicated systems and as a starting point for perturbation expansions, is resonant tunnelling through a single, spinless electronic level, which is coupled to two Fermi-gas electrodes. Anderson's original model comprises a spin-degenerate level. In this thesis, we do not consider electronic spin at all, since its first appearance in the transport dynamics is for fourth-order expansions in the tunnelling Hamiltonian. This is, however, beyond the scope of the weak-coupling limit, for which we want to derive and discuss the Markovian kinetic equation in this chapter.

On-site interactions like Coulomb repulsion render the resonant tunnelling problem highly non-trivial, and only approximative solutions of the Schrödinger equation can be obtained. For the study of molecular-electronics devices, however, electron–phonon interactions are those of primordial interest. The polaron model, an interaction being linear in both the occupation number of the device and the coordinate of the local oscillator, can be solved in closed form. If the vibronic frequency is sufficiently large, it is the coupling of the device to the electrodes, which remains the complicating perturbation. The model can be solved exactly for transport through a single electronic level interacting with a single vibrational mode using single-particle techniques like an S-matrix treatment (Glazman & Shekhter, 1988; Wingreen *et al.*, 1988, 1989). As soon as one takes into account the many-body nature of the electronic reservoirs, only approximate solutions by either expanding the equations of motion of the many-body Green functions (Flensberg, 2003) or by applying the Keldysh method for strong coupling to the electrodes (Mitra *et al.*, 2004) have been obtained so far. In both approaches, the investigation of the many-body dynamics of the problem shows non-zero correlations between the localised system and the electronic reservoirs.

The tunnelling interaction couples two intrinsically different systems: a finite-sized nanostructure, and an infinitely extended bath that can be assumed to be so inert that the interaction only affects the properties of the nanostructure and the backaction of the system to the bath can be neglected. With being "finite sized", we mean being modelled in a finite-dimensional Hilbert space. Although the oscillator spectrum is unbounded, the polaron model can be well approximated by a finite truncation of the oscillator rendering

it essentially finite-dimensional. If the coupling is assumed to be weak, an obvious approximation of the Schrödinger equation or more precisely the von Neumann equation, for the transport problem is a non-equilibrium problem, is to find a linear equation for the *reduced* density matrix ρ_S of the quantum nanostructure. The reduced density matrix is the full density matrix being traced over the environment's degrees of freedom in thermal equilibrium. By interpreting this object as the *state* of the system, we effectively incorporate the assumption of vanishing backaction onto the reservoirs. A theory in terms of the reduced density matrix can only make sense, if there are no persistent correlations between between the localised states and the bath, a setting which is opposed to the discussion for instance of Flensberg (2003). This can safely be assumed, when the temperature of the reservoirs is sufficiently large, definitely larger than the Kondo temperature. The equation ought to be linear, for it is supposed to describe the lowest-order correction due to the tunnel coupling. It is also required to be Markovian, because we are interested in the stationary or long-time behaviour of the system, where we can neglect transient dynamics and memory effects. The equation we are interested in is the master equation in the abstract form

$$\frac{\mathrm{d}}{\mathrm{d}t}\rho_S(t) = \mathcal{K}\rho_S(t).$$

The infinitesimal generator $\mathcal{K}$ has to fulfil several formal conditions that are obtained from physical reasoning. First, $\mathcal{K}$ has to define a semi-group of bounded operators $U(t)$. Then the time-evolution is Markovian. We cannot, and we do not, expect U to be a group, in which case the dynamics would be reversible. The full Schrödinger dynamics, of course, defines a unitary group that can be evolved both forwards and backwards in time. Due to the coupling to an *infinite* reservoir, the reduced dynamics will show dissipative effects rendering an evolution backwards in time impossible. The semi-group property also allows the dynamics to converge to a unique stationary state regardless of the initial condition. This property is very important, because here we are interested in the long-time behaviour, the asymptotic dynamics, and the steady-state properties of the system. Second, in order to map density matrices onto density matrices, U has to be trace preserving, $\mathrm{Tr}\big(U(t)\rho\big) = \mathrm{Tr}(\rho) = 1$. Third, since any density matrix has non-negative spectrum, U also has to map positive matrices onto positive matrices. Contrary to physical intuition, positivity alone is not enough. In fact, we require U to fulfil the condition of being *completely positive*. Not just for the ease of mathematical proof but also from the physicists' point of view one can argue for this property to hold. Stinespring (1955) defines a linear, positive map T acting on a C^*-algebra[1] $\mathcal{A}$ to be completely positive, when the map $\tilde{T}$ acting on $\mathcal{A}\otimes\mathbb{C}^{n\times n}$ by $\tilde{T}(\mathcal{A}\otimes\mathbb{C}^{n\times n}) := T(\mathcal{A})\otimes\mathbb{C}^{n\times n}$ is positive *for all* $n\in\mathbb{N}$. A completely positive map is a linear, positive map that remains positive when the system space is trivially extended by one that does not take part in the mapping at all. Davies (1976b) gives an intuitive argument why complete positivity is indeed a physical requirement and not just a mathematical subtlety.

> "If $\mathcal{H}$ is the Hilbert space of a system localised in some box and there exists a particle with n degrees of freedom so far away from the box that there is no interaction between the two then the Hilbert space for the system plus particle is $\mathcal{H}\otimes\mathbb{C}^n$. An operation on the system which does not affect the distant particle is described by a positive linear map T_n on[2] $\mathcal{L}(\mathcal{H}\otimes\mathbb{C}^n)$

[1] Since the density matrix is an operator itself, the infinitesimal generator of its time evolution has to be defined on a space of operators, which is closed under multiplication. The mathematical concept of C^*-algebras realises such a space.

[2] Davies denotes the set of all bounded linear operators acting on a vector space V by $\mathcal{L}(V)$. Since the notation collides with our notation for the Liouvillian, we shall not use it any further except for this quote.

such that

$$T_n(A \otimes B) = T(A) \otimes B$$

for some positive linear map on $\mathcal{L}(\mathcal{H})$ and all $A \in \mathcal{L}(\mathcal{H})$ and $B \in \mathcal{L}(\mathbb{C}^n)$. But $\mathcal{L}(\mathcal{H} \otimes \mathbb{C}^n)$ is isomorphic to the $n \times n$ matrix algebra over $\mathcal{L}(\mathcal{H})$ and T_n is the map described above. Therefore T_n is positive, and T is completely positive."

As simple the definition of complete positivity is and as easy it is to understand, one is tempted to ask why complete positivity is actually *more* than positivity alone. Is there an example of a map that is positive but not completely positive? Benatti & Floreanini (2005) in their review on completely positive maps and entanglement give a such an example:

Let T be the transposition map on $\mathbb{C}^{2\times 2}$, $T(N) := N^T$ for a matrix $N \in \mathbb{C}^{2\times 2}$. Since the spectrum is invariant under transposition, $\mathrm{sp}(N) = \mathrm{sp}(N^T)$, positive matrices are mapped onto positive matrices: T is positive. Consider the matrix

$$M := \frac{1}{2}\begin{pmatrix} 1 & 0 & 0 & 1 \\ 0 & 0 & 0 & 0 \\ 0 & 0 & 0 & 0 \\ 1 & 0 & 0 & 1 \end{pmatrix} \quad \in \mathbb{C}^{2\times 2} \otimes \mathbb{C}^{2\times 2}.$$

The matrix M is clearly positive as its spectrum is $\mathrm{sp}(M) = \{1, 0\}$. The operator $T \otimes \mathrm{Id}$ on $\mathbb{C}^{2\times 2} \otimes \mathbb{C}^{2\times 2}$ maps M into

$$M' := (T \otimes \mathrm{Id})(M) = \frac{1}{2}\begin{pmatrix} 1 & 0 & 0 & 0 \\ 0 & 0 & 1 & 0 \\ 0 & 1 & 0 & 0 \\ 0 & 0 & 0 & 1 \end{pmatrix},$$

with $\mathrm{sp}(M') = \{\pm\frac{1}{2}\}$. Hence, M' is *not* positive. It is obvious that the choice of M is crucial in this example and that M is a very special matrix. Indeed M is the projection $|\psi\rangle\langle\psi|$ of $|\psi\rangle := \frac{1}{\sqrt{2}}(|0\rangle \otimes |0\rangle + |1\rangle \otimes |1\rangle) \in \mathbb{C}^2 \otimes \mathbb{C}^2$. The vector $|\psi\rangle$ is the state vector of an entangled state. The definition of complete positivity and the above example suggest that the notion of entanglement, which is *the* non-classical effect of quantum mechanics, and complete positivity are closely related. Peres (1996) and Horodecki *et al.* (1996) combine this in the observation that for any entangled state ρ on the product space $\mathcal{A} \otimes \mathcal{B}$ there is a positive map T on $\mathcal{A}$ whose lift $T \otimes \mathrm{Id}_{\mathcal{B}}$ has negative eigenvalues. They prove that also the reverse implication holds true, thus being able to characterise separable and entangled states by the action of an operator and not by knowing its factorisation. For simple cases they can even identify a linear map that can be employed as an entanglement detector.

Theorem. *A state ρ acting on $\mathbb{C}^2 \otimes \mathbb{C}^2$ or $\mathbb{C}^2 \otimes \mathbb{C}^3$ is separable if and only if its partial transposition[3] is a positive operator.*

The requirement of complete positivity severely restricts the form of the generators of Markovian master equations. This is the essence of a representation theorem for completely positive maps by Stinespring (1955) stating that it is necessary and sufficient for a linear operator T on a C^*-algebra $\mathcal{A}$ to be completely positive

[3] The partial transposition is a map acting on a product space. It factorises into the transposition operator on one of the factors and the identity map on the other $T \otimes \mathrm{Id}$, like in the above example.

that is has the representation $T(A) = V^\dagger AV$, for $A, V \in \mathcal{A}$. The representation of a trace-preserving, strongly-continuous, completely positive semi-group is due to a theorem by Lindblad (1976) and simultaneously by Gorini *et al.* (1976), which states as a necessary and sufficient condition for its infinitesimal generator to have the form

$$\dot{\rho} = -\imath[H, \rho] + \sum_{kl} a_{kl} \left(V_i \rho V_j^\dagger - \frac{1}{2}\{V_j^\dagger V_i, \rho\} \right),$$

with the coefficient matrix (a_{kl}) being hermitian and positive. The equation can be diagonalised

$$\dot{\rho} = -\imath[H, \rho] + \sum_{k} \gamma_k \left(2A_k \rho A_k^\dagger - A_k^\dagger A_k \rho - \rho A_k^\dagger A_k \right).$$

The first term of the above representations is a Hamiltonian term, for example the free evolution of an unperturbed system. The second term, which describes the influence of a perturbation or coupling to an infinite reservoir generates the dissipative dynamics and hence is called "dissipator". The striking implication of Lindblad's theorem[4] is that the representation is not only sufficient but also necessary. Any Markovian master equation that has to meet the requirements of generating trace-preserving and completely positive dynamics has to have Lindblad form. If not, the generated dynamics will lack either the property of trace-preservation or that of complete positivity. Due to the representation theorem of Stinespring (1955), we can see that most often, an improper master equation will be likely to violate complete positivity.

That the dynamics has to be completely positive and not just positive alone has been identified as the source of many restrictions on the dynamics. Gorini *et al.* (1976, sec. III) show for example that for the reduced dynamics of a two-level system, the relaxation times of the diagonal and the off-diagonal elements of the density matrix ρ, called transverse and longitudinal relaxation times, respectively, have to obey the inequality $\frac{1}{2} T_\perp \leq T_\parallel$. This inequality is well-known and has been verified experimentally in many cases (Blum, 1981, chap. 7.4.2). Yet, Pechukas (1994) refers to experiments with strong system–bath coupling where it is violated. He thus questions the requirement of complete positivity for the dynamics of open quantum systems, because he does not believe in the argument that the dynamics has to take care of an additional inert system—called the witness or ancilla W—that does not interact with the system itself. Pechukas says

> "One may reasonably well doubt this argument. It is very powerful magic: W sits apart from $S+R$ [R being the reservoir] and does absolutely nothing; by doing so, it forces the motion of S to be completely positive, with dramatic physical consequences …"

He further claims that

> "… completely positive dynamics is an artifact of product initial conditions. In general, reduced dynamics need not be completely positive."

He therefore suggests to drop complete positivity as a condition for the quantum-dynamical semigroup. Since, however, there is no mathematical criterion for the generators of positive quantum-dynamical semigroups, Pechukas restricts the set of initial conditions to those that generate positive dynamics. Alicki (1996) responds to Pechukas, and he is right with his statement, that this set of initial conditions cannot be characterised. In their review, Shaji & Sudarshan (2005) embark on the problem again. They claim that for instance in quantum-information processing "there is sufficient control over the system to be able

[4] Although, the theorem has been proven both by Lindblad and Gorini *et al.*, we adopt the reference to Lindblad, which is widely used in the literature.

to initialize its state to one that is decoupled from its environment". They also stress, however, "that it is perfectly reasonable to assume that in many situations there might be initial correlations between the system and its environment". This statement leaves the question open, as to which are the proper conditions on the quantum-dynamical semigroup when initial correlations do matter. Due to the close relation of complete positivity and entanglement, the topic might come into the focus of quantum information processing and entanglement theory again. But the discussion also clearly states that as long as a factorisation of the density matrix can be assumed at least for the initial conditions, complete positivity is the formally correct form of positivity to be required. In this thesis, we go along with this assumption; we follow the general route in the literature on quantum transport theory and do not assume any initial correlations between the localised system and its fermionic environments. Such correlations are the signatures of strong coupling and low temperatures, which are not the parameter regimes we want to discuss here. We thus incorporate the Born approximation of factorised density matrices in the initial conditions alone, well aware that it implies a completely positive quantum dynamics.

2.1 Standard Derivations

In the physics literature, one finds several derivations of Markovian master equations for the quantum transport problem through weakly-coupled systems. Most common are three variants, an expansion of the propagator of the von Neumann equation (Rammer, 1998), a real-time diagrammatic technique that is an application of the Keldysh idea (König, 1998), and the iteration of the von Neumann equation (Breuer & Petruccione, 2002, chap. 3.3). Timm (2008) reviews all of these proving their equivalence. This result is not surprising, since all these techniques rely on an expansion of the propagator of the Schrödinger equation. In the following, we sketch the iterative method according to Breuer & Petruccione (2002) and use it to introduce the necessary assumptions and approximations with which the resulting equation is made a Lindblad-compliant master equation.

Consider the abstract Hamiltonian $H = H_\mathrm{S} + H_\mathrm{E} + H_\mathrm{S\text{–}E}$ of a system H_S, its environment H_E, and a system–bath interaction $H_\mathrm{S\text{–}E}$. We shall further specify the system–bath interaction in the course of the derivation; at this stage we only require it to be bi-linear, that is both linear in the system and the bath operators. In the interaction picture, the von Neumann equation for the density matrix is

$$\frac{\mathrm{d}}{\mathrm{d}t}\rho^\mathrm{I}(t) = -\imath[H^\mathrm{I}_\mathrm{S\text{–}E}, \rho^\mathrm{I}(t)] \tag{2.1.1}$$

with its formal solution

$$\rho^\mathrm{I}(t) = \rho^\mathrm{I}(0) - \imath \int_0^t [H^\mathrm{I}_\mathrm{S\text{–}E}(s), \rho^\mathrm{I}(s)]\, ds.$$

Re-inserting this expression into Equation (2.1.1) and tracing over the bath with its equilibrium distribution $\rho^\mathrm{I}_\mathrm{E}$, where $\mathrm{Tr}_\mathrm{E}\big([H^\mathrm{I}_\mathrm{S\text{–}E}(t), \rho^\mathrm{I}(0)]\big) = 0$ is assumed,[5] we obtain the first iteration of the von Neumann equation for the reduced density matrix $\rho^\mathrm{I}_\mathrm{S} = \mathrm{Tr}_\mathrm{E}(\rho^\mathrm{I})$

$$\frac{\mathrm{d}}{\mathrm{d}t}\rho^\mathrm{I}_\mathrm{S}(t) = -\int_0^t \mathrm{Tr}_\mathrm{E}\Big(\big[H^\mathrm{I}_\mathrm{S\text{–}E}(t), [H^\mathrm{I}_\mathrm{S\text{–}E}(s), \rho^\mathrm{I}(s)]\big]\Big)\, ds.$$

[5] The vanishing of this commutator amounts to factorised initial conditions like the ones we have discussed before as well as centred bath operators, whose equilibrium expectation value is zero.

This equation is simplified by the Born approximation $\rho(t) \approx \rho_S(t) \otimes \rho_E$ stating that correlation effects between the system and the bath are neglected. As we shall see in the next section and also is pointed out by Timm (2008), the use of projection operators in the derivation of this equation, only requires the Born approximation for the *initial* conditions. After changing the integration over s into one over $t-s$, the Markov approximation is justified by assuming a fast decay of the correlations of the system itself thus extending the range of integration to infinity while keeping the density matrix in the integrand constant,

$$\frac{\mathrm{d}}{\mathrm{d}t}\rho_S^I(t) = -\int_0^\infty \mathrm{Tr}_E\Big(\big[H_{S\text{–}E}^I(t), [H_{S\text{–}E}^I(t-s), \rho^I(t)]\big]\Big)\, ds. \tag{2.1.2}$$

When dealing with fermions, the system–bath interaction—in the interaction picture—is generally set to (Breuer & Petruccione, 2002, pp. 134)

$$H_{S\text{–}E}^I(t) = \sum_{k\sigma} e^{\imath\varepsilon_\sigma t} d_\sigma^\dagger c_k(t) + c_k^\dagger(t) d_\sigma e^{-\imath\varepsilon_\sigma t},$$

with bath operators $c_k(t)$ in the interaction picture and system operators d_σ in the Schrödinger picture. The eigenvalue of H_S with respect to $|\sigma\rangle$ is denoted ε_σ. For simplicity of notation, we have set all tunnel amplitudes $t_{\alpha\sigma} = 1$. For the derivation of a concrete set of equations, they can easily be inserted in the final form of the abstract master equation. We further abbreviate the bath correlation functions

$$\Gamma_k(\varepsilon_\sigma) := \int_0^\infty e^{\imath\varepsilon_\sigma s}\, \mathrm{Tr}_E\left(c_k^\dagger(s) c_k(0)\rho_E\right) ds \quad \text{and} \quad \tilde{\Gamma}_k(\varepsilon_\sigma) := \int_0^\infty e^{\imath\varepsilon_\sigma s}\, \mathrm{Tr}_E\left(c_k(s) c_k^\dagger(0)\rho_E\right) ds,$$

where the time evolution of the bath operators is with respect to the free bath Hamiltonian. The master equation for a non-interacting system, meaning without any on-site interaction like Coulomb repulsion, is, after an expansion of the double-commutator structure of Equation (2.1.2) and replacing the bath correlation functions as well as the eigenvalues of the system's Hamiltonian in the free time evolution,

$$\begin{aligned}\frac{\mathrm{d}}{\mathrm{d}t}\rho_S^I(t) = \sum_k \sum_{\sigma\sigma'} \Big\{ & e^{-\imath(\varepsilon_{\sigma'}-\varepsilon_\sigma)t} d_\sigma^\dagger \rho_S^I(t) d_{\sigma'} \Gamma_k(-\varepsilon_\sigma) + e^{\imath(\varepsilon_{\sigma'}-\varepsilon_\sigma)t} d_\sigma \rho_S^I(t) d_{\sigma'}^\dagger \tilde{\Gamma}_k(\varepsilon_\sigma) \\ & - e^{\imath(\varepsilon_{\sigma'}-\varepsilon_\sigma)t} d_{\sigma'}^\dagger d_\sigma \rho_S^I(t) \tilde{\Gamma}_k(\varepsilon_\sigma) - e^{-\imath(\varepsilon_{\sigma'}-\varepsilon_\sigma)t} d_\sigma d_{\sigma'}^\dagger \rho_S^I(t) \Gamma_k(-\varepsilon_\sigma) \Big\} + \text{h.c.}\end{aligned} \tag{2.1.3}$$

The equation in the Schrödinger picture is obtained by transforming the reduced density matrix back into that picture.

If we consider the same theory again, albeit with an interaction that only depends on the particle numbers such as Coulomb repulsion, the expressions are modified; however, only slightly. In this case we have to care about the order of the free system's propagator U_S within the chain of operators. In principle, this means that the state $d_{\sigma_2}^\dagger |\sigma_1\rangle$ propagates with a frequency including the interaction energy, that is the charging energy due to Coulomb repulsion. Assume that for one additional particle, we have to pay the extra energy ε_{int} in addition to the added particle's energy. As an example, we pick one of the $H_{S\text{–}E} H_{S\text{–}E} \rho_S \otimes \rho_E$ terms in the expansion of the double commutator of Equation (2.1.2) without replacing the bath correlation functions and the system's Hamiltonian

$$\int_{\mathbb{R}^+} e^{\imath H_S t} d_\sigma^\dagger e^{-\imath H_S t} e^{\imath H_S (t-s)} d_{\sigma'} e^{-\imath H_S (t-s)} \rho_S^I(t) \langle c_k(t) c_k(t-s) \rho_E \rangle\, ds.$$

Such a term describes the self-energy correction of the retarded branch of the density matrix by an electron tunnelling off and back onto the system. As the expression is written, the frequency generated by the free system's Hamiltonian depends on the wave function provided by the reduced density matrix. Assume this wave function to be some unspecified $|\psi\rangle$, which is a many-body wave function, a Fock state of particles, say a doubly-occupied quantum dot. We consider the dynamical phase due to the time evolution and connect the individual exponential factors to the terms of the non-interacting master equation[6]

$$\begin{aligned} e^{\imath H_\mathrm{S}(t-s)} d_{\sigma'} e^{-\imath H_\mathrm{S}(t-s)} |\psi\rangle &= e^{\imath H_\mathrm{S}(t-s)} d_{\sigma'} e^{-\imath \varepsilon_\psi (t-s)} |\psi\rangle \\ &= e^{\imath (\varepsilon_{\psi\setminus\sigma'} - \varepsilon_\psi)(t-s)} |\psi\setminus\sigma'\rangle \\ &= e^{-\imath (\varepsilon_{\sigma'} - \varepsilon_\mathrm{int})(t-s)} |\psi\setminus\sigma'\rangle \end{aligned}$$

In the second step, we add the particle $|\sigma\rangle$

$$e^{\imath H_\mathrm{S} t} d_\sigma^\dagger e^{-\imath H_\mathrm{S} t} |\psi\setminus\sigma'\rangle = e^{\imath H_\mathrm{S} t} d_\sigma^\dagger e^{-\imath \varepsilon_{\psi\setminus\sigma'} t} |\psi\setminus\sigma'\rangle = \exp\left(\imath(\varepsilon_{(\psi\setminus\sigma')\cup\sigma} - \varepsilon_{\psi\setminus\sigma'})\right) |(\psi\setminus\sigma')\cup\sigma\rangle$$

In total, we obtain the exponential factor

$$\begin{aligned} &\exp\left(\imath(\varepsilon_{(\psi\setminus\sigma')\cup\sigma} - \varepsilon_{\psi\setminus\sigma'} - \varepsilon_{\sigma'} + \varepsilon_\mathrm{int})t\right) \exp\left(\imath(\varepsilon_{\sigma'} + \varepsilon_\mathrm{int})s\right) \\ &= \exp\left(\imath(\varepsilon_{\psi\setminus\sigma'} + \varepsilon_\sigma + \varepsilon_\mathrm{int} - \varepsilon_{\psi\setminus\sigma'} - \varepsilon_{\sigma'} - \varepsilon_\mathrm{int})t\right) \exp\left(\imath(\varepsilon_{\sigma'} + \varepsilon_\mathrm{int})s\right) \\ &= \exp\left(\imath(\varepsilon_\sigma - \varepsilon_{\sigma'})t\right) \exp\left(\imath(\varepsilon_{\sigma'} + \varepsilon_\mathrm{int})s\right). \end{aligned}$$

Only the frequency of the time evolution for the period when the electron has been removed from the nanostructure is modified by the interaction energy, which in this example is released in addition to the single-particle energy $\varepsilon_{\sigma'}$. The oscillatory pre-factor of the non-interacting master equation, which is given by the part of the above term depending on t, persists. In the chosen example,[7] it is the Fourier transform of the bath–bath correlation function, which includes the factor depending on s, that has to account for the number of particles in the wave function it actually operates on. The simple accounting for Coulomb interaction like this is not possible for higher-order expansions, when, in order to simplify the computations, Wick's theorem has to be applied. Although the Coulomb interaction maps the single- and many-particle states onto themselves with the correct value of the energy, the Hamiltonian is not diagonal in the sense of being a direct product of single-particle Hamiltonians. Hence, a reduction of the many-body dynamics to the evaluation of single-particle Green functions is not possible.

As the master equation (2.1.3) stands, it is obvious that it cannot fulfil Lindblad's conditions for a completely positive, trace-preserving dissipator. For example, the second factor for the $d_\sigma^\dagger \rho d_{\sigma'}$ term, for $\sigma \neq \sigma'$, can only come from the hermitian conjugate part of the line in which $\sigma \leftrightarrow \sigma'$; however, the bath correlation functions $\Gamma_{\boldsymbol{k}}(-\varepsilon_\sigma) \neq \Gamma_{\boldsymbol{k}}^*(-\varepsilon_{\sigma'})$. The only remedy of this problem is to formally impose a restriction on the terms by inserting $\delta_{\sigma\sigma'}$ into the sum. Then the $d_\sigma^\dagger \rho d_\sigma$ terms actually are $2 d_\sigma^\dagger \rho_\mathrm{S}(t) d_\sigma \mathrm{Re}\Gamma_{\boldsymbol{k}}(-\varepsilon_\sigma)$, which is the wanted term. The thus obtained equation decouples populations from coherences between states of different energy. It does, however, retain coherences between degenerate states.

The approximation $\delta_{\sigma\sigma'}$ is either called *secular* or *rotating-wave* approximation, the latter due to its analogy in quantum optics (Breuer & Petruccione, 2002, chap. 3.3). It is justified when the intrinsic time

[6] Our notation is reminiscent of set theory: $|\psi\setminus\sigma\rangle$ is the many-body wave function $|\psi\rangle$ with the particle σ being removed.

[7] One can show that this is the case for all terms.

scale of the system τ_S is much larger than the relaxation time τ_E of the reservoir. It is, of course, clear that in the case when both time scales are approximately equal, $\tau_S \sim \tau_E$, the rotating-wave approximation cannot be used.

2.2 The Necessity of a Rigorous Approach

The above presented derivation of a master equation in the weak-coupling limit and its equivalent formulations are very intuitive and can be applied straightforwardly to many different problems. It is possible to expand the equation to higher orders, including for example co-tunnelling (König *et al.*, 1997; Leijnse & Wegewijs, 2008). The approach is perturbative and as such the full machinery of quantum many-body theory can be applied (König, 1998). On the contrary, there are also some disadvantages, which suggest a more rigorous approach. The Markov property, for example, is not a natural result of the second-order expansion of the propagator, but it has to be justified with the relaxation times of the bath correlation functions that such an approximation is actually valid. This becomes more and more complicated as higher-order processes take place on different time scales, and it is by far not clear whether the Markov property holds for all of them simultaneously. The Born approximation, the factorisation of ρ into the system's and the bath's density matrices for all times, is introduced by assuming fully inert reservoirs. Several attempts have been made, particularly in the discussion of the low-temperature properties of molecular-electronics devices, to include correlations of system and bath and then arrive at a Markovian master equation. Flensberg (2003), for example, uses such obtained equations to correct the single-particle S-matrix calculations of Wingreen *et al.* (1989). The most critical approximation of the whole derivation is the rotating-wave approximation. It is necessary to make the master equation compliant with Lindblad's conditions. The drawback is its assumption on the large separation of time scales τ_S and τ_E. Each of these approximations has its own justification. Yet, all of them are needed at the same time to derive a sensible Markovian master equation. One may therefore raise the question to which extent these approximations can be built into the theory: in which way do they emerge from a rigorous treatment of the von Neumann equation? In the seventies of the twentieth century, the theory of Markovian master equations has been put on rigorous mathematical grounds. The work of Lindblad (1976) and Gorini *et al.* (1976) defines the goal by proving necessary and sufficient conditions for completely positive and trace-preserving infinitesimal generators. Davies (1974, 1976a) provides an extensive set of articles on the derivation of Markovian master equations and their properties. Dümcke & Spohn (1979) discuss the various generators being used in the literature, and they single out Davies's result as the only one compliant with Lindblad's conditions.

The great advantage of the mathematical treatment over the straightforward perturbative one is the emergence of all of the above approximations just by a careful choice of conditions on the system–bath Hamiltonian. As we shall show in chapter 6, it is also suitable to access the regime $\tau_S \sim \tau_E$ where the rotating-wave approximation fails and thereby stains the master equation with the property of non-positivity.

2.3 Davies's Method

We consider the abstract Hamiltonian $H = H_S \otimes \mathrm{Id} + \mathrm{Id} \otimes H_E + H_{S\text{–}E}$ acting on the product Hilbert space of the system and its environment $\mathcal{H}_S \otimes \mathcal{H}_E$. Since we want to use projection operators on the individual Hilbert spaces in order to separate the reduced dynamics from the full dynamics, we formulate the theory in terms of direct products of Hamiltonians. H_S describes a finite-dimensional system S, a microscopic

quantum system like a quantum dot or a single molecule, being coupled to an infinitely large environment E, a Bose or Fermi bath, say, via a bi-linear interaction term $H_{\mathrm{S-E}}$. Davies's derivation of a Markovian master equation for the reduced dynamics consists of three steps. First, the system–bath interaction is considered a perturbation and the Hamiltonian is rewritten with a scaling parameter. Second, the dynamics of the system is obtained by using projection operators, which essentially trace out the environment's degrees of freedom. Third, the von Neumann equation is integrated and the strength of the perturbation is sent to zero on the slow Markovian time scale.

2.3.1 Scaling Method

Any expansion of a complicated function or operator is in fact a limit process. The definition of the differential of any function $f : \mathbb{R} \to \mathbb{R}$ is given by the limit of the difference quotient

$$f'(x) := \lim_{\varepsilon \to 0} \frac{f(x+\varepsilon) - f(x)}{\varepsilon}.$$

This means that the first-order Taylor expansion of any differentiable function, which equivalently serves as the definition of the derivative itself, is

$$f(x+\varepsilon) = f(x) + f'(x)\varepsilon + \varphi(x,\varepsilon).$$

The remainder $\varphi(x,\varepsilon)$ has the property that it vanishes fast enough, when $\varepsilon \to 0$, which means that it is of higher order than $\mathcal{O}(\varepsilon)$

$$\lim_{\varepsilon \to 0} \frac{\|\varphi(x,\varepsilon)\|}{\varepsilon} = 0.$$

In this sense, perturbation theory for operators would have to attach a small parameter to the perturbation, perform an expansion and finally let the small parameter tend to zero. Hence, we should rather work with the rescaled Hamiltonian

$$H^{\xi} := H_{\mathrm{S}} \otimes \mathrm{Id} + \mathrm{Id} \otimes H_{\mathrm{E}} + \xi H_{\mathrm{S-E}},$$

in order to rigorously account for the perturbative nature of $H_{\mathrm{S-E}}$. From the mathematical point of view, Kato (1966) is the key reference for properties of perturbed (semi-)groups. Given a solvable differential equation with some unspecified operator A,

$$\dot{u} = Au$$

with solution $u(t) = U(t)u(0)$ and a (bounded) perturbation B, the equation $\dot{u} = A + \xi B$ can be solved and yields the perturbed solution $u(t) = U(t;\xi)u(0)$. The important property of the perturbed solution is that for t in a finite interval, $U(t;\xi) \to U(t)$ uniformly as $\xi \to 0$. On first sight this means that we would not be able to arrive at a non-trivial result for the perturbative treatment of the system–bath coupling problem by letting $\xi \to 0$. However, the uniform convergence only holds on *finite* time intervals. The long-time dynamics and in particular the stationary properties do not comply with Kato's theorems, leaving us in a position to employ a proper limit process to derive a non-trivial perturbative result for the dynamics on a long time scale. Although this is rather non-intuitive from the perspective of Rayleigh-Schrödinger perturbation theory, where the expansion parameter is finally set to unity, we shall show in chapter 4 how the perturbed stationary solution of the resonant tunnelling problem can be obtained exactly the way pursued in this chapter.

2.3.2 Projection Operators

The problem we want to solve consists of two separate ingredients: the free evolution of the system and the bath, both of which we can solve analytically, and the system–bath interaction that mixes these dynamics. The projection-operator approach aims at a formal separation of the underlying Hilbert space that respects the natural structure of the problem $\mathcal{H} = \mathcal{H}_S \otimes \mathcal{H}_E$ being a product space. One defines a linear projection $\mathcal{P}$ onto the system's variables; its complement $\mathcal{Q} = 1 - \mathcal{P}$ then projects onto the bath's degrees of freedom. The projection operator approach, known as the Zwanzig–Mori technique in statistical mechanics,[8] can also be employed in the generic derivation of Markovian master equation for quantum transport problems (Timm, 2008).

For the given problem, we define the image of $\mathcal{P}$ as the set of reduced density matrices of the Hilbert space multiplied by the equilibrium distribution of the bath. We are only interested in the dynamics of the system and consider the bath so large and so inert that it can be assumed to rest in equilibrium for all times,

$$\mathcal{P}\rho := (\mathrm{Tr}_E\, \rho) \otimes \rho_E.$$

Again, this is the point, where the backaction of the system onto the bath is effectively neglected for the definition of the system's actual state. The backaction is, however, not set to zero as all its effects are described by the complementary projection due to $\mathcal{Q}$. In order for the projections to separate system and bath dynamics and leave this mixing to the system–bath interaction untouched, some assumptions have to be posed on the system–bath coupling. We have to require that $\mathcal{P} H_{S-E} \mathcal{P}$ vanishes as well as its projection under $\mathcal{Q}$. This is generally the case for a bi-linear coupling of the form $V \otimes B$ with system operators V and bath operators B, which are centred with respect to the equilibrium distribution, $\mathrm{Tr}_E(B) = 0$. The Liouville operator $\mathcal{L}\rho := [H, \rho]$ is split into its individual contributions similarly to the Hamiltonian H, $\mathcal{L}^\xi = \mathcal{L}_S \otimes \mathrm{Id} + \mathrm{Id} \otimes \mathcal{L}_E + \xi \mathcal{L}_{S-E}$. The following properties hold for projections of $\mathcal{L}^\xi$ under $\mathcal{P}$ and $\mathcal{Q}$ (Benatti & Floreanini, 2005, sec. 3.2)

1. Factorised density matrices form an invariant subspace of $\mathcal{P}$:

$$\mathcal{P}(\rho_S \otimes \rho_E) = \rho_S \otimes \rho_E.$$

2. The system's Liouvillian $\mathcal{L}_S \otimes \mathrm{Id}$ commutes with $\mathcal{P}$

$$\mathcal{P}(\mathcal{L}_S \otimes \mathrm{Id})\rho = \mathrm{Tr}_E(\mathcal{L}_S \otimes \mathrm{Id})\rho) \otimes \rho_E = (\mathcal{L}_S \otimes \mathrm{Id})\, \mathrm{Tr}_E(\rho) \otimes \rho_E = (\mathcal{L}_S \otimes \mathrm{Id})\mathcal{P}\rho.$$

3. The environment's Liouvillian $\mathrm{Id} \otimes \mathcal{L}_E$ is both an element of the right and the left kernel of $\mathcal{P}$:

$$(\mathrm{Id} \otimes \mathcal{L}_E)\mathcal{P}\rho = (\mathrm{Id} \otimes \mathcal{L}_E)\, \mathrm{Tr}_E\, \rho \otimes \rho_E = \mathrm{Tr}_E\, \rho \otimes \mathcal{L}_E \rho_E = 0,$$

and

$$\mathcal{P}(\mathrm{Id} \otimes \mathcal{L}_E)\rho = \mathrm{Tr}_E\big((\mathrm{Id} \otimes \mathcal{L}_E)\rho\big) \otimes \rho_E = 0.$$

The second property holds, because of $\mathcal{L}^\xi$ being a commutator, the trace over the environment degrees of freedom only involving the product of $\mathcal{L}_E$ and ρ, and by the cyclic property of the trace $\mathrm{Tr}([A, B]) = 0$ for every A, B.

[8] See for instance Reichl (1998, chap. S10.I.1) or Forster (1975).

4. Due to the above,

$$\begin{aligned}\mathcal{P}\mathcal{L}^{\xi}\mathcal{P}(\rho_{\mathrm{S}}\otimes\rho_{\mathrm{E}}) &= \mathcal{P}(\mathcal{L}_{\mathrm{S}}\otimes\mathrm{Id})(\rho_{\mathrm{S}}\otimes\rho_{\mathrm{E}}) = \mathcal{L}_{\mathrm{S}}(\rho_{\mathrm{S}}\otimes\rho_{\mathrm{E}}),\\ \mathcal{P}\mathcal{L}^{\xi}\mathcal{Q}\rho &= \xi\mathcal{P}\mathcal{L}_{\mathrm{S\text{–}E}}\mathcal{Q}\rho = \xi\,\mathrm{Tr}_{\mathrm{E}}(\mathcal{L}_{\mathrm{S\text{–}E}}\mathcal{Q}\rho)\otimes\rho_{\mathrm{E}},\\ \mathcal{Q}\mathcal{L}^{\xi}\mathcal{P}(\rho_{\mathrm{S}}\otimes\rho_{\mathrm{E}}) &= \xi\mathcal{Q}\mathcal{L}_{\mathrm{S\text{–}E}}(\rho_{\mathrm{S}}\otimes\rho_{\mathrm{E}}).\end{aligned}$$

For the easy application of the projection operators in the following calculations, we shall use the condensed notation $\mathcal{L}^{\mathcal{P}\mathcal{Q}} := \mathcal{P}\mathcal{L}\mathcal{Q}$ for any Liouvillian $\mathcal{L}$.

2.3.3 Derivation and Proof

With the preparations from the previous two sections, we derive a Markovian master equation from the von Neumann equation. The route we shall be following has first been published by Davies (1974) and is pedagogically reviewed by Spohn & Lebowitz (1978, sec. 3).

Given a Hamiltonian H and the projection $\mathcal{P}$ onto the space of factorised density matrices, the von Neumann equation, $\dot{\rho} = -\imath[H,\rho] = -\imath\mathcal{L}\rho$, can be split into two coupled equations,

$$\frac{\mathrm{d}}{\mathrm{d}t}\mathcal{P}\rho(t) = -\imath\mathcal{P}\mathcal{L}\mathcal{P}\rho(t) - \imath\mathcal{P}\mathcal{L}\mathcal{Q}\rho(t) \tag{2.3.1a}$$

$$\frac{\mathrm{d}}{\mathrm{d}t}\mathcal{Q}\rho(t) = -\imath\mathcal{Q}\mathcal{L}\mathcal{P}\rho(t) - \imath\mathcal{Q}\mathcal{L}\mathcal{Q}\rho(t). \tag{2.3.1b}$$

Equation (2.3.1b) can be integrated by use of the variation-of-constants formula[9]

$$\mathcal{Q}\rho(t) = e^{-\imath\mathcal{L}^{\mathcal{Q}\mathcal{Q}}t}\mathcal{Q}\rho(0) - \imath\int_0^t e^{-\imath\mathcal{L}^{\mathcal{Q}\mathcal{Q}}(t-s)}\mathcal{L}^{\mathcal{Q}\mathcal{P}}\mathcal{P}\rho(s)\,ds. \tag{2.3.2}$$

As we have pointed out before, we have to choose a particular initial condition, namely a factorised density matrix, such that $\mathcal{Q}\rho(0) = 0$. By inserting the integral into Equation (2.3.1a) and using the definition of $\mathcal{P}$, we obtain an equation for the reduced density matrix ρ_{S},

$$\frac{\mathrm{d}}{\mathrm{d}t}\rho_{\mathrm{S}}(t)\otimes\rho_{\mathrm{E}} = -\imath\mathcal{L}^{\mathcal{P}\mathcal{P}}\rho_{\mathrm{S}}(t)\otimes\rho_{\mathrm{E}} - \int_0^t \mathcal{L}^{\mathcal{P}\mathcal{Q}}e^{-\imath\mathcal{L}^{\mathcal{Q}\mathcal{Q}}(t-s)}\mathcal{L}^{\mathcal{Q}\mathcal{P}}\rho_{\mathrm{S}}(s)\otimes\rho_{\mathrm{E}}\,ds.$$

Before proceeding with another application of the variation-of-constants formula, we use the already calculated projections of $\mathcal{L}^{\xi}$ and simplify the equation symbolically,[10]

$$\frac{\mathrm{d}}{\mathrm{d}t}\rho_{\mathrm{S}}(t)\otimes\rho_{\mathrm{E}} = -\imath(\mathcal{L}_{\mathrm{S}}\otimes\mathrm{Id})\big(\rho_{\mathrm{S}}(t)\otimes\rho_{\mathrm{E}}\big) - \xi^2\int_0^t \mathrm{Tr}_{\mathrm{E}}\Big(\mathcal{L}_{\mathrm{S\text{–}E}}e^{-\imath\mathcal{L}^{\xi}(t-s)}\mathcal{L}_{\mathrm{S\text{–}E}}\Big)\big(\rho_{\mathrm{S}}(s)\otimes\rho_{\mathrm{E}}\big)\,ds. \tag{2.3.3}$$

In this form the equation is very reminiscent of the standard results of perturbation theory, except one

[9] The theory of ordinary differential equations, whose results can, at least formally, be used here, provides the variation-of-constants formula (Königsberger, 2000, p. 154) to obtain a particular solution x_p of an inhomogeneous ordinary differential equation. If $\Phi(t)$ is the fundamental matrix of the homogeneous problem $\dot{x} = A(t)x$, a particular solution of the inhomogeneous problem $\dot{x} = A(t)x + b(t)$ is then given by

$$x_p(t) = \Phi(t)\int_{t_0}^t \Phi^{-1}(s)b(s)\,ds.$$

[10] We make use of the idempotence of the projection operators, which yields $\mathcal{Q}e^{-\imath\mathcal{L}^{\mathcal{Q}\mathcal{Q}}t}\mathcal{Q} = \mathcal{Q}e^{-\imath\mathcal{L}t}\mathcal{Q}$.

very important property: Equation (2.3.3) is an equation for the reduced density matrix $\rho_S \otimes \rho_E$ *alone*. The Born-approximation, explicitly using a factorised density matrix for all times, is not necessary here. For factorised initial conditions, it is no approximation at all but exact. The integral form of Equation (2.3.3) is

$$\rho_S(t) = e^{-\imath\mathcal{L}_S t}\rho_S(0) - \xi^2 \int_0^t e^{-\imath\mathcal{L}_S(t-s)} \left\{ \int_0^s \mathrm{Tr}_E \left(\mathcal{L}_{S\text{–}E} e^{-\imath\mathcal{L}^\xi(s-u)} \mathcal{L}_{S\text{–}E} \rho_E \right) \rho_S(u)\, du \right\} ds,$$

where we dropped the tensor-product notation for convenience, keeping the notion of ρ_E only for the trace over the environment's degrees of freedom. In this form, we still have to work with an equation where the dissipative part is of the abstract form

$$\int_0^t \int_0^s K(t, s-u)\rho(u)\, du\, ds.$$

The actual strategy for deriving a *Markovian* master equation should be to manipulate the equation so long until it assumes a form that is again a variation-of-constants formula for $\rho_S(t)$ and then obtain the associated differential equation. We therefore first reverse the order of integration and then shift the inner integral by setting $s := u + v$,

$$\int_0^t \int_0^s du\, ds \quad \mapsto \quad \int_0^t \int_u^t ds\, du \quad \mapsto \quad \int_0^t \int_0^{t-u} dv\, du.$$

With these manipulations, we actually transform

$$\int_0^t \int_0^s K(t, s-u)\rho(u) du\, ds = \int_0^t \int_0^{t-u} K(t, v) dv \rho(u) du,$$

which is close to the aimed goal. In our context, the kernel $K(t,v)$ actually is $K^\xi(t,v)$, which, due to the now simpler form, is more open for limiting procedures than before. The integral equation for the reduced density matrix for finite ξ is

$$\rho_S(t) = e^{-\imath\mathcal{L}_S t}\rho_S(0) - \xi^2 \int_0^t e^{-\imath\mathcal{L}_S(t-s)} \left\{ \int_0^{t-s} e^{\imath\mathcal{L}_S v} \mathrm{Tr}_E \left(\mathcal{L}_{S\text{–}E} e^{-\imath\mathcal{L}^\xi v} \mathcal{L}_{S\text{–}E} \rho_E \right) dv \right\} \rho_S(s) ds.$$

We change to the interaction picture by factorising out the time-evolution due to $\mathcal{L}_S$,

$$\rho_S(t) = e^{-\imath\mathcal{L}_S t}\rho_S^I(t),$$

and multiply the whole equation with $e^{\imath\mathcal{L}_S t}$. Then,

$$\rho_S^I(t) = \rho_S^I(0) - \xi^2 \int_0^t e^{\imath\mathcal{L}_S s} \left\{ \int_0^{t-s} e^{\imath\mathcal{L}_S v} \mathrm{Tr}_E \left(\mathcal{L}_{S\text{–}E} e^{-\imath\mathcal{L}^\xi v} \mathcal{L}_{S\text{–}E} \rho_E \right) dv \right\} e^{-\imath\mathcal{L}_S s} \rho_S^I(s) ds. \tag{2.3.4}$$

The final step is to rescale time $\tau = \xi^2 t$, because, as we have pointed out before, our interest lies in the long-time behaviour of the system, whose asymptotic time scale is τ. The integration over s is transformed into one over $\sigma = \xi^2 s$, and thus

$$\rho_S^I(\tau) = \rho_S^I(0) - \int_0^\tau e^{\imath\mathcal{L}_S \frac{\sigma}{\xi^2}} \left\{ \int_0^{\frac{\tau-\sigma}{\xi^2}} e^{\imath\mathcal{L}_S v} \mathrm{Tr}_E \left(\mathcal{L}_{S\text{–}E} e^{-\imath\mathcal{L}^\xi v} \mathcal{L}_{S\text{–}E} \rho_E \right) dv \right\} e^{-\imath\mathcal{L}_S \frac{\sigma}{\xi^2}} \rho_S^I(\sigma) d\sigma. \tag{2.3.5}$$

From here on, the derivation of the Markovian master equation reduces to a discussion of the limiting behaviour of the operator in curly brackets, which due to the term $e^{-\imath\mathcal{L}^{\xi}\nu}$ still depends on the scaling variable. We then need to understand the action of the free system's evolution operators, which also depend on ξ, and finally prove that the solutions of the integral equation converge to the solution of the limiting equation.

It is plausible that in our context the integral operator

$$K^{\xi}(\tau) := \int_0^{\tau/\xi^2} e^{\imath\mathcal{L}_{\mathrm{S}}\nu}\,\mathrm{Tr}_{\mathrm{E}}\left(\mathcal{L}_{\mathrm{S\text{–}E}}e^{-\imath\mathcal{L}^{\xi}\nu}\mathcal{L}_{\mathrm{S\text{–}E}}\rho_{\mathrm{E}}\right)d\nu$$

converges in some sense[II] for $\xi\to 0$ to

$$K := \int_0^{\infty} e^{\imath\mathcal{L}_{\mathrm{S}}\nu}\,\mathrm{Tr}_{\mathrm{E}}\left(\mathcal{L}_{\mathrm{S\text{–}E}}e^{-\imath(\mathcal{L}_{\mathrm{S}}\otimes\mathrm{Id}+\mathrm{Id}\otimes\mathcal{L}_{\mathrm{E}})\nu}\mathcal{L}_{\mathrm{S\text{–}E}}\rho_{\mathrm{E}}\right)d\nu.$$

This suffices to approximate

$$e^{\imath\mathcal{L}_{\mathrm{S}}\frac{\sigma}{\xi^2}}\left\{\int_0^{\frac{\tau-\sigma}{\xi^2}} e^{\imath\mathcal{L}_{\mathrm{S}}\nu}\,\mathrm{Tr}_{\mathrm{E}}\left(\mathcal{L}_{\mathrm{S\text{–}E}}e^{-\imath\mathcal{L}^{\xi}\nu}\mathcal{L}_{\mathrm{S\text{–}E}}\rho_{\mathrm{E}}\right)d\nu\right\}e^{-\imath\mathcal{L}_{\mathrm{S}}\frac{\sigma}{\xi^2}}$$

by

$$e^{\imath\mathcal{L}_{\mathrm{S}}\frac{\sigma}{\xi^2}}\left\{\int_0^{\infty} e^{\imath\mathcal{L}_{\mathrm{S}}\nu}\,\mathrm{Tr}_{\mathrm{E}}\left(\mathcal{L}_{\mathrm{S\text{–}E}}e^{-\imath(\mathcal{L}_{\mathrm{S}}\otimes\mathrm{Id}+\mathrm{Id}\otimes\mathcal{L}_{\mathrm{E}})\nu}\mathcal{L}_{\mathrm{S\text{–}E}}\rho_{\mathrm{E}}\right)d\nu\right\}e^{-\imath\mathcal{L}_{\mathrm{S}}\frac{\sigma}{\xi^2}}.$$

In the beginning, we had assumed the system S to be of finite dimension. The free propagator, due to H_{S} being self-adjoint, has a representation in terms of its eigenvalues and spectral projections

$$e^{-\imath\mathcal{L}_{\mathrm{S}}t} = \sum_{\alpha} e^{-i\omega_\alpha t}\mathcal{E}_\alpha,$$

with α indexing the eigenspaces of $\mathcal{L}_{\mathrm{S}}$. The spectral projections $\mathcal{E}_\alpha$ are related to the spectral projections $\mathcal{P}_j$ of $H_{\mathrm{S}} = \sum_j \varepsilon_j\mathcal{P}_j$ by

$$\mathcal{E}_\alpha\rho \quad = \sum_{\varepsilon_m-\varepsilon_n=\omega_\alpha}\mathcal{P}_m\rho\mathcal{P}_n.$$

For any operator A on $\mathcal{H}_{\mathrm{S}}$, we note the following property:

$$\begin{aligned}\lim_{\xi\to 0}\int_0^{\tau} e^{-\imath\mathcal{L}_{\mathrm{s}}\frac{\sigma}{\xi^2}}Ae^{-\imath\mathcal{L}_{\mathrm{s}}\frac{\sigma}{\xi^2}}\rho(\sigma)d\sigma &= \sum_{\alpha,\beta}\mathcal{E}_\alpha A\mathcal{E}_\beta\lim_{\xi\to 0}\int_0^{\tau} e^{-\imath(\omega_\alpha-\omega_\beta)\frac{\sigma}{\xi^2}}\rho(\sigma)d\sigma\\ &= \sum_{\alpha,\beta}\mathcal{E}_\alpha A\mathcal{E}_\beta\lim_{t\to\infty}\frac{1}{2t}\int_{-t}^{t} e^{-\imath(\omega_\alpha-\omega_\beta)s}\rho(s)ds\\ &= \sum_{\alpha,\beta}\mathcal{E}_\alpha A\mathcal{E}_\beta\delta_{\alpha,\beta}\int_0^{\tau}\rho(\sigma)d\sigma = \sum_{\alpha}\mathcal{E}_\alpha A\mathcal{E}_\alpha\int_0^{\tau}\rho(\sigma)d\sigma.\end{aligned}$$

We define the time average of A to be

$$\bar{A} := \sum_{\alpha}\mathcal{E}_\alpha A\,\mathcal{E}_\alpha = \lim_{t\to\infty}\frac{1}{2t}\int_{-t}^{t} e^{-\imath\mathcal{L}_{\mathrm{S}}s}A\,e^{\imath\mathcal{L}_{\mathrm{S}}s}\,ds,$$

[II] See appendix A for the details.

and conclude with the limit of Equation (2.3.5) after τ has been re-substituted

$$\rho_{\mathrm{S}}^{\mathrm{I}}(t) = \rho_{\mathrm{S}}^{\mathrm{I}} - \xi^2 \int_0^t \bar{K}\rho_{\mathrm{S}}^{\mathrm{I}}\, ds, \tag{2.3.6}$$

which solves the Markovian master equation

$$\frac{\mathrm{d}}{\mathrm{d}t}\rho_{\mathrm{S}}^{\mathrm{I}}(t) = -\xi^2 \bar{K}\rho_{\mathrm{S}}^{\mathrm{I}}(t). \tag{2.3.7}$$

The concrete form of this master equation for the single-molecule devices treated in this thesis is formulated in appendix B.

Up to now, convergence has only been established for the integral operator. Proving the convergence of the solutions ρ^ξ of Equation (2.3.5) to the solution ρ of Equation (2.3.7) is of purely mathematical interest and provides no additional physical insight. Since here we are mainly interested in the *derivation* of the master equation and an understanding of its individual contributions and where they come from, we refer for the mathematical subtleties and formal details to Davies (1974).

Spohn & Lebowitz (1978) and Davies (1974) give a very elegant argument why the time average of K produces the secular or rotating-wave approximation, which decouples the populations from the coherences of non-degenerate states of ρ. They note that the generator of the dissipative dynamics $\bar{K}$ commutes with the free evolution of the system. By definition $\bar{K} = \sum_\alpha \mathcal{E}_\alpha K \mathcal{E}_\alpha$ and $\exp(-\imath\mathcal{L}_{\mathrm{S}}t) = \sum_\alpha \exp(-\imath\omega_\alpha t)\mathcal{E}_\alpha$, which leaves

$$e^{-\imath\mathcal{L}_{\mathrm{S}}t}\bar{K}e^{\imath\mathcal{L}_{\mathrm{S}}t} = \sum_{\alpha,\beta}\mathcal{E}_\alpha\bar{K}\mathcal{E}_\beta e^{\imath(\omega_\alpha-\omega_\beta)t} = \sum_{\alpha,\beta}\sum_\gamma \mathcal{E}_\alpha\mathcal{E}_\gamma K\mathcal{E}_\gamma\mathcal{E}_\beta e^{\imath(\omega_\alpha-\omega_\beta)t} = \sum_\gamma \mathcal{E}_\gamma K\mathcal{E}_\gamma = \bar{K}.$$

We assume that H_{S} is non-degenerate, which renders its eigenspaces one-dimensional. A system Hamiltonian H_{S} with spin degeneracy due to electronic spin should be considered non-degenerate in the present context. For generic Anderson models, the system–bath interaction, which is the tunnelling Hamiltonian H_{T}, respects the spin symmetry such that H as a whole commutes with the spin operator. Electronic spin is therefore conserved in the dynamics, and coherent superpositions of states with different spin need not be taken care of.[12] Denote the space of diagonal density matrices by $\mathcal{D}$. The free system's evolution leaves $\mathcal{D}$ and only[13] $\mathcal{D}$ invariant, for

$$\rho \in \mathcal{D} \quad \Leftrightarrow \quad e^{-\imath\mathcal{L}_{\mathrm{S}}t}\rho = \rho.$$

But due to the vanishing commutator of $\bar{K}$ and $\exp(-\imath\mathcal{L}_{\mathrm{S}}t)$ and the non-degeneracy of H_{S} also

$$\rho \in \mathcal{D} \quad \Rightarrow \quad \bar{K}\rho \in \mathcal{D}.$$

[12] The only effect of spin degeneracy in the master-equation dynamics is, as we shall see in chapter 3, repulsion of particles due to the on-site Coulomb interaction as well as an additional factor of 2 for all rates that describe tunnelling of a particle onto the device. This factor accounts for the freedom to choose an electron of either spin from the fermionic reservoir, a freedom that is not given for the tunnelling back to the electrodes, as there the spin of the particle is already fixed and only jumping into a hole of the same spin is allowed.

[13] For the reverse implication, assume $\rho = \big(|\alpha\rangle + |\beta\rangle\big)\big(\langle\alpha| + \langle\beta|\big) = |\alpha\rangle\langle\alpha| + |\beta\rangle\langle\beta| + 2\mathrm{Re}|\alpha\rangle\langle\beta|$. Then the time evolution of the density matrix in terms of the time evolution of the states is

$$\rho(t) = |\alpha\rangle\langle\alpha| + |\beta\rangle\langle\beta| + 2\,\mathrm{Re}\, e^{\imath(\omega_\alpha-\omega_\beta)t}\,|\alpha\rangle\langle\beta|,$$

which is different from ρ unless $\omega_\alpha = \omega_\beta$.

It is plausible that also the semi-group generated by $\bar{K}$ leaves $\mathcal{D}$ invariant. The consequence of this is that for non-degenerate systems, the master equation splits into two equations, a rate equation for the populations ρ_{ii} of the reduced density matrix, and one only transforming its coherences ρ_{ij}. In particular, any long-time limit or stationary state described by a master equation in the weak-coupling limit will *not* retain coherences between states of different energy in the density matrix. In view of an energy–time uncertainty relation, the theory is physical, because for $t \to \infty$, we would expect all states to be of sharp energy, where the energy is only renormalised by the perturbation on a scale given by $\mathcal{O}(\xi^2 H_{\text{S–E}}^2)$. In our model, all energy differences are assumed to be much larger than $\mathcal{O}(\xi^2 H_{\text{S–E}}^2)$. For $\xi \to 0$, any energy involved in the problem, be it the thermal energy $k_\text{B}T$ or a vibrational excitation quantum $\hbar\omega$, is much larger than $\xi^2 H_{\text{S–E}}^2$. In chapter 6, we shall present a formulation of the master equation and its derivation that describes the situation when the energy scale induced by the tunnel coupling is not the smallest scale of the problem. The above argument can be generalized to partially degenerate Hamiltonians. Then the space $\mathcal{D}$ comprises the density matrices that are block-diagonal in the energy basis and coherences between degenerate states have to be taken into account, while coherences between non-degenerate states can be ignored in the dynamics.

One may ask why this derivation of the master equation goes the route via integral equations instead of integro-differential equations that appear in the standard perturbative treatment. The reasons are two-fold. First, the mathematical treatment of integro-differential equations is much more complicated, because differential operators always induce a question of the domain of definition. The integral calculus is much more handy, as integrability is a much weaker condition on a function than differentiability. Second, the outer integral that arose from using the variation-of-constants formula provides the averaging of the fast oscillating time scale of H_S, which, although it is exact, is termed the rotating-wave *approximation* in the literature. The differential derivation lacks this and as thus cannot lead to a completely positive generator unless the averaging is inserted by hand.

Without the secular approximation, the resulting equations are known as the Bloch–Redfield equations (Timm, 2008), which are widely used in the literature. Dümcke & Spohn (1979) discuss four generators of semi-groups, among which are Davies's results $\bar{K}$ and the Bloch–Redfield generator. They show that by construction Davies's generator is the limit of a positive operator and therefore positive itself. Using $H_\text{S} = \Omega\sigma_z$, a non-degenerate two-level system, being linearly coupled to a bath of thermal bosons, Dümcke & Spohn (1979) and Benatti & Floreanini (2005, Example 3.4) show that the Bloch–Redfield generator is positive only for $\beta = 0$ that is an infinitely hot bath. Although the Bloch–Redfield equation derives from a perturbative ansatz, perturbation theory for non-equilibrium problems has to care for the positivity of ρ. Since positive operators do not form a vector space but only a convex cone, this implies restrictions to the theory when compared with standard perturbation theory for retarded Green functions, which actually does take place in a Hilbert space.

2.4 Expectations of Observables

Besides computing the stationary solution of the master equation, we are also interested in the calculation of experimentally observable quantities. As these are generally traces of a self-adjoint operator with respect to the stationary density matrix, they only show some and not the full non-equilibrium information that is encoded in ρ.

Here, we concentrate on the stationary current $\langle I_\alpha \rangle$ through the tunnel junction of electrode α. The higher moments, describing the fluctuation and noise characteristics of the current, provide information

about the time-dependent dynamics. The giant Fano factor in Anderson–Holstein type single-molecule junctions deep in the Franck–Condon blockade regime for example (Koch & von Oppen, 2005b) is a signature for the self-similar avalanche transport of electrons through such a device.

In the specific setting of molecular electronics, the system–bath interaction is the tunnel Hamiltonian

$$H_{\mathrm{T}} = \sum_{\boldsymbol{k}\alpha\sigma} t_{\alpha\sigma} c^{\dagger}_{\boldsymbol{k}\alpha} d_{\sigma} + \mathrm{h.c.}$$

for a localised, spinless[14] system with its electronic levels being labelled by σ. Any electron–phonon interaction is assumed to have been eliminated by means of the polaron transformation or numerical diagonalisation of H_{S}, such that the tunnel amplitudes $t_{\alpha\sigma}$ are in fact matrices.

The stationary current I_α is the time-derivative of the number operator N_α of particles in the respective reservoir and can be evaluated using the Heisenberg equation of motion (Wingreen & Meir, 1992)

$$I_\alpha = \frac{\imath e}{\hbar} \sum_{\boldsymbol{k}\sigma} t_{\alpha\sigma} c^{\dagger}_{\boldsymbol{k}\alpha} d_{\sigma} - \mathrm{h.c.}$$

In natural units $\hbar = 1$, $e = 1$, this is twice the negative imaginary part of the operator $\sum_{\boldsymbol{k}\sigma} t_{\alpha\sigma} c^{\dagger}_{\boldsymbol{k}\alpha} d_{\sigma}$. The tunnelling Hamiltonian H_{T} is twice the real part of this operator. By definition of the operators and $\mathrm{Tr}_{\mathrm{E}}(c^{\dagger}_{\boldsymbol{k}\alpha}\rho_{\mathrm{E}}) = 0$, it is clear that the system trace of I_α with respect to the reduced density matrix vanishes,

$$\mathrm{Tr}_{\mathrm{S+E}}(I_\alpha \rho_{\mathrm{S}} \otimes \rho_{\mathrm{E}}) = 0.$$

The straightforward approach to compute the stationary current following the idea of section 2.1 is to start with the *full*, that is system plus bath, density matrix ρ in the trace,

$$\langle I_\alpha \rangle = \mathrm{Tr}_{\mathrm{S+E}}(I_\alpha \rho).$$

Integrating the von Neumann equation once and inserting the result in the above equation yields

$$\langle I_\alpha \rangle(t) = \mathrm{Tr}_{\mathrm{S+E}} \left(I_\alpha \rho(0) - \imath \int_0^t I_\alpha [H, \rho(s)]\, ds \right).$$

In the interaction picture, the commutator only involves the tunnelling Hamiltonian $H^{\mathrm{I}}_{\mathrm{T}}$ and as such

$$\langle I_\alpha \rangle(t) = \mathrm{Tr}_{\mathrm{S+E}} \left(I^{\mathrm{I}}_\alpha(s) \rho^{\mathrm{I}}(0) - \imath \int_0^t [I^{\mathrm{I}}_\alpha(t), H^{\mathrm{I}}_{\mathrm{T}}(s)] \rho^{\mathrm{I}}(s)\, ds \right).$$

At this stage, the crucial Born approximation $\rho = \rho_{\mathrm{S}} \otimes \rho_{\mathrm{E}}$ and the Markov approximation are used to yield a formula that can be evaluated by simple integration

$$\langle I_\alpha \rangle(t) = -\imath\, \mathrm{Tr}_{\mathrm{S+E}} \left(\int_0^\infty [I^{\mathrm{I}}_\alpha(t), H^{\mathrm{I}}_{\mathrm{T}}(t-s)] \rho^{\mathrm{I}}(t)\, ds \right). \tag{2.4.1}$$

As straightforward and easy to use this approach may seem, it bears a very serious problem in the last step. As it is clear from the above calculation, the Born-approximation has to be applied exactly at the right

[14] We ignore the electronic spin for convenience, since here it does not add any new physics to the problem but due to the necessary bookkeeping of the spin indices complicates the notation.

step of the derivation. Using a factorised density matrix and integrating the von Neumann equation do not commute. But any approximation, if it were well-defined, should be valid from the very beginning of a derivation or not at all. One assumes that ρ has a certain form globally, not just from the third step onwards. We therefore discard this derivation and revert to the projection-operator approach.

We split the expectation value $\langle I_\alpha \rangle$ into two parts by inserting $\mathrm{Id} = \mathcal{P} + \mathcal{Q}$,

$$\langle I_\alpha \rangle = \mathrm{Tr}_{\mathrm{S+E}}(I_\alpha \mathcal{P}\rho) + \mathrm{Tr}_{\mathrm{S+E}}(I_\alpha \mathcal{Q}\rho).$$

The first term naturally vanishes, because $\mathcal{P}\rho = (\mathrm{Tr}_{\mathrm{E}}\rho)\otimes\rho_{\mathrm{E}}$, and by construction the system–bath coupling and hence I_α has zero expectation value with respect to the equilibrium distribution of the electrodes. The time evolution of $\mathcal{Q}\rho_{\mathrm{S+E}}$ is due to Equation (2.3.2),

$$\mathcal{Q}\rho(t) = e^{-\imath\mathcal{L}^{\xi\mathcal{Q}\mathcal{Q}}t}\rho(0) - \imath\int_0^t e^{-\imath\mathcal{L}^{\xi\mathcal{Q}\mathcal{Q}}(t-s)}\mathcal{L}^{\xi\mathcal{Q}\mathcal{P}}\mathcal{P}\rho(s)ds.$$

The Liouvillian $\mathcal{P}\mathcal{L}^{\xi}\mathcal{Q}$ acting on a factorised density matrix is $\xi\mathcal{L}_{\mathrm{S–E}}$. Like before, we use a factorised density matrix only as the initial condition. By definition of the current operator $I_\alpha = \dot{N}_\alpha = -\imath[N_\alpha, H] = -\imath[N_\alpha, H_{\mathrm{T}}]$ being the time derivative of the number operator of electrode α, it also acquires a factor ξ and shares the properties of H_{T} under the projection operators,

$$\langle I_\alpha \rangle(t) = -\imath\,\mathrm{Tr}_{\mathrm{S+E}}\left(\xi^2 I_\alpha \int_0^t e^{-\imath\mathcal{L}^{\xi}(t-s)}\mathcal{L}_{\mathrm{S–E}}\mathcal{P}\rho(s)\,ds\right).$$

We shall apply the same approximations as before, essentially repeating the calculations that led to the Markovian master equation in section 2.3.3. There, the derivation was facilitated by the use of an integral representation. The current operator itself also is a time derivative, and thus an integral representation is realised by considering the number operator N_α. The formal manipulations of section 2.3.3 lead to

$$\langle N_\alpha \rangle(t) = -\imath\,\mathrm{Tr}_{\mathrm{S+E}}\left(\xi^2 \int_0^t \int_0^{t-s} I_\alpha e^{-\imath\mathcal{L}^{\xi}v}\mathcal{L}_{\mathrm{S–E}}\,dv\,\mathcal{P}\rho(s)\,ds\right)$$

On the Markovian time scale, this is

$$\langle N_\alpha \rangle(\tau) = -\imath\,\mathrm{Tr}_{\mathrm{S+E}}\left(\int_0^\tau \int_0^{\frac{\tau-\sigma}{\xi^2}} I_\alpha e^{-\imath\mathcal{L}^{\xi}v}\mathcal{L}_{\mathrm{S–E}}\,dv\,\mathcal{P}\rho(\sigma)\,d\sigma\right),$$

which, by the same arguments, converges to

$$\lim_{\xi\to 0}\langle N_\alpha \rangle(\tau) = -\imath\,\mathrm{Tr}_{\mathrm{S+E}}\left(\int_0^\tau \int_0^\infty I_\alpha e^{-\imath(\mathcal{L}_{\mathrm{S}}+\mathcal{L}_{\mathrm{E}})v}\mathcal{L}_{\mathrm{S–E}}\,dv\,\mathcal{P}\rho(\sigma)\,d\sigma\right).$$

This result is the integral representation of Equation (2.4.1) in the Schrödinger picture; however, its derivation is consistent with all approximations. An explicit formula for the application to single-molecule devices is given in appendix B.1.

Chapter 3

The Rate Equation

By the action of the rotating-wave approximation—the averaging over the fast oscillating time scale defined by the localised system's Hamiltonian—the dynamics in the weak-coupling limit can be classified according to the spectral structure of H_S. For degenerate states, one has to compute the master equation for all elements of the reduced density matrix, not only the populations but also the off-diagonal elements, the coherences. We term this equation the "degenerate master equation" or master equation for short. For non-degenerate states, on the contrary, the large energy differences[1] occurring in the averaging imply a decoupling of the populations from the coherences. The dynamics of these states is described by a rate equation. The full master equation of a weakly coupled quantum nanostructure is a rate equation between the degenerate subspaces[2] and a degenerate master equation inside each of them.

It is the paradigm of this thesis to begin the discussion with simple and intuitive models and, after having understood these, add complexity step by step. We reflect the classification of the kinetic equations depending on the system's Hamiltonian in the structure of the following chapters.

In this chapter, we ignore the substructure of the energy manifolds and only discuss dynamics between states of different energies. We shall see that the rate equation describing these systems or this part of the full system shows a very rich phenomenology. In chapters 4 and 5, we discuss the case of degenerate states; near-degenerate states, where the energy difference is small compared with all other energy scales of the problem and is of the order of the tunnelling-induced broadening Γ, are treated in chapter 6.

Rate equations are an intuitive description of the transport problem: although they have to be derived from the von Neumann equation rigorously, their dynamics can be understood as a succession of jump processes between well-defined states with the rates being given by Fermi's Golden Rule. Sequential tunnelling of electrons onto and off the device is the lowest-order effect, namely of order $\mathcal{O}(H_T^2)$, that is second-order perturbation theory in the system–bath interaction.

The rate-equation description has been applied to various problems of molecular electronics, for instance strong electron–phonon coupling (Koch & von Oppen, 2005b) and pseudo-Jahn–Teller effects (Reckermann *et al.*, 2008). Using an effective low-energy Hamiltonian, as it is obtained by means of the Schrieffer–Wolff transformation (Schrieffer & Wolff, 1966), tunnelling of two electrons, pair-tunnelling, or co-tunnelling, becomes accessible by rate equations. Alternatively, higher-order expansions of the single-particle T-matrix[3]

[1] In this respect, "large" always means large with respect to the energy scale of the tunnelling-induced broadening $\Gamma = \mathcal{O}(H_T^2)$.

[2] We shall also use the term "energy manifold" in the following.

[3] See for instance Averin & Nazarov (1990) for the general idea and Koch *et al.* (2004) for the application to rate equations in molecular electronics.

of the scattering problem also provide rates for pair- and co-tunnelling processes that can be included in a rate-equation treatment. Although a consistent expansion of the von Neumann equation would have to account for off-diagonal elements of ρ via virtual processes like in the implementation of Leijnse & Wegewijs (2008), the rate equation formalism yields a remarkably good qualitative description (Koch *et al.*, 2006a). A rigorous derivation of rate equations for higher-order tunnelling processes is, unfortunately, difficult if not infeasible. The Markov regime only covers one distinguished time scale $\xi^2 t$. Co-tunnelling occurs on a time scale $\xi^4 t$, which is much shorter. It is thus problematic to judge whether the dynamics on both time scales are concurrently Markovian and, if not, what the non-Markovian dynamics look like.

The general form of the rate equation for a single-molecule device in the weak-coupling limit, which describes the sequential-tunnelling regime, is

$$\dot{p}_n^q = \sum_{p,m} W_{m\to n}^{p\to q} p_m^p - \sum_{p,m} W_{n\to m}^{q\to p} p_n^q. \tag{3.0.1}$$

The occupation probabilities p_n^q are the diagonal elements of the reduced density matrix $p_n^q := |n;q\rangle\langle n;q|$. The system Hamiltonian H_S operates on a product space of electronic and vibrational degrees of freedom $\mathcal{H}_S = \mathcal{H}_{el} \otimes \mathcal{H}_{vib}$. We therefore divide the labelling of the states into charge states n, m and vibronic excitations q, p. Since we want to avoid the use of too many primed symbols like q', our notation using the symbol p is more subtle. Equipped with an upper or lower index, for example p_n or p_n^q, the symbol is the *occupation probability* of the state indicated by the index. Without an index, the label p is like q just a variable counting vibronic excitations. Due to this distinction, there should be no ambiguity. The devices we want to describe have only three charge states, neutral $n = 0$, singly charged $n = 1$, and doubly charged $n = 2$. For all of the examples and problems in this chapter, we assume spinless electrodes and single-level molecules, which implies no double occupation. For the application in chapter 3.5, we consider the much more common modelling with spin-degenerate electrodes and nanostructures where we exclude double occupation by additionally assuming strong Coulomb blockade $U \to \infty$. In this case, however, the freedom to choose electrons of either spin for tunnelling has to be accounted for by factor of 2 in all rates that describe tunnelling onto the device. Apart from this, there is no qualitative difference in the two approaches as long as we only describe sequential tunnelling. Higher-order tunnel processes show Kondo correlations due to spin-exchange in co-tunnelling (Pustilnik & Glazman, 2005).

The rates $W_{n\to m}^{q\to p}$ are proportional to the probability for jumping from $|n;q\rangle$ to $|m;p\rangle$. Sequential tunnelling, that is tunnelling of single particles, immediately implies $|m-n| = 1$. In the molecular-electronics framework with an Anderson–Holstein Hamiltonian the rates $W = f\Gamma$ are a product of two terms: a Fermi function f,which is the probability to find an electron or hole in the leads to match the energy difference $\varepsilon_m^p - \varepsilon_n^q$, and the Golden-Rule rate for the actual transition. For our model of a single-molecule junction, this rate is $\Gamma_\alpha^{pq} = \frac{2\pi}{\hbar} \nu t_\alpha^2 M^{pq}$—the product of the Golden-Rule rate Γ_α of the bare tunnelling Hamiltonian H_T and the Franck–Condon factor M^{pq}, which is the squared overlap integral of the oscillator wave functions associated with either charge state in the polaron picture. For the transition from neutral to singly charged, this is the overlap between the undisplaced and the displaced wave function $M^{pq} = |\langle p|e^{-\lambda(b^\dagger - b)}|q\rangle|^2$. For the Anderson–Holstein molecule, the Franck–Condon matrix is symmetric in p and q. For other electron–phonon couplings, for instance charge-dependent oscillators, this need not be the case.

The description in terms of a rate equation does not include signatures of tunnel-induced broadening; the temperature of the reservoirs is so large with respect to the energy scale of the tunnelling Hamiltonian that the device's levels become sharp. Compared with the exact transmission function of the resonant tunnelling

problem, the weak-coupling limit is the regime $\Gamma/k_\mathrm{B}T \to 0$, when the Lorentzian spectral function, whose width is the tunnelling-induced broadening Γ of the electronic levels, converges to a δ-function localised at the unperturbed system's energy.

The rate equation (3.0.1) has a gain and a loss term. The first term describes probability flowing into the state $|n;q\rangle$ and thus increasing p_n^q, while the second accounts for processes reducing the probability p_n^q. In the stationary state, both contributions balance each other. The steady-state condition, $\dot{p}_n^q = 0$ for all n and q, differs from the condition of detailed balance, which is much stronger. Detailed balance implies that the flow of probability between *every* pair of states is balanced: $W_{n\to m}^{p\to q} p_n^p = W_{m\to n}^{q\to p} p_m^q$.

The time-dependent dynamics of the rate equation can be simulated with the help of the Metropolis–Hastings algorithm of Monte-Carlo theory presented in appendix C. This algorithm computes the quantum trajectories of individual electrons that tunnel onto and off the device with probabilities being given by the rates W. This intuitive picture of the physics makes the understanding of the time-dependent dynamics easy, as one can trace such a Monte-Carlo simulation easily by hand. The properties of the long-time behaviour and the stationary distribution are, however, not easy to grasp by simply iterating the hopping dynamics manually. For the Monte-Carlo simulation to converge, a huge number of trajectories has to be computed. Thus, for the stationary distribution, one has to revert to the picture of balanced flows of probability, which is considerably different from the simple electron-hopping picture. For the identification of tunnelling cascades in the time-dependent dynamics and the thus induced fundamental transport processes, the Monte-Carlo simulation of the rate equation are an invaluable, which the application for instance in Koch & von Oppen (2005b) or the discussion of the $E\otimes e$ Jahn–Teller molecule in chapter 3.5 show.

We can use the balance condition implied by the equation $\dot{p}_n^q = 0$ to identify different classes of states and their properties in the long-time limit. Consider a state $|j\rangle$ with population p_j, its loss rate W_out and the gain rates from other states $|i\rangle$, W_in^i. Depending on W_out and W_in^i, we distinguish three categories of states, which are sketched in Figure 3.1.

Generic States

By interpreting all states $|j\rangle$ communicates with as one large state manifold, this part of the rate equations reduces to an effective two-level system: the state in question and everything else. The stationary-state equation thus is

$$W_\mathrm{out} p_j = \sum_i W_\mathrm{in}^i p_i \le W_\mathrm{in}.$$

The ratio $W_\mathrm{in}/W_\mathrm{out}$ is an upper bound for the steady-state occupation of $|j\rangle$. A lower bound can be established by noting that $1 \ge p_j \ge W_\mathrm{in}^i/W_\mathrm{out} p_i$ for every i, which is not very handy unless more is known about the p_i. The intuitive feeling, however, is that states with large outflow and small inflow will acquire small, states with large inflow but small outflow will acquire a large population in the stationary state. The other two classes of states are the extreme cases of this situation.

Sources of Probability

These states are characterised by $W_\mathrm{in}^i = 0$ for all i, or at least for all states i that take part in the dynamics after a vibrational cut-off has been introduced. These states occur rather rarely. They do not play a significant role in the dynamics, since every bit of occupation probability that is put into them is immediately pushed out: they are emitting probability, such that $p_j = 0$ is a valid solution for these emitting states. This class of

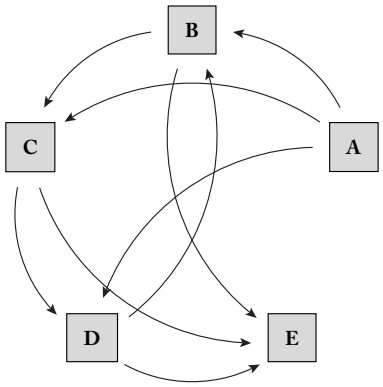

Figure 3.1: Illustration of the three classes of states. Sources (A), which emit probability and therefore solve the master equation with $p_A = 0$, sinks (E), which absorb probability and therefore solve the stationary equation with $p_E = 1$, and states that are populated and depopulated by the dynamics by the respective entry and exit rates (B,C,D).

states is also a good description for states with a large number of exit but only a small number of entry channels, because $W_{in}/W_{out} \approx 0$. Consider for example the high-lying vibronic states of a single-molecule device at moderate bias voltage. These states can be populated from all other states above, but from none of those lying energetically lower. We consider these as sources of probability and of not much relevance for the dynamics, thus also legitimating a finite cut-off of the phonon number in the numerical evaluation of the rate equation. This fact is also explained by Koch *et al.* (2006b) where for small electron–phonon coupling, the large number of exit states generates a drift towards the low-lying vibrational states, eventually stabilising the system against the heating dynamics caused by the large Franck–Condon factors $M^{q\pm1,q}$, which allow the system to slowly climb the vibrational ladder towards highly excited vibronic states.

Sinks of Probability

These states are the opposite of those discussed before. They have a finite inflow, but $W_{out} = 0$. An example is the state $|1;0\rangle$ in Figure 3.2. In contrast to the sources of probability, these states occur quite frequently. If such a state appears in the dynamics, the solution of the rate equation is $p_j = 1$; ρ is a pure state. Due to $W_{out} = 0$, for all other states $W^j_{in} = 0$, too. And as such, this state does not occur in the rate equation except for its own dynamics. We call such states absorbing, because they absorb probability. If there is more than one absorbing state in a system, the rate equation cannot be solved uniquely. In order to restore uniqueness, a relaxation mechanism or some other form of communication between the states has to be included that provides a small exit rate W_{out}, which serves as a regularisation of the rate equation and restores the uniqueness of the stationary solution. Absorbing states are also called "dark states", because since all probability is locked in them, there cannot be a finite current through the system. As we shall see in the next paragraph, a finite stationary current is always connected to both non-zero probability *and* non-zero exit rates. In the presence of a dark state, no state can fulfil both conditions simultaneously.

The stationary current through a molecular-electronics device in the rate-equation formalism follows from similar considerations: the current is increased by processes that add electrons to the nanostructure, and it is decreased when electrons are extracted from it. For the single-level Anderson–Holstein model, the actual expression[4] is

$$I_\alpha = \sum_{p,q} \left[W^{p\to q}_{0\to1,\alpha} p^p_0 - W^{p\to q}_{1\to0,\alpha} p^p_1 \right], \tag{3.0.2}$$

[4] Although this is just the expectation value of the stationary current, we tacitly drop the angular brackets, since in this thesis, the current will only appear as its expectation value.

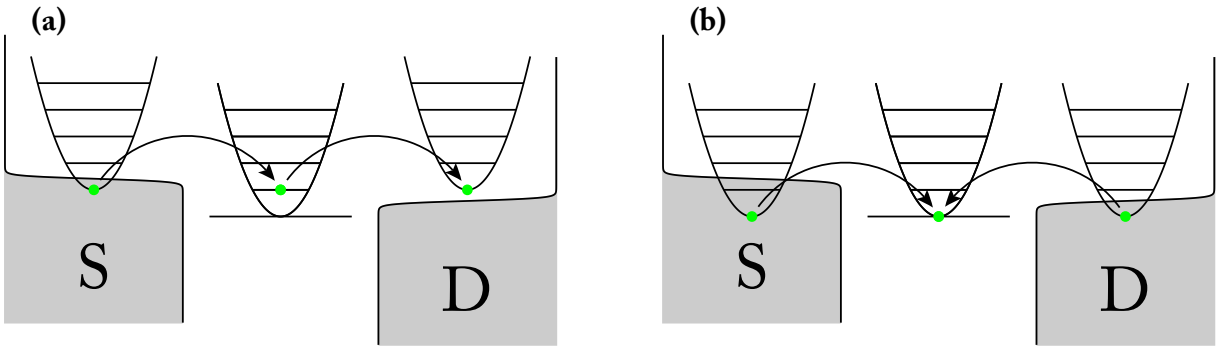

Figure 3.2: Illustration of possible jump processes for a molecule in the Coulomb blockade. We use the common picture showing Fermi functions for the electronic reservoirs L/R, which for the chosen bias voltage act as source (S) and drain (D), respectively, and the single-impurity level of the molecule. The vibronic degrees of freedom is indicated by the parabolic potentials. Since not only the charged but also the neutral molecule has a vibronic quantum number, we keep track of the vibrational state by also drawing the oscillator potential on top of the Fermi levels of the electrodes. The possible tunnelling processes thus are very intuitive to understand by means of conservation of energy. (a) The transition that theoretically could carry a finite current. (b) The transition that locks the electron on the molecule, thus obstructing any finite current.

where the lead-dependent rates $W^{p\to q}_{m\to n,\alpha}$ only take into account tunnelling at electrode α, that is $W^{p\to q}_{m\to n} = \sum_\alpha W^{p\to q}_{m\to n,\alpha}$. Using the rate equation (3.0.1) for the single-level model, one immediately finds

$$I_\mathrm{L} + I_\mathrm{R} = -\sum_q \dot{p}^q_0,$$

which in the stationary state $\dot{p} = 0$ amounts to equal currents through the left and the right tunnel junction and is a manifestation of the Ramo–Shockley theorem (Blanter & Büttiker, 2000, chaps. 3.1 and 5.2).

The computation of the stationary current is a two-step process: first, one has to compute the stationary distribution p_stat, which balances the in- and outflow of probability for every state. One then uses p_stat to compute I_α. While the second step is easy and complies with the electron-hopping picture, the first is not. We consider a trivial example, an Anderson–Holstein molecule inside the Coulomb-blockade, like it is sketched in Figure 3.2. We choose $eV_\mathrm{sd} \geq 2\hbar\omega$ and $eV_\mathrm{g} < -\frac{1}{2}eV_\mathrm{sd}$. The hopping of single electrons could, in principle, go on forever, as the transition $|0;0\rangle \to |1;1\rangle$ is inside the conduction window and not obstructed by the conservation of energy. However, since there is a finite probability to jump into $|1;0\rangle$, which cannot be left at all, the probability for sustaining the current-carrying transition converges to zero as $t \to \infty$.

The stationary distribution of the vibronic excitations is in general not a Gibbs ensemble with respect to the temperature of the reservoirs. The tunnelling dynamics produce vibrational non-equilibrium. Physically, there, however, are many mechanisms that are not part of our model, which cause relaxation and drive the vibronic distribution back to its equilibrium state. We therefore include a phenomenological relaxation term in the rate equation that precisely fulfils this purpose (Koch *et al.*, 2004). The additional term in the equation for $\dot{p}^q_n$ is

$$-\frac{1}{\tau}\left[p^q_n - p^q_\mathrm{eq}\sum_p p^p_n\right], \tag{3.0.3}$$

where p^q_eq is the Gibbs ensemble of the harmonic oscillator $p^q_\mathrm{eq} := Z^{-1}e^{-\beta q\hbar\omega}$ with $Z = \sum_q p^q_\mathrm{eq}$ and β being the inverse temperature of the Fermi-gas electrodes. Such a term drives the non-equilibrium distribution p^q_n

towards the equilibrium ensemble on a typical time scale τ. In contrast to tunnelling, the relaxation term induces transitions *within* a charge manifold. Thus, as relaxation and tunnelling take place in different sectors of the dynamics, they will define two time scales. Their mutual interaction will be shown to determine the precise form of differential conductance peaks in chapter 3.5. However, for the first three of the following sections, we restrict the discussion to the full non-equilibrium dynamics of the rate equation (3.0.1)

3.1 Generic Observations

In contrast to the intrinsic model parameters charging energy, electron–phonon coupling, and tunnel amplitudes, the experimentally accessible quantities are the temperature of the reservoirs, the gate voltage V_g, and the source–drain voltage V_sd. These enter the rate equation through the Fermi factors in the rates $W_{n\to m}^{p\to q}$, which only change significantly when the chemical potential of an electrode matches the energy difference of the transition $|n;p\rangle \mapsto |m;q\rangle$, $\mu_\alpha = \varepsilon_m^q - \varepsilon_n^p$. From the perspective of the vibronic ground state, this means that by sweeping the voltages, a resonance occurs whenever a molecular level passes the Fermi level of one of the leads, which is a picture compatible with the resonant-tunnelling model. Due to the changes in the rates, the stationary distribution and hence also the stationary current through the device will only change at these resonances. The steps in the current–voltage diagram or equivalently the peaks in the differential conductance can thus be mapped onto the spectrum of the system's Hamiltonian H_S. In this sense, the current–voltage diagram given by the rate equation provides a spectroscopy of the free, unperturbed molecule. Computations using S-matrix or many-body techniques come to a similar conclusion. The non-interacting formulation of the famous Meir–Wingreen formula (Wingreen *et al.*, 1989, Equation (37)), which is essentially the Landauer formula, depends on the transmission function, hence the retarded propagator and thus the spectral function of the device. In the weak-coupling limit $\Gamma \to 0$, the spectral function converges to a sequence of δ-functions each localised at the various excitation frequencies of the molecule's vibrational modes. The height of the thus produced steps in the stationary current profile and whether they increase or decrease the current is a result of the complex interplay of Franck–Condon factors, tunnel amplitudes, and the internal dynamics of the system.

In the differential-conductance diagram dI/dV_sd as a function of both source–drain and gate voltage, as shown for example in Figures 3.5 or 3.9, the resonances appear as straight lines marking the change of the involved Fermi functions from zero to one. Given the difference in energy of a resonance by $\Delta\varepsilon$, the equation for such a line is

$$\Delta\varepsilon + eV_\mathrm{g} - \mu_\alpha = \Delta\varepsilon + eV_\mathrm{g} \pm \frac{1}{2}eV_\mathrm{sd} = 0.$$

For an Anderson–Holstein molecule, $\Delta\varepsilon$ is the difference in vibrational energy $\Delta\varepsilon = (p-q)\hbar\omega$, when the resonance is $|0;q\rangle \mapsto |1;p\rangle$.We assume positive bias such that the left electrode acts as source with $\mu_\mathrm{L} = \frac{1}{2}eV_\mathrm{sd}$. The upper sign is due to processes at the drain electrode; the lower sign describes processes at the source electrode. Rewriting the above equation as one for the bias,

$$eV_\mathrm{sd} = \mp 2\big(eV_\mathrm{g} + \Delta\varepsilon\big).$$

Lines with negative slope occur for resonances at the drain electrode, lines with positive slope indicate resonances at the source electrode. This property of the dI/dV diagram is very helpful for the spectroscopic identification of tunnel processes and the reverse engineering of the physical mechanisms that lead to a certain phenomenology. It can also be obtained by a simple gedankenexperiment. Fix the bias voltage at

some value and scan the gate voltage through the conduction window defined by eV_{sd}. The left boundary of the Coulomb-blockade diamond, the one with negative slope, occurs at negative gate voltages and thus corresponds to hitting the Fermi level of the drain electrode with the molecular level. Similarly, the positive-slope line marks the alignment of the molecular level with the source electrode's Fermi edge.

For a rate equation, the stationary solution has to fulfil several conditions. If the $n=0$ or $n=1$ charge sector has zero occupation probability, the stationary current is zero. Consider the current at the source electrode. The forward current is given by the outflow rates of the $n=0$ sector, the backward current by those from the $n=1$ sector. If $\sum_q p_0^q = 0$, the current at the source electrode is only determined by the backscattering contribution from the molecule to the lead. The same argument holds for the current through the drain's tunnel junction, such that there is a net current flowing *from* the molecule to both electrodes and not *through* the device as the relation $I_{\mathrm{L}} = -I_{\mathrm{R}}$ requires for the stationary state. In the same spirit, it is clear that states with a finite rate W_{out} can never acquire unit occupation. The dynamics can never lock the electrons in actually transparent states. In the description of a two-level system by a degenerate master equation, the particles can, however, be locked on the device due to destructive interference of two degenerate wave functions, which each taken individually are transparent.[5] In the rate-equation description, there are situations where due to selection rules and spectral distortions the molecule develops absorbing states, but these require complex molecular Hamiltonians, for example the $E\otimes e$ Jahn–Teller molecule, which we discuss in chapter 3.5.

The decision whether the addition of new tunnelling channels due to a change in bias actually increases the stationary current or not crucially depends on the Franck–Condon factors and thus on the quantum mechanical modelling of the molecule. If the Franck–Condon matrix M^{pq} is well-behaved, that is with a maximum at the elastic vibronic transitions $|q\rangle \to |q\rangle$ and the matrix elements M^{pq} being decreasing for inelastic transitions, that is larger $|p-q|$, the differential conductance at the vibronic resonances will in general be positive. Such behaviour of the Franck–Condon matrix elements can be found for rather small electron–phonon coupling λ, see Figure 3.3 (a) and (b). Under certain circumstances, the addition of a new resonance by increasing the bias can *reduce* the stationary current. We view such behaviour as a signature of non-trivial Franck–Condon factors, where the maximal wave function overlap is for elastic and inelastic transitions with a finite number of oscillator quanta being excited and other elastic or low-energy transitions being suppressed, Figure 3.3 (c). Negative differential conductance essentially means that by adding more channels for tunnelling, the effective through-put of current decreases. The new channel must have certain non-trivial properties, for example having extremely small Franck–Condon matrix elements or being an (almost) absorbing state.

3.2 Franck–Condon Blockade

The structure of the Franck–Condon factors strongly depends on the precise quantum mechanical model of the electron–phonon interaction. The matrix not only shows the parabolic behaviour that moves the maximum from M^{00} for a larger coupling strength. It also shows oscillations, which for example lead to $M^{11} = 0$ for $\lambda = 1$. The behaviour of the Franck–Condon matrix elements becomes more intuitive by only considering the slice M^{q0}. These are the matrix elements of the displacement operator $e^{-\lambda(b^\dagger - b)}$ with respect to the harmonic oscillator ground state. The displacement of the harmonic oscillator ground state generates a coherent state. As it is well-known from the quantum mechanics of the harmonic oscillator,

[5] See chapter 5.3.

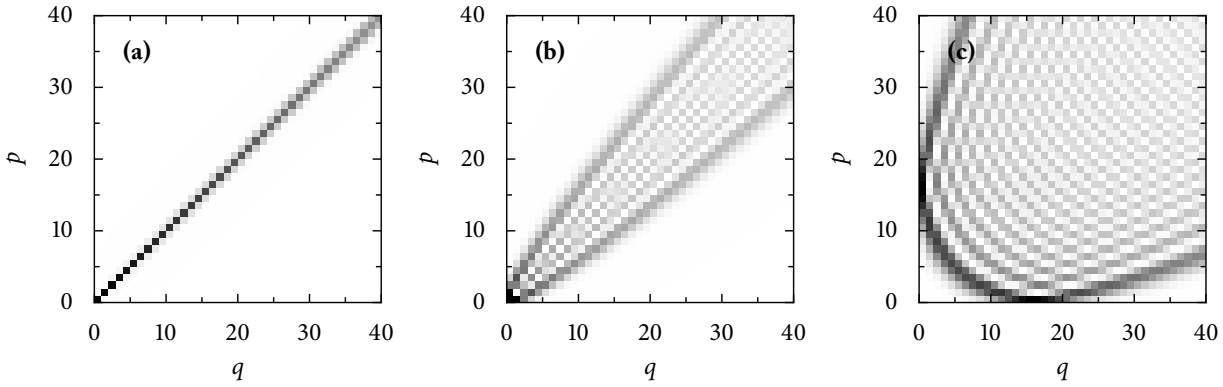

Figure 3.3: Franck–Condon matrices M^{pq} for different values of the electron–phonon coupling λ. Weak coupling $\lambda = 0.1$ (a), intermediate coupling $\lambda = 1$ (b), and strong coupling $\lambda = 4$ (c).. The Franck–Condon factors are normalised to the unit interval for each value of the electron–phonon coupling constant to increase contrast. The colour code is white for zero and black for unity.

the expansion of the coherent state in the undisplaced Fock-state basis is given by the Poisson distribution, and as such

$$M^{q0} = \frac{\lambda^{2q}}{q!} e^{-\lambda^2}.$$

This distribution has the property that for large enough λ, it develops a maximum at non-zero q. A similar property follows for all other slices M^{pq}, see Figure 3.3. The immediate consequence for electronic transport through a molecule with strong electron–phonon coupling is an exponential suppression of the low-lying $q \to p$ transitions. And as such, due to the very small exit rate W_{out} of the $|n;q\rangle$ states with small q at low bias, these states will acquire the largest part of probability, which in turn implies an exponentially suppressed stationary current. The time-dependent dynamics, accessible through a computation of the current–current autocorrelation function or a Monte-Carlo simulation of the electron hopping, shows how the electrons are transported in charge avalanches over the device (Koch & von Oppen, 2005b).

In the Anderson–Holstein model, the Franck–Condon blockade effect is immediately seen in the formal structure of the Franck–Condon matrix. Yet, the blockade effect is generic for general linear electron–phonon couplings, which depending on the type of model can be very complicated and only be solved numerically. Any linear electron–phonon coupling describes a displacement of the equilibrium position of the molecular vibrations. It is the spatial confinement of the low-lying vibronic wave functions by the adiabatic potential and the implementation of the Franck–Condon principle, which demands to treat electronic transitions from one adiabatic potential to another locally in space, which cause an exponential suppression of the overlap integrals of the low-lying vibronic excitations for strongly displaced adiabatic potentials. Regardless of the precise nature of the linear electron–phonon coupling, Franck–Condon blockade physics are a generic effect due to strong coupling. Leturcq *et al.* (2009) demonstrate the Franck–Condon blockade experimentally in suspended carbon nanotubes. As it is shown in this article, the longitudinal stretching mode of the nanotube has a linear electron–phonon coupling of order $\mathcal{O}(1)$, which is the regime in which a Franck–Condon blockade should appear in conductance measurements. In Figure 3.4, we show their experimental data for several Coulomb-blockade diamonds. In addition to the suppression of the stationary current, there is more structure that is caused by the Franck–Condon physics. There is a pronounced asymmetry of the current maximum of each charge resonance with respect to the gate voltage, such that

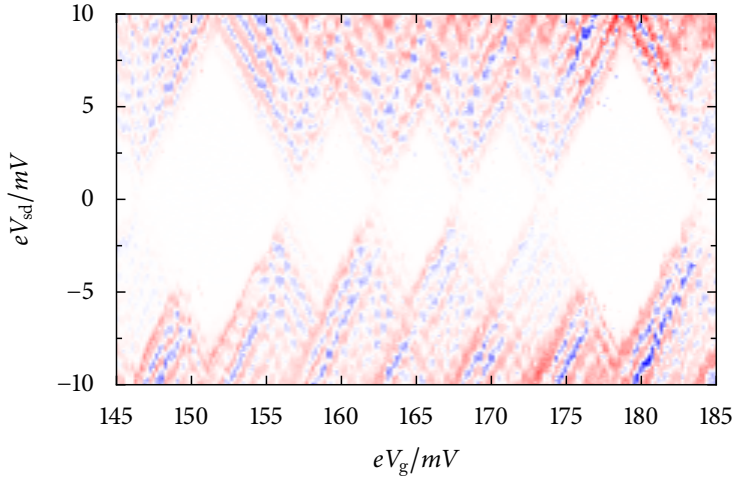

Figure 3.4: Differential conductance measurements of a suspended carbon nanotube quantum dot. The data is courtesy of R. Leturcq and C. Stampfer. The colour code is blue for negative, white for zero, and red for positive differential conductance. The tips of the Coulomb-blockade diamonds do not touch due to the strong electron–phonon coupling, which drives the system into the Franck–Condon blockade. The asymmetry in the tunnel amplitudes causes a shift of the conduction maxima, which appears as a tilt of the diamond. The strong negative-differential conductance peaks parallel to the vibronic sidebands cannot be explained by the rate-equation theory.

the Coulomb diamonds appear to be tilted. This is an immediate consequence of asymmetric coupling of the molecular structure to the electrodes and the exponential suppression of the low-lying Franck–Condon matrix elements. A detailed discussion of this physics is given in the next section. The negative differential conductance peaks in Figure 3.4 are probably the most puzzling phenomenon in the nanotube's conductance properties, because it is difficult to imagine from the electronic hopping picture how negative differential conductances can appear in a single-level rate equation. We shall show in the following that there are indeed structures in the Franck–Condon matrix that can produce negative differential conductance peaks; however, a direct comparison of Figures 3.4 and 3.5 (a) reveals that the Franck–Condon effect as it manifests itself in the rate-equation treatment is not the cause of the experimentally observed structure. Although we cannot fully explain the measured effect in the Franck–Condon blockaded regime, we believe that an extension of the model to include degenerate orbitals like in chapter 5.5, and thus accounting for the complicated electronic structure of carbon nanotubes, is better suited to explain this phenomenology than the single-level rate-equation treatment.

In the following, we stick to the abstract Anderson–Holstein model and discuss the effects due to the generic structure of its Franck–Condon matrix. Besides the Franck–Condon blockade itself, this is the appearance of negative differential conductance peaks in Figure 3.5 (a), which is a result of the complicated interplay of balancing probability flow in the stationary state and the oscillatory structure of the Franck–Condon factors.

We choose the voltages such that the molecular ground state is placed slightly above the Fermi level of the drain electrode. Raising the bias voltage, there is a resonance $|0;0\rangle \to |1;q_0\rangle$ passing the Fermi level of the source electrode and thereby generating a step in the current–voltage characteristics. As it is apparent from Figure 3.5 (b), there is a certain q_0 that results in an, albeit small, *negative* step. Obviously, exactly at this point, the shape of the Franck–Condon matrix has a special form. By inspection of the matrix, we find that due to the parabolic structure of the Franck–Condon matrix and the oscillations inside the parabola, the newly added channel for this particular resonance is characterised by both a very small inelastic matrix element, as it is typical for the Franck–Condon blockade, and a very small elastic factor $M^{q_0 q_0}$. This property is contrary to the behaviour at the resonances before q_0, where although the inelastic rates are still small, the elastic rates are rapidly increasing to values of order unity.

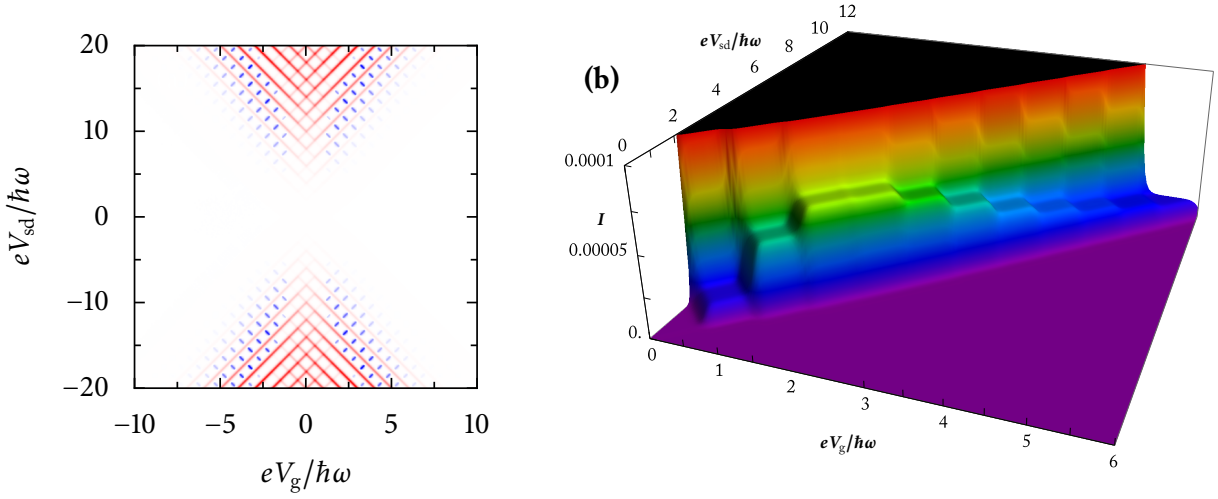

Figure 3.5: Negative differential conductance due to non-trivial Franck–Condon matrix elements. $\lambda = 4$, $k_B T = 0.05\hbar\omega$. (a) Full dI/dV diagram. The colour code is blue for negative, white for zero, and red for positive values. The short blue lines perpendicular to the respective strong vibrational sidebands show negative differential conductance peaks for this model. (b) Zoom into the first vibronic sideband to show that the effect is not restricted to the large-bias regime, where it is most pronounced, but is generic to all vibronic sidebands. The effect also occurs for resonances at the source electrodes, which are discussed in the text. Due to the absence of spin degeneracy, the problem is invariant under changing the sign of the gate voltage by simultaneously exchanging the role of molecule and leads.

We consider a two-state model, whose possible transitions are sketched in Figure 3.6, to show that the addition of channels that are not only weakly coupled to the vibronic ground state but also lacking transparency in the elastic tunnelling process is likely to reduce the transmitted current. In this model, we have introduced the quantity f, reminiscent of a Fermi function, to account for the availability of the resonance at the source electrode, that is $f \in \{0,1\}$. All other resonances are either available or not for either value of f. The effect also occurs for resonances at the drain electrode pictured in Figure 3.5 (b), which, due to the negligence of electronic spin, is obtained from the situation discussed here by exchanging the role of molecule and leads. According to the diagram in Figure 3.6, the matrix representation[6] of this model is

$$\mathcal{L}\rho = \begin{pmatrix} -\Gamma^{10} f - \Gamma^{00} & 0 & \Gamma^{00} & (2-f)\Gamma^{10} \\ 0 & -\Gamma^{11} - 2\Gamma^{10} & 0 & \Gamma^{11} \\ \Gamma^{00} & 2\Gamma^{10} & -\Gamma^{00} & 0 \\ f\Gamma^{10} & \Gamma^{11} & 0 & -(2-f)\Gamma^{10} - \Gamma^{11} \end{pmatrix} \begin{pmatrix} p_0^0 \\ p_0^1 \\ p_1^0 \\ p_1^1 \end{pmatrix}. \tag{3.2.1}$$

The stationary state for the situation before the vibronic resonance is easily computed. Before the resonance, when $f = 0$, it is only the vibronic ground states, which contribute to the dynamics. Due to lack of energy of the tunnelling electrons, the excited vibronic states cannot be populated and are thus emitting states with zero stationary probability. The stationary solution before the resonance is thus $p_0^0 = p_1^1 = \frac{1}{2}$, and the stationary current is $\frac{1}{2}\Gamma^{00}$. If we choose generic values for the rate Γ^{10} and Γ^{11} of the order of Γ^{00}, opening the resonance will increase the stationary current as the additional tunnel channels compensate the loss of

[6] The Golden-Rule rates are $\Gamma^{pq} = \frac{2\pi}{\hbar} \nu M^{pq}$ without the Fermi function. The rates in the rate equation (3.0.1) are $W = f\Gamma$. We only denote the reduced density matrix as a column vector of the diagonal elements, not mentioning any off-diagonal elements, since the master equation we use is only a rate equation.

stationary probability in p_0^0 due to the normalisation $\mathrm{Tr}(\rho) = 1$ more than enough. Consider the simple example of identical rates $\Gamma^{ij} = \Gamma$; the resonance is equivalent to the ground-state transition and also has the same inelastic rate. In this case, the Liouvillian itself is proportional to Γ, and as such the stationary solution of the rate equation (3.2.1) is independent of Γ

$$p_0^0 = \frac{5}{16}, \quad p_0^1 = \frac{1}{16}, \quad p_1^0 = \frac{7}{16}, \quad p_1^1 = \frac{3}{16}.$$

The neutral ground state is less populated than before the resonance, but with the additional inelastic channel the stationary current $I_\mathrm{L} = 2\Gamma p_0^0 + 2\Gamma p_0^1 = \frac{3}{4}\Gamma$ is larger than $I_\mathrm{L}(f=0) = \frac{1}{2}\Gamma$. The addition of such a resonance produces a positive step in the stationary current.

In order to illustrate the effect of a non-trivial Franck–Condon matrix, where the additional resonance has both small inelastic and elastic rate, we consider the extreme case with $\Gamma^{11} = 0$. We set $\Gamma^{00} = 1$ for simplicity. From the diagram in Figure 3.6, it is immediately clear that p_0^1 is an emitting state, hence $p_0^1 = 0$. For $f = 1$, when the additional tunnelling channel is opened and the resonance is contributing to the dynamics, there are two equivalent and independent possibilities for electrons to traverse the nanostructure

$$|0;0\rangle \overset{\Gamma^{00}}{\longmapsto} |1;0\rangle \overset{\Gamma^{00}}{\longmapsto} |0;0\rangle \quad \text{and} \quad |0;0\rangle \overset{\Gamma^{10}}{\longmapsto} |1;1\rangle \overset{\Gamma^{10}}{\longmapsto} |0;0\rangle\,,$$

and hence $p_0^0 = p_1^0$ as well as $p_0^0 = p_1^1$. The stationary solution of the rate equation is thus

$$p_0^0 = \frac{1}{3}, \quad p_0^1 = 0, \quad p_1^0 = \frac{1}{3}, \quad p_1^1 = \frac{1}{3}.$$

The stationary current is $I_\mathrm{L}(f=1) = \frac{1}{3}(1+\Gamma^{10})$, which is larger than $I_\mathrm{L}(f=0) = \frac{1}{2}$, only if $\Gamma^{10} > \frac{1}{2}$. For vanishing elastic rate Γ^{11}, the inelastic rate Γ^{10} has to be at least half the elastic rate Γ^{00} to produce a positive step in the stationary current when the resonance has been made available by an increased bias. If not, the system will show negative differential conductance.

There is one value of the linear electron–phonon coupling λ, which exactly corresponds to the situation $\Gamma^{11} = 0$, namely $\lambda = 1$. In this situation, the Franck–Condon matrix elements are given by the Poisson distribution, which determines the Franck–Condon factors M^{q0} and as such $M^{00} = M^{10} = e^{-1}$. Thus $\Gamma^{10} = \Gamma^{00}$ and, according to the above discussion, the current step has to be positive, which is indeed the observed phenomenology.

In Figure 3.6, we show the numerical solution of the rate equation for arbitrary tunnel rates. We plot the difference $I_\mathrm{L}(f=1) - I_\mathrm{L}(f=0)$ as a function of the ratio of the elastic rates Γ^{11}/Γ^{00}. The different curves correspond to different values of Γ^{00}, and Γ^{10} has been set to unity. The first observation is that no matter what the inelastic rate is, for equal elastic rates, the current step will always be positive. Indeed, even for $\Gamma^{11}/\Gamma^{00} > 1$, negative differential conductance will never be observed. If, however, the ratio is much less than one, the blue curves become negative, which corresponds to the case $\Gamma^{11}, \Gamma^{10} \ll \Gamma^{00}$. The Franck–Condon matrix of the Anderson–Holstein molecule shows oscillations along the diagonal elements for strong electron–phonon couplings. The maximal elastic rate appears for a vibronic excitation $q \approx 4{,}5$. For higher excitations, the elastic rates decrease. As also the inelastic rates are very small in this regime, we encounter the situation discussed exemplary with the two-state model.

In general, the dynamics of the full vibronic system is more complicated than in our two-state model, because also higher-order inelastic transitions $|0;q\rangle \mapsto |1;q+k\rangle$ and their mutual interplay control the

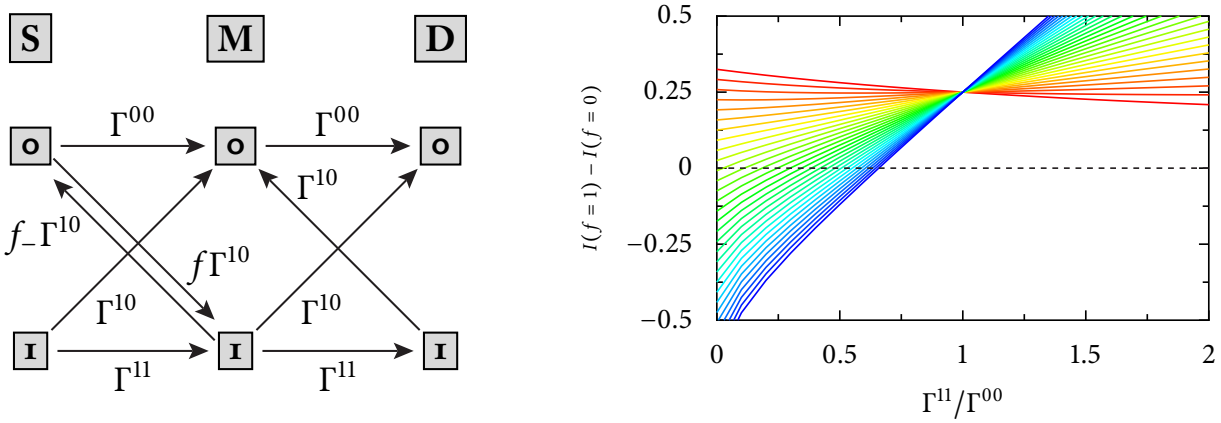

Figure 3.6: Two-state model to illustrate the mechanism that generates negative differential conductance in the rate-equation treatment. Left: The sequential-tunnelling processes between source and drain (S/D) and the molecule M are indicated. The states are resolved with respect to the electrodes. The neutral population is given by the sum of the S and the D contributions. The rate for the process $|0;1\rangle \to |1;0\rangle$ is $(2-f)\Gamma^{10}$, one addend for jumping from the source and one for jumping from the drain electrode onto the molecule. We abbreviate $f_- := 1-f$. Right: The difference of the stationary currents before ($f=0$) and after the resonance ($f=1$). The inelastic rate Γ^{10} is set to unity, and Γ^{00} is scanned between 0.05 (red) and 6 (blue). Negative differential conductance can be observed when both $\Gamma^{11} \ll \Gamma^{00}$ and $\Gamma^{10} \ll \Gamma^{00}$, and hence $\Gamma^{11} \sim \Gamma^{10} \ll \Gamma^{00}$.

stationary dynamics. The elastic rates are, however, generically suppressed and due to the enormous spreading of the Franck–Condon parabola, most of the inelastic rates are also very small. The mechanism we have shown here therefore persists to higher-order transitions, rendering the appearance of negative differential conductance a generic effect of Franck–Condon blockaded single-molecule devices.

3.3 Asymmetry

Besides the intrinsic properties of the molecular device's model itself, also the bare tunnel couplings Γ_α have a significant influence on the qualitative steady-state transport behaviour. Two main effects will be in the focus of our attention: negative differential conductance effects and a shift of the maxima of the differential conductance, best visible in the Franck–Condon blockade regime. The precise value of the coupling of the molecule to the conducting leads is probably the least controllable parameter in the problem. A profound understanding of its effect on the transport characteristics is therefore essential for the application of simple molecular models like the Anderson–Holstein model to experiments.

3.3.1 Negative Differential Conductance

Koch & von Oppen (2005a) report negative differential conductances for asymmetrically coupled devices. The numerical results for the stationary current at zero gate voltage shown in Figure 3.8 show exaggerated steps that, for larger voltages, reduce to a value that is independent of the asymmetry. A numerical simulation with various ratios of Γ_L/Γ_R shows two effects: the height of the exaggerated step is independent of the asymmetry, and the width of the exaggerated current step at each vibrational resonance broadens as the ratio of the couplings increases. Since we already know that it is the Fermi functions in the rates that define the positions of the steps, this effect suggests a competition of the decreasing Fermi function $1-f$ for backscattering the particle from the new resonance into the electrode with the respective tunnel coupling.

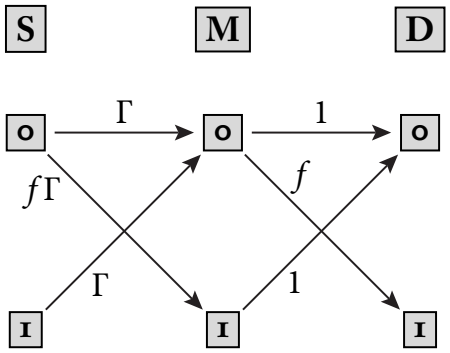

Figure 3.7: Transition rates in the highly asymmetric set-up $\Gamma = \Gamma_L/\Gamma_R \gg 1$ at zero gate voltage. The electron–phonon coupling is assumed to be $\lambda \approx 1$, such that the Franck–Condon matrix element $\Gamma^{11} \approx 0$, which is a condition for observing negative differential conductance due to asymmetric coupling. By setting $\Gamma_R = 1$, we ignore the finite value of the Franck–Condon matrix element M^{00}, which however only rescales the stationary current.

We analyse this effect within a simple two-state model. For simplicity, we assume $M^{11} = 0$, which actually is the case for electron–phonon couplings $\lambda = 1$ and M^{11} being very small for λ close to unity, which is the regime of intermediate electron–phonon coupling. This choice of λ is essential for the effect to occur. In the discussion of the Franck–Condon blockade in the previous section, we have already seen that the generic oscillations of the Franck–Condon matrix elements along the $q' = q$ line have a non-negligible effect on the stationary-state properties of the system. We further set the coupling to the right electrode to unity as well as all other Franck–Condon factors keeping $\Gamma_L/\Gamma_R = \Gamma$ as the only parameter. The rate equation for this model, whose structure is shown in Figure 3.7, is

$$\mathcal{L}\rho = \begin{pmatrix} -\Gamma(1+f) & 0 & 1 & 1+\Gamma(1-f) \\ 0 & -\Gamma-(1-f) & f & 0 \\ \Gamma & \Gamma+(1-f) & -(1+f) & 0 \\ f\Gamma & 0 & 0 & -1-\Gamma(1-f) \end{pmatrix} \begin{pmatrix} p_0^0 \\ p_0^1 \\ p_1^0 \\ p_1^1 \end{pmatrix}$$

In contrast to the model of the previous section, here we consider zero gate voltage such that the additional inelastic resonance is opened for tunnelling both at the source and at the drain electrode. The stationary solution of the rate equation is

$$\rho^{\mathrm{T}} = \left(1, \frac{f\Gamma}{\Gamma + (1-f)}, \Gamma, \frac{f\Gamma}{1 + \Gamma(1-f)}\right) p_0^0$$

The occupation probability of the vibronic ground state p_0^0 is determined by the normalisation condition $\sum_{np} p_n^q = 1$. The stationary current at the resonance, shown in Figure 3.8, is characterised by three regimes.

Before the First Vibronic Resonance

If the first vibronic resonance is not yet part of the dynamics, the system has too little energy to excite oscillator quanta and $f = 0$. The solution of the rate equation in this regime is

$$\rho^{\mathrm{T}} = (1, 0, \Gamma, 0)\, \frac{1}{1+\Gamma}.$$

The stationary current through the left lead becomes $I_L(f=0) = \Gamma p_0^0 = \frac{\Gamma}{1+\Gamma}$, which is the resonant tunnelling result $I = \frac{\Gamma_L \Gamma_R}{\Gamma_L + \Gamma_R}$ with $\Gamma_R = 1$ and $\Gamma_L = \Gamma$. For very large asymmetry, this becomes approximately $I_L(f=0) \approx 1$.

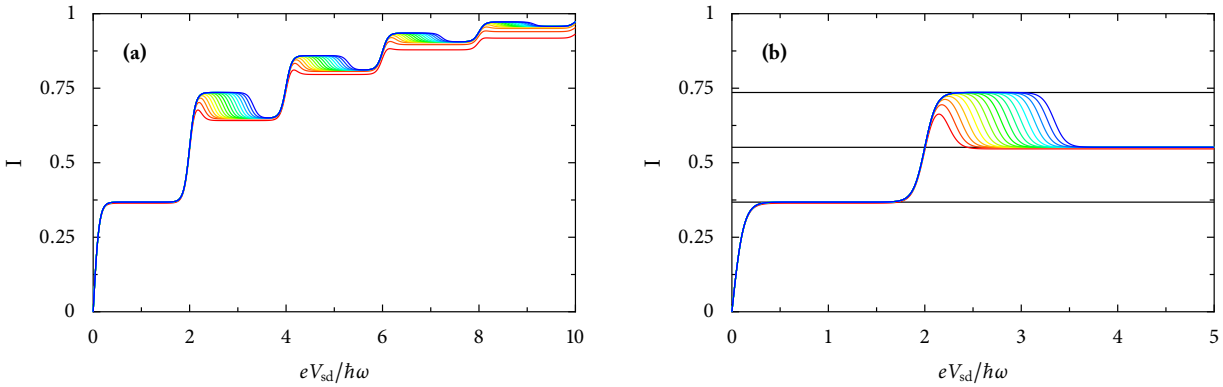

Figure 3.8: Negative differential conductance due to asymmetric coupling to the electrodes for a full molecule (a) and a model system with cut-off at $q=1$ like the one treated exemplary in the text (b). The solid line in graph (b) indicate $I(f=0)$, $\frac{3}{2}I(f=0)$, and $2I(f=0)$. The parameters are $\lambda=1$, $k_BT=0.03\hbar\omega$, and Γ_L is varied from $10\Gamma_R$ (red) to the unphysical value of $10000\Gamma_R$ (blue), which, however, shows the effect discussed in the text.

Far Beyond the First Vibronic Resonance

When the bias voltage is large enough to excite the additional oscillator quantum, there is a region in the current–voltage characteristics, where the effect of the asymmetry is no longer present. In the model this condition is expressed by only setting $f=1$. Here, the solution of the rate equation is

$$\rho^{\mathrm{T}} = (1,1,\Gamma,\Gamma)\,\frac{1}{2(1+\Gamma)}.$$

The stationary current is larger than before the resonance, because the electrons have more tunnel channels at their disposal

$$I_{\mathrm{L}}(f=1) = 2\Gamma p_0^0 + \Gamma p_0^1 = \frac{3}{2}\frac{\Gamma}{1+\Gamma} = \frac{3}{2}I_{\mathrm{L}}(f=0).$$

The Exaggerated Regime

Due to the asymmetric coupling to the electrodes, there is an intermediate, a cross-over regime, where the current is exaggerated with respect to the just discussed regime in which the resonance is fully developed. This cross-over is characterised by already $f=1$ but still $\Gamma(1-f)=\delta>\mathcal{O}(1)$. In this regime, the rate equation is solved by

$$\rho^{\mathrm{T}} = (1,1,\Gamma,\Gamma)\,\frac{\delta}{2+\Gamma\frac{2+\delta}{1+\delta}}.$$

For these parameters, the stationary current acquires a backscattering contribution from the molecule to the lead, which due to $\Gamma(1-f)=\delta$ has a finite rate,

$$I_{\mathrm{L}}(\delta\gg 1) = 2\Gamma p_0^0 + \Gamma p_0^1 - \delta p_1^1 = \left(3-\frac{\delta}{1+\delta}\right)\frac{\Gamma}{2+\Gamma\frac{2+\delta}{1+\delta}}.$$

For the larger part of this regime, we can safely assume $\delta\gg 1$ such that $\frac{\delta}{1+\delta}\approx 1$ as well as $\frac{2+\delta}{1+\delta}\approx 1$, leading to $I_{\mathrm{L}}\approx\frac{2\Gamma}{2+\Gamma}$. For large values of Γ, this current can again be approximated by $I_{\mathrm{L}}\approx 2$, which is independent of

the asymmetry, as it is expected from the numerics. For generic values of Γ, we can compare I_L with the current at the fully established resonance, where no backscattering is present,

$$I_L(\delta \gg 1) - I_L(\delta = 0) = \frac{2\Gamma}{2+\Gamma} - \frac{3}{2}\frac{\Gamma}{1+\Gamma} = C\Gamma(\Gamma - 2),$$

with the common denominator C being a positive number. The difference is positive for $\Gamma > 2$. For most asymmetric couplings, the stationary current in the intermediate regime, where there is a significant backscattering from the molecule to the strongly coupled electrode, is larger than the one in the fully developed first vibronic sideband. Moreover, the actual value of the current only slightly depends on the backscattering rate, rendering the current profile in this regime the saturated plateau shown in Figure 3.8.

3.3.2 Asymmetry of the Differential Conductance Diagram

Besides the observation of negative differential conductance, another generic effect of asymmetric coupling in the sequential-tunnelling regime is the shift of the region of maximal current in the current–voltage diagram. The such induced asymmetry in the diagram itself generates the impression of a tilted diagram, particularly in the Franck–Condon blockade regime, where the Coulomb diamonds do not touch. This effect has recently been observed in experiments on suspended carbon nanotubes (Leturcq *et al.*, 2009). In Figure 3.9, we show the numerical evaluation of the rate equation for the Anderson–Holstein molecule in the Franck–Condon blockade regime, $\lambda = 3.3$, with symmetric coupling $\Gamma_L = \Gamma_R$ (a) and with asymmetric couplings $\Gamma_L = 100\Gamma_R$ (b). The symmetry of the current–voltage diagram with respect to the gate voltage is broken: the graph appears to be tilted.

The balance condition in steady-state helps to understand the long-time behaviour of the reduced density matrix, from which the stationary current is computed easily. The Franck–Condon blockade regime is helpful insofar as due to the exponential suppression of the low-lying vibrational excitations, the exit rates of these states are small compared with the ones of highly-excited vibronic states. With the reasoning of the introduction to this chapter we infer that only the states close to the vibronic ground state can acquire significant occupation probability and thus only these have to be considered in the calculation of the stationary current. The numerical results of Figures 3.9 (c) and (d) corroborate this reasoning. We analyse the system's properties by slicing the current–voltage diagram at a source–drain voltage of about $eV_{sd} = 10\hbar\omega$ and only changing the gate voltage from either side of the Coulomb-blockade diamond through the conduction window. The energetic situation in the three extreme cases, alignment of the vibronic ground state at either Fermi edge or symmetrically in-between, is pictured in Figure 3.10. We first discuss the symmetric-coupling case and explicate the differences due to asymmetric coupling.

If the vibronic ground state of the molecule is aligned close to the Fermi level of the drain electrode like in Figure 3.10 (a), the only transition allowed from $|1;0\rangle$ is the elastic one into $|0;0\rangle$. Due to the Franck–Condon blockade, its rate is exponentially suppressed. The neutral state, on the contrary, has a much higher exit rate. The source–drain voltage has been chosen so large that those states for which the Franck–Condon matrix elements M^{q0} are finite are inside the conduction window. Thus the exit rate of $|0;0\rangle$ is at least $\max\{\Gamma^{q0} | q \in \mathbb{N}\}$, which is of order unity. With the balance condition for the stationary state, we conclude that almost all of the probability will be stored in the almost absorbing state $|1;0\rangle$, such that the stationary current is determined by the Franck–Condon factor for the transition $|1;0\rangle \mapsto |0;0\rangle$ to the drain electrode. In the opposite case, the vibronic ground state being slightly below the Fermi edge of the source electrode, Figure 3.10 (c), the roles of the charged and neutral state are exchanged. The Franck–Condon

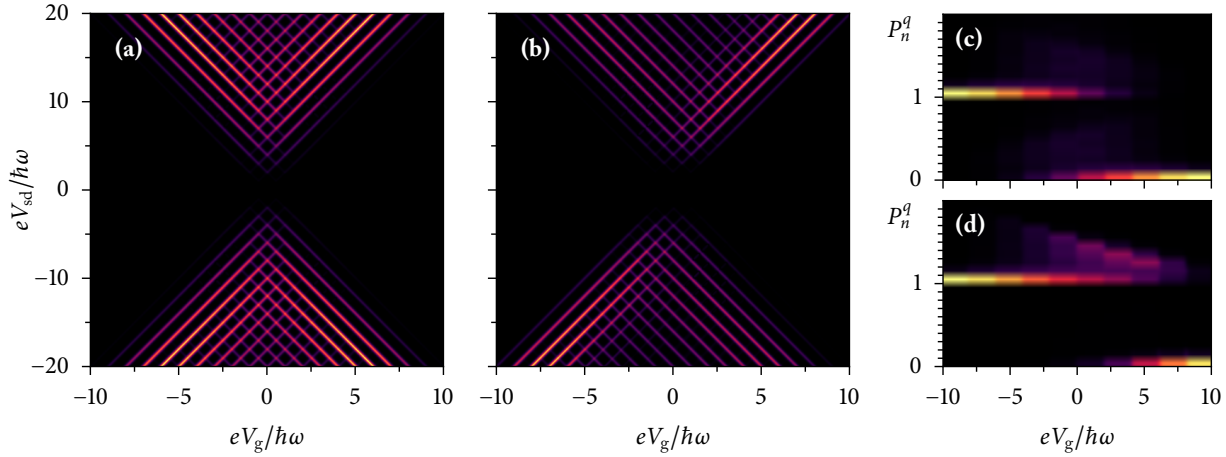

Figure 3.9: Asymmetry of the dI/dV due to asymmetric coupling to the electrodes. The parameters are $k_BT = 0.05\hbar\omega$, $\lambda = 3.3$. The symmetric configuration $\Gamma_L = \Gamma_R$ is shown in (a) for the differential conductance and in (c) for the stationary population as a function of the gate voltage, when $eV_{sd} = 10\hbar\omega$ is held fixed. The same diagrams for asymmetric coupling $\Gamma_L = 100\Gamma_R$ are shown in (b) and (d).

suppressed rates affect the transition $|0;0\rangle \mapsto |1;0\rangle$, leaving the *neutral* state with an exponentially suppressed exit rate. The charged state, on the contrary, can be left by exciting many vibronic states on the molecule by an electron tunnelling to the drain electrode. By the same reasoning as before, in this situation, almost all of the occupation probability will be stored in the neutral state $|0;0\rangle$, and the stationary current, this time evaluated as I_L, is again small. The only situation, where there is significant population both in the charged and in the neutral state, is for a symmetric alignment of the level between the two Fermi edges, Figure 3.10 (b). There, the exit rate from $|0;0\rangle$ equals that of $|1;0\rangle$, and we expect maximal current through the device, symmetrically decreasing for a change of the gate voltage in either direction.

By introducing an asymmetry in the tunnel amplitudes, the above argument is modified. Assume that it is the coupling to the source electrode, which is greater. Then the point of maximal current, being the one for which both rates onto and off the molecule are approximately equal, is shifted to higher gate voltage, Figures 3.9 (c) and (d). The reduced number of accessible vibronic states for tunnelling from the source electrode compensates the larger bare coupling. The argument can be repeated for any value of the source–drain voltage, finally yielding the tilted form of the current–voltage diagram in Figure 3.9 (b).

3.4 Strong Relaxation

All of the phenomenology of rate equations presented so far is intrinsically vibrational non-equilibrium physics. It is a result of the ideal model of the nanostructure being only coupled to the fermionic reservoirs. For a more realistic description of quantum transport through single-molecule devices, other effects due to a non-ideal environment have to be modelled. In the introduction to this chapter, we have set-up the phenomenological mechanism (3.0.3) for incorporating thermal equilibration of the vibrational distribution into the rate-equation formalism. In this section, we sketch how in the regime of strong relaxation, which corresponds to very small τ, the stationary current profile can be calculated and by comparison with experiments can be used to extract an estimate for the linear electron–phonon coupling constant from the data (Leturcq *et al.*, 2009).

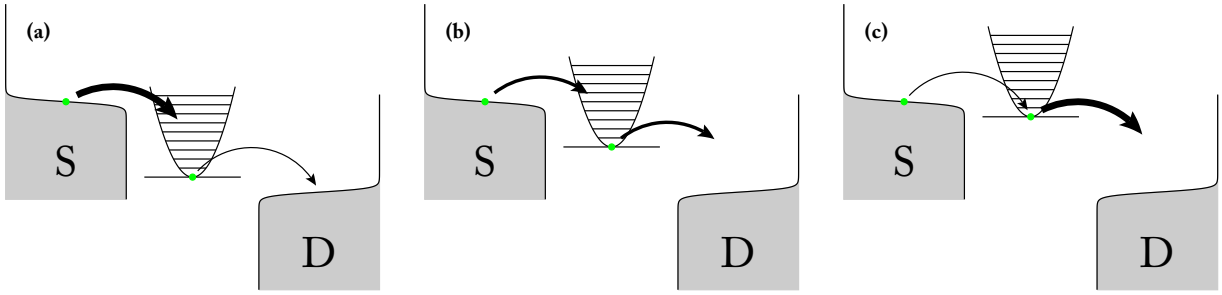

Figure 3.10: Energetic situation for the three stages encountered by sweeping the gate voltage of a single-molecule junction in the Franck–Condon blockade: (a) Ground state close to the drain electrode. Due to the large number of oscillator quanta that can be excited, the rate for populating the molecule from the source electrode is large, whereas due to the exponentially suppressed Franck–Condon factors, the rate for leaving the vibronic ground state towards the drain electrode is very small. (b) Ground state symmetrically placed in the conduction window. The rates for tunnelling onto and off the molecule are approximately equal as due to the rather large number of oscillator levels inside the conduction window, the Franck–Condon blockade is overcome for either tunnelling process. (c) Ground state close to the source electrode. This is the same situation like in (a) just with the rates at the tunnel junctions being interchanged.

The general formula for the stationary current through the tunnel junction at electrode α of a single-molecule junction is

$$I_\alpha = \sum_{qp} W^{p\to q}_{0\to 1;\alpha} p^p_0 - \sum_{qp} W^{q\to p}_{1\to 0;\alpha} p^q_1.$$

If the stationary density matrix is sufficiently strongly localised in the low-energy states or the bias voltage is large enough such that for the current I_S through the source electrode, the backscattering contribution of p^q_1 is negligible, the formula becomes a function of p^p_0 alone

$$I_S = \Gamma_S \sum_{qp} M^{qp} f\big((q-p)\hbar\omega + eV_g - \frac{1}{2}eV_{sd}\big) p^p_0.$$

This expression can be evaluated by hands, when both the Franck–Condon matrix elements M^{qp} and the form of the stationary density matrix, the distribution of the vibronic occupations, are known. Most often, especially for strong electron–phonon coupling, the vibrational distribution function cannot be accessed analytically, because this effect is a genuine non-equilibrium dynamics.

For very strong vibronic relaxation, $\tau \to 0$, the rate equation[7] $\dot\rho = \big(\mathcal{L}_T + \frac{1}{\tau}\mathcal{L}_R\big)\rho$ is dominated by the relaxation term $\mathcal{L}_R$, the dissipation due to tunnelling $\mathcal{L}_T$ being a small perturbation and thus almost negligible. Then p^q_n assumes a thermal equilibrium distribution with respect to the vibronic excitations. For small temperatures $k_B T \ll \hbar\omega$, we effectively have $p^q_n = p^0_n \delta_{0,q}$, and

$$p^0_0 = \frac{\Gamma_D}{\Gamma_D + \Gamma_S}.$$

In this case, the stationary current for zero gate voltage, close to a certain resonance, $|0;0\rangle \mapsto |1;q'\rangle$, say, is

$$I_S = \Gamma_S \sum_{q<q'} M^{q0} p^0_0 + \Gamma_S f_S M^{q'0} p^0_0,$$

[7] This is a symbolic notation of the rate equation in terms of Liouville operators $\mathcal{L}$.

because we can safely assume $f\big((q-p)\hbar\omega - \frac{1}{2}eV_{\mathrm{sd}}\big) = 1$ for $p = 0$ and $q < q'$. The Fermi function for the resonance $|0;0\rangle \mapsto |1;q'\rangle$ is abbreviated by f_{S}. Its derivative with respect to the source–drain voltage is

$$\frac{d}{d(eV_{\mathrm{sd}})} f_{\mathrm{S}} = \frac{1}{2k_{\mathrm{B}}T} f_{\mathrm{S}}(1 - f_{\mathrm{S}})$$

and as such, since directly at the resonance $f_{\mathrm{S}}(eV_{\mathrm{sd}} = 2q'\hbar\omega) = \frac{1}{2}$,

$$\frac{dI}{d(eV_{\mathrm{sd}})}(eV_{\mathrm{sd}} = 2q'\hbar\omega) = \Gamma_{\mathrm{S}} P_0^0 M^{q'0} \frac{d}{d(eV_{\mathrm{sd}})} f_{\mathrm{S}} = \frac{\Gamma_{\mathrm{S}}\Gamma_{\mathrm{D}}}{\Gamma_{\mathrm{S}} + \Gamma_{\mathrm{D}}} M^{q'0} \frac{f_{\mathrm{S}}(1 - f_{\mathrm{S}})}{2k_{\mathrm{B}}T} = \frac{1}{8k_{\mathrm{B}}T} \frac{\Gamma_{\mathrm{S}}\Gamma_{\mathrm{D}}}{\Gamma_{\mathrm{S}} + \Gamma_{\mathrm{D}}} M^{q'0}.$$

Apart from system parameters like temperature and tunnel couplings, the differential conductance at the q'th resonance is proportional to the Franck–Condon matrix element of the inelastic transition $|0;0\rangle \mapsto |1;q'\rangle$. This number is the Poisson distribution, which we have discussed in connection with the Franck–Condon blockade in section 3.2. In Figure 3.11, we show the differential conductance for zero gate voltage and various values of the electron–phonon coupling λ, as well as the Poisson distribution that fits the peaks heights.

One thing is striking, when we compare the numerical plots with the Poisson distribution, namely the height of the resonant tunnelling peak $|0;0\rangle \mapsto |1;0\rangle$. This peak is higher than it ought to be according to the above reasoning: for equal and unit coupling $\Gamma_{\mathrm{S}} = \Gamma_{\mathrm{D}} = 1$, like in Figure 3.11, it is actually twice as high. At zero bias $eV_{\mathrm{sd}} = 0$, we also have to include the backscattering contribution due to p_1^0 in the stationary current. Then

$$I_{\mathrm{S}} = \Gamma_{\mathrm{S}} M^{00} \left(f_{\mathrm{S}} p_0^0 - (1 - f_{\mathrm{S}}) p_1^0 \right) = \Gamma_{\mathrm{S}} M^{00} (f_{\mathrm{S}} - p_0^1).$$

The differential conductance at zero bias is therefore

$$\frac{dI_{\mathrm{S}}}{d(eV_{\mathrm{sd}})}(eV_{\mathrm{sd}} = 0) = \Gamma_{\mathrm{S}} M^{00} \frac{d}{d(eV_{\mathrm{sd}})} f_{\mathrm{S}} = \frac{1}{8k_{\mathrm{B}}T} \Gamma_{\mathrm{S}} M^{00}.$$

The resonant tunnelling peak is scaled by a factor $1/p_0^0 = \frac{\Gamma_{\mathrm{D}} + \Gamma_{\mathrm{S}}}{\Gamma_{\mathrm{D}}}$ compared to what we expect from the discussion of the inelastic peaks. For equal and unit coupling to the leads, like in Figure 3.11, this factor is just 2.

The distribution of the differential conductance peaks according to a Poisson distribution has been successfully measured experimentally for suspended carbon nanotubes by Leturcq *et al.* (2009) and used for an estimate of the actual value of λ. The agreement with the experiment shows that not only the Franck–Condon blockade is an observable phenomenon in quantum transport through single-molecules, but also supports the applicability and the use of the Anderson–Holstein model, which causes the actual form of the Franck–Condon matrix elements.

3.5 The $E \otimes e$ Jahn–Teller Effect

As a conclusion to this chapter, we discuss a model in which relaxation effects as well as selection rules and spectral distortions characterise the current–voltage diagram. The model gives some insight into the transport properties of more complex molecules and serves as an application of the previously discussed techniques. The material covered in section has been published in Schultz *et al.* (2008).

We consider a molecular Hamiltonian with two degenerate electronic levels, labelled by a pseudo-spin σ being linearly coupled to two degenerate vibronic modes with coordinates Q_θ and Q_ε. We assume that these

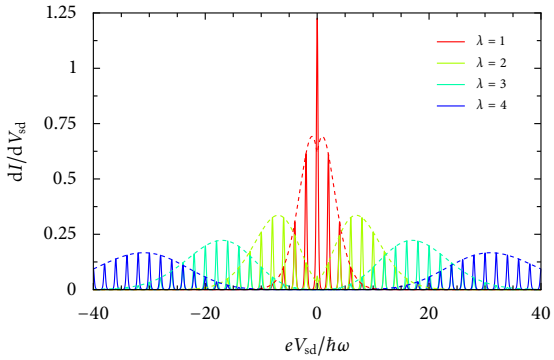

Figure 3.11: Differential conductance for various values of the electron–phonon coupling λ. The parameters are $eV_g = 0$, $\tau = 10^{-5}\tau_0$, $k_B T = 0.05\hbar\omega$, and $\Gamma_L = \Gamma_R = 1$. The time scale defined by the tunnelling Hamiltonian is $\tau_0^{-1} = \frac{2\pi}{h}\nu$. The peaks are fitted with a scaled Poisson distribution as an envelope (dashed). Due to a backscattering contribution, the zero-bias peak is twice as high as expected from the fit.

degeneracies derive from geometric symmetries of the molecule and that the electron–phonon interaction respects this symmetry as well. As Jahn & Teller (1937) show, such molecules are geometrically unstable. The energetic ground state is a non-symmetric conformation of the molecular frame and appears to be distorted. This effect, the Jahn–Teller effect, is due to a type of electron–phonon interaction, whose complexity and phenomenological richness goes beyond the simple Anderson–Holstein model. In principle it can also be extended to quadratic or higher order in the normal-mode coordinates. In appendix D, we discuss details of the Jahn–Teller effect in general. For the model treated in this section, whose quantum-mechanics we discuss in appendix E, we assume that in the neutral state, there is no electron–phonon coupling and the vibrational physics are that of an isotropic two-dimensional harmonic oscillator. In the singly-charged configuration, however, we model the molecule to be Jahn–Teller active, featuring an electron–phonon coupling of the respective type. Jahn–Teller effects are commonly classified according to the degeneracy of the interacting electronic and vibronic degrees of freedom. The group-theoretical symbols explained in the appendix denote a double degeneracy by E; non-degenerate modes are denoted A or B. To avoid confusion, one labels the electronic degeneracy with capital letters, E, and the vibronic degeneracy with lower-case letters, e. A particular Jahn–Teller effect is then denoted as the tensor product of both spaces. The model we have defined so far is thus of $E\otimes e$-type. Typical examples of molecular geometries that show this type of Jahn–Teller effect are triangular, tetrahedral, and octahedral molecules. Bersuker (2006) discusses real-world examples of such molecules, their physics, and their chemistry. For an octahedral complex, a central atom surrounded by an octahedron of six ligands, the double degeneracy can be traced back to the crystal-field splitting of the five-fold degenerate d-orbitals of the central atom into a three-fold degenerate sector—denoted by T—and an energetically lower-lying two-fold degenerate sector, which is the E sector we are considering here (Ludwig & Falter, 1988, chap. 8.3). In Bersuker's formulation, the Hamiltonian of the linear $E\otimes e$ Jahn–Teller effect is

$$H_{E\otimes e} = eV_g n_d + \frac{1}{2}(P_\theta^2 + \omega^2 Q_\theta^2) + \frac{1}{2}(P_\varepsilon^2 + \omega^2 Q_\varepsilon^2) + \lambda\frac{\hbar\omega}{\ell_0}\left(Q_\theta\sigma_x + Q_\varepsilon\sigma_y\right) n_d, \tag{3.5.1}$$

where the Pauli matrices σ_i operate in the electronic Hilbert space; scalars are to be understood as being multiplied with the identity matrix in this space. Although the model has degenerate electronic orbitals, we describe its transport properties using rate equations. This has several reasons. First, although they cannot grasp the full physics due to the degenerate eigenspaces of the system's Hamiltonian, rate equations do, however, model the physics *between* energy manifolds. It is the purpose of this example to show how selection rules and spectral distortions influence the transport characteristics. We shall show in the following

section that the observed effects are independent of the chosen basis of the degenerate subspace, which renders the rate-equation description a good approximation of this dynamics. Second, we assume infinite charging energy $U \to \infty$. As we shall show in chapter 5, effects due to the coherent interaction of the degenerate levels are most pronounced for finite and non-zero U. Infinite U drives the phenomenology towards the one observed in the rate-equation setting. Third, as we finally prove in chapter 6, the rate-equation description for degenerate systems has a well-defined physical meaning as the correct theory for levels whose energy difference Ω is large compared to the tunnelling-induced broadening Γ but small compared to $k_B T$. Since placing a symmetric molecule inside a tunnel junction will always have some effect on the degenerate level structure, the degenerate rate-equation description can serve to account also for these effects.

3.5.1 Berry Phase and Selection Rule

Since its adiabatic potential, which is invariant under rotations in the $(Q_\theta, Q_\varepsilon)$-plane, the two-dimensional isotropic harmonic oscillator has a conserved integer angular-momentum quantum number that is defined by the displacement of the degenerate oscillations θ and ε

$$L_z := \frac{1}{\hbar}\left(Q_\theta P_\varepsilon - Q_\varepsilon P_\theta\right).$$

Due to the presence of an electron–phonon coupling, it is the total angular momentum,

$$J := L_z + \frac{1}{2}\sigma_z,$$

which is conserved in the $E\otimes e$ Jahn–Teller effect. There are two arguments to prove this, an algebraic one and one that utilises the conical intersection of the adiabatic potentials sketched in Figure D.1 in the appendix. Given the fundamental commutators for Pauli matrices, $[\sigma_i, \sigma_j] = 2\imath \sum_k \varepsilon_{ijk}\sigma_k$ and those for coordinates and momenta $[Q_i, P_j] = \imath\hbar\delta_{ij}$, we can evaluate the commutator of J with the $E\otimes e$ Hamiltonian. The only relevant terms come from the electron–phonon coupling:

$$\begin{aligned} [Q_\theta\sigma_x, L_z] &= \imath Q_\varepsilon \sigma_x, & [Q_\varepsilon\sigma_y, L_z] &= \imath Q_\theta \sigma_y, \\ [Q_\theta\sigma_x, \frac{1}{2}\sigma_z] &= -\imath Q_\theta \sigma_y, & [Q_\varepsilon\sigma_y, \frac{1}{2}\sigma_z] &= -\imath Q_\varepsilon \sigma_x. \end{aligned}$$

And thus $[Q_\theta\sigma_x + Q_\varepsilon\sigma_y, J] = 0$, and the eigenvalues of J are good quantum numbers.

If we diagonalise the electron–phonon interaction in the electronic Hilbert space, we obtain a potential energy surface in the adiabatic basis. When we use polar coordinates (r, φ) in the space spanned by the displacements Q_θ and Q_ε such that $Q_\theta = r\cos\varphi$ and $Q_\varepsilon = r\sin\varphi$, this transformation is for the $E\otimes e$ Jahn–Teller Hamiltonian (Bersuker & Polinger, 1989, chap. 3.1.1)

$$S = \frac{1}{\sqrt{2}}\begin{pmatrix} e^{-\imath\varphi/2} & e^{-\imath\varphi/2} \\ e^{\imath\varphi/2} & -e^{\imath\varphi/2} \end{pmatrix}.$$

The diagonal basis of the potential energy obtained by this transformation is a mixture of electronic and vibrational degrees of freedom as the polar angle of the degenerate vibronic Hilbert space appears explicitly. The thus computed potential energy surface is the well-known mexican-hat potential, a graphical illustration

of which is shown in Figure D.1 in the appendix,

$$U_{E\otimes e} = \frac{1}{2}\omega^2 r^2 + \lambda\frac{\hbar\omega}{\ell_0} r\sigma_z.$$

In the transformed vibronic coordinates, this potential is also $U(1)$-symmetric, and the angular wave function ought to have the form

$$\psi \sim e^{\imath j\varphi}.$$

Due to the conical intersection at the origin, the potential has an intrinsic geometric phase that determines the properties of the angular momentum j. Berry (1984) has introduced the concept of geometric phases in contrast to the dynamical phase $e^{-\imath/\hbar Et}$ of quantum mechanics. He shows that for certain potentials, a system that is adiabatically transported around a closed path in its parameter space acquires an additional phase that strongly depends on the path. This dependence is only on the homotopy class of the path. The phase is invariant under homeomorphisms, that is smooth deformations of the path. It is a topological property of the adiabatic potential. The probably best-known example of a geometric phase is the Aharonov–Bohm effect, where the geometric phase is caused by a magnetic flux and experimentally visible in an interference pattern. Mead (1992) and Yarkony (1996) extensively review the role of both geometric phases and conical intersections in molecular physics. They remark that despite their abstract formulation these concepts are important for the quantum mechanics of molecules as they involve and result from the symmetry properties of the problem. Berry (1984) explicitly computes the geometric phase for the mexican-hat potential, the electron–phonon coupling of the linear $E\otimes e$ Jahn–Teller problem. The phase has the value π if the path encloses the point of degeneracy and zero else. This means that the irreducible representations of the symmetry group of the mexican-hat potential, which actually rotate the potential or, equivalently, transport the system around the degeneracy, also add the geometric phase to the wave function. And as such, to restore invariance under the symmetry group, the total angular momentum has to be *half integer*: $|j| \in \frac{1}{2}(2\mathbb{N}+1)$.

If there was no Berry phase in the system and the conserved angular-momentum quantum number in the Jahn–Teller active state was an integer, the sequential-tunnelling dynamics would also conserve the angular momentum. The tunnelling would factorise with respect to the angular motion and split into several non-interacting angular-momentum sectors, which would have their individual tunnelling dynamics. Tunnelling could only change the radial excitation of the wave function and the only relevant physical effect would be the distortion of the harmonic oscillator spectrum. Besides the problem of a non-unique stationary solution of the master equation, the model would behave like a parallel array of Anderson–Holstein models with distorted oscillator spectra. But in the $E\otimes e$ Jahn–Teller Hamiltonian there is a Berry phase, which due to the half-integer angular momentum couples the individual angular sectors of the eigenfunctions and thus yields non-trivial transport properties of the single-molecule junction. Any eigenstate of the linear $E\otimes e$ Hamiltonian can be expanded in terms of an electronic wave function and the eigenstates of the two-dimensional harmonic oscillator in polar coordinates, which are discussed in detail in appendix E.1 (Longuet-Higgins *et al.*, 1958)

$$|1; j, n\rangle = \sum_{n'}\left[A^{jn}_{n'}\,|+\rangle\,|j-\frac{1}{2}, n'\rangle + B^{jn}_{n'}\,|-\rangle\,|j+\frac{1}{2}, n'\rangle\right].$$

We keep the expansion coefficients $A^{jn}_{n'}$ and $B^{jn}_{n'}$ as symbols without further specification. As it is shown in appendix E, the matrix elements $\langle 0; m, n'|H_{\mathrm{T}}|1; j, n\rangle$ of the tunnel Hamiltonian H_{T} vanish unless the

angular momenta of the neutral and the charged state satisfy the selection rule

$$j = m \pm \frac{1}{2}.$$

The implications of this selection rule are two-fold. First, it causes many zeros in the Franck–Condon matrix and thereby drastically reduces the complexity of the tunnelling dynamics. And second, in contrast to the factorised tunnelling dynamics sketched above for the case of zero Berry phase, the angular momentum sectors of the linear $E\otimes e$ Jahn–Teller molecule are connected and thus allowing for transitions

$$|0;m\rangle \mapsto |1;m\pm\frac{1}{2}\rangle \mapsto \left\{\begin{array}{c}|0;m\rangle\\|0;m\pm1\rangle\end{array}\right\} \mapsto \dots$$

By the tunnelling-induced change of the angular momentum of the oscillator dynamics, there can be a step-by-step advancing in angular momentum space. Koch *et al.* (2006b) find a similar phenomenon for Anderson–Holstein systems with a single harmonic oscillator in the limit of very small electron–phonon coupling. For small λ, the polaron transformation—the displacement operator—is approximated

$$e^{-\lambda(b^\dagger - b)} \approx 1 - \lambda(b^\dagger - b),$$

such that the predominant inelastic sequential tunnel events are

$$|0;q\rangle \mapsto \left\{\begin{array}{c}|1;q\rangle\\|1;q\pm1\rangle\end{array}\right\} \mapsto \left\{\begin{array}{c}|0;q\rangle\\|0;q\pm1\rangle\\|0;q\pm2\rangle\end{array}\right\} \mapsto \dots$$

This slow advancing yields a highly non-equilibrium vibrational distribution, which is eventually stabilised by relaxation processes.

In the linear $E\otimes e$ Jahn–Teller problem, the selection rule is exact, meaning that forbidden transitions have zero probability and can only be observed if some other mechanism such as vibrational relaxation interferes with the selection rule. We shall show in the course of this discussion that such treatment is absolutely necessary to render the stationary solution of the rate equation for the transport problem unique and obtain a well-defined current–voltage profile.

3.5.2 Current Blockade

In the previous section, we have introduced and derived a selection rule for sequential-tunnelling transitions in the angular-momentum quantum number. As it is shown in appendix E.2, the charged system is spectrally distorted: the radial excitation spectrum is not equidistant. In Figure 3.13 we show the eigenvalues of both charge states ordered by their respective (half-)integer angular momentum. The reduction of the energy in the Jahn–Teller active state with respect to the harmonic oscillator energy grows with angular momentum. Figure E.1 shows the eigenvalues of the $E\otimes e$ Jahn–Teller Hamiltonian plotted against the electron–phonon coupling: the radial ground states of higher lying angular-momentum eigenstates experience a much faster fall-off than the states with small j. This property of the Jahn–Teller spectrum leads to an isolation of radial ground states with large j in the tunnelling dynamics for certain well-chosen voltages. In Figure 3.14, we have chosen such voltages and shifted the spectra accordingly such that the transitions in the master

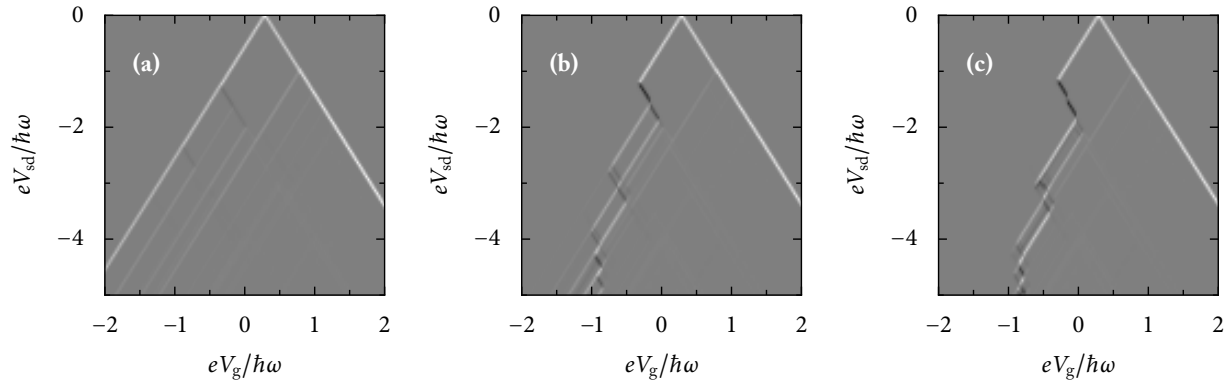

Figure 3.12: Differential conductance of the $E\otimes e$ Jahn–Teller molecule with intermediate electron–phonon coupling $\lambda = 1$ and strong Coulomb-blockade $U \to \infty$, such that only single occupancy of the molecule is possible. The parameters are $k_B T = 0.01\hbar\omega$, equal coupling Γ_0 of the electronic levels to the electrodes, and relaxation times (a) $\tau = 10\,\tau_0$, (b) $\tau = 10^5\,\tau_0$, and (c) $\tau = 10^6\,\tau_0$, where $\tau_0 = 1/\Gamma_0$. The colour code is black for negative, grey for zero, and white for positive values. The numerics show a strong current blockade for negative gate voltage only and a step-like pattern of positive and negative differential conductance peaks.

equation can only proceed from diamonds (charged state) to lower-lying circles (neutral states), which accounts for the conservation of energy, and only to adjacent columns, which implements the selection rule.

Given the parameters of the figure, we see that all states $|1;j,0\rangle$ with $|j| \geq \frac{3}{2}$ are isolated. Once they are occupied, there is no allowed transition to a neutral state, and hence no possibility for uncharging the molecule. Transitions to neutral states that are allowed by energy conservation, for example $|1;\frac{5}{2},0\rangle \mapsto |0;0,0\rangle$ are forbidden by the selection rule. And those that are accessible by the selection rule have too high energy due to the spectral distortion of the Jahn–Teller effect. In this situation the electron is locked on the device and, due to the infinite charging energy, no current can flow through the molecule. The particular states $|1;j,0\rangle$ for larger j are absorbing states and hence are dark and non-conducting states. In contrast to the already explained theory, there is not just one absorbing state but a large, actually an infinite number of them. Without further alterations of the model, this would lead to non-unique stationary states of the equation. We therefore have to include the phenomenological relaxation mechanism (3.0.3) that, accounting for higher-order tunnel processes or relaxation of the vibronic configuration towards thermal equilibrium, breaks the selection rule slightly. Besides ensuring a unique solution of the stationary rate equation, such mechanisms define a second time scale, whose effects on the transport properties will be discussed in section 3.5.3.

Any relaxation mechanism will ultimately drive the system to the lowest energy state, the ground state. Whenever one of the absorbing states can be reached by a tunnel cascade from $|0;0,0\rangle$, there is a finite probability of locking the system in that absorbing state for very long time. The stationary current through the device will be strongly suppressed in these regimes, the amount of suppression strongly depending on the magnitude of the relaxation time scale.

This mechanism of a current blockade is different from the Coulomb blockade. Here, we make explicit use of *excited* absorbing states, that is states that are non-conducting whereas at the same time, the electronic ground states, whose conductance properties define the Coulomb-blockade diamonds in the current–voltage diagram, are transparent. It is the two-dimensional spectrum, the dependence on two quantum numbers, that allows for a selection rule, which, in cooperation with the spectral distortions leads to the observed phenomenology.

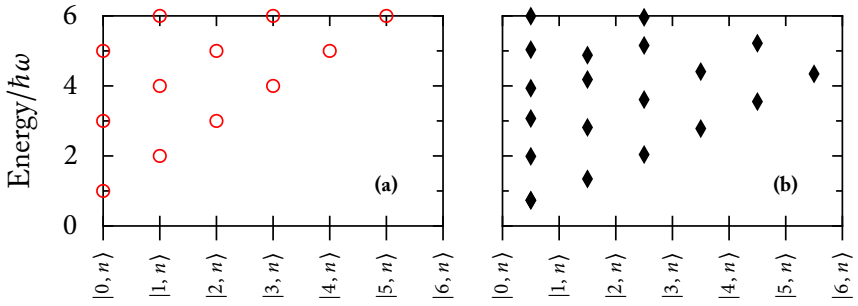

Figure 3.13: Spectra of both the neutral (a) and the charged (b) state of the Jahn–Teller molecule ordered by angular momentum. Since each state is doubly degenerate due to the symmetry $m \mapsto -m$, we only show the spectra for positive angular momenta.

In Figure 3.12, we show numerical results for the differential conductance of our model with equal coupling to the electrodes $\Gamma_\alpha^\sigma = \Gamma_0$ for some Γ_0. The graphs have been obtained by a treatment of the problem with rate equations. If one were strictly applying the rules of chapter 2, rate equations would be unsuitable as the problem has many degeneracies. Indeed, it is the degeneracies of the Jahn–Teller Hamiltonian that actually produce the rich phenomenology. Due to the selection rule in angular momentum, we can, however, show that the current blockade is a generic effect, which is independent of the implementation of the model as a rate equation or a degenerate master equation.

In chapter 2, we have argued that any weak-coupling dynamics naturally split into a rate equation between the different energy manifolds and a degenerate master-equation description inside each degenerate subspace. Given any coherent superposition of neutral states of the Jahn–Teller molecule of the same energy

$$|\gamma\rangle := \sum a_{m,n} |0; m, n\rangle ,$$

where m and n are related by the condition $m+2n = \text{const}$. In contrast to the harmonic oscillators, the Jahn–Teller-active states are only doubly degenerate, such that a general wave function of its degenerate eigenspace has the form

$$|\beta\rangle := b_j |1; j, n'\rangle + b_{-j} |1; -j, n'\rangle .$$

The Franck–Condon factor for a transition $|\beta\rangle \mapsto |\gamma\rangle$ would be

$$|\langle\gamma | H_\mathrm{T} | \beta\rangle|^2 = \left| \sum_{m,n,\pm j} a^*_{m,n} b_j \langle 0; m, n | H_\mathrm{T} | 1; j, n'\rangle \right|^2 = \left| \sum_{\pm j} a^*_{j\pm\frac{1}{2},n} b_j \langle 0; j \pm \frac{1}{2}, n | H_\mathrm{T} | 1; j, n'\rangle \right|^2 .$$

Whatever coherent superposition the system actually is in, due to the breaking of the large degeneracy of the isotropic harmonic oscillator down to $E_j = E_{-j}$ in the Jahn–Teller active state, the selection rule still isolates the absorbing states. The isolation of these is a property of the whole energy manifold, which in this case comprises only two states. The observed phenomenology is the phenomenology of the rate-equation dynamics between the energy manifolds and not related to any effects of the coherent master equation at all. By this reasoning describing electronic transport through the linear $E\otimes e$ Jahn–Teller molecule using rate equations for the study of its generic current blockade is justified.

The numerical results plotted in Figure 3.12 show this current blockade and reveal two important aspects of its phenomenology. It obviously breaks the structural—not only quantitative—symmetry of the differential conductance in the sign of the gate voltage. The spectral trapping of the system only occurs in the charged state, and the relevant distortions are related to a lowering of the energy due to the Jahn–Teller effect. For

negative bias, trapping occurs when the molecular ground state is aligned or energetically close to the Fermi level of the drain electrode, which means negative gate voltage. Alignment with the Fermi level of the source electrode, and hence positive gate voltage, cannot produce the trapping effect in this model, as it is seen in the energy diagrams in Figure 3.14 (b) and (d). In this voltage regime, the cross-over of the equidistant harmonic oscillator levels with the distorted Jahn–Teller eigenenergies appears at too large angular momenta that can never be reached from the current-carrying states.

The current suppression itself shows up as a cascade of negative and positive conductance peaks. We already showed that in the linear $E\otimes e$ Jahn–Teller effect, there is not just one absorbing state; due to the large spectral distortions at high angular momentum, they appear as an infinite set. Once such a state is connected to the current-carrying, low-lying states by a tunnel cascade with finite probability,[8] the system is blockaded and, if it was conducting at lower bias, will show negative differential conductance. In contrast, if the bias is raised to such a magnitude that the absorbing state becomes conducting again, which means that the cross-over of harmonic oscillator levels with Jahn–Teller eigenenergies is shifted to higher angular momentum, the system can become transparent again, permit a stationary current, and thus produces a positive differential conductance peak. This mechanism applies for each state $|1;j,0\rangle$ individually, which causes the step-like pattern in the differential conductance diagram.

The cascade that produces the first "block" of suppressed current for low bias, kicks the system into the first absorbing state $|1;\frac{3}{2},0\rangle$ by advancing from the ground state

$$|0;0,0\rangle \mapsto |1;\frac{1}{2},1\rangle \mapsto |0;1,0\rangle \mapsto |1;\frac{3}{2},0\rangle\,. \tag{3.5.2}$$

The positive differential conductance peak is determined by the availability of energy for the transition

$$|1;\frac{3}{2},0\rangle \mapsto |0;1,0\rangle$$

from the molecule to the drain electrode. The line is therefore *parallel* to the boundary of the Coulomb-blockade diamond at negative gate voltage. The negative differential conductance peak, on the contrary, marks the availability of sufficient energy for the transitions

$$|0;0,0\rangle \mapsto |1;\frac{1}{2},1\rangle \quad \text{and} \quad |0;1,0\rangle \mapsto |1;\frac{3}{2},0\rangle\,,$$

which, since they are transitions from the neutral to the charged molecule, involve tunnelling processes at the source electrode and thus are marked by lines *perpendicular* to the negative-gate boundary of the Coulomb-blockade diamond.

3.5.3 A Second Time Scale due to Relaxation

The analysis of the linear $E\otimes e$ Jahn–Teller effect's transport properties and the attempt to attribute negative and positive differential conductance peaks to certain tunnelling transitions—the spectroscopy of the rate equations—proves to be more difficult *in praxi* than it has been suggested by the theory developed so far. There is an obvious mismatch of the peaks' maxima and their theoretically predicted positions. What, on first sight, is even more disturbing but actually is the key to the problem, is a dependence of these shifts on

[8] This means that the cascade has to be rather short, and the Franck–Condon matrix elements have to be sufficiently large.

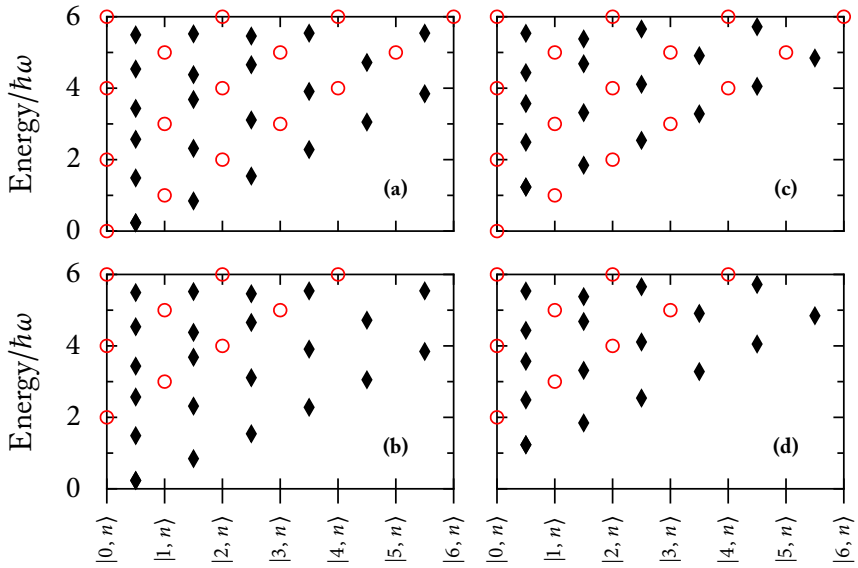

Figure 3.14: Illustration how the spectral distortions due to the $E\otimes e$ Jahn–Teller effect and the Berry-phase induced selection rule characterise the possible tunnelling processes, the emergence of absorbing states, and the qualitative asymmetry of the dI/dV diagram with respect to the gate voltage. The spectra of both the neutral (circles) and the charged (diamonds) state of the system have been overlaid and shifted with respect to each other to indicate the energetic situation for the respective tunnelling. The electron–phonon coupling is $\lambda = 1$. (a) and (b) $eV_{\mathrm{sd}} = 2\hbar\omega$ and $eV_{\mathrm{g}} = -\frac{1}{2}\hbar\omega$. The molecule is aligned close to the Fermi level of the drain electrode. (a) Tunnelling at the drain electrode, where the emergence of absorbing states is clearly seen. (b) Tunnelling at the source electrode, where no tunnelling channels are obstructed. (c) and (d) Alignment of the molecule close to the Fermi level of the source electrode, $eV_{\mathrm{g}} = \frac{1}{2}\hbar\omega$. (c) Tunnelling at the drain electrode, where in the low-j sector no absorbing states are observed and hence no current blockade. (d) Tunnelling at the source electrode. Although the energy difference are smaller than in (b) still no channel is obstructed.

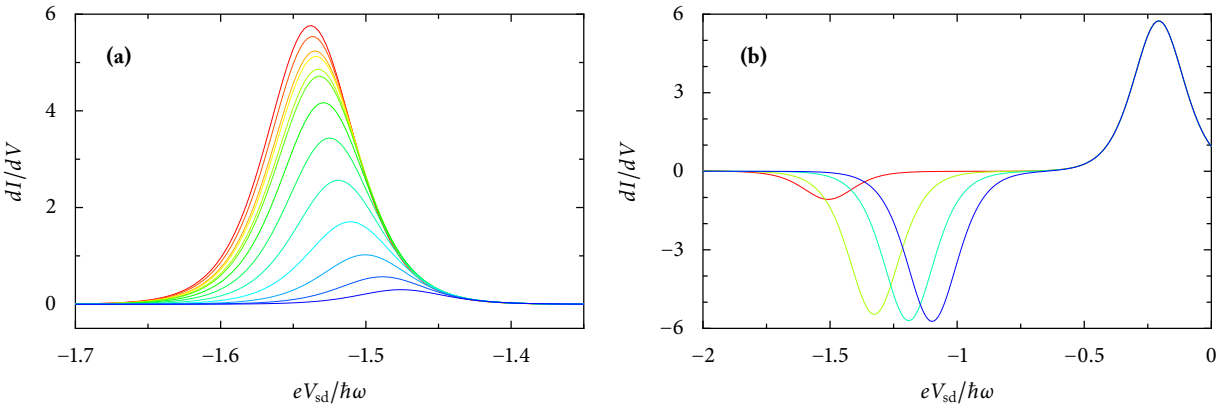

Figure 3.15: The two types of peak-shifts due to vibronic relaxation. (a) Nestling shifts, which continuously change the line shape and the position of the maximum due to the presence of two time scales. The relaxation time assumes values between $\tau = 4\tau_0$ (red) and $\tau = 1280\tau_0$ (blue). (b) Discrete rigid shifts, which are due to high-energy entry states into the trapping cascades and a signature of the non-equilibrium stationary vibronic distribution. The relaxation time is chosen between $\tau = 10\tau_0$ (red) and $\tau = 40960\tau_0$ (blue). The other parameters are $\lambda = 1$, $k_{\mathrm{B}}T = 0.05\hbar\omega$, $eV_{\mathrm{g}} = -0.5\hbar\omega$ (a) and $eV_{\mathrm{g}} = -0.26\hbar\omega$ (b).

the relaxation time τ, which we have introduced in order to regularise the strict selection rule and remove the thus caused non-uniqueness of the stationary density matrix. Inspection of the numerical data reveals two types of shifts, which we plot exemplary in Figure 3.15. The first type, Figure 3.15 (a), is a "nestling" of the high-τ curves against the low-energy shoulders of the low-τ limit, which serves as an envelope function for all relaxation effects of this type. The second type, Figure 3.15 (b), is a rigid shift of the negative differential conductance peak towards lower energy. The rigid shifts can be easily understood by noting that in contrast to the nestling shifts, they are of discrete nature. Their position cannot be tuned continuously by changing the relaxation time τ. By verification with the Jahn–Teller spectrum, one can match the position of the lines with transitions in the tunnelling dynamics, although not the low-energy cascades, which we used to explain the current blockade. The shifted negative differential conductance peaks correspond to high-energy transitions that open the cascade into the absorbing state. Weaker relaxation implies a stationary vibrational distribution that is less concentrated at the vibronic ground state: it is in stronger non-equilibrium. And as such, highly excited states can play a more important role in the stationary tunnelling dynamics. They eventually determine the energetic threshold for the current blockade if such a resonance has lower energy than the one emerging from the vibronic ground state. The spectrum of the linear $E\otimes e$ Jahn–Teller effect, Figures 3.13 and 3.14, is so much distorted also in the higher radial excitations that such a behaviour is plausible. In the Anderson–Holstein model, such an effect is not found, as there the oscillator spectrum is equidistantly spaced and undistorted. Whether different tunnelling processes involve high-energy states or low-energy states does not leave its fingerprint in the spectroscopic picture of the differential conductance diagram.

The mechanism causing the rigid shifts of the resonances is contrasted by the properties of the nestling shifts. Depending on the strength of the phenomenological relaxation, the maxima move continuously and are damped. But they never leave the area marked by the curve given by the low-τ limit. In order to explain this phenomenon, we have to understand the time-dependent dynamics of the system. We consider the Monte-Carlo trajectory of the system at the voltages $(eV_g, eV_{sd}) = (-0.5\hbar\omega, -2\hbar\omega)$, which is shown in Figure 3.16 (a). The implementation of the Monte-Carlo simulation is the Metropolis–Hastings algorithm presented in appendix C. The curve in Figure 3.16 (a) shows the number of charges that have passed through the left tunnel junction after the simulation time t. The current is then given by the slope of the graph. By inspection of the figure, one notices two properties of the dynamics. The increase of transmitted charge with time is interrupted once in a while for a relatively long period. The closer look at the Monte-Carlo data shows that this happens whenever the system is in a absorbing state and is waiting to be freed by the relaxation mechanism. But apart from these interruptions, the current flow is apparently undisturbed. This is seen in the quite regular and identical slope of the curve for every section between two trapping events. We infer that the relaxation mechanism, and thus the trapping effect itself, constitutes a second time scale in the transport problem, being opposed to the tunnelling dynamics, which is of order $\mathcal{O}(H_T^2)$. The bare tunnelling time is defined as $\tau_0 := 1/\Gamma_0$: the second time scale due to relaxation is of order τ. We combine our observations and conclusions to state an *ad-hoc* two-level model, with which we can simulate the effect of the two time scales' interplay and thereby understand their influence on the resonance positions.

Consider the two-level system, which is sketched in Figure 3.16 (b), with a absorbing state $|\beta\rangle$ and a state $|\alpha\rangle$ from which the electron can tunnel to the drain electrode, say the absolute ground state of the charged molecule. The current is given by the inverse of the time τ_{total} the electron spends on the molecule. In our model, this time is characterised by the sum of the trapping time τ and the time the electron needs to leave the second, non-absorbing state. The rate to leave this latter state is the product of the bare tunnelling

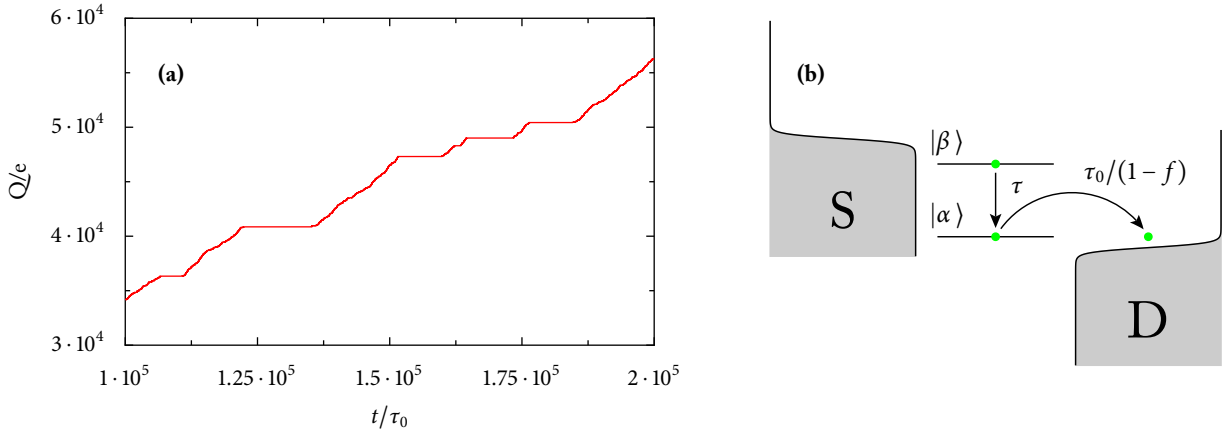

Figure 3.16: (a) Monte-Carlo simulation of electron transport through the $E\otimes e$ Jahn–Teller molecule in the regime of current suppression. $\lambda = 1, k_\mathrm{B}T = 0.05\hbar\omega, \tau = 5000\,\tau_0, (eV_\mathrm{g}, eV_\mathrm{sd}) = (-0.5\hbar\omega, -2\hbar\omega)$. The transport of electrons through the single-molecule junction is once in a while interrupted for a rather long period of time, when the electron is locked in one of the absorbing states and waiting for relaxation towards a conducting state. (b) Effective two-level model for the explanation of the two time scales' interplay. The state $|\beta\rangle$ is assumed to be an absorbing state, which can only be left towards $|\alpha\rangle$ via an internal relaxation process on a typical time scale τ. From the state $|\alpha\rangle$, the electron can tunnel off to the drain electrode on a time scale $\tau/(1-f)$ as it is explained in the text.

rate $1/\tau_0$ and the probability $1-f$ to find an empty state of appropriate energy in the drain electrode, where f is this electrode's Fermi function $f(eV_\mathrm{g}-\mu_\mathrm{D})$. The typical time for tunnelling from $|\alpha\rangle$ out to the leads is thus $\tau_0/(1-f)$ and the stationary current can be estimated as

$$I \propto \frac{1}{\tau_\mathrm{total}} = \frac{1}{\tau + \frac{\tau_0}{(1-f)}} = \frac{1-f}{(1-f)\tau + \tau_0}. \tag{3.5.3}$$

Being differentiated with respect to the source–drain voltages, this yields the relation

$$\frac{\mathrm{d}I}{\mathrm{d}V} \propto If\,\frac{1-\tau I}{2k_\mathrm{B}T}.$$

For vanishing τ, that is for instantaneous relaxation or absence of absorbing states, the current of this model would be

$$I_0 = \frac{(1-f)}{\tau_0}.$$

The differential conductance is accordingly

$$\frac{\mathrm{d}I_0}{\mathrm{d}V} = \frac{1}{2k_\mathrm{B}T} I_0 f,$$

where the peak's maximum is defined by the condition

$$\frac{\mathrm{d}I_0^2}{\mathrm{d}^2V} = I_0\left(\frac{f}{2k_\mathrm{B}T}\right)^2 - \left(\frac{I_0}{2k_\mathrm{B}T}\right)^2 f = 0.$$

It is at the very voltage for which $f = \frac{1}{2}$, which is the usual resonance condition. For a model with just a single

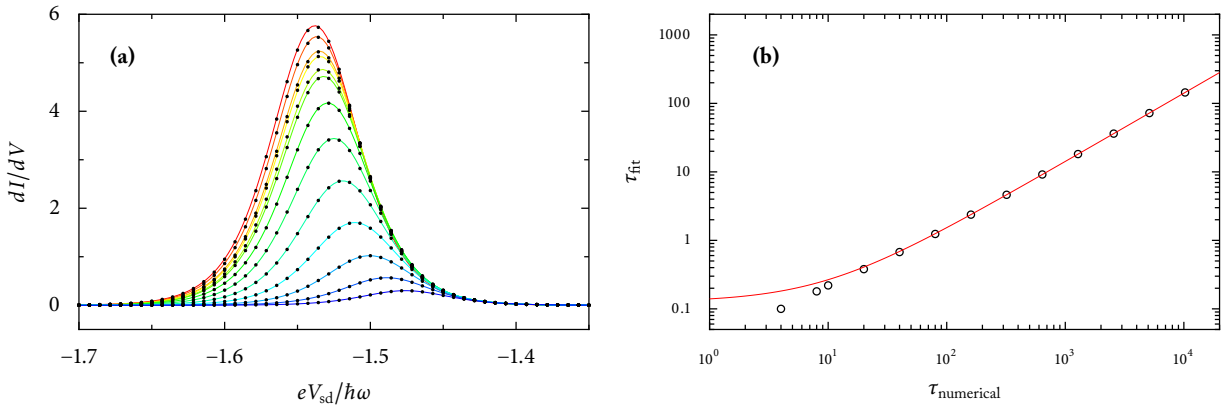

Figure 3.17: (a) Fit of the differential conductance peaks of the nestling shifts of Figure 3.15 with the result (3.5.3) of the minimalistic model shown in Figure 3.16 (b) minimalistic model. (b) Correlation of the fit values of τ with the ones used in the numerical simulations. Apart from the regime, where the relaxation-induced physics happens at the same time scale as the tunnelling, $\tau_{\text{fit}} \propto \tau_{\text{numerical}}$, which corroborates our explanation of the data using the two-level model.

time scale, be it a quantum dot or a single-level molecule, the stationary current through the drain electrode in the configuration we are considering is only determined by the Fermi function $1-f(\varepsilon_1^q-\varepsilon_0^{q'}-\mu_D)$, that is the probability to find an empty state in the leads with just the energy necessary for the vibrational transition $|1;q\rangle \mapsto |0;q'\rangle$. The maximum of the differential conductance peak is thus located at the bias voltage for which $\mu_\alpha = \varepsilon_1^q - \varepsilon_0^{q'}$. Of course, this result has been expected from the resonant tunnelling model and is reproduced by our model. With a finite relaxation time τ and hence more than one time scale present in the problem, the position of the peak is given by the roots of the second derivative of I in Equation (3.5.3). The maximum of the peak is thus to be found at the very voltages $2eV_g+eV_{sd}$ for which

$$f(eV_g - \mu_D) = \frac{\tau_0}{2\tau_0 + \tau} \quad \text{or equivalently} \quad 2eV_g + eV_{sd} = 2k_BT \ln\left(\frac{\tau_0 + \tau}{\tau_0}\right).$$

The consequences of finite τ for the line shape are twofold. As a purely quantitative effect, the height of the peak in dI/dV decreases with increasing τ. As a qualitative effect, however, the position of the peak is shifted logarithmically slow towards higher bias voltages.

The simple model compares remarkably well to the numerical rate-equation results. We focus on a single peak in the dI/dV diagram and study its line shape for different values of the phenomenological relaxation rate τ. The effect of increasing τ—red to blue curves in Figure 3.17 (a)—is a reduction of the peak's height and a shift of its maximum towards lower energy. Since the resonance occurs at negative source–drain voltages, this means increasing eV_{sd}, just as it is predicted by the model. We finally fit the results of the model, Equation (3.5.3), to the data in Figure 3.17 (a). Comparing the fitted values for τ with the parameters of the numerical simulation, in Figure 3.17 (b), we see how well this simplified model describes the interplay of the two time scales. The only deviations occur when both time scales are of comparable magnitude, $\tau = \mathcal{O}(\tau_0)$. For a sufficiently large separation of time scales, the agreement is nearly perfect.

Chapter 4

Non-Interacting Two-Level Quantum Dots

In the previous chapter, we have given a thorough discussion of quantum transport through single molecules in the sequential-tunnelling regime using rate equations. These equations, which describe the tunnelling dynamics between the different degenerate subspaces of the system Hamiltonian, are very versatile in their application and show a rich phenomenology in the stationary current. The dynamics inside a degenerate, or near-degenerate, subspace of H_S, cannot be described by rate equations as the rotating-wave approximation, which essentially removes all coherences in the density matrix, cannot be applied to such systems. For these, the master equation for the full density matrix has to be solved including its off-diagonal elements. Of course, the density matrix is a self-adjoint operator and can thus be diagonalised. The associated master equation for the stationary state is then rewritten as a rate equation. But *a priori* we do not know anything about the nature of the eigenbasis of ρ. In the simplest case, it would be constant in the (eV_g, eV_{sd})-plane and as such the difference between the proper master equation and an *ad-hoc* rate-equation description would only be of quantitative nature. In the general case, however, the eigenbasis will show a non-trivial dependence on the voltages causing a qualitative influence of the coherences onto the steady-state properties.

In this chapter, as an intermediate step between the discussions of rate equations and the full molecular master equation, we present the treatment of a non-interacting two-level quantum dot to model the electronic part of a degenerate two-orbital molecule. This system can be discussed both by kinetic equations and in the weak-coupling limit of an exact Keldysh treatment. With the Keldysh formalism, we compute the analytic solution of the sequential-tunnelling problem and the diagonal basis of the stationary density matrix. The result can be integrated into a pseudo-spin formulation of the internal dynamics of the quantum dot. Such a formulation will become more important in chapter 5, as it turns out that most of the master-equation phenomenology for molecules can be understood in this picture best.

The physics of non-interacting quantum dots is actually rather simple and unspectacular. It becomes more interesting and colourful in the interacting case; however, then a closed analytic solution cannot be obtained. The physics of the interacting quantum dot can be discussed using various methods, most prominently renormalisation group methods[1] at zero or small temperature. Although these methods give some insight into the physics of the interacting quantum dot, their full power has not yet been unleashed as even the formulation for physically interesting cases, such as large temperatures, proves to be very complicated and involved. Most of the two-level quantum dot physics that is discussed with weak-coupling methods and master equations, relates to serial quantum dots, when the tunnelling electrons traverse the two dots

[1] See for example (Karrasch *et al.*, 2006).

sequentially (Gurvitz, 1998). Here, we focus on *parallel* structures: both levels of the dot are coupled to both electrodes. This set-up resembles the degenerate Anderson–Holstein and Jahn–Teller molecules that we shall discuss in the next chapter. Resonant tunnelling through parallel quantum dots in different settings has been discussed by Shahbazyan & Raikh (1994), who investigate the connection of the two-level and the single-level problem, and Braun *et al.* (2004), where the spin-degeneracy of a quantum dot coupled to ferromagnetic leads is investigated.

In the following discussion of non-interacting degenerate quantum dots, we shall acquaint ourselves with some intuition for the role of the physics introduced by the off-diagonal elements of the density matrix. From the rate-equation point of view, their physical consequences are difficult to imagine, because the interpretation of sequential tunnelling as electrons hopping between well-defined states like in the Monte-Carlo simulation of the rate equation is not possible due to the inclusion of linear superpositions of the degenerate orbitals in the dynamics.

4.1 Resonant Tunnelling

The resonant tunnelling model is a toy-model for studying transport through quantum nanostructures. In the non-interacting case, it can be solved exactly using an abundance of different methods. Here, we present a way using the Keldysh method (Brouwer, 2005) that permits the computation of the occupation numbers in the long-time limit. The presented method will then be extended to the case of two degenerate levels in the next section. We assume the electronic reservoirs to be spinless and perfect non-interacting Fermi gases held in equilibrium at temperature $k_\mathrm{B}T$. Their density of states is assumed to be constant over the relevant energy interval, the wide-band limit, and denoted by ν. With the notation introduced in chapter 1, the resonant-tunnelling Hamiltonian is

$$H_{\mathrm{R.T.}} = \varepsilon_d d^\dagger d + \sum_{k\alpha} \varepsilon_k c^\dagger_{k\alpha} c_{k\alpha} + \sum_{k\alpha} \left(t_\alpha c^\dagger_{k\alpha} d + t^*_\alpha d^\dagger c_{k\alpha} \right).$$

We refrain from mentioning the gate voltage eV_g explicitly; it can be restored in the Hamiltonian by shifting the single-particle energy $\varepsilon_\mathrm{d} \mapsto \varepsilon_\mathrm{d} + eV_\mathrm{g}$. The Golden-Rule expressions[2] for the hopping rates induced by the tunnelling Hamiltonian are $\Gamma_\alpha := \frac{2\pi}{\hbar}\nu|t_\alpha|^2$. The rate-equation for weak-coupling transport through the nanostructure is

$$\begin{aligned} \dot{p}_1 &= \sum_\alpha \Gamma_\alpha f_\alpha(\varepsilon_d) p_0 - \sum_\alpha \Gamma_\alpha \big(1 - f_\alpha(\varepsilon_d)\big) p_1 \\ 1 &= p_0 + p_1. \end{aligned}$$

This equation has the stationary solution

$$p_0 = \frac{1}{\Gamma} \sum_\alpha \big(1 - f_\alpha(\varepsilon_d)\big) \quad \text{and} \quad p_1 = \frac{1}{\Gamma} \sum_\alpha \Gamma_\alpha f_\alpha(\varepsilon_d).$$

Using the exact solution of the Dyson equation for the dot operators, we shall recover this result in the limit $\Gamma \to 0$. We denote the Green functions as follows: G_d is the Green function of the free resonant

[2] Although this is the general definition, in the following, we shall discard the constants and set $\nu = 1$ and use natural units $\hbar = 1$. We also stick to the notational convention introduced in appendix B.1 that left out indices imply the respective sum.

level. The dot's Green function with respect to the full Hamiltonian will simply be denoted by G. The electrode's free Green functions are given an index to indicate the lead—left or right—and the wave vector of the respective particles $G_{k\alpha}$. The upper index R, A, or K is an abbreviation for the retarded, advanced, or Keldysh Green function, respectively. Green functions without this index are matrices in Keldysh space. In terms of the dot's operators, these are (Brouwer, 2005)

$$G^{\mathrm{R}}(t) = -\imath\theta(t)\langle\{d(t), d^\dagger(0)\}\rangle \qquad G^{\mathrm{A}}(t) = G^{\mathrm{R}*}$$
$$G^{<}(t) = \imath\langle d^\dagger(t) d\rangle \qquad G^{>}(t) = -\imath\langle d(t) d^\dagger\rangle$$
$$G^{\mathrm{K}}(t) = G^{<}(t) + G^{>}(t) = -\imath\langle\left[d, d^\dagger(t)\right]\rangle \qquad \mathcal{A}(t) = \imath(G^{<}(t) - G^{>}(t)).$$

For the stationary solution, we only need to consider equal-time correlators, which relate to their Fourier decomposition by

$$G = \int G(\omega)\frac{d\omega}{2\pi}.$$

The occupation number of the charged state is related to the lesser Green function

$$p_1 = \mathrm{Tr}\left(\rho(t)\, d^\dagger d\right) = \mathrm{Tr}\left(\rho_{\mathrm{stat}}\, d^\dagger(t) d(t)\right) = -\imath G^{<}(t, t). \tag{4.1.1}$$

By ρ_{stat}, we denote the stationary, long-time limit of the reduced density matrix. The Dyson equation $G = G_{\mathrm{d}} + G_{\mathrm{d}}\Sigma G$ is solved for the dot's Green function

$$G = \left(G_{\mathrm{d}}^{-1} - \Sigma\right)^{-1}.$$

The retarded and advanced components as well as the Keldysh component of the dot's self-energy are

$$\Sigma^{\mathrm{R/A}}(\omega) = \sum_{k\alpha} |t_\alpha|^2 G^{\mathrm{R/A}}_{k\alpha}(\omega) = \mp\imath\pi \sum_{k\alpha} |t_\alpha|^2 \delta(\varepsilon_k - \omega) = \mp\imath \sum_\alpha \frac{\Gamma_\alpha}{2} = \mp\imath\frac{\Gamma}{2},$$
$$\Sigma^{\mathrm{K}}(\omega) = \sum_{k\alpha} |t_\alpha|^2 G^{\mathrm{K}}_{k\alpha}(\omega) = -2\pi\imath \sum_{k\alpha} |t_\alpha|^2 \delta(\varepsilon_k - \omega)\left(1 - 2f_\alpha(\varepsilon_k)\right) = -\imath \sum_\alpha \Gamma_\alpha\left(1 - 2f_\alpha(\omega)\right).$$

The free fermions' Green functions are

$$G^{\mathrm{R/A}}_{k\alpha}(\omega) = \mp\imath\pi\delta(\varepsilon_k - \omega), \qquad G^{\mathrm{K}}_{k\alpha}(\omega) = -2\pi\imath\delta(\varepsilon_k - \omega)\left(1 - 2f_\alpha(\varepsilon_k)\right).$$

The free Green function of the dot itself in Keldysh space is[3]

$$G_{\mathrm{d}}^{-1}(\omega) = \begin{pmatrix} \frac{1}{\omega - \varepsilon_{\mathrm{d}} + \imath\eta} & -2\pi\imath\delta(\varepsilon_{\mathrm{d}} - \omega) G_{\mathrm{d}}^{\mathrm{K}} \\ 0 & \frac{1}{\omega - \varepsilon_{\mathrm{d}} - \imath\eta} \end{pmatrix}^{-1}$$
$$= \begin{pmatrix} \omega - \varepsilon_{\mathrm{d}} + \imath\eta & 2\pi\imath\delta(\varepsilon_{\mathrm{d}} - \omega) G_{\mathrm{d}}^{\mathrm{K}}\left((\omega - \varepsilon_{\mathrm{d}})^2 + \eta^2\right) \\ 0 & \omega - \varepsilon_{\mathrm{d}} - \imath\eta \end{pmatrix}$$

[3] The retarded and advanced components of the free dot's Green function are obvious, the infinitesimal $\imath\eta$ is for a convenient treatment of unbounded integrals and will be sent to zero later. The Keldysh component is noted for completeness. It is the anticommutator of the free level's operators, which in analogy to the free fermionic Keldysh Green function is $\delta(\varepsilon_{\mathrm{d}} - \omega)$ times the occupation number, essentially a constant, which will drop out in the course of the calculations.

As we see from this expression, the Keldysh component of the free dot's inverse Green function G_d^{-1} is proportional to $\delta(\omega-\varepsilon_\mathrm{d})\big((\omega-\varepsilon_\mathrm{d})^2+\eta^2\big)$. This term vanishes identically in the limit $\eta\to 0$, because the δ-function is only supported on the roots of the second factor. Then, in the limit $\eta\to 0$,

$$\begin{aligned} G(\omega) &= \begin{pmatrix} \omega-\varepsilon_\mathrm{d}+\imath\frac{\Gamma}{2} & \imath\sum_\alpha\Gamma_\alpha\big(1-2f_\alpha(\omega)\big) \\ 0 & \omega-\varepsilon_\mathrm{d}-\imath\frac{\Gamma}{2} \end{pmatrix}^{-1} \\ &= \frac{1}{(\omega-\varepsilon_\mathrm{d})^2+\left(\frac{\Gamma}{2}\right)^2}\begin{pmatrix} \omega-\varepsilon_\mathrm{d}-\imath\frac{\Gamma}{2} & -\imath\sum_\alpha\Gamma_\alpha\big(1-2f_\alpha(\omega)\big) \\ 0 & \omega-\varepsilon_\mathrm{d}+\imath\frac{\Gamma}{2} \end{pmatrix}. \end{aligned}$$

The Keldysh component and the spectral function are

$$\begin{aligned} G^\mathrm{K}(\omega) &= -2\pi\imath\frac{\frac{\Gamma}{2\pi}}{(\omega-\varepsilon_\mathrm{d})^2+\left(\frac{\Gamma}{2}\right)^2}\frac{\sum_\alpha\Gamma_\alpha\big(1-2f_\alpha(\omega)\big)}{\Gamma}, \\ \imath\mathcal{A}(\omega) &= G^\mathrm{A}(\omega)-G^\mathrm{R}(\omega) = \imath\frac{\Gamma}{(\omega-\varepsilon_\mathrm{d})^2+\left(\frac{\Gamma}{2}\right)^2}. \end{aligned}$$

The occupation of the dot's level in the stationary state is given by $p_1=-\imath\int G^<(\omega)\frac{d\omega}{2\pi}$ where

$$G^<(\omega) = \frac{1}{2}\big(G^\mathrm{K}(\omega)+\imath\mathcal{A}(\omega)\big) = -\frac{2\pi\imath}{2}\frac{\frac{\Gamma}{2\pi}}{(\omega-\varepsilon_\mathrm{d})^2+\left(\frac{\Gamma}{2}\right)^2}\left(\frac{\sum_\alpha\Gamma_\alpha\big(1-2f_\alpha(\omega)\big)}{\Gamma}-1\right),$$

such that finally

$$p_1 = \sum_\alpha\frac{\Gamma_\alpha}{\Gamma}\int f_\alpha(\omega)\frac{\Gamma}{(\omega-\varepsilon_\mathrm{d})^2+\left(\frac{\Gamma}{2}\right)^2}\frac{d\omega}{2\pi}.$$

In the weak-coupling limit $\Gamma\to 0$, the Lorentzian in the integral turns into a δ-function centred at $\omega=\varepsilon_d$, from which we recover the rate-equation result in Equation (4.1.1).

4.2 Two-Level Resonant Tunnelling

By adding a second level to the resonant-tunnelling Hamiltonian, we generalise the previous calculation from scalar Green functions to matrix-valued Green functions. The linear algebra used in the Keldysh treatment is extended to using block-matrices.

A parallel quantum dot, which is the bare electronic model for the single-molecule junctions we shall treat in the next chapter, is equivalent to the resonant tunnelling model with two degenerate levels. The levels are non-interacting, such that the nanostructure can hold two particles at the same time without additional cost in energy and Wick's theorem can be applied. With the same fermionic reservoirs as before, the Hamiltonian is

$$H_\mathrm{R.T.2} = \sum_\sigma\varepsilon_\sigma d_\sigma^\dagger d_\sigma + \sum_{\boldsymbol{k}\alpha}\varepsilon_{\boldsymbol{k}}c_{\boldsymbol{k}\alpha}^\dagger c_{\boldsymbol{k}\alpha} + \sum_{\boldsymbol{k}\alpha\sigma}\left(t_{\alpha\sigma}c_{\boldsymbol{k}\alpha}^\dagger d_\sigma + t_{\alpha\sigma}^* d_\sigma^\dagger c_{\boldsymbol{k}\alpha}\right).$$

For simplicity, we assume real tunnel amplitudes $t_{\alpha\sigma}\in\mathbb{R}$. For the degenerate model, $\varepsilon_\sigma=\varepsilon_\mathrm{d}$. The two levels define a pseudo-spin $|\uparrow\rangle$ and $|\downarrow\rangle$, the indices σ and τ denote either orientation in summations. In analogy

to electronic spin notation, $\bar{\sigma}$ has the opposite value of σ; a similar notation applies to the lead index α. We keep the different energies ε_σ as long as possible in the following derivation, because we shall need some of these expressions in chapter 6. The Golden-Rule rates acquire an additional index for the electronic level, $\Gamma_\alpha^\sigma := \frac{2\pi}{\hbar}\nu|t_{\alpha\sigma}|^2$, and the cross-coupling rate $\gamma_\alpha := \frac{2\pi}{\hbar}\nu t_{\alpha\uparrow}t_{\alpha\downarrow}$ is introduced.

4.2.1 Solution Using the Keldysh Formalism

In the first part of the discussion, we solve the degenerate two-level resonant tunnelling problem with the Keldysh formalism as it has been introduced in the previous section. The calculation shows how the exact solution and the weak-coupling approach by the master equation coincide in the limit $\Gamma \to 0$.

For the free propagators of the dot, we set in analogy to the discussion before

$$G_\mathrm{d}^{\mathrm{R/A}}(\omega) = \begin{pmatrix} \frac{1}{\omega-\varepsilon_\uparrow \pm \imath\eta} & 0 \\ 0 & \frac{1}{\omega-\varepsilon_\downarrow \pm \imath\eta} \end{pmatrix} \quad \text{and} \quad G_\mathrm{d}^{\mathrm{K}}(\omega) = -2\pi\imath \begin{pmatrix} \delta(\omega-\varepsilon_\uparrow)G_\uparrow^{\mathrm{K}}(\omega) & 0 \\ 0 & \delta(\omega-\varepsilon_\downarrow)G_\downarrow^{\mathrm{K}}(\omega) \end{pmatrix}.$$

The last equation follows from $\langle d_\sigma^\dagger d_\tau\rangle_0 \propto \delta_{\sigma\tau}$; there are no off-diagonal elements of the unperturbed system's Green functions. Like before, we have introduced the free dot's Keldysh Green function, which will drop out from the calculation when $\eta \to 0$. Inverting the free Green function is straightforward. We just have to keep in mind that all matrices are indeed matrices of block matrices. We thus find

$$G_\mathrm{d}^{-1} = \begin{pmatrix} G_\mathrm{d}^{\mathrm{R}} & G_\mathrm{d}^{\mathrm{K}} \\ 0 & G_\mathrm{d}^{\mathrm{A}} \end{pmatrix}^{-1} = \begin{pmatrix} \left(G_\mathrm{d}^{\mathrm{R}}\right)^{-1} & -\left(G_\mathrm{d}^{\mathrm{R}}\right)^{-1} G_\mathrm{d}^{\mathrm{K}} \left(G_\mathrm{d}^{\mathrm{A}}\right)^{-1} \\ 0 & \left(G_\mathrm{d}^{\mathrm{A}}\right)^{-1} \end{pmatrix}.$$

Its Keldysh part is the diagonal matrix

$$\left(G_\mathrm{d}^{-1}\right)^{\mathrm{K}}(\omega) = 2\pi\imath \begin{pmatrix} G_\uparrow^{\mathrm{K}}(\omega)\delta(\omega-\varepsilon_\uparrow)\left((\omega-\varepsilon_\uparrow)^2+\eta^2\right) & 0 \\ 0 & G_\downarrow^{\mathrm{K}}(\omega)\delta(\omega-\varepsilon_\downarrow)\left((\omega-\varepsilon_\downarrow)^2+\eta^2\right) \end{pmatrix}.$$

This term vanishes identically in the limit $\eta \to 0$. In contrast to the dot's free Green functions, the self-energy acquires an off-diagonal part in the pseudo-spin variables,

$$\Sigma_{\sigma\tau}^{\mathrm{R/A}}(\omega) = \sum_{\boldsymbol{k}\alpha} t_{\alpha\sigma}t_{\alpha\tau}G_{\boldsymbol{k}\alpha}^{\mathrm{R/A}}(\omega) \quad \text{and} \quad \Sigma_{\sigma\tau}^{\mathrm{K}}(\omega) = \sum_{\boldsymbol{k}\alpha} t_{\alpha\sigma}t_{\alpha\tau}G_{\boldsymbol{k}\alpha}^{\mathrm{K}}(\omega).$$

The solution of the Dyson equation is

$$\begin{aligned} G = \left(G_\mathrm{d}^{-1} - \Sigma\right)^{-1} &= \begin{pmatrix} \left(G_\mathrm{d}^{\mathrm{R}}\right)^{-1} - \Sigma^{\mathrm{R}} & -\left(G_\mathrm{d}^{\mathrm{R}}\right)^{-1} G_\mathrm{d}^{\mathrm{K}} \left(G_\mathrm{d}^{\mathrm{A}}\right)^{-1} - \Sigma^{\mathrm{K}} \\ 0 & \left(G_\mathrm{d}^{\mathrm{A}}\right)^{-1} - \Sigma^{\mathrm{A}} \end{pmatrix}^{-1} = \begin{pmatrix} \left(G_\mathrm{d}^{\mathrm{R}}\right)^{-1} - \Sigma^{\mathrm{R}} & -\Sigma^{\mathrm{K}} \\ 0 & \left(G_\mathrm{d}^{\mathrm{A}}\right)^{-1} - \Sigma^{\mathrm{A}} \end{pmatrix}^{-1} \\ &= \begin{pmatrix} \left(\left(G_\mathrm{d}^{\mathrm{R}}\right)^{-1} - \Sigma^{\mathrm{R}}\right)^{-1} & \left(\left(G_\mathrm{d}^{\mathrm{R}}\right)^{-1} - \Sigma^{\mathrm{R}}\right)^{-1} \Sigma^{\mathrm{K}} \left(\left(G_\mathrm{d}^{\mathrm{A}}\right)^{-1} - \Sigma^{\mathrm{A}}\right)^{-1} \\ 0 & \left(\left(G_\mathrm{d}^{\mathrm{A}}\right)^{-1} - \Sigma^{\mathrm{A}}\right)^{-1} \end{pmatrix} = \begin{pmatrix} G^{\mathrm{R}} & G^{\mathrm{R}}\Sigma^{\mathrm{K}}G^{\mathrm{A}} \\ 0 & G^{\mathrm{A}} \end{pmatrix}. \end{aligned}$$

From this expression, the lesser Green function follows to be

$$G^< = \frac{1}{2}\left(G^{\mathrm{K}} + \imath\mathcal{A}\right) = \frac{1}{2}\left[\left(1 + \frac{1}{2}G^{\mathrm{R}}\Sigma^{\mathrm{K}}\right)G^{\mathrm{A}} - G^{\mathrm{R}}\left(1 + \frac{1}{2}\Sigma^{\mathrm{K}}G^{\mathrm{A}}\right)\right].$$

In the following calculation, we first compute the retarded and advanced components of the Green functions to obtain the spectral function and discuss its properties; in the second step, we cover the Keldysh component.

The Spectral Function

In the limit $\eta \to 0$, we evaluate the retarded and advanced Green functions by simply inverting the two-by-two matrix given by the Dyson equation

$$G^{\mathrm{R/A}}(\omega) = \left(\left(G_{\mathrm{d}}^{\mathrm{R/A}}\right)^{-1} - \Sigma^{\mathrm{R/A}}\right)^{-1}(\omega) = \begin{pmatrix} \omega - \varepsilon_\uparrow \pm \imath\frac{\Gamma^\uparrow}{2} & \pm\imath\frac{\gamma}{2} \\ \pm\imath\frac{\gamma}{2} & \omega - \varepsilon_\downarrow \pm \imath\frac{\Gamma^\downarrow}{2} \end{pmatrix}^{-1}$$
$$= \begin{pmatrix} \left(\omega - \varepsilon_\uparrow \pm \imath\frac{\Gamma^\uparrow}{2}\right)^{-1} & \mp\imath\frac{\gamma}{2}\left((\omega - \varepsilon_\uparrow \pm \imath\frac{\Gamma^\uparrow}{2})(\omega - \varepsilon_\downarrow \pm \imath\frac{\Gamma^\downarrow}{2})\right)^{-1} \\ \mp\imath\frac{\gamma}{2}\left((\omega - \varepsilon_\uparrow \pm \imath\frac{\Gamma^\uparrow}{2})(\omega - \varepsilon_\downarrow \pm \imath\frac{\Gamma^\downarrow}{2})\right)^{-1} & \left(\omega - \varepsilon_\downarrow \pm \imath\frac{\Gamma^\downarrow}{2}\right)^{-1} \end{pmatrix}.$$

From here on, we restrict the discussion to the degenerate problem $\varepsilon_{\mathrm{d}} := \varepsilon_\uparrow = \varepsilon_\downarrow$. The determinant of the inverse Green function $(G^{\mathrm{R}})^{-1}$ is

$$\det\left(G^{\mathrm{R}}\right)^{-1}(\omega) = (\omega - \varepsilon_{\mathrm{d}})\left(\omega - \varepsilon_{\mathrm{d}} + \imath\frac{\Gamma}{2}\right) - \frac{1}{4}(\Gamma^\uparrow\Gamma^\downarrow - \gamma^2) =: (\omega - \varepsilon_{\mathrm{d}})\left(\omega - \varepsilon_{\mathrm{d}} + \imath\frac{\Gamma}{2}\right) - \frac{1}{4}\Delta.$$

The quantity $\Delta := \Gamma^\uparrow\Gamma^\downarrow - \gamma^2$ is proportional to $\det(\Sigma^{\mathrm{R/A}})$ and describes the asymmetry of the couplings to the electrodes. If all couplings were equal, $t_{\alpha\sigma} = 1$, then $\Gamma^\sigma = \gamma$ and thus $\Delta = 0$. Also in the case of proportional coupling $t_{\alpha\uparrow} = \zeta t_{\alpha\downarrow}$, with ζ being independent of the lead index α, we find $\Delta = 0$. For the full Green function, we find for non-zero Δ

$$G^{\mathrm{R}}(\omega) = \frac{1}{(\omega - \varepsilon_{\mathrm{d}})(\omega - \varepsilon_{\mathrm{d}} + \imath\frac{\Gamma}{2}) - \frac{1}{4}\Delta}\begin{pmatrix} \omega - \varepsilon_{\mathrm{d}} + \imath\frac{\Gamma^\downarrow}{2} & -\imath\frac{\gamma}{2} \\ -\imath\frac{\gamma}{2} & \omega - \varepsilon_{\mathrm{d}} + \imath\frac{\Gamma^\uparrow}{2} \end{pmatrix}.$$

Its imaginary part and thus the spectral function is

$$\mathcal{A}(\omega) = -2\,\mathrm{Im}\,G^{\mathrm{R}}(\omega) = \frac{1}{\left|\omega - \varepsilon_{\mathrm{d}} + \imath\frac{\Gamma}{2} - \frac{\Delta}{4(\omega - \varepsilon_{\mathrm{d}})}\right|^2}\left[\begin{pmatrix} \Gamma^\uparrow & \gamma \\ \gamma & \Gamma^\downarrow \end{pmatrix} + \frac{\Delta}{4(\omega - \varepsilon_{\mathrm{d}})^2}\begin{pmatrix} \Gamma^\downarrow & -\gamma \\ -\gamma & \Gamma^\uparrow \end{pmatrix}\right].$$

Performing the limit $\Delta \to 0$ properly,[4] this expression converges to

$$\mathcal{A}(\omega) = -2\,\mathrm{Im}\,G^{\mathrm{R}}(\omega) = \frac{1}{\left|\omega - \varepsilon_{\mathrm{d}} + \imath\frac{\Gamma}{2}\right|^2}\begin{pmatrix} \Gamma^\uparrow & \gamma \\ \gamma & \Gamma^\downarrow \end{pmatrix} + \frac{2}{\Gamma}\begin{pmatrix} \Gamma^\downarrow & -\gamma \\ -\gamma & \Gamma^\uparrow \end{pmatrix}\delta(\omega - \varepsilon_{\mathrm{d}}).$$

[4] Due to the formal structure of these terms being $f_n(\omega) = \frac{a_n}{\omega - \varepsilon_0}$ with a null sequence $a_n \to 0$ for $n \to \infty$, these functions converge to zero pointwise for almost every ω. Indeed, the only value of ω, where the pointwise convergence cannot be established is the root $\omega = \varepsilon_0$. Depending on the speed of convergence of a_n and thus on the integral $F_n := \int_{\mathbb{R}} f_n(\omega)d\omega$, there are three possible scenarios:

1. If $a_n \to 0$ faster than the denominator diverges. Then $F_n \to 0$, too, and the limit $f_n(\omega) \to 0$ pointwise for all ω is established.
2. If, however, $a_n \to 0$ slower than the divergence of the denominator, $F_n \to \infty$ and the limit of $f_n(\omega)$ is ill-defined.
3. In the intermediate case, the integral $F_n = F$ is constant. All mass of f_n will then be concentrated at the singular point $\omega = \varepsilon_0$, and accordingly $f_n(\omega) \to F\delta(\omega - \varepsilon_0)$.

It is the third case, the convergence to a δ-function, which we usually encounter in our calculations.

Due to the condition $\Delta = 0$, both matrices in the above expression have zero determinant. They also commute and thus admit a common eigenbasis for their eigenvalues $\lambda_1 = 0$ and $\lambda_2 = \Gamma$. The eigenvectors are $e_1 = (\gamma, -\Gamma^{\uparrow})$ and $e_2 = (\gamma, \Gamma^{\downarrow})$. The first matrix maps e_1 onto $\lambda_1 e_1 = 0$ and e_2 onto $\lambda_2 e_2$, the second matrix does the opposite. In this basis the spectral function decouples into a resonant tunnelling contribution and an orthogonal localised state,

$$\mathcal{A}_{\mathrm{diag}}(\omega) = \frac{1}{\left|\omega - \varepsilon_{\mathrm{d}} + \imath\frac{\Gamma}{2}\right|^2}\begin{pmatrix}\Gamma & 0\\ 0 & 0\end{pmatrix} + \frac{2}{\Gamma}\begin{pmatrix}0 & 0\\ 0 & \Gamma\end{pmatrix}\delta(\omega - \varepsilon_{\mathrm{d}}).$$

The decoupling into a single resonant tunnelling model and an additional localised state is a consequence of the Hamiltonian of the system. A unitary transformation in the dot's electronic Hilbert space $\mathcal{H}_{\mathrm{el}}$ can accomplish a decoupling of one level from the electronic leads. The degeneracy $\varepsilon_{\uparrow} = \varepsilon_{\downarrow}$ guarantees the invariance of the free dot's Hamiltonian under any unitary transformation. In this regime, the two-level problem reduces to an effective single-level problem. This property, which will become important for the transport properties of the interacting molecular model, has already been noted by Shahbazyan & Raikh (1994) and Chudnovskiy (2005). The quantity Δ is, by definition, proportional to the determinant of the retarded or advanced self-energy $\Sigma^{\mathrm{R/A}}$. This determinant being zero causes at least one of the eigenvalues to be zero as well, which means that in the eigenbasis of the self-energy, the corresponding eigenstate has zero self-energy. It is therefore not influenced by the presence of the fermionic reservoirs: it is decoupled from the electrodes. The δ-function in the spectral function is the signature of this effect.

A generalisation of the decoupling to an arbitrary number of localised levels being coupled to an arbitrary number of electrodes is due to Berkovits *et al.* (2004), who show that the rank of the coupling matrix defines the number of effectively coupled levels. If the coupling constants $t_{\alpha\sigma}$ form a matrix $(W)_{\alpha\sigma} = t_{\alpha\sigma} \in \mathbb{C}^{m\times n}$, the retarded/advanced self energy is proportional to $\Sigma^{\mathrm{R/A}} \propto W^{\dagger}W \in \mathbb{C}^{n\times n}$, a square matrix in the vector space spanned by the electronic states (Mahaux & Weidenmüller, 1969, chap. 4.2). The rank of a matrix is defined as the dimension of its image. Let $A \in \mathbb{C}^{m\times n}$ be an arbitrary matrix, then

$$\operatorname{rank}(A) := \dim\bigl(\operatorname{range}(A)\bigr) \leq \min(m, n).$$

If A was surjective, for example, $\operatorname{rank}(A) = m$; if A was injective, $\operatorname{rank}(A) = n$. For the product of two matrices, one therefore finds

$$\operatorname{rank}(A \cdot B) \leq \min\bigl(\operatorname{rank}(A), \operatorname{rank}(B)\bigr).$$

The rank of the self energy and therefore the number of levels that are effectively coupled to the electrodes is less than $\operatorname{rank}(\Sigma^{\mathrm{R/A}}) \leq \min(m,n)$. For example, three levels coupled to five electrodes cannot be reduced generically. But four levels coupled to two electrodes are at most two levels coupled to two electrodes.

The Keldysh Component

The Keldysh component of the Green function G is the product $G^{\mathrm{R}}\Sigma^{\mathrm{K}}G^{\mathrm{A}}$ of the retarded and advanced Green functions with the Keldysh component of the self energy

$$\Sigma^{\mathrm{K}}(\omega) = -\imath\sum_{\alpha}\bigl(1 - 2f_{\alpha}(\omega)\bigr)\begin{pmatrix}\Gamma_{\alpha}^{\uparrow} & \gamma_{\alpha}\\ \gamma_{\alpha} & \Gamma_{\alpha}^{\downarrow}\end{pmatrix}.$$

Since we assume all couplings to be real, the Green functions read in symbolic notation

$$G^{\mathrm{R}} = \begin{pmatrix} A & B \\ B & D \end{pmatrix}, \qquad \Sigma^{\mathrm{K}} \sim \begin{pmatrix} \Gamma^{\uparrow} & \gamma \\ \gamma & \Gamma^{\downarrow} \end{pmatrix}, \quad G^{\mathrm{A}} = G^{\mathrm{R}*},$$

and their product is

$$G^{\mathrm{R}}\Sigma^{\mathrm{K}}G^{\mathrm{A}} = \begin{pmatrix} |A|^2\Gamma^{\uparrow} + A\gamma B^* + B\gamma A^* + |B|^2\Gamma^{\downarrow} & A\Gamma^{\downarrow}B^* + A\gamma D^* + |B|^2\gamma + B\Gamma^{\downarrow}D^* \\ B\Gamma^{\uparrow}A^* + |B|^2\gamma + D\gamma A^* + D\Gamma^{\downarrow}B^* & |B|^2\Gamma^{\uparrow} + B\gamma D^* + D\gamma B^* + |D|^2\Gamma^{\downarrow} \end{pmatrix}.$$

We first consider the diagonal elements

$$G^{\mathrm{K}}_{\uparrow\uparrow}(\omega) = \frac{-\imath \sum_\alpha \big(1 - 2f_\alpha(\omega)\big)}{\left|(\omega - \varepsilon_{\mathrm{d}})(\omega - \varepsilon_{\mathrm{d}} + \imath\frac{\Gamma}{2}) - \frac{1}{4}\Delta\right|^2}\left[\left[(\omega - \varepsilon_{\mathrm{d}})^2 + \left(\frac{\Gamma^{\downarrow}}{2}\right)^2\right]\Gamma^{\uparrow}_{\alpha} - \frac{1}{4}\gamma_\alpha\left(\Gamma^{\uparrow} - \Gamma^{\downarrow}\right) + \Gamma^{\downarrow}_{\alpha}\frac{\gamma^2}{4}\right].$$

The element $G^{\mathrm{K}}_{\downarrow\downarrow}$ follows by replacing $\uparrow \leftrightarrow \downarrow$. We use the original definitions of Γ and γ in terms of the coupling constants $t_{\alpha\sigma}$ to reduce the complexity of this expression

$$\begin{aligned} G^{\mathrm{K}}_{\uparrow\uparrow}(\omega) &= \frac{-\imath\sum_\alpha\big(1-2f_\alpha(\omega)\big)}{(\omega-\varepsilon_{\mathrm{d}})^2\left|\omega-\varepsilon_{\mathrm{d}}+\imath\frac{\Gamma}{2}-\frac{\Delta}{4(\omega-\varepsilon_{\mathrm{d}})}\right|^2}\left(\Gamma^{\uparrow}_{\alpha}(\omega-\varepsilon_{\mathrm{d}})^2+\frac{\Delta}{4}\Gamma^{\downarrow}_{\bar\alpha}\right) \\ G^{\mathrm{K}}_{\downarrow\downarrow}(\omega) &= \frac{-\imath\sum_\alpha\big(1-2f_\alpha(\omega)\big)}{(\omega-\varepsilon_{\mathrm{d}})^2\left|\omega-\varepsilon_{\mathrm{d}}+\imath\frac{\Gamma}{2}-\frac{\Delta}{4(\omega-\varepsilon_{\mathrm{d}})}\right|^2}\left(\Gamma^{\downarrow}_{\alpha}(\omega-\varepsilon_{\mathrm{d}})^2+\frac{\Delta}{4}\Gamma^{\uparrow}_{\bar\alpha}\right). \end{aligned}$$

The off-diagonal element of G^{K} is

$$G^{\mathrm{K}}_{\uparrow\downarrow}(\omega) = \frac{-\imath \sum_\alpha \big(1 - 2f_\alpha(\omega)\big)}{(\omega - \varepsilon_{\mathrm{d}})^2\left|\omega - \varepsilon_{\mathrm{d}} + \imath\frac{\Gamma}{2} - \frac{\Delta}{4(\omega-\varepsilon_{\mathrm{d}})}\right|^2}\left(\gamma_\alpha(\omega - \varepsilon_{\mathrm{d}})^2 + \imath\frac{\gamma}{2}(\omega - \varepsilon_{\mathrm{d}})(\Gamma^{\downarrow}_{\bar\alpha} - \Gamma^{\uparrow}_{\bar\alpha}) - \frac{\Delta}{4}\gamma_{\bar\alpha}\right).$$

We add the spectral function and the Keldysh component of the full Green function to obtain $G^{<}(\omega)$, which integrated over the frequencies is the occupation number of the pseudo-spin states.

$$\begin{aligned} G^{<}_{\uparrow\uparrow}(\omega) &= \frac{\sum_\alpha f_\alpha(\omega)}{\left|\omega-\varepsilon_{\mathrm{d}}+\imath\frac{\Gamma}{2}-\frac{\Delta}{4(\omega-\varepsilon_{\mathrm{d}})}\right|^2}\left(\Gamma^{\uparrow}_{\alpha}+\frac{\Delta}{4(\omega-\varepsilon_{\mathrm{d}})^2}\Gamma^{\downarrow}_{\bar\alpha}\right) \\ G^{<}_{\downarrow\downarrow}(\omega) &= \frac{\sum_\alpha f_\alpha(\omega)}{\left|\omega-\varepsilon_{\mathrm{d}}+\imath\frac{\Gamma}{2}-\frac{\Delta}{4(\omega-\varepsilon_{\mathrm{d}})}\right|^2}\left(\Gamma^{\downarrow}_{\alpha}+\frac{\Delta}{4(\omega-\varepsilon_{\mathrm{d}})^2}\Gamma^{\uparrow}_{\bar\alpha}\right) \\ G^{<}_{\uparrow\downarrow}(\omega) &= \frac{1}{\left|\omega-\varepsilon_{\mathrm{d}}+\imath\frac{\Gamma}{2}-\frac{\Delta}{4(\omega-\varepsilon_{\mathrm{d}})}\right|^2}\sum_\alpha\left\{f_\alpha(\omega)\left(\gamma_\alpha-\frac{\Delta}{4(\omega-\varepsilon_{\mathrm{d}})^2}\gamma_{\bar\alpha}\right)-\imath\frac{\gamma}{4}\frac{1-2f_\alpha(\omega)}{(\omega-\varepsilon_{\mathrm{d}})}\left(\Gamma^{\downarrow}_{\bar\alpha}-\Gamma^{\uparrow}_{\bar\alpha}\right)\right\}. \end{aligned}$$

We reduce these results to the expressions we would expect from a master-equation treatment. Since there are many variables of order $\mathcal{O}(H_{\mathrm{T}}^2)$, we adopt the scaling-variable approach from chapter 2.3.1. We rescale the tunnel amplitudes $t_{\alpha\sigma} \mapsto \xi t_{\alpha\sigma}$. Then $\Gamma^{\sigma}_{\alpha} \mapsto \xi^2\Gamma^{\sigma}_{\alpha}$, $\gamma_\alpha \mapsto \xi^2\gamma_\alpha$, and $\Delta \mapsto \xi^4\Delta$. The limit $\xi \to 0$ is performed in the same manner as the previously discussed limit $\Delta \to 0$, such that the weak-coupling result for the

integrated lesser Green function of the two-level resonant tunnelling problem is

$$G^< = \frac{1}{\Gamma}\sum_\alpha f_\alpha(\varepsilon_\mathrm{d})\begin{pmatrix}\Gamma_\alpha^\uparrow+\Gamma_{\bar\alpha}^\downarrow & \gamma_\alpha-\gamma_{\bar\alpha}\\ \gamma_\alpha-\gamma_{\bar\alpha} & \Gamma_\alpha^\downarrow+\Gamma_{\bar\alpha}^\uparrow\end{pmatrix} \tag{4.2.1}$$

Before we continue with the discussion of the master equation for this system, we remark on the discrepancy of the descriptions by either Green functions or density matrices. In contrast to the density matrix, which is a projection onto wave functions, the many-particle methods work with occupation numbers. In the two-level problem, the diagonal matrix elements of $G^<$ are *not* occupation probabilities of the individual levels like they are given by the diagonal elements of the respective density matrix. Due to the definition

$$G^<_{\sigma\sigma} = \langle d_\sigma^\dagger d_\sigma\rangle,$$

there is also a contribution of the two-particle wave function term $|{\uparrow\downarrow}\rangle\langle{\uparrow\downarrow}|$ of the density matrix. The two-particle state has a different wave function than the single-particle states; moreover, $\langle\sigma|\sigma\bar\sigma\rangle = 0$. The number operator n_σ, however, has non-zero and equivalent matrix elements on both $|\sigma\rangle$ and $|\sigma\bar\sigma\rangle$. We thus have the identity

$$G^<_{\sigma\sigma} = \rho_\sigma + p_2,$$

which implies that at least the difference of the diagonal elements of both $G^<$ and ρ are the same

$$G^<_{\uparrow\uparrow} - G^<_{\downarrow\downarrow} = \rho_\uparrow - \rho_\downarrow.$$

The off-diagonal elements of both operators also coincide, $G^<_{\sigma\bar\sigma} = \rho_{\sigma\bar\sigma}$. By interchanging particles and holes, we can compare the probability for neutral and double occupation, p_0 and p_2. For vanishing eV_g, $p_0 = p_2$, for then the non-interacting system is particle-hole symmetric. In the general case, however, $p_2 = \langle d_\sigma^\dagger d_\sigma d_{\bar\sigma}^\dagger d_{\bar\sigma}\rangle$ and $p_0 = \langle(1-d_\sigma^\dagger d_\sigma)(1-d_{\bar\sigma}^\dagger d_{\bar\sigma})\rangle$. And thus $p_0 - p_2 = 1 - \mathrm{Tr}G^<$. Using the solution for the lesser Green function in the weak-coupling limit, Equation (4.2.1), $\mathrm{Tr}G^< = \sum_\alpha f_\alpha(\varepsilon_\mathrm{d})$ and hence

$$p_0 - p_2 = 1 - \sum_\alpha f_\alpha(\varepsilon_\mathrm{d}). \tag{4.2.2}$$

4.2.2 The Master Equation

We use the master equation, which we have derived in chapter 2 and explicitly formulated in appendix B.1, and set the Coulomb-interaction term to zero: $U = 0$. From this point of view on the master equation, we can see, after some reformulation, the immediate effect of the virtual interaction of the two degenerate levels, which is expressed in the off-diagonal element of the self energy, $\Sigma_{\uparrow\downarrow}$. The non-interacting master equation, where we drop the argument of the Fermi function $f_\alpha(\varepsilon_\mathrm{d})$ for notational convenience, because it is only the single-particle energy or the gate voltage, respectively, is

$$\begin{aligned}
\dot p_0 &= -\sum_\alpha f_\alpha\Gamma_\alpha p_0 + \sum_\alpha(1-f_\alpha)(\Gamma_\alpha^\sigma\rho_\sigma + \Gamma_\alpha^{\bar\sigma}\rho_{\bar\sigma} + 2\gamma_\alpha\mathrm{Re}\rho_{\uparrow\downarrow})\\
\dot p_2 &= -\sum_\alpha(1-f_\alpha)\Gamma_\alpha p_2 + \sum_\alpha f_\alpha(\Gamma_\alpha^{\bar\sigma}\rho_\sigma + \Gamma_\alpha^\sigma\rho_{\bar\sigma} - 2\gamma_\alpha\mathrm{Re}\rho_{\uparrow\downarrow})\\
\dot\rho_\sigma &= \sum_\alpha\Big(f_\alpha\Gamma_\alpha^\sigma p_0 + (1-f_\alpha)\Gamma_\alpha^{\bar\sigma}p_2\Big) - \sum_\alpha\Big(f_\alpha\Gamma_\alpha^{\bar\sigma} + (1-f_\alpha)\Gamma_\alpha^\sigma\Big)\rho_\sigma - \sum_\alpha\gamma_\alpha(1-2f_\alpha)\mathrm{Re}\rho_{\uparrow\downarrow}
\end{aligned}$$

$$\dot{\rho}_{\uparrow\downarrow} = \sum_\alpha \Big(f_\alpha \gamma_\alpha p_0 - (1-f_\alpha)\gamma_\alpha p_2 \Big) - \frac{1}{2}\sum_\alpha (1-2f_\alpha)\gamma_\alpha p_1 - \frac{1}{2}\Gamma \rho_{\uparrow\downarrow}.$$

The imaginary part of the density matrix, $\mathrm{Im}\rho_{\uparrow\downarrow}$, does neither couple to the populations ρ_i, nor to the real part of the off-diagonal element $\mathrm{Re}\rho_{\uparrow\downarrow}$. It solves the von Neumann equation

$$\mathrm{Im}\,\dot{\rho}_{\uparrow\downarrow} = -\frac{\Gamma}{2}\,\mathrm{Im}\,\rho_{\uparrow\downarrow}, \tag{4.2.3}$$

with $\mathrm{Im}\rho_{\uparrow\downarrow}(t) = \mathrm{Im}\rho_{\uparrow\downarrow}(0)e^{-\frac{\Gamma}{2}t}$. We are only interested in the stationary state of the reduced density matrix and are thus allowed to assume $\mathrm{Im}\rho_{\uparrow\downarrow}(0) = 0$; hence $\mathrm{Im}\rho_{\uparrow\downarrow}(t) = 0$ for all t is a valid solution.

The Equation for the Stationary State

In the stationary state, $\dot{\rho} = 0$, the left-hand side of the above master equation vanishes identically. The equation for the off-diagonal element of ρ can thus be solved

$$\rho_{\sigma\bar{\sigma}} = \frac{1}{\Gamma}\Big[2\sum_\alpha \gamma_\alpha \big(f_\alpha p_0 - (1-f_\alpha)p_2 \big) - \sum_\alpha (1-2f_\alpha)\gamma_\alpha p_1 \Big].$$

We insert this expression into the master equation and obtain an effective rate equation for the diagonal elements of ρ; however, the rates and hopping processes have a more complicated structure than before. The technique of rewriting the full master equation as an effective rate equation for the populations has been introduced by Gurvitz (1998) in the discussion of serial quantum dots in the high-voltage limit, $eV_{\mathrm{sd}} \to \infty$. The interpretation of the effective rates as rates is difficult. They do have a functional dependence on the voltages that goes beyond that of a Golden-Rule expression. They can also become zero or negative, such that this equation ought to be interpreted more as a balance equation for the probability flow between the states than hopping processes. The equation for example for $\dot{p}_0 = 0$ becomes

$$p_0 \sum_\alpha f_\alpha \left[\Gamma_\alpha - 4\sum_\beta (1-f_\beta)\frac{\gamma_\alpha\gamma_\beta}{\Gamma} \right] + 4p_2 \sum_{\alpha\beta} \left[\frac{(1-f_\alpha)(1-f_\beta)\gamma_\alpha\gamma_\beta}{\Gamma} \right] - \sum_{\nu\alpha} \rho_\nu \left[\Gamma_\alpha^\nu - 2\sum_\beta (1-2f_\beta)\frac{\gamma_\alpha\gamma_\beta}{\Gamma} \right] = 0.$$

This equation describes incoherent tunnelling over the device by adding two coherent tunnelling processes. By the same procedure, a similar equation is obtained for the population of the doubly occupied state, from $\dot{p}_2 = 0$,

$$p_2 \sum_\alpha f_\alpha \left[\Gamma_\alpha - 4\sum_\beta (1-f_\beta)\frac{\gamma_\alpha\gamma_\beta}{\Gamma} \right] + 4p_0 \sum_{\alpha\beta} \left[\frac{(1-f_\alpha)(1-f_\beta)\gamma_\alpha\gamma_\beta}{\Gamma} \right] - \sum_{\nu\alpha} \rho_\nu \left[\Gamma_\alpha^{\bar{\nu}} - 2\sum_\beta (1-2f_\beta)\frac{\gamma_\alpha\gamma_\beta}{\Gamma} \right] = 0.$$

The equation for either charged state, $\dot{\rho}_\sigma = 0$, couples both parts of the pseudo-spin $\rho_\sigma \leftrightarrow \rho_{\bar{\sigma}}$:

$$p_0 \sum_\alpha \left[\Gamma_\alpha^\sigma - 2\sum_\beta (1-2f_\beta)\frac{\gamma_\alpha\gamma_\beta}{\Gamma} \right] + p_2 \sum_\alpha (1-f_\alpha) \left[\Gamma^{\bar{\sigma}} + 2\sum_\beta (1-2f_\beta)\frac{\gamma_\alpha\gamma_\beta}{\Gamma} \right]$$
$$- \rho_\sigma \sum_\alpha \left[f_\alpha \Gamma^{\bar{\sigma}} + (1-f_\alpha)\Gamma_\alpha^\sigma - (1-2f_\alpha)\sum_\beta (1-2f_\beta)\frac{\gamma_\alpha\gamma_\beta}{\Gamma} \right] + \rho_{\bar{\sigma}} \sum_{\alpha\beta} (1-2f_\alpha)(1-2f_\beta)\frac{\gamma_\alpha\gamma_\beta}{\Gamma} = 0.$$

The Pseudo-Bloch Equation

In analogy to the discussion of electronic spin valves by Braun *et al.* (2004), one can describe the dynamics by a rate equation for the populations and a Bloch-equation for the pseudo-spin $\vec{S} = (2\mathrm{Re}\rho_{\uparrow\downarrow}, 2\mathrm{Im}\rho_{\uparrow\downarrow}, \rho_{\uparrow} - \rho_{\downarrow})$. The equation for the populations of the different charge states is[5]

$$\frac{d}{dt}\begin{pmatrix} p_0 \\ p_1 \\ p_2 \end{pmatrix} = \frac{1}{2}\sum_{\alpha}\Gamma_{\alpha}\begin{pmatrix} -2f_{\alpha} & (1-f_{\alpha}) & 0 \\ 2f_{\alpha} & -1 & 2(1-f_{\alpha}) \\ 0 & f_{\alpha} & -2(1-f_{\alpha}) \end{pmatrix}\begin{pmatrix} p_0 \\ p_1 \\ p_2 \end{pmatrix} + \frac{1}{2}\sum_{\alpha}\begin{pmatrix} 1-f_{\alpha} \\ -(1-2f_{\alpha}) \\ -f_{\alpha} \end{pmatrix}\vec{S}\cdot\vec{n}_{\alpha}. \tag{4.2.4}$$

The Bloch-equation for the pseudo-spin is

$$\frac{d}{dt}\vec{S} = \frac{1}{2}\sum_{\alpha}\Big[2f_{\alpha}p_o - (1-2f_{\alpha})p_1 - 2(1-f_{\alpha})p_2\Big]\vec{n}_{\alpha} - \frac{1}{2}\Gamma\vec{S}. \tag{4.2.5}$$

We express the stationary current in terms of the occupations and the pseudo-spin. Since

$$I_{\alpha} = f_{\alpha}\Gamma_{\alpha}p_0 - (1-f_{\alpha})\Gamma_{\alpha}p_2 + f_{\alpha}\Big(\sum_{\nu}\Gamma_{\alpha}^{\bar{\nu}}\rho_{\nu} - 2\gamma_{\alpha}\,\mathrm{Re}\,\rho_{\sigma\bar{\sigma}}\Big) - (1-f_{\alpha})\Big(\sum_{\nu}\Gamma_{\alpha}^{\nu}\rho_{\nu} + 2\gamma_{\alpha}\,\mathrm{Re}\,\rho_{\sigma\bar{\sigma}}\Big),$$

this expression reads in pseudo-spin notation

$$I_{\alpha} = \frac{1}{2}\Gamma_{\alpha}\begin{pmatrix} 2f_{\alpha} \\ -(1-2f_{\alpha}) \\ -2(1-f_{\alpha}) \end{pmatrix}\cdot\begin{pmatrix} p_0 \\ p_1 \\ p_2 \end{pmatrix} - \frac{1}{2}\vec{S}\cdot\vec{n}_{\alpha}.$$

This equation shows the influence of the alignment of the pseudo-spin on the magnitude of the stationary current. If $\sum_{\alpha}\vec{S}\cdot\vec{n}_{\alpha} = 0$, the current would only be determined by the populations of the nanostructure. Moreover, since $S_z = \rho_{\uparrow} - \rho_{\downarrow}$ and in the non-interacting model $S_y = 0$, the influence of the off-diagonal elements of ρ is only encoded in the x-component of the pseudo-spin.

4.2.3 The Diagonal Basis

In the final section of this chapter, we join the two paths leading to the description of the non-interacting two-level quantum dot: the Keldysh method, which provides the exact solution for the stationary transport problem in terms of expectation values of the number operators, and the weak-coupling master equation, which in its pseudo-spin formulation allows an intuitive perception of its physics. We use the Keldysh result to find the diagonal basis of the density matrix, which transforms the master equation into a rate equation for the populations. The stationary integrated lesser Green function of the problem in the weak-coupling limit is, according to the calculations of section 4.2.1,

$$G^{<} = \frac{1}{\Gamma}\sum_{\alpha}f_{\alpha}(\varepsilon_{\mathrm{d}})\begin{pmatrix} \Gamma_{\alpha}^{\uparrow} + \Gamma_{\bar{\alpha}}^{\downarrow} & \gamma_{\alpha} - \gamma_{\bar{\alpha}} \\ \gamma_{\alpha} - \gamma_{\bar{\alpha}} & \Gamma_{\alpha}^{\downarrow} + \Gamma_{\bar{\alpha}}^{\uparrow} \end{pmatrix}. \tag{4.2.1}$$

The two addends of the sum over the lead index α commute and therefore admit a common eigenbasis. Although the lesser Green function is not the reduced density matrix but rather $G^{<} = \rho + p_2\mathrm{Id}$, we are still

[5] See appendix B.2 for the full equation, of which this is the non-interacting version.

allowed to use the linear algebra of $G^<$ to determine the eigenbasis of ρ, because by definition also $G^<$ and ρ commute. The unitary transformation that maps the states $|\uparrow\rangle$ and $|\downarrow\rangle$ into the eigenbasis $|\pm\rangle$ is

$$\begin{pmatrix} + \\ - \end{pmatrix} := V \begin{pmatrix} \uparrow \\ \downarrow \end{pmatrix} := \frac{1}{\sqrt{2d}} \begin{pmatrix} \sqrt{d+b} & \sqrt{d-b} \\ -\sqrt{d-b} & \sqrt{d+b} \end{pmatrix} \begin{pmatrix} \uparrow \\ \downarrow \end{pmatrix},$$

where the coefficients a, b, and d are defined by

$$a := \gamma_\alpha - \gamma_{\bar{\alpha}}, \quad b := \Gamma_\alpha^\uparrow + \Gamma_{\bar{\alpha}}^\downarrow - (\Gamma_\alpha^\downarrow + \Gamma_{\bar{\alpha}}^\uparrow), \quad d^2 := 4a^2 + b^2.$$

The transformation of the reduced density matrix follows immediately

$$\begin{aligned} \rho_\uparrow &= \frac{1}{2d}\big((d+b)\rho_+ + (d-b)\rho_- - 4a\,\mathrm{Re}\rho_{+-}\big) \\ \rho_\downarrow &= \frac{1}{2d}\big((d-b)\rho_+ + (d+b)\rho_- + 4a\,\mathrm{Re}\rho_{+-}\big) \\ \mathrm{Re}\rho_{\uparrow\downarrow} &= \frac{1}{2d}\big(2a(\rho_+ - \rho_-) + 2b\,\mathrm{Re}\rho_{+-}\big). \end{aligned}$$

Since the transformation V is unitary, the trace of the density matrix is the same in both coordinate systems. The y-component of the pseudo-spin is irrelevant for the dynamics and therefore omitted: here, our notation is compressed to $\vec{S} = (S_x, S_y)$. Under V, the pseudo-spin transforms according to

$$\vec{S}_\mathrm{d} := V\vec{S} := \frac{1}{d}\begin{pmatrix} b & -2a \\ 2a & b \end{pmatrix}\vec{S}.$$

Using these transformations, we are able to show that the master equation collapses into a rate equation. We consider the pseudo-Bloch equation and show that the equation for the populations is actually independent of $\mathrm{Re}\rho_{+-}$. Then, similarly to the argument for setting $S_y = 0$, $S_x = 0$ is a valid solution for the reduced dynamics, which then only depends on the populations of the states without admitting coherent superpositions. The invariance of the scalar product under a unitary transformation implies

$$\vec{S}\cdot\vec{n}_\alpha = (V^{-1}\vec{S}_\mathrm{d})\cdot\vec{n}_\alpha = \vec{S}_\mathrm{d}\cdot V\vec{n}_\alpha =: \vec{S}_d\cdot\vec{n}_\alpha^\mathrm{d}.$$

The pseudo-magnetisation $\vec{n}_\alpha$ in the diagonal basis is

$$\vec{n}_\alpha^\mathrm{d} = \frac{1}{d}\begin{pmatrix} 2\big(b\gamma_\alpha - a(\Gamma_\alpha^\uparrow - \Gamma_\alpha^\downarrow)\big) \\ 4a\gamma_\alpha + b(\Gamma_\alpha^\uparrow - \Gamma_\alpha^\downarrow) \end{pmatrix} =: \frac{1}{d}\begin{pmatrix} 2\sum_\beta \gamma_\beta(\Gamma_{\bar{\beta}}^\downarrow - \Gamma_{\bar{\beta}}^\uparrow) \\ 4a\gamma_\alpha + b(\Gamma_\alpha^\uparrow - \Gamma_\alpha^\downarrow) \end{pmatrix}.$$

The eigenbasis of $G^<$ is defined by the property that the projection of $\vec{n}_\alpha$ onto the x-axis of the eigenbasis is independent of α. The equation for the x-component in the pseudo-Bloch equation (4.2.5) is, also due to the normalisation $p_0 + p_1 + p_2 = 1$,

$$\begin{aligned} \Gamma S_x &= \sum_\alpha \Big[2f_\alpha p_0 - (1-2f_\alpha)p_1 - 2(1-f_\alpha)p_2\Big]\big(\vec{n}_\alpha^\mathrm{d}\big)_x \\ &= 2\Big[p_0 - p_2 - 1 + \sum_\alpha f_\alpha\Big]\big(\vec{n}_\alpha^\mathrm{d}\big)_x = 0. \end{aligned}$$

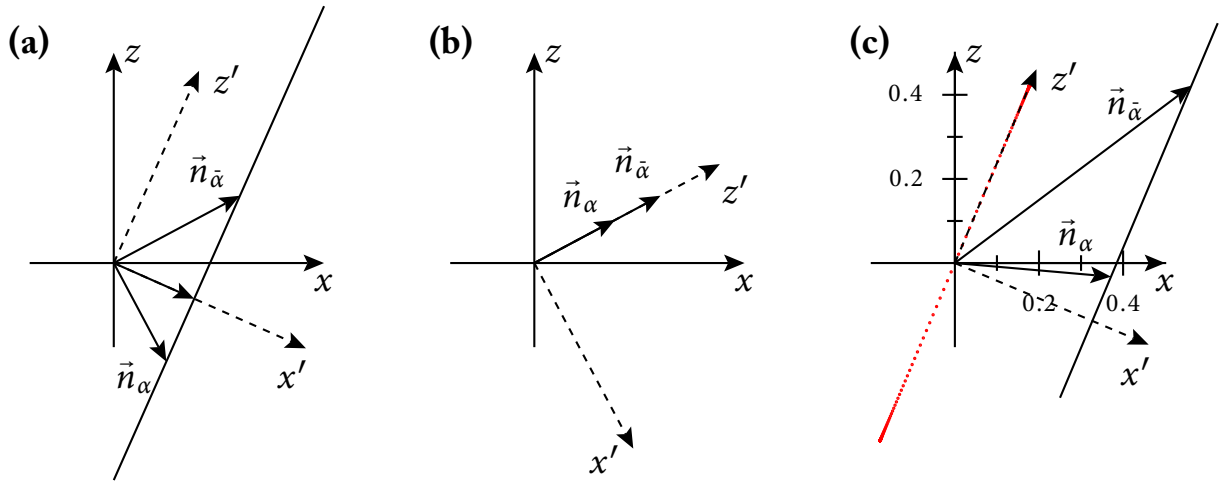

Figure 4.1: Geometric construction of the diagonal system of the stationary reduced density matrix in pseudo-spin space. The pseudo-spin aligns parallel to a line that connects the tips of the pseudo-magnetisations $\vec{n}_\alpha$. The diagonal system is rotated such that the pseudo-spin is along the z'-axis and has no x'-component, which renders the master equation a rate equation. In Figure (a) a rather general choice of tunnel amplitudes is shown; in Figure (b) the case of parallel magnetisations shows that in the eigensystem, the pseudo-magnetisations are parallel to the z'-axis, which is also the axis along which the pseudo-spin aligns. (c) Numerical results for the evolution of the pseudo-spin while sweeping the bias voltage from −5 to 5. The tunnel amplitudes are $t_{\mathrm{L}\uparrow} = 1.1$, $t_{\mathrm{L}\downarrow} = 1.2$, $t_{\mathrm{R}\uparrow} = 2$, and $t_{\mathrm{R}\downarrow} = 1$. The red line drawn by the pseudo-spin is parallel to the z'-axis of the rotated (and rescaled) coordinate system.

The last equality, the vanishing of the bracket and thus S_x itself, is a property of the stationary solution of the problem, which we have obtained in the Keldysh analysis, Equation (4.2.2), $p_0 - p_2 = 1 - \sum_\alpha f_\alpha$.

We have thus found, by a discussion of the Keldysh Green functions in the weak-coupling limit, the diagonal basis of the reduced density matrix. This diagonal basis is that basis, in which the stationary master equation assumes the form of a rate equation. Without interactions, be it electron–electron or electron–phonon interaction, this basis is independent of the external parameters, that is both the bias and the gate voltage. The plot of a numerical simulation in Figure 4.1 (c) shows this behaviour clearly. The trace of the pseudo-spin is a straight line through the origin; its slope is what is expected from the criterion on the pseudo-magnetisations in the eigensystem, we have established above.

The results from the combined analysis of Green functions and master equation lead to a graphical construction of the diagonal system of ρ. From the perspective of pseudo-Bloch equations, this seems most natural: the pseudo-spin $\vec{S}$ aligns parallel to the z'-axis of a coordinate system, whose x'-axis is oriented such that the projections of the magnetisations onto this axis are equal. In Figure 4.1, we show several thus constructed coordinate systems. Diagram (a) is a rather general choice of pseudo-magnetisations. Diagram (c) shows the numerically evaluated pseudo-spin aligning along the z'-component of the eigensystem. Diagram (b) shows the construction for $n_\alpha \uparrow\uparrow n_{\tilde{\alpha}}$, which corresponds to that line in parameter space on which the Hamiltonian can be rotated into a single impurity scattering problem plus an isolated electronic level. When $\Delta = 0$, that is there is some number ζ being independent of α such that, $t_{\alpha\downarrow} = \zeta t_{\alpha\uparrow}$,

$$\vec{n}_\alpha = \Gamma_\alpha^\uparrow \begin{pmatrix} 2\zeta \\ 0 \\ (1-\zeta^2) \end{pmatrix} \quad \text{and} \quad \vec{n}_{\tilde{\alpha}} = \Gamma_{\tilde{\alpha}}^\uparrow \begin{pmatrix} 2\zeta \\ 0 \\ (1-\zeta^2) \end{pmatrix}$$

and both magnetisations are parallel. Then the geometric alignment and the normalisation $|\vec{n}_\alpha| = \Gamma_\alpha = (1+\zeta^2)\Gamma_\alpha^\uparrow$ imply in the eigensystem of the stationary reduced density matrix

$$\vec{n}_\alpha^{\,\mathrm{d}} = (0, 0, \Gamma_\alpha).$$

The x'-components of the magnetisations in the eigensystem are not only equal, but they are zero. Since $S_z = \rho_\uparrow - \rho_\downarrow$ and $p_1 = \rho_\uparrow + \rho_\downarrow$ the occupation probabilities in terms of the pseudo-spin components are $\rho_{\uparrow/\downarrow} = \frac{1}{2}(p_1 \pm S_z)$. Then the master equation for $\rho_\uparrow$ and $\rho_\downarrow$ in the eigenbasis reads

$$\begin{aligned}
\frac{d}{dt}(p_1 \pm S_z) &= \frac{1}{2}\sum_\alpha \Gamma_\alpha \big(2f_\alpha p_0 - p_1 + 2(1-f_\alpha)p_2 + (1-2f_\alpha)S_z\big) \\
&\quad \mp \frac{1}{2}\sum_\alpha \Gamma_\alpha \big(2f_\alpha p_0 - (1-2f_\alpha)p_1 - 2(1-f_\alpha)p_2 + S_z\big) \\
&= \begin{cases} 2\sum_\alpha \Gamma_\alpha f_\alpha p_0 - \sum_\alpha \Gamma_\alpha f_\alpha (p_1 + S_z) & \text{for } + \\ 2\sum_\alpha \Gamma_\alpha (1-f_\alpha) p_2 - \sum_\alpha \Gamma_\alpha (1-f_\alpha)(p_1 - S_z) & \text{for } - \end{cases}
\end{aligned}$$

Choosing the plus sign, this equation reduces to the rate equation of the single-level resonant tunnelling problem. Choosing the minus sign instead, the equation becomes a resonant tunnelling problem that switches between singly and doubly occupied states of the quantum dot. In this case, there is one state that is always occupied but does not take part in the tunnelling dynamics, which is a picture fully consistent with the decoupling property of the full Hamiltonian.

Chapter 5

The Master Equation

In the previous chapter, we have analysed the transport theory of a non-interacting resonant tunnelling model with two degenerate levels from two different points of view, an exact Keldysh treatment and the weak-coupling limit using a master equation. We have shown how the asymmetric coupling of the device to the conducting electrodes uniquely determines the diagonal basis of the reduced density matrix and that this basis is independent of the applied voltages. The simplicity of this result relies on the absence of any interaction in the model. In the field of molecular electronics, interactions are of two fundamentally different types: electron–electron interactions, which is essentially Coulomb-repulsion, and electron–phonon interactions, which are a conceptual extension of the resonant tunnelling model to single-molecule junctions and thus constitute their defining property. Electron–phonon interactions not only give rise to inelastic transitions when a tunnelling electron excites internal vibrations, but due to the renormalisations of the Hamiltonian by the polaron transformation, they also induce an effective electron–electron interaction, which, depending on the molecular model, can be attractive or repulsive. Models for single-molecule junctions have a generic electron–electron interaction, $U \neq 0$. In our treatment, we therefore always include a repulsive Coulomb interaction in the model. The steady-state transport phenomenology will roughly distinguish two regimes: vibronic excitations below the double charging threshold, defined by the charging energy U, where the system's physics will be determined by the electron–electron interaction, and excitations above the double charging threshold, where the current–voltage characteristics are similar to those of a non-interacting, $U = 0$, system.

The direct formal consequence of interactions in the transport problem is that the y-component of the pseudo-spin cannot be set to zero in the master equation; it does not decouple from the populations like in Equation (4.2.3). The pseudo-Bloch dynamics will take place in the full three-dimensional unit ball. The y-component of the pseudo-spin couples to the x-component and the populations via the principal-value integrals that define pseudo-magnetic fields in the pseudo-Bloch equations of appendix B.2. These integrals, which are the imaginary parts of the bath correlation function (Breuer & Petruccione, 2002, p. 135), are due to the *continuum* of bath states and both types of the aforementioned *interactions*. We therefore expect more complicated pseudo-spin dynamics than in the non-interacting quantum dot, where this dynamics essentially is the motion along a line in the (x,z)-plane of the pseudo-spin components when the bias voltage is swept. The slope of this line is uniquely determined by the pseudo-magnetisations of the electrodes, hence the tunnel amplitudes $t_{\alpha\sigma}$. In contrast to the non-interacting resonant tunnelling model, where the effect of the system's multi-level structure on the stationary current profile is only of quantitative nature, the

models for single-molecule junctions discussed in this chapter will show physics being qualitatively different from the rate-equation treatment. The pseudo-magnetic field induces a precession of the pseudo-spin in the time-dependent dynamics and thus cause processes *inside* the singly charged sector of the reduced density matrix. The new dynamics is extending the physics of rate equations: it consists of processes that do neither involve a change in the electron number of the device nor do they modify the vibronic quantum number, as they only mediate between the degenerate electronic states.

In this chapter, we shall first present the two generic molecular models and their properties under unitary transformations in the electronic Hilbert space $\mathcal{H}_{\mathrm{el}}$. These will turn out to be of general interest as the discussion in chapter 4 has shown that certain choices of the tunnel amplitudes $t_{\alpha\sigma}$ in H_{T} reduce the complexity of the problem by decoupling single levels from both of the conducting electrodes. We shall see that the notion of decoupling single levels from single electrodes is of paramount importance for understanding the physics of the degenerate master equation. The generic behaviour below the double-charging threshold is discussed by stripping the model of all its vibronic structure and considering a two-level interacting quantum dot only. The effect of the coherent dynamics, a suppression of the stationary current and the non-trivial deformation of the differential conductance peaks along with regions of strong negative differential conductance will be most clear in such a treatment. In a second step, we shall analyse the role of the pseudo-magnetic fields, the Coulomb interaction, and the vibronic level structure for the stationary transport properties. Most of the new phenomenology will be restricted to the low-lying vibrational excitations, except for strong electron–phonon coupling, where it is the also highly excited states that are affected by the intrinsic pseudo-spin dynamics. The discussion of the $E\otimes b$ Jahn–Teller molecule, which will take place in the last but one section of this chapter, will show how the breaking of the rotational symmetry of the full Hamiltonian in the electronic Hilbert space removes the generality of the previously discussed physics from the model. The parameter space will develop regions of completely different phenomenology. For certain couplings, the effects of the degenerate level structure will be striking, for others the transport properties will hardly differ from a rate-equation treatment. Motivated by recent transport measurements on suspended carbon nanotubes, we conclude the chapter by generalising our findings to systems with electronic multi-mode reservoirs.

5.1 Electron–Phonon Coupling and Polaron Transformation

Our model of a single-molecule junction with electronic degeneracies is the generalisation of the spinless Anderson–Holstein model, which has been introduced in chapter 1.2 and has been used throughout most of chapter 3:[1]

$$H_{\mathrm{S}} = (\varepsilon_{\mathrm{d}} + eV_{\mathrm{g}})(n_\uparrow + n_\downarrow) + Un_\uparrow n_\downarrow + \hbar\omega b^\dagger b + H_{\mathrm{el-ph}}.$$

The generic form of a linear electron–phonon coupling is

$$H_{\text{el-ph}} = \hbar\omega(b^\dagger + b)\frac{1}{2}\sum_{\sigma\tau} d_\sigma^\dagger d_\tau \lambda_{\sigma\tau} = \hbar\omega(b^\dagger + b)\left(\lambda_0 \mathrm{Id} + \sum_i \lambda_i \sigma_i\right),$$

where we adopt the pseudo-spin notation from the previous chapter using Pauli matrices σ_i. Since the system is assumed to be degenerate in the electronic Hilbert space $\mathcal{H}_{\mathrm{el}}$, we can diagonalise the electron–phonon

[1] In general, we shall set $\varepsilon_{\mathrm{d}} = 0$ as it only renormalises the gate voltage. We nonetheless keep it in this section to illustrate the renormalisations of the energies by the polaron transformation.

coupling matrix

$$H_{\text{el-ph}} = \lambda\hbar\omega(b^\dagger + b)(\lambda_0 \mathrm{Id} + \lambda_z\sigma_z).$$

Due to the polaron transformation, the energies of the bare electronic levels will be shifted by $(\lambda_0 \pm \lambda_z)^2$, the polaron-shift. In the polaron picture, which is the starting point for the derivation of a weak-coupling theory, degeneracy of the on-site levels is only guaranteed for either λ_0 or λ_z being zero. If not, the theory will either result in a rate-equation treatment as the large energy differences will trigger the decoupling of coherences due to the rotating-wave approximation or, if the coupling constants are small enough, in a theory that is able to catch near-degeneracies. Such a theory will be the central focus of chapter 6.

The electron–phonon coupling we shall be concerned with in this chapter is thus

$$H_{\text{el-ph}} = \lambda\hbar\omega(b^\dagger + b)(n_\uparrow \pm n_\downarrow).$$

Choosing the plus sign, we obtain the simplest generalisation of the Anderson–Holstein molecule to two electronic levels. We refer to this model as the "Anderson–Holstein molecule" in the following.[2] The minus sign, on the contrary, makes the electron–phonon coupling that of an $E\otimes b$ Jahn–Teller effect. This flavour of the Jahn–Teller effect is a simplified version of the $E\otimes(b_1+b_2)$ Jahn–Teller effect, which, as it is shown in appendix D, arises as the second possible decomposition of the degenerate E^2 term besides the $E\otimes e$ effect. Bersuker & Polinger (1989) discuss the $E\otimes(b_1+b_2)$ model in their chapter 3.2.1. If the frequency of the second harmonic oscillator becomes very large, such that only its vibrational ground state contributes to the tunnelling dynamics, this oscillator becomes irrelevant and thus leads to the notion of the $E\otimes b$ Jahn–Teller effect, with two electronic levels being linearly coupled to a single oscillator mode only.

The electronic reservoirs are the usual free Fermi-gas electrodes without electronic spin, and the tunnelling part of the Hamiltonian is the same as in the two-level resonant tunnelling model of chapter 4,

$$H_{\mathrm{T}} = \sum_{\boldsymbol{k}\alpha\sigma} t_{\alpha\sigma} c^\dagger_{\boldsymbol{k}\alpha} d_\sigma + \text{h.c.}$$

For notational convenience, because we shall use and discuss many different points and regions in the parameter space of H_{T}, we define the tuple $\boldsymbol{\Gamma} := \left(\Gamma^\uparrow_{\mathrm{L}}, \Gamma^\downarrow_{\mathrm{L}}, \Gamma^\uparrow_{\mathrm{R}}, \Gamma^\downarrow_{\mathrm{R}}\right)$ to refer to the chosen tunnel couplings.[3] The elimination of the linear electron–phonon interaction in the full Hamiltonian H is achieved by a generalisation of the polaron transformation from one to two electronic levels. The transformation of the oscillator's operators is

$$b \mapsto b - \sum_\sigma \lambda_\sigma n_\sigma.$$

The free oscillator's Hamiltonian and the electron–phonon interaction become

$$\hbar\omega b^\dagger b + \hbar\omega(b^\dagger + b)\sum_\sigma \lambda_\sigma n_\sigma \mapsto \hbar\omega b^\dagger b - \hbar\omega\left(\sum_\sigma \lambda_\sigma n_\sigma\right)^2.$$

[2] Although, we have used the terms Anderson–Holstein molecule and Jahn–Teller molecule before to name different models, we shall use them nonetheless for notational convenience. There will be no ambiguity, as we do not discuss single-level models in this chapter.

[3] Note that the Γ's are the bare Golden-Rule rates and not the tunnel couplings $t_{\alpha\sigma}$ of the tunnelling Hamiltonian. Since they only differ by numerical factors and the square, we do, however, use the Γ's as the reference and therefore call them coupling constants or tunnel couplings. Due to our numerical implementation being in terms of $t_{\alpha\sigma}$, most of the numerical tunnel couplings that we are using will appear as squares.

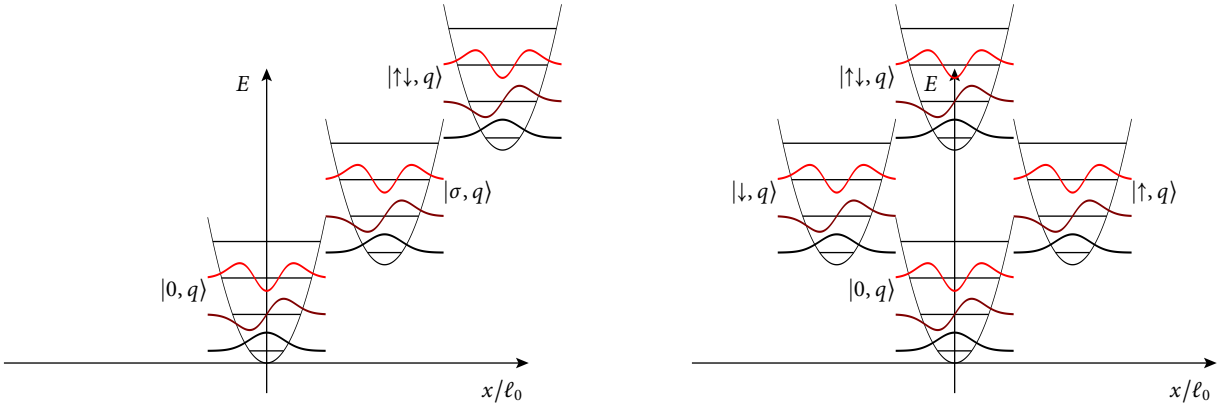

Figure 5.1: Adiabatic potentials of the molecular models considered in this chapter in units of the oscillator length $\ell_0 = \sqrt{\hbar/\omega}$ in the polaron picture. Anderson–Holstein molecule (left) and the $E\otimes b$ Jahn–Teller molecule (right) after the polaron transformation. The first three vibronic wave functions are indicated in order to visualise the dependence of their overlap integrals on the involved electronic states in the Jahn–Teller case.

Distributing the contributions proportional to n_σ to a renormalisation of the single-particle energies and the product term to a renormalisation of the Coulomb interaction, the renormalisation of the physical quantities is[4]

$$\varepsilon_\mathrm{d} \mapsto \varepsilon_\mathrm{d} - \lambda^2\hbar\omega, \quad U \mapsto U - 2\,\mathrm{sgn}(\lambda_\uparrow\lambda_\downarrow)\lambda^2\hbar\omega, \text{ and } \quad t_{\alpha\sigma} \mapsto t_{\alpha\sigma}e^{-\lambda_\sigma(b^\dagger - b)}.$$

The shift of the single-particle energies can be absorbed in a global shift of energy and hence a mere renormalisation of the gate voltage eV_g. The renormalisation of the charging energy U can pose a problem in the Anderson–Holstein case, because due to the possible presence of two electrons on the molecule, an initially non-interacting system acquires a negative charging energy. Quantum transport through nanostructures with negative U and thus attractive Coulomb interaction are discussed in Koch *et al.* (2007). The problem of negative U is not present in the Jahn–Teller molecule, as there the shift is positive: $-\mathrm{sgn}(\lambda_\uparrow\lambda_\downarrow) = 1$. The polaron transformation is usually interpreted as a displacement of the adiabatic potentials for the vibronic degrees of freedom, see Figure 5.1. Occupying a Jahn–Teller molecule with two electrons amounts to shifting the potential once in one direction and then back. The adiabatic potential of the two-electron state is the same as the potential of the neutral one only shifted in energy by $2\varepsilon_\mathrm{d} + U$. Hence in the two-particle state the total renormalisation of ε_d and U due to the unitary transformation is zero. If, in order to compare to the Anderson–Holstein case, it is split into contributions to ε_d and U, the renormalisation of U is *positive*. The Jahn–Teller effect induces a repulsive interaction between the electrons in the polaron picture, and the case of negative U need not be considered here.

5.2 Decoupling of an Electronic Level

For specific choices of the tunnel couplings $t_{\alpha\sigma}$, the Hamiltonian can be further simplified. In the previous chapter, such simplifications have occurred in the sense that the actual two-level problem reduced to an effective single-level problem whenever the coupling constants met certain conditions, namely a vanishing

[4] We set $\lambda := |\lambda_\sigma|$ for notational convenience.

determinant of the non-interacting self energy. On the level of the full Hamiltonian this condition can also be implemented using unitary transformations in $\mathcal{H}_{\mathrm{el}}$; however, due to the polaron transformation, there is additional vibronic structure in the tunnelling Hamiltonian.

The two electronic levels of the molecule are degenerate, and as such any linear combination of the two ought to be a solution of the Schrödinger equation. We look for distinguished bases of the electronic Hilbert space in which the problem takes a manageable form. Glazman & Raikh (1988) use such an approach to transform a system initially coupled to two electrodes into one that is only coupled to a single electrode and then show the existence of a Kondo effect in that problem. Crucial in their case is the condition of zero bias, which amounts to the energetic degeneracy of the two electronic leads. We proceed in the same fashion, only transforming the system's levels instead of the electrodes', a variation of the theme, which is also used for instance in Shahbazyan & Raikh (1994) or more generally in Berkovits *et al.* (2004). We apply a unitary transformation in the two-dimensional complex vector space $\mathcal{H}_{\mathrm{el}}$ spanned by the operators $d_\uparrow$ and $d_\downarrow$,

$$d_+ := \cos\theta d_\uparrow + e^{\imath\varphi}\sin\theta d_\downarrow \quad \text{and} \quad d_- := -e^{-\imath\varphi}\sin\theta d_\uparrow + \cos\theta d_\downarrow.$$

All parts of the Hamiltonian except the tunnelling are invariant under this transformation. The tunnelling Hamiltonian H_{T} becomes

$$H_{\mathrm{T}} = \sum_{k\alpha} c^\dagger_{k\alpha}\big((t_{\alpha\uparrow}\cos\theta + t_{\alpha\downarrow}e^{\imath\varphi}\sin\theta)d_+ + (t_{\alpha\downarrow}\cos\theta - t_{\alpha\uparrow}e^{-\imath\varphi}\sin\theta)d_-\big) + \mathrm{h.c.} \tag{5.2.1}$$

If the condition $t_{\alpha\downarrow}\cos\theta = t_{\alpha\uparrow}e^{-\imath\varphi}\sin\theta$ is fulfilled for every α, the second term in Equation (5.2.1) will vanish, and the system will only couple the state d_+ to the electrodes, thus reducing it to an effective single-level system with tunnelling matrix elements $\left|t^{\mathrm{eff}}_\alpha\right|^2 = |t_{\alpha\uparrow}|^2 + |t_{\alpha\downarrow}|^2$. In the case of scalar couplings, that is a system without phonons, this condition, which we call the *decoupling condition*, reads

$$\varphi = \arg\frac{t_{\alpha\uparrow}}{t_{\alpha\downarrow}} \quad \text{and} \quad \theta = \arctan\frac{|t_{\alpha\downarrow}|}{|t_{\alpha\uparrow}|}, \tag{5.2.2}$$

being independent of α. For real[5] $t_{\alpha\sigma}$, this condition is exactly the condition $\Delta \propto \det(\Sigma) = 0$ of chapter 4. Applied to the transport problem through a single-molecule junction, this condition being satisfied would reduce all the coherent dynamics due to the degenerate two-level structure to the rate-equation transport problem of a single-level Anderson–Holstein molecule. For generic tunnel couplings, which do not fulfil the decoupling condition (5.2.2), one can fix one particular electrode α and apply the unitary transformation with the thus defined φ_α and θ_α. This suffices to decouple the electronic level $|-\rangle$ from electrode α. Hence without satisfying the decoupling condition, the generic tunnel coupling $\mathbf{\Gamma}$ has at least one zero entry.

Including phonons in the model, we have to distinguish the Anderson–Holstein and the Jahn–Teller case; for their decoupling properties are different. We assume arbitrary real tunnel amplitudes $t_{\alpha\sigma}$ and choose α to be either the source or the drain electrode. We then define the unitary transformation with angles according to Equation (5.2.2), $\tan\theta = t_{\alpha\downarrow}/t_{\alpha\uparrow}$. For the particular electrode α, the second term in Equation (5.2.1) then reads

$$c^\dagger_{k\alpha} t_{\alpha\downarrow}\cos\theta\,(e^{-\lambda_\downarrow(b^\dagger - b)} - e^{-\lambda_\uparrow(b^\dagger - b)})d_-. \tag{5.2.3}$$

The electron-phonon coupling of the Anderson–Holstein molecule is characterised by the condition $\lambda_\uparrow = \lambda_\downarrow$

[5] In this chapter, we always assume real $t_{\alpha\sigma}$, which means $\varphi = 0$.

thus rendering the term (5.2.3) zero. In the decoupling regime, this term is zero for both values of α, that is for both electrodes; such a molecule is equivalent to a single-level molecule.

The Jahn–Teller molecule has $\lambda_\uparrow = -\lambda_\downarrow$ making a detailed discussion of the matrix-valued tunnel amplitudes necessary. Transforming the molecular Hamiltonian into the polaron picture corresponds to shifting the adiabatic potential of the oscillator by $\sqrt{2}\lambda_\sigma \ell_0$, where ℓ_0 is the oscillator length, $\ell_0 = \sqrt{\hbar/\omega}$. The element of the Franck–Condon matrix at row q and column q' is the overlap integral of the original vibrational state q' with the shifted oscillator's state q—the scalar product of the displaced and the undisplaced wave function. Compared to the Anderson–Holstein model, in the Jahn–Teller molecule the adiabatic potential of the electronic state $|\uparrow\rangle$ is shifted to the opposite side of the adiabatic potential of $|\downarrow\rangle$. The modulus of the matrix elements is independent of the direction of the shift; however, the sign is not. A transition between states that differ by an even number of excited oscillator quanta is independent of the direction of the displacement, because the wave functions have the same parity, and their scalar product is symmetric under a parity transformation. Such a parity transformation $x \mapsto -x$ is equivalent to reversing the direction of the displacement due to the polaron transformation. A transition involving an odd number of excitations, $|q-q'| = 2k+1$, is sensitive to the direction of the shift, because the parity of the scalar product of the initial and final state is different. In the matrix $e^{\lambda(b^\dagger - b)} - e^{-\lambda(b^\dagger - b)}$, only the matrix elements belonging to excitations of an even number of oscillator quanta cancel. In the pre-factor of d_+, the matrix $t_{\alpha\uparrow}\cos\theta e^{-\lambda(b^\dagger - b)} + t_{\alpha\downarrow}\sin\theta e^{\lambda(b^\dagger - b)}$, there are no cancellations expected. Only in the case of equal coupling, $t_{\alpha\sigma} = 1$ for all α and σ, the matrix elements for excitations of an odd number of quanta cancel in this matrix. In that special case, the Hamiltonian decouples transitions with an even number of excited quanta, $|q-q'| = 2k$, from d_- and all transitions with $|q-q'| = 2k+1$ from d_+. The system decouples into two independent subsystems with disjoint spectra, each of which could be treated by rate equations in the weak-coupling limit, because the decoupling also removes the degeneracy in each subsystem. As simple and tempting such a configuration and a treatment by rate equations may seem, the resulting system of equations cannot be solved uniquely.

5.3 Anderson–Holstein Molecules

The behaviour of the system at energies below the first vibronic sideband can be understood by considering a quantum nanostructure without phonons or with just one excited vibronic level. This simplifies the equations drastically. We split the treatment into two more instances: we first analyse the numerics for a master equation without the principal-value terms. The thus obtained equations are much easier to understand than the full equations, albeit they miss a vital part of the dynamics and as such should be considered unphysical. In the second step, we include the principal-value terms, which in the pseudo-Bloch description for the pseudo-spin of the degenerate two-level system of appendix B.2 define pseudo-magnetic fields. Most often the result will be a mere regularisation or smoothing of the result without principal values. There are some cases, for example very large charging energy, where the principal-value integral significantly influence the numerical results driving the phenomenology towards the one already seen in rate-equation treatments of the problem.

The electron–phonon coupling of the Anderson–Holstein molecule is proportional to the unit matrix in the degenerate electron space $\mathcal{H}_{\mathrm{el}}$. For every choice of basis of the degenerate electrons, the electron–phonon coupling is the same, because by such transformations only the tunnelling Hamiltonian is affected. We fix the charging energy between the first and the second vibronic sideband, $U = 2.35\hbar\omega$, such that we

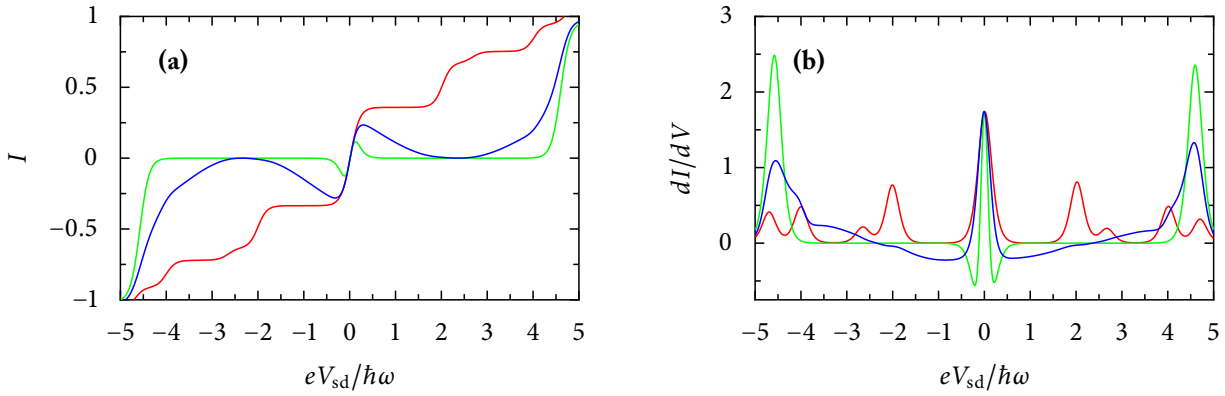

Figure 5.2: Generic behaviour of the Anderson–Holstein molecule at zero gate voltage with parameters $U = 2.35\hbar\omega$, $k_B T = 0.05\hbar\omega$, $\lambda = 1.1$, and couplings $\mathbf{\Gamma} = (1, 1.5^2, 1.1^2, 1.6^2)$. (a) Stationary Current I, (b) differential conductance dI/dV. The colour code is Red: rate equations, Green: master equation without principal-value terms, Blue: master equation with principal-value integrals. The rate-equation treatment shows the expected spectroscopy of the molecular Hamiltonian. The master equation without principal-value terms describes a system that is non-conducting between zero bias and the double-charging threshold $eV_{sd} = 2U$. The principal-value terms partially restore a finite current and smooth the current suppression on an energy scale, which is independent of $k_B T$.

can observe vibronic effects both with and without double occupation, and we set the temperature to $k_B T = 0.05\hbar\omega$. We always contrast the numerical master-equation result with the one obtained from a rate-equation description of the same system. Although *prima facie* such a treatment is an uncontrolled simplification of the problem, it gives some insight into the physics of the coherent dynamics. It will be an important result of chapter 6 to give a physical meaning of the rate-equation description of degenerate nanostructures as being the proper treatment for near-degenerate systems with energy differences much larger than the tunnelling-induced energy scale.

The numerical results for the stationary current and the differential conductance for a typical coupling $\mathbf{\Gamma}$ are shown in Figure 5.2. As it is expected, the rate equation (red) shows a spectroscopic picture of the different elastic and inelastic transitions of the molecule. At zero bias, there is the elastic transition $|0,q\rangle \to |\sigma,q\rangle$. At $eV_{sd} = 2n\hbar\omega$, we see the inelastic vibrational transitions $|0,q\rangle \to |\sigma,q+n\rangle$. At the double-charging threshold $eV_{sd} = 2U$, the two-particle excitation peak $|\sigma,q\rangle \to |\sigma\bar{\sigma},q\rangle$ is visible, and at $eV_{sd} = 2U - n\hbar\omega$, there is a peak from the transition $|\sigma\bar{\sigma},q\rangle \to |\sigma,q+n\rangle$, where Coulomb energy is converted into vibronic energy. The master equation (green and blue), on the contrary, shows a much less intuitive behaviour. The spectral resonances are smeared out or completely suppressed, there is a negative differential conductance peak close to zero bias, also at certain voltages, there is no current flowing through the device at all. Most importantly, there is a significant difference between the treatment with principal-value terms (blue) and without them (green).

Using the master equation in its original form (B.3.1a)–(B.3.1d), we give an explanation of the mechanism that renders the stationary current of the Anderson–Holstein molecule zero for certain values of the applied voltages. For $eV_{sd} = 2eV_g + U$, the suppression occurs irrespectively whether we take the principal-value terms into account or not, because as we shall see in the following sections, at this very voltage the principal-value terms cancel to zero. We work in a low-bias regime and at moderate couplings. There is no Franck–Condon blockade effect, such that we can restrict the discussion to just the electronic states without phonons and no double occupation of the system. We choose the coupling constants to be $\mathbf{\Gamma} = (1,1,0,2)$, for as we have shown in the previous section, this choice of couplings with one tunnel amplitude being zero is generic for

the master equation. The only exception is the case of the decoupling regime, in which the Hamiltonian can be reduced to a single impurity problem and thus be treated by rate equations. The generic form of the tunnelling Hamiltonian, where we use the original labels $|\uparrow\rangle$, $|\downarrow\rangle$ instead of $|\pm\rangle$, is

$$H_{\mathrm{T}} = \sum_{\boldsymbol{k}} \left[c^{\dagger}_{\boldsymbol{k}\mathrm{L}} (t_{\mathrm{L}\uparrow} d_{\uparrow} + t_{\mathrm{L}\downarrow} d_{\downarrow}) + c^{\dagger}_{\boldsymbol{k}\mathrm{R}} d_{\downarrow} t_{\mathrm{R}\downarrow} \right] + \mathrm{h.c.}$$

We consider a positive bias voltage, $0 < eV_{\mathrm{sd}} < 2U$, the distance between these values being larger than $k_{\mathrm{B}}T$. In this case, $f_{\alpha 2} = 0$, and we drop the index 1 from the Fermi factors for singly charging the molecule: $f_{\alpha} \equiv f_{\alpha 1}$ such that we have for the Fermi-factors

$$f_{\mathrm{R}} = 0 = 1 - f_{\mathrm{L}}.$$

By definition $t_{\mathrm{R}\uparrow} = 0$, and hence $\gamma_{\mathrm{R}} = 0$, such that the $|\uparrow\rangle$-level is completely decoupled from the *drain* electrode. We see from the master equation (B.1.1a) without the principal-value terms that $\rho_{\uparrow\downarrow}$ does not couple to the singly-charged populations ρ_{σ}. The neutral population p_0 also does not couple to $\rho_{\uparrow\downarrow}$, and due to the small bias $p_2 = 0$. The master equation thus reduces to a rate equation with the state $\rho_{\uparrow}$ becoming absorbing: it is a state that can be populated but not depopulated by the tunnelling dynamics. Due to $f_{\mathrm{L}}\Gamma_{\mathrm{L}\uparrow} \neq 0$, there is a finite flow of probability into $\rho_{\uparrow}$: however, its exit rate vanishes,

$$\sum_{\alpha} (1 - f_{\alpha}) \Gamma_{\alpha\uparrow} = (1 - f_{\mathrm{L}}) \Gamma_{\mathrm{L}\uparrow} + (1 - f_{\mathrm{R}}) \Gamma_{\mathrm{R}\uparrow} = 0 \cdot \Gamma_{\mathrm{L}\uparrow} + (1 - f_{\mathrm{R}}) \cdot 0 = 0.$$

Since we are not in the decoupling regime, the system does not split into two subsystems with a non-unique stationary solution. The unique stationary density matrix of the problem as we discuss it here is the pure state

$$\rho = |\uparrow\rangle \langle\uparrow|. \tag{5.3.1}$$

In this configuration, the system is locked in $|\uparrow\rangle$, and because of the high charging energy, no other electron can be used to transport a stationary current across the device. The system develops a dark state. In contrast to the dark states encountered in the physics of the $E\otimes e$ Jahn–Teller molecule in chapter 3.5, here the state is dark because of destructive interference of the two paths that the electron can use to traverse the nanostructure. Although none of the rates need to be zero explicitly, the linear superposition of states due to the electronic degeneracy produces an effective zero exit rate. By this property, the presence of dark states and the decoupling of levels from the drain electrode emerges as a paradigm in the physics of degenerate two-level nanostructures. This pattern is modified by the pseudo-magnetic fields and vibronic effects both in intermediate and strong electron–phonon coupling regimes.

We remark that the density matrix of a dark state outside the Coulomb blockade can only be of the form

$$\big(c_1 |\uparrow, q\rangle + c_2 |\downarrow, q\rangle\big)\big(c_1^{*} \langle\uparrow, q| + c_2^{*} \langle\downarrow, q|\big),$$

with constants $c_i \in \mathbb{C}$, and cannot involve neutral or doubly charged populations. If the dark state were $\rho = \sum_q a_q p_0^q$ with all $a_q \geq 0$, the stationary current through the source lead would be

$$I_{\mathrm{S}} = \sum_{pq} f_{\mathrm{S}}\big((p - q)\hbar\omega + eV_{\mathrm{g}}\big) \Gamma_{\mathrm{S}}^{pq} a_q p_0^q \neq 0,$$

which amounts to the statement that the state is not dark at all. A similar argument shows the property for the doubly occupied state $\rho = \sum_q b_q p_2^q$. If the solution of the master equation is unique, only a pure state with a single electron can be locked on the device, when the coherent superposition of both degenerate electronic states interfere destructively. If the state was a mixed state, each participating wave function would have to be a dark state of its own. Thus each wave function would define a stationary solution of the master equation, which would thus be no longer uniquely solvable.

For the chosen tunnel coupling $\mathbf{\Gamma} = (1,1,0,2)$, the stationary solutions are the following. For positive bias, the Hamiltonian is already in the generic form with the $|\uparrow\rangle$-level being decoupled from the drain electrode. The stationary solution is given by Equation (5.3.1). For negative bias, the states have to be rotated into a suitable basis in which the state $|-\rangle := \frac{1}{\sqrt{2}}(|\uparrow\rangle - |\downarrow\rangle)$ is decoupled from the left electrode, which for negative bias acts as drain. The stationary density matrix, which solves the master equation, is then the pure state $\rho = |-\rangle\langle -|$ and hence

$$\rho = \frac{1}{2}\begin{pmatrix} 0 & 0 & 0 & 0 \\ 0 & 1 & -1 & 0 \\ 0 & -1 & 1 & 0 \\ 0 & 0 & 0 & 0 \end{pmatrix}.$$

For a more quantitative understanding and also in order to explain the finite linear conductance at zero bias, we turn to the explanation of the zero-bias behaviour of the system. We discard the principal-value terms for the time being and neglect all vibrational excitations. For $eV_{\mathrm{sd}} < 2\hbar\omega$, there is not enough energy in the system to permanently excite the oscillator. Using the vector structure of the pseudo-Bloch equations of appendix B.2 without the principal-value terms, the number of equations reduces to just three. Using the normalisation of the density matrix, $p_0 + p_1 = 1$, we only have to consider two equations. The equation for the pseudo-spin $\vec{S}$ is then solved by

$$\vec{S} = \frac{\sum_\alpha \big(2f_\alpha p_0 - (1-f_\alpha)p_1\big)}{\sum_\beta (1-f_\beta)\Gamma_\beta}\,\vec{n}_\alpha.$$

The equation for the populations on the other hand is

$$\sum_\alpha \big(-2f_\alpha p_0 + (1-f_\alpha)p_1\big)\Gamma_\alpha + \sum_{\alpha\beta} \frac{2f_\beta p_0 - (1-f_\beta)p_1}{\sum_\gamma (1-f_\gamma)\Gamma_\gamma}\,\vec{n}_\alpha \cdot \vec{n}_\beta = 0.$$

Using the normalisation condition of the occupation probabilities and inserting one equation into the other, we obtain

$$p_1 = \frac{\sum_{\alpha\beta} 2f_\alpha(1-f_\beta)\left[\Gamma_\alpha\Gamma_\beta - \vec{n}_\alpha\cdot\vec{n}_\beta\right]}{\sum_{\alpha\beta}(1-f_\alpha)(1+f_\beta)\left[\Gamma_\alpha\Gamma_\beta - \vec{n}_\alpha\cdot\vec{n}_\beta\right]}, \tag{5.3.2}$$

from which the remaining density matrix is easily derived. The graph in Figure 5.3 shows a plot of the thus computed pseudo-spin $\vec{S}$ in the (x,z)-plane. It displays the cross-over from one dark-state solution to another when the bias voltage changes sign. Equation (5.3.2) is readily evaluated in two limiting cases. At zero bias, $f_\alpha = \frac{1}{2}$ and thus $p_1 = \frac{2}{3}$, $p_0 = \frac{1}{3}$. There the pseudo-spin is evaluated zero, $\vec{S} = \frac{2}{\Gamma}\sum_\alpha \vec{n}_\alpha\big(p_0 - \frac{1}{2}p_1\big) = 0$ and also the stationary current vanishes as it is expected at this voltage $I(eV_{\mathrm{sd}} = 0) = f_\alpha\Gamma_{\mathrm{L}}p_0 - \frac{1}{2}(1-f_\alpha)\Gamma_{\mathrm{L}}p_1 = 0$. For finite bias, when only the Fermi factor of the source electrode will contribute to the dynamics, $f_\alpha = \delta_{\alpha,\mathrm{S}}$, and due to the normalisation of the pseudo-magnetisation $|\vec{n}_\alpha|^2 = \Gamma_\alpha^2$, we find $p_1 = 1$. Here,we recover the

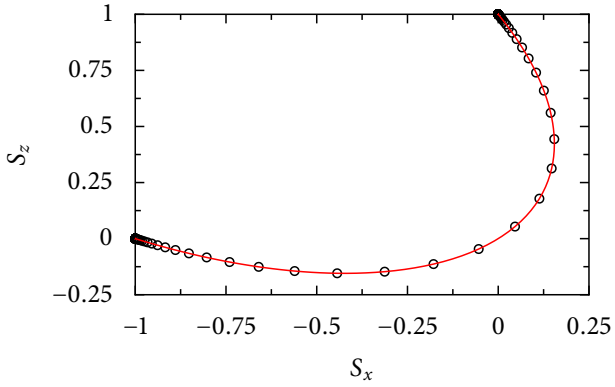

Figure 5.3: The graph shows the dynamics of the pseudo-spin evaluated by the master equation without principal-values terms for $\mathbf{\Gamma} = (1,1,0,2)$, $k_B T = 0.05\hbar\omega$, and $V_{sd} \in [-3\hbar\omega, 3\hbar\omega]$. Since the y-component vanishes identically, we only plot the dynamics in the (x,z)-plane. As it is explained by the calculation in the text, the pseudo-spin aligns at $\vec{S} = (-1,0)$ for $eV_{sd} = -3\hbar\omega$ and at $\vec{S} = (0,1)$ for $eV_{sd} = 3\hbar\omega$. It vanishes identically at zero bias. The dots are placed equidistantly in the bias voltage and show how $\vec{S}$ accelerates its rotation at the zero-bias resonance.

dark state of the above discussion with $\vec{S} = -\Gamma_D^{-1}\vec{n}_D$.

The finite current close to zero-bias can formally be explained by a contradiction argument. Assume that for the chosen coupling $\mathbf{\Gamma}$, the current through the left lead, I_L, is zero,

$$I_L = f_L\Gamma_L(1-p_1) - \frac{1}{2}(1-f_L)\Gamma_L p_1 - (1-f_L)2\gamma_L \operatorname{Re}\rho_{\uparrow\downarrow} = 0.$$

The stationary master equation $\dot{\rho}_\downarrow = 0$ is, with $\Gamma_L^\downarrow = \frac{1}{2}\Gamma_L$,

$$f_L\Gamma_L(1-p_1) - \frac{1}{2}(1-f_L)\Gamma_L\rho_\downarrow - (1-f_L)2\gamma_L \operatorname{Re}\rho_{\uparrow\downarrow} = 0.$$

Subtracting these two, we obtain the condition

$$\frac{1}{2}(1-f_L)\Gamma_L(\rho_\uparrow - \rho_\downarrow) = 0.$$

Given this equation, a necessary condition for $I_L = 0$ therefore is that either the bias is so large that $f_L = 1$ or $S_z = 0$. From the above discussion, we know that for positive bias, when $f_L = 1$, $S_z \neq 0$, and at $V_{sd} = 0$, $f_L = \frac{1}{2}$, and $S_z = 0$. For finite temperature, both quantities f_L and S_z are continuous in eV_{sd}, such that the condition cannot be fulfilled at all up to a voltage of order $k_B T$ above zero bias. By contradiction $I_L \neq 0$ in this range. Physically, the finite current stems from the finite $1-f_L$ in this range, where the decoupled state is not dark. In the picture of sequentially hopping electrons, the particle populates the decoupled state from the source electrode and then, with finite probability, can leave it again towards the *source* electrode. A similar backscattering effect is the source of the exaggerated vibronic sidebands discussed in chapter 3.3, where due to the asymmetric coupling of the device, $\Gamma_S(1-f_S)$ is of order unity for a large range of voltages.

5.3.1 The Role of the Pseudo-Magnetic Fields

The most non-intuitive terms in the master equation for the two-level system immersed in a fermionic bath are the pseudo-magnetic fields that essentially are principal-value integrals over the bath degrees of freedom. The bath itself, a collection of uncountably many degrees of freedom, is the source of two physical phenomena: Due to the infinite recurrence time of a particle that is scattered into the bath degrees of freedom back to the localised state, a continuum of states essentially acts as a source of relaxation. Renormalisation of the localised states' energies, also known as Lamb shift, is the second effect of such

an environment. Breuer & Petruccione (2002, chap. 3.3.1) show in their microscopic derivation of the weak-coupling limit that the Lamb shift is the imaginary part of the bath–bath correlation function. We shall return to the Hamiltonian interpretation of the Lamb shift in more detail in chapter 6.

We begin the discussion of the principal-value terms by an analysis of the self energy of a localised level interacting with a continuous bath via a scalar interaction such as the tunnelling Hamiltonian H_T. The free retarded Green function of the bath, with $\hbar$ being set to unity for convenience, is $G^\mathrm{R}_{\boldsymbol{k}}(t) = -\imath\Theta(t)e^{-\imath\varepsilon_k t}$. The self energy of the localised level $|\sigma\rangle$ is

$$\begin{aligned}\Sigma_\mathrm{d} &= \sum_{\boldsymbol{k}} \int_{\mathbb{R}^+} H_\mathrm{T} G^\mathrm{R}_{\boldsymbol{k}}(t) H_\mathrm{T}\, dt = -\imath \int_{\mathbb{R}} \int_{\mathbb{R}^+} \nu(\varepsilon)|t_\sigma|^2 e^{-\imath\varepsilon t}\, dt\, d\varepsilon \\ &= -\imath \int_{\mathbb{R}} \frac{\nu(\varepsilon)}{\varepsilon} d\varepsilon |t_\sigma|^2 = \left(-\mathcal{P}\int \frac{\nu(\varepsilon)}{\varepsilon} d\varepsilon + \imath\pi\nu(0)\right)|t_\sigma|^2 \approx \imath\pi|t_\sigma|^2\nu.\end{aligned}$$

The principal-value integral vanishes in the wide-band limit $\nu(\varepsilon) \equiv \nu = 1$ of the model for the electronic reservoir. So there is no signature of these terms in non-interacting single-particle physics. Here, we are interested in the non-equilibrium dynamics of the *reduced* density matrix of the localised system. The diagrammatic technique that one should apply here is due to an expansion of the von Neumann equation for $\mathrm{Tr}_\mathrm{E}(\rho)\otimes\rho_\mathrm{E}$. This implies additional steps compared to the standard treatment of resonant tunnelling: the density matrix is a projector and as such, the perturbative expansion applies to both the vector with the retarded propagator and its dual with the advanced propagator. Since we only consider the reduced density matrix, all self-energy terms include the trace over the environmental degrees of freedom. In contrast to the derivation above, the energy integrals are over the density of states times the *Fermi function*, which under suitable conditions destroys the symmetry of the integrand and therefore causes a finite principal-value integral. The diagrams that are relevant for these terms are those that relate the singly charged sector of the reduced density matrix to itself. In the graphical language of Rammer (1998) these are the following two diagrams

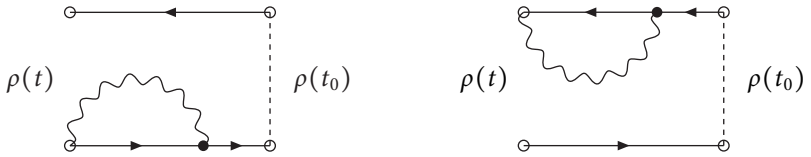

These diagrams relate the reduced density matrix ρ at time t to one at some earlier time t_0. The circles mark the bra- and the ket-vector of $\rho = |\psi\rangle\langle\psi|$. The upper branch is the retarded propagator of the ket, while the lower branch is the advanced propagator of the bra. Similar to the Keldysh technique or the real-time diagrammatic technique by König (1998), the interaction is not restricted to one branch but can rather connect the two. The wiggly line represents the virtual emission or absorption of a bath electron. The left diagram corresponds to terms of the symbolic form $\langle\rho H_\mathrm{T} G^\mathrm{A} H_\mathrm{T}\rangle$ and the right term represents terms of the form $\langle H_\mathrm{T} G^\mathrm{R} H_\mathrm{T}\rho\rangle$. We denote the vertices due to the tunnelling Hamiltonian as matrices

$$\Sigma_0 = \begin{pmatrix}\Gamma^\uparrow & \gamma \\ \gamma & \Gamma^\downarrow\end{pmatrix} \qquad \Sigma_2 = \begin{pmatrix}\Gamma^\downarrow & -\gamma \\ -\gamma & \Gamma^\uparrow\end{pmatrix}.$$

The matrix Σ_0 is used when the virtual intermediate state is neutral, Σ_2 is used for intermediate states that are doubly occupied. The minus sign in the off-diagonal element as well as the interchanged order on

the diagonals is due to this definition, which is also explained in appendix B.1. We obtain the following expression—modulo constant factors—for the sum of the two diagrams

$$\lim_{\eta\to 0}\int_{\mathbb{R}}\int_{\mathbb{R}^+}\Big\{\Sigma_0\rho(1-f)e^{\imath(\varepsilon_1-\varepsilon_0-\varepsilon+\imath\eta)t}+\Sigma_2\rho f e^{-\imath(\varepsilon_2-\varepsilon_1-\varepsilon-\imath\eta)t} \\ +\rho\Sigma_0(1-f)e^{-\imath(\varepsilon_1-\varepsilon_0-\varepsilon-\imath\eta)t}+\rho\Sigma_2 f e^{\imath(\varepsilon_2-\varepsilon_1-\varepsilon+\imath\eta)t}\Big\}\,dt\,d\varepsilon.$$

This expression is a matrix. For simplicity we refrain from mentioning the index of the source and drain electrode. We also use the convergence-generating factor $e^{-\eta t}$, whose justification and necessity is illustrated in appendix A. After performing the integral over time, we obtain

$$\lim_{\eta\to 0}\int_{\mathbb{R}}\Big\{\Sigma_0\rho(1-f)\frac{1}{\varepsilon_1-\varepsilon_0-\varepsilon+\imath\eta}-\Sigma_2\rho f\frac{1}{\varepsilon_2-\varepsilon_1-\varepsilon-\imath\eta} \\ -\rho\Sigma_0(1-f)\frac{1}{\varepsilon_1-\varepsilon_0-\varepsilon-\imath\eta}+\rho\Sigma_2 f\frac{1}{\varepsilon_2-\varepsilon_1-\varepsilon+\imath\eta}\Big\}\,d\varepsilon. \tag{5.3.3}$$

In the case of a rate-equation treatment of the reduced dynamics, we only consider the diagonal elements of the above matrix and assume ρ to be diagonal. The matrix structure reduces to $\Sigma_0\rho=\rho\Sigma_0$. Then, and the same property holds for the terms involving Σ_2, the integrals for the terms with Σ_0,

$$\lim_{\eta\to 0}\int_{\mathbb{R}}\left\{\Sigma_0\rho(1-f)\frac{1}{\varepsilon_1-\varepsilon_0-\varepsilon+\imath\eta}-\rho\Sigma_0(1-f)\frac{1}{\varepsilon_1-\varepsilon_0-\varepsilon-\imath\eta}\right\}d\varepsilon \tag{5.3.4}$$

only yield the *imaginary* part of the integral formula (A.0.2), which is the δ-function contribution that amounts to the direct hopping transitions. If, on the contrary, the full reduced density matrix is used, the commutator of ρ and the Σ's is non-zero. The upper diagonal element of the matrix defined by the expression (5.3.3), and we only discuss this as an example, because it couples coherences to populations, is

$$\lim_{\eta\to 0}\int_{\mathbb{R}}\Big\{(\Gamma^{\uparrow}\rho_{\uparrow}+\gamma\rho^*_{\uparrow\downarrow})(1-f)\frac{1}{\varepsilon_1-\varepsilon_0-\varepsilon+\imath\eta}-(\Gamma^{\downarrow}\rho_{\uparrow}-\gamma\rho^*_{\uparrow\downarrow})f\frac{1}{\varepsilon_2-\varepsilon_1-\varepsilon-\imath\eta} \\ -(\Gamma^{\uparrow}\rho_{\uparrow}+\rho_{\uparrow\downarrow}\gamma)(1-f)\frac{1}{\varepsilon_1-\varepsilon_0-\varepsilon-\imath\eta}+(\Gamma^{\downarrow}\rho_{\uparrow}-\rho_{\uparrow\downarrow}\gamma)f\frac{1}{\varepsilon_2-\varepsilon_1-\varepsilon+\imath\eta}\Big\}\,d\varepsilon.$$

The contribution from $\rho_{\uparrow}$ is treated like in Equation (5.3.4) before and only yields the δ-function contribution, which need not worry. The contribution involving the off-diagonal element, however, is

$$\lim_{\eta\to 0}2\,\mathrm{Im}\,\gamma\rho^*_{\uparrow\downarrow}\left\{\int_{\mathbb{R}}(1-f)\frac{1}{\varepsilon_1-\varepsilon_0-\varepsilon+\imath\eta}d\varepsilon+\int_{\mathbb{R}}f\frac{1}{\varepsilon_2-\varepsilon_1-\varepsilon-\imath\eta}d\varepsilon\right\}.$$

Due to the fact that in the wide-band limit $\mathcal{P}\!\int\frac{1}{\varepsilon}d\varepsilon=0$, the principal-value contribution of this expression cancels exactly only in the absence of interactions, $\varepsilon_2-\varepsilon_1=\varepsilon_1-\varepsilon_0$, in which case the expression becomes the direct, the δ-function contribution.

Summing the above findings, the principal value integrals that appear in the weak-coupling theory of system–bath interactions only appear for systems with degeneracies or near-degeneracies. Interactions render the frequencies of the free unperturbed propagator for the virtual intermediate states that involve either zero or two particles different: $\varepsilon_2-\varepsilon_1\neq\varepsilon_1-\varepsilon_0$. Then the principal-value terms for the self-energy terms

that couple populations with off-diagonal elements will not cancel. They therefore express an interference phenomenon of the free evolution of the two different virtual paths of the system.

Reversal of the Current Suppression

The finite principal-value integrals and thus the pseudo-magnetic fields have a well hidden origin in the self-energy terms of the perturbative expansion of the reduced density matrix. They are rather difficult to fully understand by the intuition coming from the hopping-electron picture of rate equations. But they serve an important physical purpose. In the previous section, we have seen that without the pseudo-magnetic fields, the stationary state of *any* device below the double-charging threshold is a dark state with the electron being locked on the molecule. In a suitably chosen coordinate system of the electronic Hilbert space $\mathcal{H}_{\mathrm{el}}$, the stationary pseudo-spin aligns parallel to $\hat{e}_z$. Without loss of generality, we can assume that the pseudo-magnetic field $\vec{B}$ is not parallel to the pseudo-spin $\vec{S}$. The direction of $\vec{S}$ is defined by the coupling constants of the *drain* electrode. We are therefore free to choose the couplings to the source electrode to generate an x-component of the full pseudo-magnetic field $\vec{B}$. The precession term $\vec{B}\times\vec{S}$ in the pseudo-Bloch equation (B.3.2a) will rotate the pseudo-spin out of the dark state into a linear superposition of states some of which have finite coupling to the drain electrode. These contributions will allow the electron to leave the nanostructure towards the drain electrode and allow for a non-zero stationary current through the device.

What we have just argued by words can be made more rigorous by an explicit discussion of the pseudo-Bloch equation below the charging threshold, where we can safely assume $p_2 = 0$. For simplicity, we consider a system without any vibronic interactions.

$$\dot{\vec{S}} = -\frac{1}{2}\sum_{\alpha}(1-f_\alpha)\Gamma_\alpha\vec{S} + \frac{1}{2}\sum_{\alpha}\Big[2f_\alpha p_0 - (1-f_\alpha)p_1\Big]\vec{n}_\alpha - \sum_{\alpha}B_\alpha\vec{n}_\alpha\times\vec{S},$$

where the pseudo-magnetic fields are of strength

$$B_\alpha = \frac{1}{2\pi}\mathcal{P}\!\int\frac{f_\alpha(\varepsilon)}{eV_{\mathrm{g}}+U-\varepsilon}d\varepsilon + \frac{1}{2\pi}\mathcal{P}\!\int\frac{1-f_\alpha(\varepsilon)}{eV_{\mathrm{g}}-\varepsilon}d\varepsilon.$$

For small temperatures, when the Fermi-functions can be approximated by $f(\varepsilon)\approx 1-\Theta(\varepsilon)$, the integrals are evaluated as

$$2\pi B_\alpha \approx \ln\frac{D+eV_{\mathrm{g}}+U}{D+eV_{\mathrm{g}}} + \ln\left|\frac{\mu_\alpha-eV_{\mathrm{g}}}{\mu_\alpha-eV_{\mathrm{g}}-U}\right| \approx \ln\left|\frac{\mu_\alpha-eV_{\mathrm{g}}}{\mu_\alpha-eV_{\mathrm{g}}-U}\right|,$$

for an electronic band with infinite bandwidth, $D\to\infty$. A finite temperature regularises the divergences at the resonances of B_α at $\mu_\alpha = eV_{\mathrm{g}}$ and $\mu_\alpha = eV_{\mathrm{g}}+U$. These divergences are the reason why in the two-level system, the limit $k_{\mathrm{B}}T\to 0$ cannot be performed easily. The physical reason for this is rather obvious. Due to the asymmetric coupling of the nanostructure to the electrodes, one expects a splitting of the degenerate levels of the order $\mathcal{O}(H_\Gamma^2)=\mathcal{O}(\Gamma)$. In the weak-coupling limit, this splitting cannot be resolved by the Fermi-gas electrodes as we shall show in chapter 6. At zero or very low temperature, however, one expects the master equation to be able to resolve the tunnelling-induced splitting completely. For this regime, a different approach than the one chosen in this thesis must be employed. The principal-value integrals have opposite sign at each of the two resonances making the pseudo-magnetic field $\vec{B}_\alpha$ vanish along the line

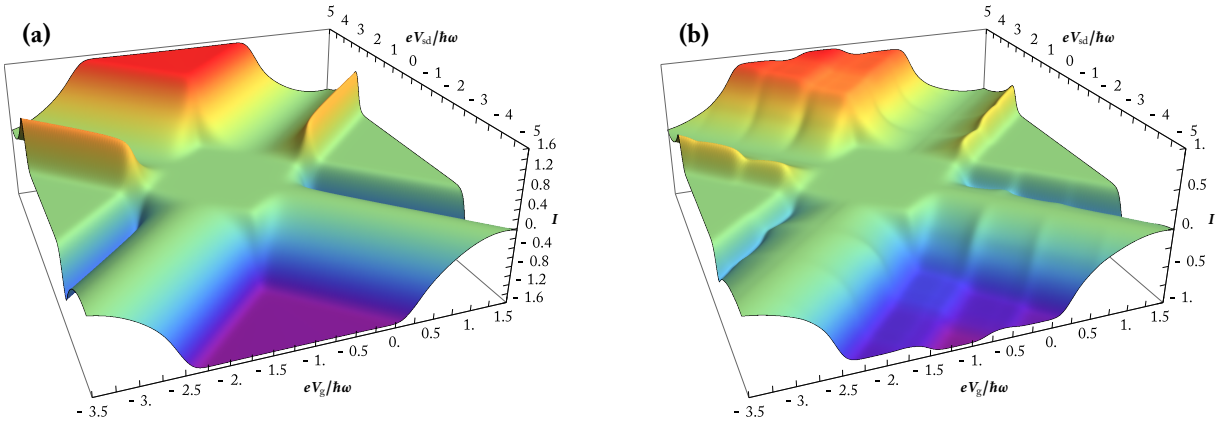

Figure 5.4: Stationary current through a single-molecule device without vibrons (a) and with vibrons (b) in the Anderson–Holstein configuration $\lambda = 1.1$. The coupling is $\mathbf{\Gamma} = (1, 1.5^2, 1.1^2, 1.6^2)$. The other parameters are $k_B T = 0.05\hbar\omega$, and $= 2.35\hbar\omega$.

$\mu_\alpha = eV_g + \frac{1}{2}U$ in the (eV_g, eV_{sd})-plane. This line crosses the eV_g-axis exactly in the particle–hole symmetric point of the Anderson model.

By mapping the electronic operators $d_\sigma^\dagger \mapsto f_\sigma$ and $c_{k\alpha}^\dagger \mapsto -g_{k\alpha}$ onto (phase shifted) holes and denoting the respective number operators by $\bar{n}$ with appropriate indices, the electronic part of the Anderson Hamiltonian is mapped into

$$H = (2eV_g + U) - \left(eV_g + U\right)\left(\bar{n}_\uparrow + \bar{n}_\downarrow\right) + U\bar{n}_\uparrow\bar{n}_\downarrow + \sum_{k\alpha} \varepsilon_{k\alpha} - \sum_{k\alpha} \varepsilon_{k\alpha}\bar{n}_{k\alpha} + H_T.$$

By interpreting the terms with sums over $\boldsymbol{k}$ as the Hamiltonian of a reservoir of *holes*, the transformed Hamiltonian is identical to the original one for zero bias and $eV_g = -\frac{1}{2}U$. For the master equation at this point in the (eV_g, eV_{sd})-plane one immediately infers the identity of electronic populations and hole populations $p_0^h = p_2$ and $p_2^h = p_0$. At zero bias, obviously $p_2 = 0$, hence $p_0 = 0$ and $I = 0$, which corresponds to the fact that at these voltages, the system is Coulomb blockaded.

The relation to particle–hole symmetry is not surprising, as a non-zero pseudo-magnetic field derives from the *asymmetry* of particles and holes, the difference of the propagation frequency in the virtual intermediate states $|0\rangle$ and $|\uparrow\downarrow\rangle$, and the source's pseudo-magnetic fields are invariant under a shift along the line $eV_{sd} = 2eV_g + U$.

According to our generic choice of tunnel couplings, the x-component of the drain's pseudo-magnetisation $\vec{n}_D$ is always zero, and the current blockade found in the previous discussion will only be visible when $B_x = B_S = 0$. Braun *et al.* (2004) find a similar behaviour for a spin-degenerate single-electron transistor; however, their current suppression does not yield $I = 0$ in general. In the final part of this chapter, we discuss a situation similar to theirs and be able to fully explain the phenomenology of their system.

For a quantitative discussion of the precise dependence of the stationary current on the pseudo-magnetic fields, we solve the stationary master equation for a tunnel coupling $\mathbf{\Gamma} = (1, \varepsilon^2, 1, 0)$ with $\varepsilon \neq 0$. Then the pseudo-magnetisations are

$$\vec{n}_L = \begin{pmatrix} 2\varepsilon \\ 0 \\ 1-\varepsilon^2 \end{pmatrix} \quad \text{and} \quad \vec{n}_R = \begin{pmatrix} 0 \\ 0 \\ 1 \end{pmatrix},$$

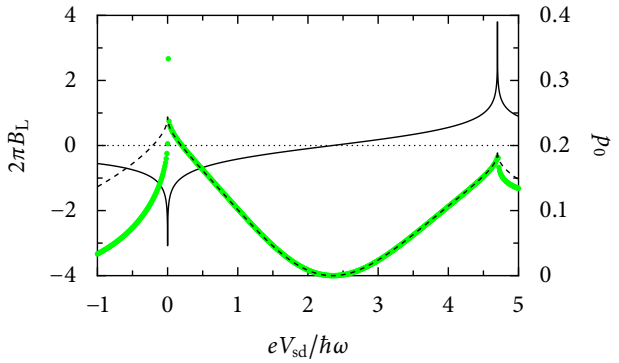

Figure 5.5: The pseudo-magnetic field $2\pi B_L$ (solid line), the stationary population of the neutral state, both in the simplified model discussed in the text (dashed) and the full solution of the stationary master equation with $k_B T = 0.001\hbar\omega$ (green), such that the logarithmic expression for the pseudo-magnetic fields can be used, and tunnel coupling $\mathbf{\Gamma} = (1,1,1,0)$. The analytic solution fits the numerical data very well in the regime $eV_{sd} \in [0,2U]$.

and for $f_L = 1 = 1 - f_R$, that is for finite and positive bias, the stationary pseudo-Bloch equation reads

$$\frac{1}{2}\vec{S} = p_0 \begin{pmatrix} 2\varepsilon \\ 0 \\ \frac{3}{2}-\varepsilon^2 \end{pmatrix} - \begin{pmatrix} 0 \\ 0 \\ \frac{1}{2} \end{pmatrix} - B_L \begin{pmatrix} -(1-\varepsilon^2)S_y \\ (1-\varepsilon^2)S_x - 2\varepsilon S_z \\ 2\varepsilon S_y \end{pmatrix} - B_R \begin{pmatrix} -S_y \\ S_x \\ 0 \end{pmatrix}.$$

The solution for the neutral population is thus

$$p_0 = \left[2 + \varepsilon^4 + \left(\frac{B_R}{B_L}\right)^2 + 2\varepsilon^2 \left(1 - \frac{B_R}{B_L}\right) + \left(\frac{1}{2B_L}\right)^2 \right]^{-1}. \tag{5.3.5}$$

The full suppression of the stationary current, which in this voltage regime is just $I_L = \Gamma_L p_0$, is obtained at the zeros of the pseudo-magnetic field associated with the source electrode. For $B_R \to 0$, the neutral population $p_0 \to 0$, and hence $I_L = 0$ in this limit. We show a numerical evaluation of Equation (5.3.5) in Figure 5.5 along with the solution of the stationary master equation. The good agreement of the numerical evaluation and the analytical discussion is not surprising, as we explicitly solve the master equation for the chosen range of voltages.

Note that although it is tempting, the limit $\varepsilon \to 0$ is not allowed in this result. Due to the decoupling of the $|\downarrow\rangle$-state from both electrodes at $\varepsilon = 0$, the equations cannot be solved uniquely. In the derivation of the above result, we had to assume $\varepsilon \neq 0$ in order to divide by ε. If we had not had assumed this, one equation would have dropped out and the uniqueness of the stationary solution would have been lifted.

5.3.2 Effects due to Charging Energy and Vibronic Excitations

After we have discussed the general role of the pseudo-magnetic fields and their importance for maintaining non-zero stationary currents through the device, we shall shortly dwell on the effect of vibronic excitations as well as the extreme cases of zero and infinite charging energy on the pseudo-magnetic fields.

A system without intrinsic Coulomb repulsion should not show effects due to principal-value integrals; the symmetry of the virtual intermediate states with either zero or two particles on the device, which is expressed in the condition $U = 0$, should yield a cancellation of the two contributing terms in the master equation. This is only true as long as the system is completely devoid of any intra-molecular interaction. Electron–phonon interactions like the one of the Anderson–Holstein molecule do break this symmetry and produce finite pseudo-magnetic fields in the master equation. When we recall the derivation of the master

equation and the relevant principal-value terms from the previous section, we realise that the frequency of the free propagation between two vertices of the scalar tunnelling interaction is either $\varepsilon_2-\varepsilon_1-\varepsilon$ or $\varepsilon_1-\varepsilon_0-\varepsilon$. In the vibration-less model with $U=0$: $\varepsilon_2-\varepsilon_1=\varepsilon_1-\varepsilon_0$. For a system with vibronic excitations, we have to keep the index of the respective vibronic excitations. The state from which we start computing the corrections due to the tunnelling interaction shall be $|1;q\rangle$ with energy $\varepsilon_1^q=\varepsilon_1+q\hbar\omega=\varepsilon_\mathrm{d}+eV_\mathrm{g}+q\hbar\omega$. The virtual transitions then involve states $|0;p\rangle$ and $|2;p\rangle$, and the energy differences become

$$\begin{aligned}\varepsilon_2^p-\varepsilon_1^q&=(p-q)\hbar\omega+\varepsilon_2-\varepsilon_1\\ \varepsilon_1^q-\varepsilon_0^p&=(q-p)\hbar\omega+\varepsilon_1-\varepsilon_0.\end{aligned}$$

Both terms are only equal for $q=p$. In general the difference in the vibronic excitations amounts to a state-specific artificial Coulomb interaction U^{pq} such that

$$\varepsilon_2^p-\varepsilon_1^q=(p-q)\hbar\omega=\varepsilon_1^q-\varepsilon_0^p+2(p-q)\hbar\omega=:\varepsilon_1^q-\varepsilon_0^p+U^{pq}.$$

By rewriting the terms in the fashion shown above, we see how the electron–phonon interaction introduces a far more subtle interaction of particles and holes than the bare Coulomb interaction would have been capable of. There is no effect, however, on the line $eV_\mathrm{g}=0$, where $\varepsilon_1-\varepsilon_0=0$, if the pseudo-magnetisations $\vec{n}^{qp}$ are symmetric matrices. For the Anderson–Holstein and the $E\otimes b$ Jahn–Teller molecule, this symmetry is provided. In models, where for instance the oscillator's frequency differs in the charged and in the neutral state, $\Gamma^{qp}\neq\Gamma^{pq}$ (Koch & von Oppen, 2005a). We illustrate the vanishing of the principal-value terms for the non-interacting molecule at zero gate voltage. Consider a typical integral term in the master equation,

$$\begin{aligned}\mathcal{P}\int\frac{f(\varepsilon)}{(p-q)\hbar\omega-\varepsilon}d\varepsilon+\mathcal{P}\int\frac{1-f(\varepsilon)}{(q-p)\hbar\omega-\varepsilon}d\varepsilon&=\mathcal{P}\int\frac{f(-\tilde{\varepsilon})}{(p-q)\hbar\omega+\tilde{\varepsilon}}d\tilde{\varepsilon}+\mathcal{P}\int\frac{1-f(\varepsilon)}{(q-p)\hbar\omega-\varepsilon}d\varepsilon\\ &=\mathcal{P}\int\frac{1-f(\tilde{\varepsilon})}{(p-q)\hbar\omega+\tilde{\varepsilon}}d\tilde{\varepsilon}+\mathcal{P}\int\frac{1-f(\varepsilon)}{(q-p)\hbar\omega-\varepsilon}d\varepsilon\\ &=0,\end{aligned}$$

which vanishes due to the symmetry of the principal-value integral. The general effect due to these terms in the transport characteristics is much less pronounced than in the setting that we have discussed before. For finite gate voltage, the main contributions of the principal-value terms are localised at the vibronic resonances. They are lost in the thermal structure of the resonance only causing a slight deviation of the shape of the differential conductance peaks from the profile determined by the Fermi functions alone, as it is shown in Figure 5.6. For finite U and generic coupling with one electronic level being decoupled from the drain electrode, the pseudo-magnetic fields in the pseudo-Bloch equation for $\vec{S}^q$ are

$$B_\mathrm{S}^{qp}(\mu_\mathrm{S})=\gamma_\mathrm{S}^{qp}\left[\mathcal{P}\int\frac{f(\varepsilon-\mu_\mathrm{S})}{(p-q)\hbar\omega+U+eV_\mathrm{g}-\varepsilon}d\varepsilon+\mathcal{P}\int\frac{1-f(\varepsilon-\mu_\mathrm{S})}{(q-p)\hbar\omega+eV_\mathrm{g}-\varepsilon}d\varepsilon\right].\tag{5.3.6}$$

We assume the electronic bands of the leads to be wide enough to ensure $\mathcal{P}\int\frac{1}{\varepsilon}d\varepsilon\approx 0$. Then to abbreviate the principal-value integrals, we define the symbol

$$P(\varepsilon_0):=\mathcal{P}\int\frac{f(\varepsilon)}{\varepsilon_0-\varepsilon}d\varepsilon,$$

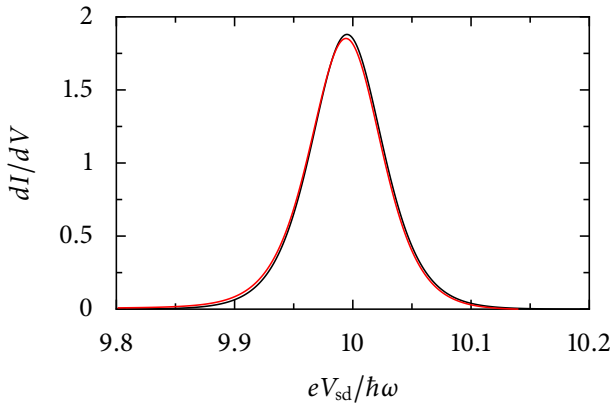

Figure 5.6: A comparison of the line shape of differential conductance peaks obtained by a rate-equation treatment (black) and a non-interacting degenerate Anderson–Holstein molecule (red). The influence of the principal-value integrals is due to $U = 0$ very small, but the peak's line shape is different from the derivative of the Fermi function, which determines the line shape in the rate equation. The maximum is slightly shifted, the peak is smaller and its shoulders are slightly asymmetric. The parameters are $k_B T = 0.01\hbar\omega$, $\mathbf{\Gamma} = (0.75^2, 1, 1.5^2, 1)$, $\lambda = 1.1$, and $eV_g = 4\hbar\omega$.

and the definition of the pseudo-magnetic fields, Equation (5.3.6), takes the simpler form

$$B_S^q(\mu_S) := \sum_p B_S^{qp}(\mu_S) := \sum_p \gamma_S^{qp}\Big[P\big((p-q)\hbar\omega + eV_g + U - \mu_S\big) - P\big((q-p)\hbar\omega + eV_g - \mu_S\big)\Big]. \quad (5.3.7)$$

The functions $P(\varepsilon_0)$ are symmetric in their argument $P(\varepsilon_0) = P(-\varepsilon_0)$. They assume their maximal value at $\varepsilon_0 = 0$ and have logarithmic tails for $|\varepsilon_0| \to \infty$. The two terms in the bracket of Equation (5.3.6) have their maxima at the resonances with $\mu_S = (p-q)\hbar\omega + eV_g + U$ and $\mu_S = (q-p)\hbar\omega + eV_g$, respectively. Their difference vanishes for $U = 2(p-q)\hbar\omega$, which is a condition that affects at most one term in the sum over p. Independently of p, all addends vanish simultaneously at $eV_g - \mu_S = \frac{1}{2}U$. Our conclusions from the previous sections remain valid as also in the full master equation of the Anderson–Holstein molecule, the pseudo-magnetic fields vanish at $eV_{sd} = 2eV_g + U$, where the coherent current blockade is re-established. The current blockade can, however, not be seen in the stationary current without a finite Coulomb interaction on the molecule, for it is a Coulomb-blockade effect. The detailed structure of the voltage-dependent magnitude of the pseudo-magnetic fields is irrelevant for the qualitative structure of the current–voltage characteristics. As long as $\vec{B}_S$ is neither diverging nor vanishing, $I(eV_g, eV_{sd})$ will represent an approximate spectroscopy of H_S. In the case $U \to \infty$, the zeros of $\vec{B}_S$ are shifted to infinity as well, and the specific structure of $\vec{B}_S$ that produces the dip in the stationary current will vanish. The coherent current blockade of the Anderson–Holstein molecule is only then clearly visible in the stationary current, when the charging energy is of the order of several $\hbar\omega$.

The discussion of the role of the pseudo-magnetic fields in the setting of the previous paragraph has provided several important results. Finite pseudo-magnetic fields ensure a non-zero stationary current through the device in contrast to the master equation with zero pseudo-magnetic fields, which is stationary in a pure and hence a non-conducting state. The finite charging energy produces two peaks in $B_S(eV_{sd})$ with opposite signs, such that there is a line in the (eV_g, eV_{sd})-plane at which the fields vanish, and a coherent current blockade is visible. The change of the fields as a function of the voltages allows for the deviations from the spectroscopic picture found in the numerical data.

5.3.3 Strong Electron–Phonon Coupling

Whenever we eliminate a linear electron–phonon coupling term in the system's Hamiltonian H_S by a polaron transformation and thereby imprint a vibronic matrix structure onto the tunnelling-matrix elements

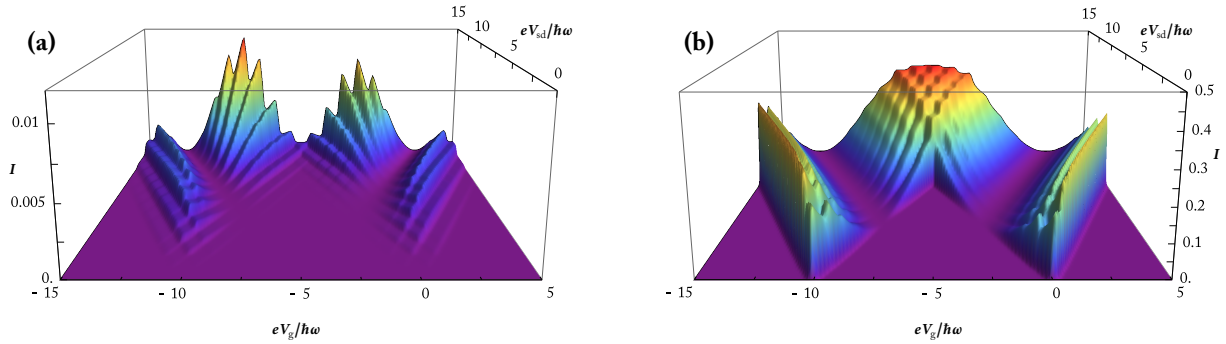

Figure 5.7: Stationary current of the Anderson–Holstein molecule in the Franck-Condon blockade regime for $\lambda = 4$ (a) and for intermediate coupling $\lambda = 1.1$ (b). Although the obvious effect of strong electron–phonon coupling is a suppression of the stationary current at the Coulomb-blockade line and the double-charging threshold, the current profile develops sharp spikes at larger bias. The parameters are $U = 10\hbar\omega$ and $\mathbf{\Gamma} = (1,1,1.5^2,0)$.

of H_T, we would like to generalise the findings for the transport properties of the bare electronic levels to the molecular model. Such is easiest when the main vibronic transitions are elastic and do not change the vibronic quantum number q of the molecule. The Franck–Condon matrix $M^{qq'}$ will often have its maximum along the line $q = q'$ and on average be monotonically decreasing for larger differences $|q - q'|$. Then the molecule will only develop vibrational sidebands in the differential conductance. The Franck–Condon matrix can also have non-trivial structure, as it is the case for strong electron–phonon couplings where the matrix elements $M^{qq'}$ are exponentially suppressed for small q, q', and the inelastic transitions with rates of order unity appear for larger vibronic quantum numbers. Such a matrix structure leads to transport effects like the Franck–Condon blockade and avalanche transport that cannot be explained by using a generalisation of the models without vibronic excitations, as has been shown first by Koch & von Oppen (2005b) and is explained in detail in several sections of chapter 3. The model of an Anderson–Holstein molecule considered in this chapter also develops non-trivial transport properties for large electron–phonon couplings. By non-trivial, we mean that an understanding of the differential conductance has to rely on the vibronic structure of the model explicitly. The obvious effect of strong electron–phonon coupling would be a mere shift of the conduction maximum. Since for finite charging energy, there is an $I = 0$ trough in the current–voltage diagram, the maxima of I, which are originally, that is for small electron–phonon couplings, located at the Coulomb-blockade peak and the double-charging threshold, move towards the trough. The vibronic sidebands' influence, little peaks at the respective voltages, becomes more and more exaggerated, resulting in the sharp peaks seen in Figure 5.7 (a).

If we compute the stationary current for large bias and Coulomb repulsion, say $eV_{sd} = 20\hbar\omega$ and $U = 10\hbar\omega$, the master equation without the principal-value terms shows a conduction window between $eV_g = -\frac{1}{2}eV_{sd}$ and $eV_g = \frac{1}{2}eV_{sd} - U$, see Figure 5.8 (a). In principle, we would not expect any Franck–Condon blockade effect in this regime, as although one level could be decoupled from the drain electrode, for $eV_g = -U$, electrons in the source still have enough energy to excite about ten oscillator quanta, which is enough to overcome the blockade. The numerical data, however, shows a strong suppression of the stationary current indicating that there is indeed a Franck–Condon blockade effect present even at such large bias. Due to the fact that in the investigated voltage regime, the two-particle state is *within* the bias window, the behaviour of the master equation will change from drain-decoupling for positive gate voltages to source-decoupling at gate voltages close to the drain's Fermi level. This is easy to understand as decoupling from the drain

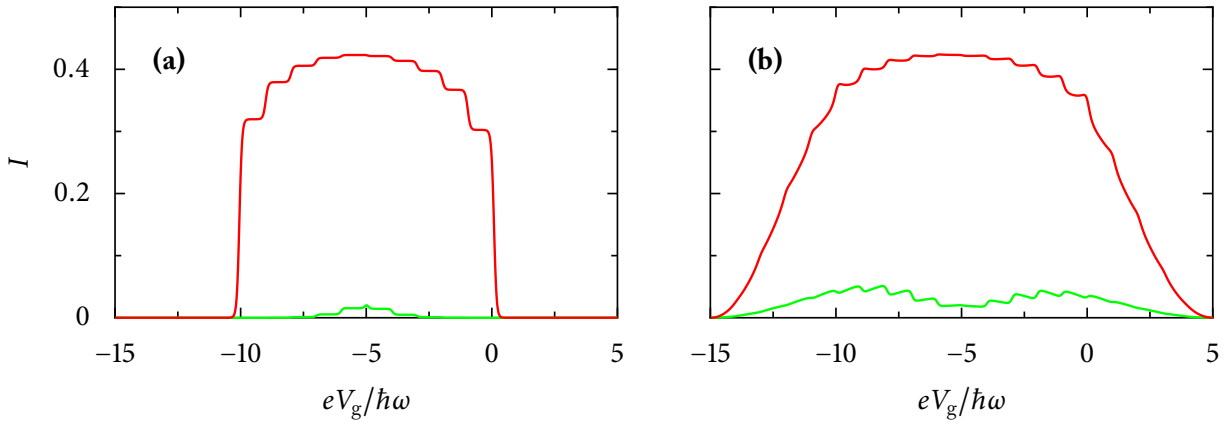

Figure 5.8: The Anderson–Holstein molecule with $U = 10\hbar\omega$, held at $eV_{sd} = 20\hbar\omega$. The gate voltage is swept from $eV_g = -15\hbar\omega$ to $eV_g = 5\hbar\omega$ and $\mathbf{\Gamma} = (1,1,1.5^2,0)$. The electron–phonon coupling is $\lambda = 1.1$ (red) and $\lambda = 4$ (green). Diagram (a) shows the stationary current without the pseudo-magnetic field contributions, where due to the decoupling of one of the electronic states from the source electrode, the Franck–Condon blockade is seen despite the large bias voltage. Diagram (b) shows the same situation for the full master equation. The additional precession of the molecule's pseudo-spin allows for a widening of the conduction window and the development of the current steps into little peaks similar to those seen in Figure 5.7.

does not produce a dark state at all; the bias window provides enough energy to overcome the double charging threshold. Deep in the Franck–Condon blockade regime, however, the $|\sigma,0\rangle \mapsto |0,0\rangle$ transition is exponentially suppressed and therefore a candidate for a dark state. The access to the two-particle state, which can convert charging energy to vibronic energy and thus overcome the Franck–Condon blockade, can be obstructed by simply decoupling one state from the source electrode. Such reasoning allows us to solve the master equation close to the Fermi level of either electrode, obtaining $I = 0$. Only when $eV_g \approx -U/2$, neither decoupling mechanism can generate a dark state and the system will transport a finite current as it is shown in Figure 5.8 (a). The pseudo-magnetic fields act as a turnstile that moves population from the dark state into the other, conducting state. This has two consequences, which are seen in Figure 5.8 (b). Independent of the strength of the electron–phonon coupling, the conduction window defined by the Coulomb blockade for double occupation is widened beyond $eV_g \in [-\frac{1}{2}eV_{sd}, \frac{1}{2}eV_{sd} - U]$. For strong electron–phonon coupling, both decoupling mechanisms can be overcome with the help of the pseudo-magnetic fields, such that we finally observe the current profile shown in Figure 5.8 (b).

5.4 Jahn–Teller Molecules

Jahn–Teller molecules, as we have defined them in section 5.1, have an electron–phonon coupling that only differs slightly from that of the Anderson–Holstein molecule. The Jahn–Teller coupling is not proportional to the unit-matrix in the electronic Hilbert space $\mathcal{H}_{el}$ but proportional to σ_z. It is diagonal but not invariant under unitary transformations of the electronic operators and thus breaks the rotational symmetry of the system Hamiltonian in $\mathcal{H}_{el}$. If we applied the rotation we have used previously to decouple one electronic level from the drain electrode, we now would also induce an off-diagonal electron–phonon coupling term,

$$\sigma_z \mapsto \begin{pmatrix} \cos\theta & \sin\theta \\ -\sin\theta & \cos\theta \end{pmatrix} \begin{pmatrix} 1 & 0 \\ 0 & -1 \end{pmatrix} \begin{pmatrix} \cos\theta & -\sin\theta \\ \sin\theta & \cos\theta \end{pmatrix} = \cos 2\theta\sigma_z - \sin 2\theta\sigma_x .$$

Although by a suitable rotation, one of the electronic levels can be decoupled from the drain electrode in H_T, it is still connected to that reservoir indirectly via the electron–phonon coupling. In the polaron picture, the decoupling can only be achieved for certain parts of the matrix-valued tunnelling elements, namely those involving even transitions $|q\rangle \to |q+2k\rangle$ with $q+2k \in \mathbb{N}_0$. The generality of a coupling $\mathbf{\Gamma} = (1,1,0,1)$ is no longer given. The physics of this model, especially for voltages beyond the first vibronic sideband, will therefore be much less generic than the one of the highly symmetric Anderson–Holstein molecule.

We discuss three different aspects of the coherent transport properties of the $E\otimes b$ Jahn–Teller molecule. Close to the decoupling line in the parameter space of the tunnel amplitudes, the low-bias behaviour is characterised by an almost vanishing pseudo-spin. This effect, which is caused by the pseudo-magnetic fields, restores a rate-equation behaviour of the system even in the stationary solution. The current suppression that is generic for transport through Anderson–Holstein molecules will be difficult to observe, as soon as vibronic excitation participate in the tunnelling dynamics. The decoupling mechanism that leads to the creation of a dark state is not independent of the tunnelling matrix elements $t_{\alpha\sigma}$. We show which conditions have to be posed on the parameters, in order to observe the current blockade also in the first vibronic sideband. The σ_z-coupling of the $E\otimes b$ Jahn–Teller molecules has also signatures in the transition matrix elements that enter the master equation. The Franck-Condon matrices[6] $\tilde{M}_\sigma^{pq}$ for transitions involving $|\uparrow\rangle$ differ from those for $|\downarrow\rangle$. By inspection of the adiabatic potentials in Figure 5.1, we have seen that the overlap of even and odd oscillator wave functions differ in their sign depending on the direction of the displacement due to the polaron transformation. A rate equation is insensitive to such a sign, because it only involves the square modulus $M_\sigma^{pq} = |\tilde{M}_\sigma^{pq}|^2$, which is independent of the direction of the displacement and therefore independent of σ. The master equation, however, allows tunnelling into and out of linear superpositions of the two degenerate states, and as such the product $\tilde{M}_\uparrow^{pq}\tilde{M}_\downarrow^{pq}$ enters the problem, which is negative for odd and positive for even differences $|p-q|$. Due to the negative sign of γ_α^{pq}, the pseudo-magnetic fields are more complicated in their structure, being less effective in restoring a finite current at low bias.

5.4.1 Killing a Pseudo-Spin

Close to the regime in the parameter space of H_T, where the decoupling condition (5.2.2) is satisfied and the electronic self-energy matrix has only rank one, the pseudo-magnetic fields show their real power in the Jahn–Teller molecule. Without them, there is an additional peak below the first vibronic sideband compared to the spectroscopic picture, see Figure 5.9 (a). Consider the system in a basis, where, like in the Anderson–Holstein molecule, one level is decoupled from the drain electrode. Since we are close to the decoupling line, this level is only very weakly coupled to the source electrode as well. In the Jahn–Teller model, the decoupling from the drain electrode only affects the *even* vibronic transitions. This is in contrast to the Anderson–Holstein molecule, where the decoupling is independent of the vibronic structure of the system. In particular, this means that in the $E\otimes b$ Jahn–Teller model, the quantities γ_α^{10} and $\Gamma_{\alpha\sigma}^{10}$ do not vanish in the rotated basis.

The additional peak is due to a balance condition. The rates for the process $|0;0\rangle \mapsto |\downarrow;0\rangle$ at the source electrode, which is suppressed due to the almost decoupling $\Gamma_{S\downarrow}^{00} \approx 0$, and those for the inelastic process $|\downarrow;0\rangle \mapsto |0;1\rangle$ at the drain electrode, which is exponentially suppressed by the Fermi function $1-f_D^{01}$, are of the same order and hence contribute to the steady-state dynamics. After we have switched on the pseudo-magnetic fields, the picture is completely different. There is no current suppression, there is no

[6] Note that in the Jahn–Teller molecule, we need to discuss the wave-function overlap $\tilde{M}_\sigma^{pq} = \langle p|e^{\lambda(b^\dagger - b)}|q\rangle$.

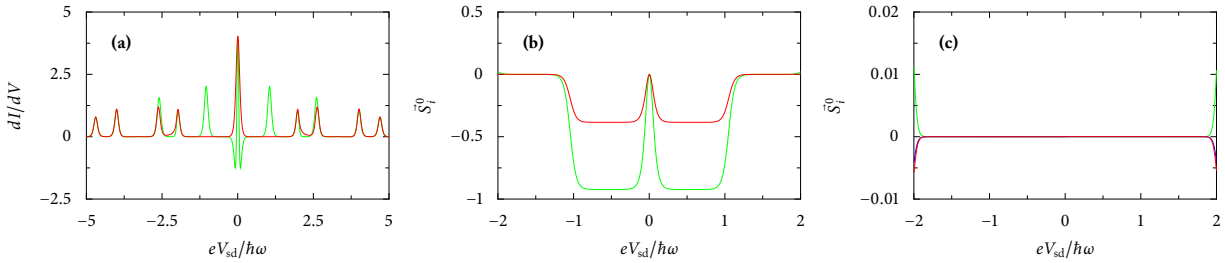

Figure 5.9: (a) Differential conductance dI/dV of the $E\otimes b$ Jahn–Teller molecule close to the decoupling line. The parameters are $U = 2.35\hbar\omega$, $k_BT = 0.02\hbar\omega$, $\lambda = 1.1$, and $\mathbf{\Gamma} = (1, 1.5^2, (1+\varepsilon)^2, 1.5^2)$ with $\varepsilon = 10^{-5}$. Green: master equation without principal-value terms, Red: master equation with principal-value terms. Components of the pseudo-spin $\vec{S}^0$: S_x (green), S_y (green), and S_z (red) for the master equation without (b) and with (c) pseudo-magnetic fields. In (c) the pseudo-spin is damped to zero.

additional peak, and the stationary distribution is reminiscent of a rate-equation result because, as it is seen in the data of Figure 5.9 (c), $\vec{S} \approx 0$. This result is striking and unexpected, because due to the complicated vibronic structure, there is no obvious reason why the pseudo-magnetic fields, which up to now only worked as a regularising and current-restoring mechanism should influence the physics so much as to force the pseudo-spin to vanish. The explanation is due to the missing decoupling of the inelastic transitions in the Jahn–Teller molecule that actually produced the additional peak in Figure 5.9 (a).

We explain the mechanism in two steps. First, we show the implications of a vanishing pseudo-spin in the decoupling regime, and then we show that $\vec{S}$ actually equals zero. Due to the partial instead of the full electronic decoupling caused by the Jahn–Teller structure, the model does not separate into two independent systems as long as not all $t_{\alpha\sigma}$ are equal. Hence the term "decoupling" has only a meaning in the case of a purely electronic nanostructure without phonons. For the sake of notational simplicity, we shall use the term nonetheless.

Consider a system with vanishing pseudo-spin. Then $\rho_\uparrow = \rho_\downarrow$, and the pseudo-Bloch equation for the populations (B.3.2b) in the chosen voltage regime before the first vibronic sideband and the double-charging threshold, where $f_S = 1$, $f_D = 0$ with $p_2 = 0$ and $\rho_{ij}^{q>0} = 0$, is

$$\Gamma_S p_0 = \frac{1}{2}\Gamma_D p_1.$$

The solution is, due to the normalisation $p_0 + p_1 = 1$,

$$p_1 = \frac{1}{1 + \frac{1}{2}\frac{\Gamma_D}{\Gamma_S}}.$$

which for example for $\Gamma_D = \Gamma_S$ results in $p_0 = \rho_\uparrow = \rho_\downarrow = \frac{1}{3}$. In contrast to a rate-equation result, where for $\Gamma_S \neq \Gamma_D$ also $\rho_\uparrow \neq \rho_\downarrow$, here both states are equally occupied. Due to $S_z = 0$, the reduced density matrix of the singly-charged wave-functions is proportional to the unit matrix and as such it is invariant under any unitary transformation in $\mathcal{H}_{el}$. It is therefore of no relevance at all in which basis of the electronic Hilbert space we work, when we want to prove the vanishing of $\vec{S}$.

We assume that the decoupling condition is satisfied exactly and consider a basis of the electronic Hilbert space, where accordingly one of the states, $|\downarrow\rangle$, say, is decoupled from both electrodes in the sense that $\Gamma_{\alpha\downarrow}^{00} = \gamma_\alpha^{00} = 0$ for all α. Due to the special vibronic matrix structure of the Jahn–Teller molecule, the pseudo-

magnetic fields *do not* vanish if the decoupling condition is satisfied exactly—in the Anderson–Holstein model, B_x would be zero in such a configuration. Consider the pseudo-Bloch equations for S_z and p_0,

$$\begin{aligned}\Gamma_S p_0 - \frac{1}{2}\Gamma_D p_1 - \frac{1}{2}\Gamma_D S_z &= B_x S_y \\ -\Gamma_S p_0 + \frac{1}{2}\Gamma_D p_1 + \frac{1}{2}\Gamma_D S_z &= 0.\end{aligned}$$

Adding both equations implies $B_x S_y = 0$, which due to $B_x \neq 0$ for the Jahn–Teller molecule means $S_y = 0$. We put this result into the pseudo-Bloch equation for the remaining components of the pseudo-spin

$$\begin{aligned}-\frac{1}{2}\Gamma_D S_x + B_z S_y &= 0 \\ -\frac{1}{2}\Gamma_D S_y + (B_x S_z - B_z S_x) &= 0.\end{aligned}$$

For $S_y = 0$, the first equation implies $S_x = 0$; then the second equation is solved by $S_z = 0$, which finally states the result $\vec{S} = 0$.

This result is somewhat non-intuitive. The Anderson–Holstein model is not continuous in parameter space at the decoupling condition, as there it decouples into two independent systems. The Jahn–Teller molecule, on the contrary is continuous at the decoupling condition except for the configuration $t_{\alpha\sigma} = 1$ for all α and σ, where also the Jahn–Teller molecule decouples into two independent systems. Since as long as the solution of the problem is unique and well-defined, the theory is continuous in H_T, this allows us to study the Jahn–Teller molecule close to the decoupling line by computing an approximate solution with parameters for which the decoupling condition is satisfied exactly.

The Jahn–Teller molecule intrinsically tends to show rate-equation dynamics in the stationary current profile. The cause of this effect is the inability to decouple one electronic level from the drain electrode for generic tunnel couplings *completely*. In some special cases, this is, however, possible thus producing a completely different phenomenology. Due to the possible cross-over of these different types of stationary physics, the Jahn–Teller molecule is difficult to understand from a generic point of view.

5.4.2 Coherent Suppression of the Stationary Current

The main result of the discussion of the Anderson–Holstein molecule of section 5.3 is the generic appearance of a coherent current blockade for bias voltages below the double-charging threshold. Due to the σ_z electron–phonon coupling in the Jahn–Teller problem, we shall lose this blockade-effect in the Jahn–Teller molecule in the first vibronic sideband. Still, there are some parameter regimes, where it re-appears, making explicit use of the vibronic structure of the problem. In Figures 5.10 (a) and (b), we show numerical data for both models illustrating the difference.

We consider a tunnel coupling $\mathbf{\Gamma} = (1,1,0,1)$. Obviously the current blockade is present in the positive bias, positive gate regime, although different from the Anderson–Holstein molecule as we shall explain in the next section. We choose the new basis $|\pm\rangle = \frac{1}{\sqrt{2}}(|\uparrow\rangle \pm |\downarrow\rangle)$ of $\mathcal{H}_{el}$. For negative bias and positive gate, the decoupling from the drain electrode is only achieved for the even excitations of the $|-\rangle$-level and the odd excitations of the $|+\rangle$-level. For the transitions at the source electrode, there are no cancellations.

In Figure 5.11, we show the available direct transitions from the source electrode to the molecule and from there to the drain electrode at voltages in the first vibronic sideband. By choosing the electron–phonon

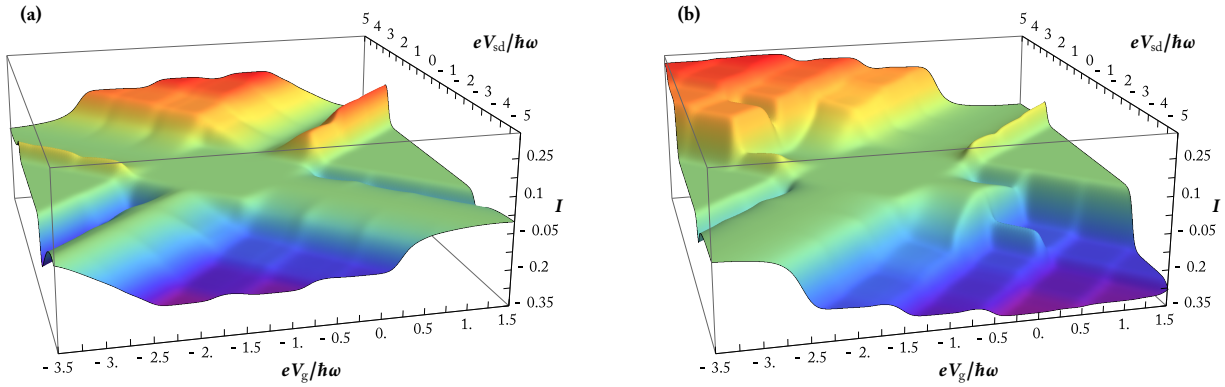

Figure 5.10: Comparison of the Anderson–Holstein (a) and the $E\otimes b$ Jahn–Teller molecule (b) at $U = 2.35\hbar\omega$, $k_BT = 0.05\hbar\omega$, $\mathbf{\Gamma} = (1,1,0,1)$, and $\lambda = 1.1$. In the Jahn–Teller molecule, the broken symmetry of the Hamiltonian in the electronic Hilbert space causes a qualitatively different behaviour for positive and negative bias. The current suppression, being the generic effect in the Anderson–Holstein molecule, is only partly visible.

coupling $\lambda = 1.1$, we place the system close to a point, where the overlap of $|0,1\rangle$ with $|\sigma,1\rangle$ is very small. For $\lambda = 1.0$, it actually vanishes. We thus obtain a situation, in which the state $|+,1\rangle$ is strongly coupled to $|0,0\rangle$, from which it gains population, and very weakly connected to everything else, especially those states it loses population to. This state will therefore achieve a very high population in steady state. The molecule will not gain significant transparency by having the first vibronic excitation in the energy window; indeed, it will rest in a stationary configuration of high vibrational non-equilibrium, even population inverted. The localisation of this current blockade effect to a small regime of the applied voltages is due to the pseudo-magnetic fields, which, like before, rotate the system out of the absorbing state thus restoring a finite current. The increment of the stationary current due to the vibronic resonance does, however, vanish at the zero of the pseudo-magnetic field. The Anderson–Holstein current blockade in the first vibronic sideband can be observed in Jahn–Teller molecules, although only for a small volume of the parameter space.

5.4.3 Signatures of Negative Franck–Condon Matrix Elements

In the Jahn–Teller molecule, the different signs of Franck–Condon matrix elements will effectively damp the x-component of the pseudo-magnetic field, which in turn results in a clearly visible current blockade with a much broader profile than it is expected from the equivalent Anderson–Holstein model, see Figure 5.10 at positive bias, positive gate and Figure 5.12. The z-component of the pseudo-magnetic field is the same both for Anderson–Holstein and Jahn–Teller molecules,[7]

$$(B_i^q)_z = \sum_{p\alpha} B_{\alpha i}^{qp} (\Gamma_{\alpha\uparrow}^{pq} - \Gamma_{\alpha\downarrow}^{pq}).$$

The Golden-Rule rates are $\Gamma_{\alpha\uparrow}^{pq} - \Gamma_{\alpha\downarrow}^{pq} = \frac{2\pi}{\hbar}\nu|\tilde{M}^{pq}|^2(t_{\alpha\uparrow}^2 - t_{\alpha\downarrow}^2)$. In the Anderson–Holstein model, the x-component of the pseudo-magnetic field, which is the current-restoring force, is

$$(B_i^q)_x = \sum_{p\alpha} B_{\alpha i}^{qp} 2\gamma_\alpha^{pq},$$

[7] For the notation, see appendix B.2.

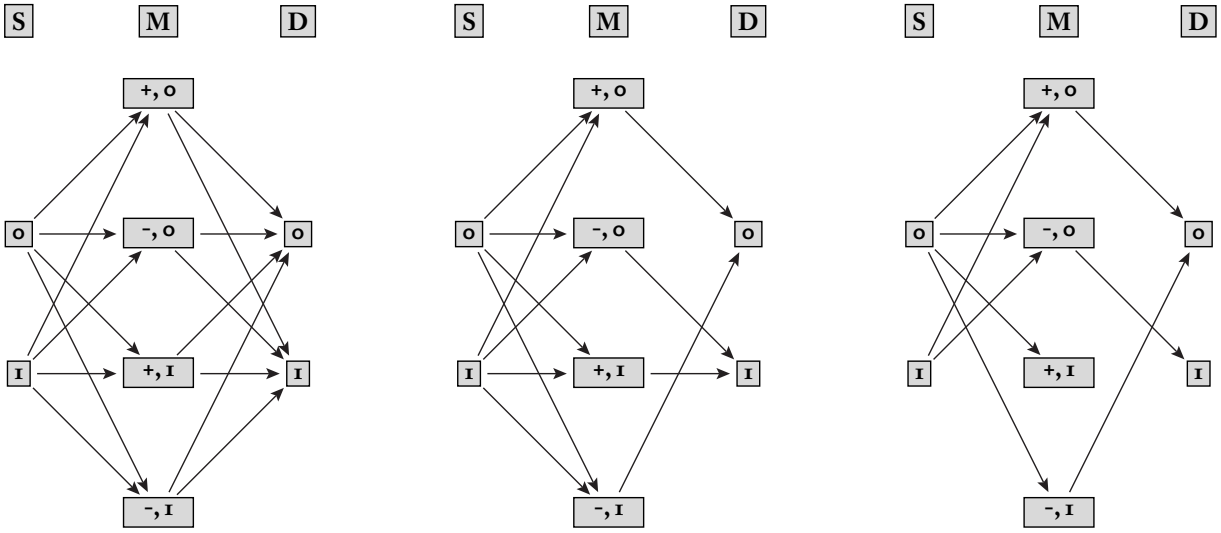

Figure 5.11: Tunnelling possibilities for the Jahn-Teller molecule at zero gate voltage and inside the first vibronic sideband. We indicate the possible transitions between source (S), molecule (M), and drain (D) by directed arrows without denoting the explicit rates. Left: General energetic situation. Middle situation after a unitary transformation in $\mathcal{H}_{\mathrm{el}}$ has decoupled the $|-\rangle$-states from the even and the $|+\rangle$-states from the odd vibronic transitions at the drain electrode. Right: Situation after the vanishing of the Franck–Condon factor for $\lambda = 1$ has been taken into account and the state $|+;1\rangle$ becomes (almost) absorbing and causes a suppression of the stationary current also in the first vibronic sideband.

where the coupling is $2t_{\alpha\uparrow}t_{\alpha\downarrow}|\tilde{M}_\sigma^{pq}|^2$. The Franck–Condon matrix elements just appear as a positive weight for the principal-value integrals. In the Jahn–Teller case, however,

$$\gamma_\alpha^{pq} = \frac{2\pi}{\hbar}\nu t_{\alpha\uparrow}t_{\alpha\downarrow}\left|\tilde{M}_\sigma^{pq}\right|^2 \operatorname{sgn}\left(\tilde{M}_\uparrow^{pq}\tilde{M}_\downarrow^{pq}\right),$$

which, when being summed over p, leads to a suppression of the fields' x-component compared with the Anderson–Holstein molecule because $\operatorname{sgn}\left(\tilde{M}_\uparrow^{pq}\tilde{M}_\downarrow^{pq}\right)$ is alternating in q and p. As an example of this effect, we compare the Anderson–Holstein molecule and its Jahn–Teller counterpart for a special choice of parameters, where the effect is most clearly seen. The numerical evaluation of the stationary current for $eV_{\mathrm{g}} = 0$ is shown in Figure 5.12 but the structure is equally well visible in Figure 5.10 (b). We use a tunnel coupling $\mathbf{\Gamma} = (1,1,1,0)$ like in the previous section, which for positive bias is already in the form of having one electronic level being decoupled from the drain electrode. This isolates the effect of the small pseudo-magnetic field by not introducing any off-diagonal electron–phonon coupling. Like for the Anderson–Holstein molecule, the system features a current blockade below the charging energy, which is partly lifted by the pseudo-magnetic fields. The numerical data, however, show that the blockade's profile resembles the one found in the treatment of the Anderson–Holstein molecule *without* the principal-value terms. Due to the σ_z-structure of the Jahn–Teller molecule's electron–phonon coupling, the current-restoring x-component of the pseudo-magnetic field is less effective. To gain some insight into the analytical structure of the effect, we solve the stationary master equation for just one occupied electronic level by assuming U to be very large, $k_{\mathrm{B}}T$ very small, and the bias voltage positive and such that neither the zero bias nor vibronic or charging effects have to be considered. We incorporate the physics of the Jahn–Teller molecule by splitting the pseudo-magnetic field into the x- and z-component. Due to our specific choice of tunnel

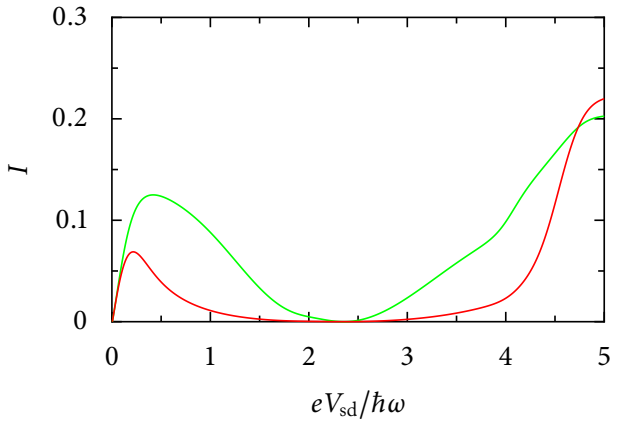

Figure 5.12: Effects of small pseudo-magnetic field in the x-direction. The parameters are $U = 2.35\hbar\omega$, $k_\mathrm{B}T = 0.05\hbar\omega$, $\lambda = 1.1$, $eV_\mathrm{g} = 0$, and $\mathbf{\Gamma} = (1,1,1,0)$. The stationary current of the Anderson–Holstein molecule is shown in green, the one of the Jahn–Teller molecule in red. The suppression of the latter to a curve reminiscent of the current suppression in absence of any pseudo-magnetic fields is due to the small value of B_x.

couplings, this is equivalent to distinguish between left and right as $\vec{n}_\mathrm{L} \uparrow\uparrow \hat{e}_x$ and $\vec{n}_\mathrm{R} \uparrow\uparrow \hat{e}_z$. With the tunnel coupling $\mathbf{\Gamma} = (1,1,1,0)$, the pseudo-Bloch equation is

$$\frac{1}{2}\dot{\vec{S}} = \begin{pmatrix} 2 \\ 0 \\ \frac{1}{2} \end{pmatrix} p_0 - \begin{pmatrix} 0 \\ 0 \\ \frac{1}{2} \end{pmatrix} - \begin{pmatrix} -B_z S_y \\ B_z S_x - 2B_x S_z \\ 2B_x S_y \end{pmatrix}.$$

The equation for the population simplifies to $S_z = 5p_0 - 1$. Using the result of the respective calculation in section 5.3, with $\varepsilon = 1$ and due to the tunnel couplings the identification $B_\mathrm{L} = B_x$ and $B_\mathrm{R} = B_z$, we obtain the population of the vibronic ground state of the neutral molecule

$$p_0 = \frac{(2B_x)^2}{1 - 18B_x^2 + 4(B_x - B_z)^2} \leq \mathcal{O}(B_x^2).$$

The precession out of the dark state is induced by the source's fields parallel to $\hat{e}_x$, whereas the perturbation induced renormalisation of the eigenenergies, being proportional to B_z, in this particular configuration are due to the interaction with the drain's continuum of states. The stationary current in this voltage regime is proportional to p_0, and in contrast to the Anderson–Holstein molecule, where the pseudo-magnetic field is in general quite large, in the Jahn–Teller case with small B_x over a wide range of voltages, we encounter a situation where current profile is determined by the master equation without the precession terms.

5.5 Multi-Mode Reservoirs

Motivated by the recent experiments on suspended carbon nanotubes by Sapmaz *et al.* (2006) and especially by Leturcq *et al.* (2009), we use the final part of this chapter to generalise the theory developed so far to multi-mode reservoirs. A multi-mode reservoir has more than one eigenstate per eigenvalue, similarly to degenerate multi-orbital quantum nanostructures. Such an extension provides the first step from our abstract models towards the description of realistic and experimentally accessible quantum nanostructures that show a steady-state current–voltage characteristics that goes beyond the descriptive capabilities of the single-level Anderson–Holstein model using rate equations. Although, as we have shown in chapter 3.2, the rate-equation treatment can well account for certain parts of the phenomenology found by Leturcq *et al.*

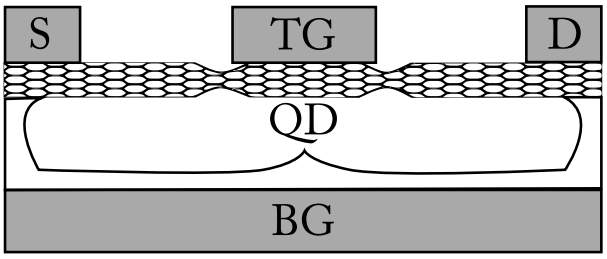

Figure 5.13: Set-up of a suspended carbon nanotube, which is used in the experiment by Leturcq *et al.* (2009). The basic configuration consists of a source electrode (S), a drain electrode (D), and a back-gate electrode (BG). Attaching the top gate (TG) on the nanotube creates the quantum dot (QD) by a deformation of the nanotube to tunnel junctions. In such set-ups, parts of the nanotube itself act as source and drain electrode.

(2009), it fails to explain the ubiquitous negative differential conductance peaks *parallel* to the vibrational sidebands in the measurements shown in Figure 3.4. The rate-equation treatment of the Franck–Condon blockaded Anderson–Holstein model only produces negative differential conductance peaks *perpendicular* to the vibrational sidebands.

Carbon nanotubes are cylindrical structures of rolled graphene sheets. Graphene itself is a two-dimensional layer of the graphite crystal. The investigation both theoretically and experimentally of graphene and carbon nanotubes has become a major branch of condensed matter theory in recent years.[8] Graphene has a bipartite honeycomb lattice. Its Brillouin zone comprises two Fermi points, called K and K', at which the dispersion forms two linear cones. The tip of these cones touch exactly in the Fermi point, such that the two degenerate "valleys" and the linearity of the dispersion relation close to the Fermi energy give rise to a description of the electronic low-energy properties in terms of a massless Dirac equation. It is this fact, which has made graphene such a grateful object for theoretical investigation. Taking into account both valley degeneracy and the degeneracy due to electronic spin, graphene is a fourfold degenerate system. Rolling a sheet of graphene into a single-wall carbon nanotube can produce different types of systems with respect to their conductance properties; the fourfold degeneracy, however, persists.

A typical transport experiment of this type has a carbon nanotube being suspended between two metallic electrodes and attached to a top gate electrode, as it is shown in Figure 5.13. In such an experiment, parts of the carbon nanotube also serve as electrodes for the central system. Due to the valley degeneracy in the electronic structure, we therefore have to model reservoirs with an additional degree of freedom. Contrary to the situation with electronic spin, the tunnel junctions, which are deformed parts of the graphene lattice, are *not* expected to conserve the valley quantum number. The Anderson–Holstein model mainly considered in this chapter is easily extended to this situation. For simplicity of the discussion, we neglect the electronic spin and only concern ourselves with the effects due to valley degeneracy. We modify the tunnel amplitudes $t_{\alpha\sigma}$ and add an index τ for the respective valley quantum number of the carbon nanotube part of the electrode: $t_{\alpha\tau,\sigma}$. The Golden-Rule rates are rewritten as well yielding $\Gamma^{\sigma}_{\alpha\tau}$ and $\gamma_{\alpha\tau}$. It is clear that with eight instead of previously four amplitudes, a decoupling of a single electronic level from one electrode is no longer generically possible. Consider the non-interacting self energy with respect to tunnelling at electrode α

$$\Sigma_\alpha = \begin{pmatrix} \sum_\tau \Gamma^{\uparrow}_{\alpha\tau} & \sum_\tau \gamma_{\alpha\tau} \\ \sum_\tau \gamma_{\alpha\tau} & \sum_\tau \Gamma^{\downarrow}_{\alpha\tau} \end{pmatrix}.$$

In general, this matrix has full rank. But since it is hermitian, we can find a basis of the electronic Hilbert space $\mathcal{H}_{\text{el}}$ that renders at least one of the Σ_α's diagonal. Since in the master equation both Σ_α's are weighed with the Fermi function of the respective electrode, a simultaneous eigenbasis for both self energies can

[8] As a general reference, see Kane & Mele (1997) and Castro Neto *et al.* (2009).

in general not be found for arbitrary voltages. The non-interacting self-energy matrix Σ_α is the product $W_\alpha^\dagger W_\alpha$ of the coupling matrix $(W_\alpha)_{\tau\sigma} = t_{\alpha\tau,\sigma}$. Due to this property, it is not only hermitian but also positive. Given any vector $\vec{x}$ with its dimension being the number of electronic levels on the nanostructure. Then,

$$\vec{x}^\dagger \Sigma_\alpha \vec{x} = \vec{x}^\dagger W_\alpha^\dagger W_\alpha \vec{x} = (W_\alpha \vec{x})^\dagger (W_\alpha \vec{x}) = |W_\alpha \vec{x}|^2 \geq 0.$$

In the eigenbasis of Σ_α, the diagonal elements therefore do define proper Golden-Rule rates. If we chose Σ_α to be the drain electrode's self energy Σ_D, its off-diagonal element is zero, and below the double-charging threshold when the voltages are chosen such that the pseudo-magnetic fields vanish, $\vec{B} = 0$, the master equation is a rate equation. The physics is similar to the situation in single-mode reservoirs treated before. Although the coupling to a two-mode reservoir thwarts the locking mechanism that produced the current suppression before, the stationary current is defined by the eigenvalues Σ^+ and Σ^- of Σ_D. In case these differ very much $0 \leq \Sigma^- \ll \Sigma^+$, the stationary distribution is almost completely localised in the eigenstate of Σ^-, hence $I \approx \Sigma^-$. Like before, the pseudo-magnetic fields provide an intra-dot coupling, which moves population to the more strongly coupled eigenstate, thereby increasing the stationary current away from the particle–hole symmetric line, where $\vec{B}_\mathrm{S} = 0$. If the smaller eigenvalue was actually zero, as it is the case for the single-mode reservoir we have discussed so far, there would be a full current suppression to $I = 0$. By adjusting the asymmetry of the couplings to the reservoirs, the dip in I due to this coherent suppression effect can be tuned over a wide range corresponding to $\Sigma^+ \neq 0$ and $\Sigma^- = 0$, where $I = 0$, to $\Sigma^+ = \Sigma^-$, where the current suppression is absent and I is maximal and finite. In Figure 5.14, we show numerical data for a vibration-less system (a) and an Anderson–Holstein molecule (b). We scan the tunnel amplitudes such that the smaller eigenvalue of Σ_D is increased from zero to Σ^+. In accordance with our reasoning, the minimal value of the current before the double-charging threshold is lifted from zero until the suppression is completely absent. A similar behaviour is found in quantum spin valves (Braun *et al.*, 2004), where due to the magnetisation of the reservoirs, the orientation of the electronic spin is not conserved in the tunnelling and the dot's electron can indeed tunnel in two equivalent electronic states of the reservoir. In contrast to our discussion, where it is wave-function overlaps that define the tunnel amplitudes and thus give raise to differences in the respective moduli, Braun *et al.* (2004) only consider phase-differences due to different alignment of the electronic spins on the dot and in the ferromagnetic leads.

In the spirit of Berkovits *et al.* (2004), we generalise our findings. Assume M to be the number of modes in the leads and N to be the number of degenerate levels on the nanostructure. According to Berkovits *et al.* (2004), the number of effectively coupled modes and levels is given by the rank of the self-energy matrix $\Sigma = \Sigma_\alpha + \Sigma_{\tilde{\alpha}}$, which is bounded from above by $\mathrm{rank}(\Sigma) \leq \min(M,N)$. Assume $\mathrm{rank}(\Sigma) = r$ and the effective self-energy matrix $\Sigma' \in \mathbb{C}^{r\times r}$ hence being quadratic. Then $\mathrm{rank}(\Sigma'_\mathrm{D})$ defines the number of levels on the dot that *cannot* be decoupled from the drain electrode. In the single-mode reservoirs discussed in this chapter, $r = 2$ and $\mathrm{rank}(\Sigma'_\mathrm{D}) = 1$. For our model of a carbon nanotube, $r = 2$ and also $\mathrm{rank}(\Sigma'_\mathrm{D}) = 2$. The number $r - \mathrm{rank}(\Sigma'_\mathrm{D})$ therefore defines the number of possible dark states of the system. For the steady-state master equation to be uniquely solvable, there can, however, be at most one dark state. One therefore has to restrict the tunnel amplitudes such that $0 \leq r - \mathrm{rank}(\Sigma'_\mathrm{D}) \leq 1$ is always ensured.

In Figure 5.14 (c), we show the differential conductance of the Anderson–Holstein molecule being coupled to a two-mode reservoir as a function of both gate and bias voltage. The numerical data exhibit regions of strong negative differential conductance for positive gate voltage being aligned parallel to the vibronic sideband. This structure is very reminiscent of the one seen in the experimental data shown in

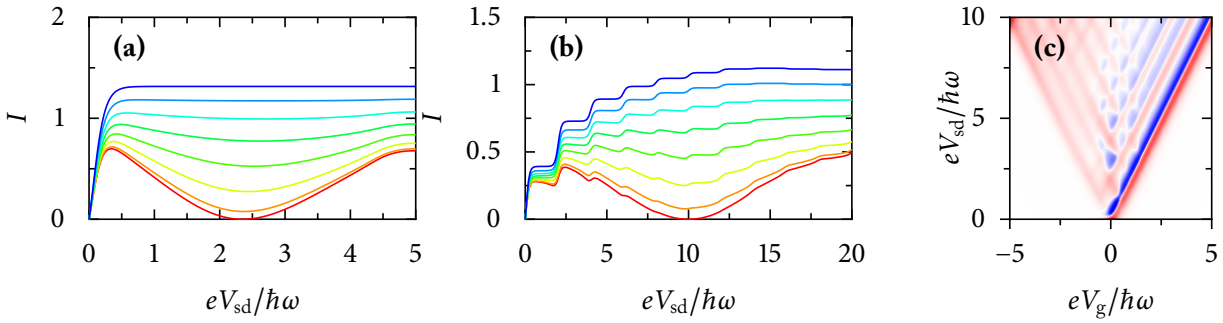

Figure 5.14: (a) Two-mode reservoir interacting with a two-level quantum dot with $U = 2.35\hbar\omega$, $k_BT = 0.05\hbar\omega$. (b) Two-mode reservoir interacting with an Anderson–Holstein molecule. $U = 10\hbar\omega$, $k_BT = 0.05\hbar\omega$, and $\lambda_\uparrow = \lambda_\downarrow = 1.1$. The coupling to the left electrodes are equal and set to unity, and the ones to the right electrode are $t_{R\uparrow,\uparrow} = 1.4$, $t_{R\uparrow,\downarrow} = t_{R\downarrow,\uparrow} = 0$. The coupling $t_{R\downarrow,\downarrow}$ is scanned from 0 to 1.4 (red to blue curves) in order to increase the eigenvalues of Σ_R from $(\Sigma^-,\Sigma^+) = (0,1.4)$, where the effect of the two-mode reservoir is absent, linearly to $(\Sigma^-,\Sigma^+) = (1.4,1.4)$, where the coherent current blockade is gone. (c) Differential conductance of the Anderson–Holstein molecule attached to a two-mode reservoir for varying source–drain and gate voltage. The couplings for the two modes of the reservoir are chosen $\Gamma_\tau = (1,1,1.5^2,0.1^2)$ and $\Gamma_{\bar\tau} = (0.8^2,1,1.4^2,0.25^2)$, and the temperature is increased to $k_BT = 0.1\hbar\omega$. The colour code is blue for negative, white for zero, and red for positive values.

Figure 3.4 and in the experiment by Leturcq *et al.* (2009). However, before an application of the theory as an explanation of the experiment, we have to issue a *caveat*.

A suspended carbon nanotube shows several modes of oscillations and vibrations, for instance longitudinal stretching modes, bending modes, or the breathing mode of the cylindrical structure. Leturcq *et al.* (2009) identify the longitudinal stretching mode as the one whose vibronic sidebands are observed in the data. Combining the effective Dirac equation for the low-energy properties of the nanotube with the theory of elasticity, they derive an estimate for the electron–phonon coupling $\lambda^2 \approx 10/L_\perp[\mathrm{nm}]$. Since the circumference of the nanotube $L_\perp$ is of the order of a few nanometres, the coupling constant is well localised in the regime of order unity. A fit of the differential conductance peaks according to the idea discussed in chapter 3.4 shows that $\lambda^2 \approx 10$, which is large enough to observe Franck–Condon blockade physics in the conductance measurements, see Figure 3.4.

Thus, Leturcq *et al.* (2009) work in the Franck–Condon blockaded regime with strong vibrational relaxation, whereas we consider the full vibrational non-equilibrium dynamics at moderate electron–phonon coupling. Our model of the single-molecule junction still does not incorporate electronic spin. We thus do not model the full fourfold degeneracy of a carbon nanotube, which is likely to introduce additional coherent physics to the dynamics. Due to the large number of tunnel amplitudes in a multi-mode model and the thus broken symmetry of the Hamiltonian in the electronic Hilbert space, the parameter space is highly non-generic, a similar behaviour as already seen in the treatment of the $E\otimes b$ Jahn–Teller molecule. As long as the generic structure of the tunnel amplitudes in suspended carbon nanotube quantum dots is unknown, a systematic study is infeasible. With these restrictions, the numerical data cannot reproduce the experiment quantitatively but only give qualitative tendencies.

Nonetheless, the interplay of the two reservoir modes and their influence on the coherent current suppression as well as the generic negative differential conductance found in the multi-orbital treatment of Anderson–Holstein-type models using master equations is expected to open the view for a profound understanding of the transport characteristics of suspended carbon nanotubes.

Chapter 6

The Singular-Coupling Limit

> The course of every intellectual, if he pursues his journey long and unflinchingly enough, ends in the obvious …
>
> Huxley, *Point Counter Point*

In the previous two parts of this thesis, we have investigated the transport properties of quantum nanostructures such as quantum dots and single-molecule junctions by two fundamentally different approaches. Although both are situated in the regime of weak system–bath interactions, whose mathematical theory we have presented in chapter 2, the applicability of a description in terms of rate equations differs from the one using degenerate master equations. The principal distinction of these two is the scale of the energy differences of the system whose transport properties are to be modelled. It is the purpose of this last chapter to embed both descriptions in a larger context and by doing so derive a theory that is able to interpolate the descriptive gap between rate equations and master equations (Schultz & von Oppen, 2008).

We shall derive and discuss a scaling regime, which in the mathematical theory of Markovian master equations is known as the "singular-coupling limit",[1] but has received rather little if no attention at all in the application to transport theory for quantum nanostructures. We give a motivation both on practical and purely theoretical, that is methodological, considerations to justify the extension of the available theoretical descriptions to the singular-coupling limit. In analogy to the introduction of the master equation in chapters 4 and 5, a simple example of a non-interacting system will help to clarify the physical idea underlying the approach and the ansatz used in the derivation of the kinetic equation. Using the methods developed in chapter 2, we then derive a suitable master equation. We also compare the result to perturbative methods typically employed in quantum transport theory and show how these have to be modified to properly reproduce the result of Davies's method. We finally prove our claim of being able to bridge the gap between rate equations and master equations by an application of the method to molecular electronics.

6.1 Motivation

At first sight, it is unclear why the description of weak-coupling quantum transport has to be extended to a larger context. In the actual derivation of the equations in chapter 2, there was no choice except modelling the system with a degenerate or a non-degenerate Hamiltonian. The first choice results in the degenerate

[1] see for example Breuer & Petruccione (2002, chap. 3.3.3) or Spohn (1980, chap. V.C).

master-equation description applied in chapter 5, while the second amounts to using rate equations as being done in chapter 3. *Tertium non datur.* In the more detailed discussion, however, it becomes apparent that there has to be a third option, as numerous questions being raised by the theory and its experimental applications could not be answered satisfactorily otherwise. These arguments naturally separate into two groups.

6.1.1 Practical

The first extension of the quantum transport theory to more complex systems than those being described by rate equations is to allow for degenerate system Hamiltonians. But when one is honest with physics, there is no real degeneracy in nature at all. Take for instance the hydrogen atom: its Hamiltonian has a large symmetry group and thus many degenerate levels. But the more detailed the discussion becomes and the better the experimental resolution of energy measurements, the less of the symmetry actually survives, for instance due to spin-orbit coupling or the Lamb shift. External perturbations that are not an intrinsic part of the isolated system in the gas-phase, for instance electric or magnetic fields, yield a splitting of formerly degenerate levels, known as the Stark or Zeeman effects. Yet, degenerate levels are a very good approximation for some systems in rather clean environments. We therefore also have to distinguish between non-degenerate and nearly degenerate systems, the precise notion of which we shall define later.

In the theory of molecular electronics, one effect is always mentioned and predominant in the discussion between experimentalists and theorists: the lifting of any degeneracy by the probably asymmetric coupling of the quantum nanostructure to the electronic reservoirs. In general, the coupling is achieved by physi- or chemisorption of the atoms at the edge of the molecule to the metallic electrodes, which necessarily implies the breaking of geometric symmetries by the junction geometry, or an underlying substrate. The theoretical model as an Anderson-type impurity does not account for these effects. It explicitly models *degenerate* levels, free baths, and the tunnelling Hamiltonian as a perturbation. Any splitting due to asymmetric coupling to the electrodes has to come out of the perturbative calculation as a renormalisation of the eigenenergies of the localised level. But all other energy renormalisations are due to symmetry-breaking mechanisms not yet incorporated in our models. How would these have to be accounted for in the Hamiltonian? We have tried to account for such effects in the concluding section of Schultz *et al.* (2008). But the answer given in that article is not satisfactory at all, because the problem turns out to be two-fold. There has to be a renormalisation of the eigenenergies of the isolated and unperturbed system *and* there has to be a way to account for small perturbations of the initially degenerate Hamiltonian. The actual problem comes about as the first is an effect that is obtained *a posteriori* by solving the master equation, while the second is an ingredient to be added *a priori* to the theoretical model. The third choice between rate equations and degenerate master equations must provide an answer, such that both types of splitting can be treated consistently and on equal footing.

6.1.2 Theoretical

Also on the purely theoretical side, the distinction of transport theory into rate equations and degenerate master equations is problematic. Considering the derivation of the Markovian master equation in the weak-coupling limit like in chapter 2, the decoupling of the off-diagonal elements of the reduced density matrix is due to the vanishing commutator of the quantum-dynamical semigroup with all diagonal density matrices provided the Hamiltonian is non-degenerate. A two-level system with energies $\varepsilon_\uparrow$ and $\varepsilon_\downarrow$, will

be described by a rate equation *for every non-zero splitting* $\Omega := \varepsilon_\uparrow - \varepsilon_\downarrow$. A degenerate Hamiltonian, on the contrary, obeys completely different physics in the weak-coupling limit and shows a phenomenology that cannot be described by rate equations. The weak-coupling theory that has been developed so far and is actually used in the quantum transport theory of nanostructures is obviously non-continuous for $\Omega \to 0$. The theory is unable to describe near-degeneracies.

One could, as a remedy, not implement the rotating-wave approximation and work with the full master equation for a finite splitting Ω while keeping all off-diagonal matrix elements of the reduced density matrix in the equation, One would expect that for large enough splitting the off-diagonal elements of ρ eventually decouple from the populations. The resulting equations, known as the *Bloch-Redfield* equations (Timm, 2008) are, however, not positive at all as has been shown by numerous authors, for instance Dümcke & Spohn (1979) and Benatti & Floreanini (2005, Example 3.4). Although the Bloch-Redfield equations are continuous for $\Omega \to 0$, where they yield the master equation used in chapter 5, they defy their proper use for finite and therefore large splitting, where one hopes to recover the rate equations and the decoupling of the off-diagonal elements of the reduced density matrix from its populations.

There is the need of a master equation that both retains coherences between near-degenerate states and fulfils the criteria for generating completely positive dynamics.

6.2 Motivation of the Ansatz

We use a simple non-interacting example calculation to illustrate the physics of our approach and to justify the ansatz for the derivation of the master equation in the singular-coupling limit. This example is in the spirit of chapter 4, where we discuss a non-interacting model to show fundamental properties of electronic transport theory for degenerate nanostructures. The process of obtaining the weak-coupling expressions from the exact solution of the problem serves as the key idea of the approach.

We consider a single-electron transistor with two electronic levels labelled by $\sigma \in \{\uparrow, \downarrow\}$, the z-component of their pseudo-spin, having an energy difference $\Omega := \varepsilon_\uparrow - \varepsilon_\downarrow$, and being coupled to two spinless fermionic reservoirs, a source and a drain electrode labelled by α. The Hamiltonian of this system is in natural units where $\hbar = 1$

$$H = \frac{\Omega}{2}(n_\uparrow - n_\downarrow) + \sum_{k\alpha} \varepsilon_{k\alpha} c^\dagger_{k\alpha} c_{k\alpha} + \sum_{k\alpha\sigma} t_{\alpha\sigma} c^\dagger_{k\alpha} d_\sigma + \text{h.c.}$$

For these non-interacting electronic states the retarded propagator can be computed exactly as it has been done for the degenerate mode in chapter 4. The spectral function is

$$\mathcal{A}(\omega) = \frac{1}{\left|\left((\omega - \frac{\Omega}{2}) + \imath\frac{\Gamma^\uparrow}{2}\right)\left((\omega + \frac{\Omega}{2}) + \imath\frac{\Gamma^\downarrow}{2}\right) + \frac{\gamma^2}{4}\right|^2} \begin{pmatrix} \Gamma^\uparrow(\omega - \frac{\Omega}{2})^2 + \Gamma^\downarrow \frac{\Delta}{4} & \gamma\left[(\omega - \frac{\Omega}{2})(\omega + \frac{\Omega}{2}) - \frac{\Delta}{4}\right] \\ \gamma\left[(\omega - \frac{\Omega}{2})(\omega + \frac{\Omega}{2}) - \frac{\Delta}{4}\right] & \Gamma^\downarrow(\omega + \frac{\Omega}{2})^2 + \Gamma^\uparrow \frac{\Delta}{4} \end{pmatrix}.$$

The coupling constants are the same as in chapter 4. For a non-trivial solution of the degenerate problem $\Omega = 0$, we have to assume $\Delta \neq 0$ generically as otherwise one of the levels would decouple from both electrodes. Since we want to show the continuity of the approach at $\Omega = 0$, $\Delta \neq 0$ has necessarily to be assumed. By replacing $w := \omega + \frac{\Omega}{2}$, the off-diagonal element of the spectral function becomes

$$\mathcal{A}_{\uparrow\downarrow}(w) = \frac{\gamma\left(w(w + \Omega) - \frac{\Delta}{4}\right)}{\left|(w + \imath\frac{\Gamma^\uparrow}{2})(w + \Omega + \imath\frac{\Gamma^\downarrow}{2}) + \frac{\gamma^2}{4}\right|^2}.$$

We discuss this expression both in the weak- and in the singular-coupling limit, showing that only in the latter it is non-zero. Following the definition and treatment of the problem in chapter 2, the weak-coupling limit can be applied, when the tunnelling-induced broadening of the electronic levels defines the smallest energy scale of the problem. We rescale $t_{\alpha\sigma} \mapsto \xi t_{\alpha\sigma}$ and then let $\xi \to 0$. The rescaled expression $\mathcal{A}^{\xi}_{\uparrow\downarrow}(w)$ converges to zero almost everywhere, except at the four roots of its denominator. The stationary properties of the system are described by the equal time correlator, the integral of the spectral function over all frequencies $\int_{\mathbb{R}} \mathcal{A}(w)\, dw$. For non-interacting electrons, one would expect the sum-rule $\int_{\mathbb{R}} \mathcal{A}_{\uparrow\downarrow}(w)\, dw = 0$ to hold. Since both levels are coupled to the same electrode, they do, however, interact. A non-zero correlation therefore indicates the renormalisation of the electronic operators due to the system–bath interaction H_{T}. In the present case, the integral $\int_{\mathbb{R}} \mathcal{A}_{\uparrow\downarrow}(w)\, dw$ can only then be non-zero if all mass of the integrand becomes localised in its singularities, which form a null set,

$$w_{1,2} = \frac{\xi^2}{4}\left[\delta\Gamma - 2\frac{\Omega}{\xi^2} + \imath\Gamma \pm 2\sqrt{\left(\frac{\Omega}{\xi^2}\right)^2 - \gamma^2}\,\right], \qquad w_{3,4} = \frac{\xi^2}{4}\left[\delta\Gamma - 2\frac{\Omega}{\xi^2} - \imath\Gamma \pm 2\sqrt{\left(\frac{\Omega}{\xi^2}\right)^2 - \gamma^2}\,\right],$$

where we also have defined the abbreviation $\delta\Gamma := \Gamma^{\uparrow} - \Gamma^{\downarrow}$. By use of the residue theorem, we evaluate the integral and find

$$\frac{1}{2\pi}\int_{\mathbb{R}} \mathcal{A}^{\xi}_{\uparrow\downarrow}(w)\, dw = \imath\big(\mathrm{Res}(w_1) + \mathrm{Res}(w_2)\big) = \frac{2\gamma\delta\Gamma^2}{\Gamma\left[\Gamma^2 + 4\left(\left(\frac{\Omega}{\xi^2}\right)^2 - \gamma^2\right)\right]} \tag{6.2.1}$$

which obviously tends to zero for $\xi \to 0$. The stationary-state properties of the non-degenerate two-level system in the weak-coupling limit do not show any correlations between the two states. This is what is expected from physical reasoning. On the level of Markovian master equations, this fact is encoded in the application of the rotating-wave approximation, which the theory owes to the derivation in chapter 2 via an integral equation for ρ in the interaction picture. Our considerations regarding the spectral function once more show that the rotating-wave approximation is not an approximation, but the exact treatment. Our result is important with respect to the judgement of the applicability of the Bloch–Redfield equations to non-degenerate systems. The discussion of the behaviour of the exact solution of the non-interacting problem shows that the decoupling of the off-diagonal elements of the reduced density matrix from the populations is indeed dictated by the weak-coupling hypothesis. The Bloch–Redfield equations are therefore no proper implementation of this setting in the theory of Markovian master equations at all.

The singular-coupling limit, on the contrary, serves as the approximation hypothesis when both the tunnelling-induced broadening Γ and the level-splitting Ω are of the same order. If we repeat the above calculation, however, with $\Omega \mapsto \xi^2\Omega$ also being rescaled, or simply replace the quantity in Equation (6.2.1), we obtain

$$\frac{1}{2\pi}\int_{\mathbb{R}} \mathcal{A}^{\xi}_{\uparrow\downarrow}(w)\, dw = \frac{2\gamma\delta\Gamma^2}{\Gamma\big(\Gamma^2 + 4(\Omega^2 - \gamma^2)\big)}, \tag{6.2.2}$$

which is finite. Already the expressions for the roots of the spectral function's denominators suggest that Ω has to scale with ξ^2. In that case

$$w_{1,2} = \frac{\xi^2}{4}\left[\delta\Gamma - 2\Omega + \imath\Gamma \pm 2\sqrt{\Omega^2 - \gamma^2}\,\right], \qquad w_{3,4} = \frac{\xi^2}{4}\left[\delta\Gamma - 2\Omega - \imath\Gamma \pm 2\sqrt{\Omega^2 - \gamma^2}\,\right].$$

Our result also shows that for general rescaling $\Omega \mapsto \xi^\beta \Omega$ neither $\beta < 2$ nor $\beta > 2$ would result in a previously unknown regime. A scaling slower than the weak-coupling due to the tunnelling Hamiltonian would result in the standard weak-coupling result for non-degenerate systems, hence a rate equation, with eventually Ω being set to zero. A faster scaling, on the contrary, would produce a system that is effectively degenerate, hence the kinetic equation will be the degenerate master equation. The limit of $\mathcal{A}^\xi_{\uparrow\downarrow}$ is therefore non-zero in the singular-coupling limit, $\beta = 2$, only, showing that although the system is non-degenerate, some correlations between the electronic levels are retained in the limit. Then Ω is called a near-degeneracy.

At first sight, this result has an unphysical feel. This is because one expects, due to the energy–time uncertainty relation, the stationary density matrix to be localised at energy-eigenstates. Coherences between non-degenerate states describe linear superpositions of these states, whose energy would not be sharp. This reasoning is, however, neglecting the fact that the weak-coupling limit, the singular-coupling limit, or in fact any expansion of the von Neumann equation for the reduced density matrix is perturbation theory up to second order in the tunnelling Hamiltonian. In perturbation theory, the unperturbed energy eigenbasis of the system is modified due to the perturbation. The above result and the persisting correlations indicate the renormalisation of the unperturbed states of the system due to second-order perturbation theory. The unperturbed states are, however, only mixed with states whose separation in energy is of the same order as the tunnelling-induced splitting, namely of order $\mathcal{O}(H_\mathrm{T}^2)$. Hence only the localised states with $\Omega \sim \Gamma$ show non-trivial coherences.

In the introduction to this chapter, we have complained that the master equation in the weak-coupling limit was not continuous in the limit $\Omega \to 0$. The singular-coupling limit, however, is. Consider Equation (6.2.1) and set $\Omega = 0$ *before* sending $\xi \to 0$. This results in exactly the same expression for the integral as if we had sent $\Omega \to 0$ in the singular-coupling expression Equation (6.2.2). On the contrary, if we let $\Omega \to \infty$ in Equation (6.2.2), the off-diagonal element of the spectral function $\mathcal{A}_{\uparrow\downarrow} \to 0$ everywhere, as we would expect from our experience with the rotating-wave approximation the weak-coupling limit. The singular-coupling limit applied to the off-diagonal correlations of the non-interacting two-level Anderson model therefore converges both for vanishing and for infinite splitting Ω to the results one would have expected from the weak-coupling limit of vanishing and finite Ω, respectively. The scaling $\Omega \mapsto \xi^2 \Omega$ is thus a good candidate for the derivation of an interpolating theory between the degenerate master equation and the non-degenerate rate equation; it is the third option asked for in the introduction.

6.3 Derivation of the Master Equation

For the derivation of the master equation in the singular-coupling limit, we recall the main result of the discussion in the previous paragraph. The exact solution of the non-interacting resonant tunnelling problem provides us with the insight that the cross-over regime, in which the lowest-order perturbative transport properties tend from correlations between degenerate levels to vanishing correlations between non-degenerate levels, is properly described by a modified scaling in which not only the tunnelling Hamiltonian is sent to zero but also the near-degenerate sector of the system Hamiltonian. The ratio of the splitting Ω and the tunnelling-induced broadening Γ is kept fixed in this process. Using a scaling approach the system's Hamiltonian or, equivalently, that part of H_S, which is considered a near-degeneracy, also has to be rescaled. In this section, we apply this result to the derivation of a Markovian master equation following the method of Davies (1974), which we have already used in chapter 2 to derive the kinetic equation in the weak-coupling limit.

After having derived the master equation in the singular-coupling limit, we shall discuss standard derivations of master equations for the transport problem. By doing so, we place the mathematical results into the physical context and also give some intuitive feeling and understanding for the underlying physics. We first consider the perturbative approach of Rammer (1998), which is related to the real-time diagrammatic perturbation theory of König (1998). We then show how the derivation of the Bloch–Redfield equations can be consistently extended to properly include correlations between non-degenerate states and thereby substantiate the findings in Braun *et al.* (2004) and Darau *et al.* (2008). Although the results are formally simple, for obtaining them in the first place one has to rely the scaling ansatz of the singular-coupling limit and consistently include it in the derivations of the kinetic equations.

6.3.1 Davies's Method Reviewed

We first review the steps used for obtaining a master equation in the weak-coupling limit in chapter 2.3 and then include the necessary modifications in the ansatz to account for the singular-coupling limit. By doing so, the difference between the two approaches will become clear from a theoretical and formal point of view.

For the derivation of the weak-coupling limit, we use the Hamiltonian

$$H^\xi = H_\mathrm{S} + H_\mathrm{E} + \xi H_\mathrm{S–E}.$$

Using projection operators $\mathcal{P}$ and $\mathcal{Q}$ to obtain a theory for the reduced density matrix of the localised system, the theory leads to an integral equation for ρ_S

$$\rho_\mathrm{S}(t) = e^{-\imath\mathcal{L}_\mathrm{S}t}\rho_\mathrm{S}(0) - \xi^2 \int_0^t e^{-\imath\mathcal{L}_\mathrm{S}(t-s)} \left\{ \int_0^{t-s} e^{\imath\mathcal{L}_\mathrm{S}v} \operatorname{Tr}_\mathrm{E}\left(\mathcal{L}_\mathrm{S–E} e^{-\imath\mathcal{L}^\xi v} \mathcal{L}_\mathrm{S–E}\rho_\mathrm{E} \right) dv \right\} \rho_\mathrm{S}(s) ds.$$

In the interaction picture, the equation is

$$\rho_\mathrm{S}^\mathrm{I}(t) = \rho_\mathrm{S}^\mathrm{I}(0) - \xi^2 \int_0^t e^{\imath\mathcal{L}_\mathrm{S}s} \left\{ \int_0^{t-s} e^{\imath\mathcal{L}_\mathrm{S}v} \operatorname{Tr}_\mathrm{E}\left(\mathcal{L}_\mathrm{S–E} e^{-\imath\mathcal{L}^\xi v} \mathcal{L}_\mathrm{S–E}\rho_\mathrm{E} \right) dv \right\} e^{-\imath\mathcal{L}_\mathrm{S}s} \rho_\mathrm{S}^\mathrm{I}(s) ds.$$

In the limit $\xi \to 0$, given the necessary conditions, the term in brackets converges to

$$\mathcal{K} := \int_0^\infty e^{-\imath\mathcal{L}_\mathrm{S}s} \operatorname{Tr}_\mathrm{E}\left(\mathcal{L}_\mathrm{S–E} e^{-\imath(\mathcal{L}_\mathrm{S}+\mathcal{L}_\mathrm{E})s} \mathcal{L}_\mathrm{S–E}\rho_\mathrm{E} \right) ds. \tag{6.3.1}$$

The oscillating terms in the integral equation yield a time average of the fast time scale of H_S, which eventually leads to the decoupling of the off-diagonal elements of ρ_S from the populations, the rotating-wave approximation.

In the singular-coupling limit, the rescaled Hamiltonian is different:

$$H^\xi = \xi^2 H_\mathrm{S} + H_\mathrm{E} + \xi H_\mathrm{S–E}.$$

Notice that with this ansatz we consider the *full* system Hamiltonian to be of order ξ^2. In a complicated molecular electronics problem, for example the Anderson–Holstein model discussed in chapter 5.3 with near-degenerate electronic levels, the scaling *only* applies to the restriction of the system's Hamiltonian to that subspace of the full Hilbert space in which is it assumed to be nearly degenerate. In our simplified

model also $\mathcal{L}_S$ is rescaled by ξ^2, and the integral equation for the reduced density matrix becomes

$$\rho_S^I(t) = \rho_S^I(0) - \xi^2 \int_0^t e^{\imath\xi^2\mathcal{L}_S s} \left\{ \int_0^{t-s} e^{\imath\xi^2\mathcal{L}_S v} \operatorname{Tr}_E \left(\mathcal{L}_{S-E} e^{-\imath\mathcal{L}^\xi v} \mathcal{L}_{S-E}\rho_E \right) dv \right\} e^{-\imath\xi^2\mathcal{L}_S s} \rho_S^I(s) ds. \quad (6.3.2)$$

The limiting equation for the reduced density matrix is then, due to the additional factors of the scaling variable ξ,

$$\dot{\rho}_S = -\imath\xi^2\mathcal{L}_S\rho_S - \xi^2 \int_0^\infty \operatorname{Tr}_E \left(\mathcal{L}_{S-E} e^{-\imath\mathcal{L}_E s} \mathcal{L}_{S-E}\rho_E \right) ds\, \rho_S. \quad (6.3.3)$$

The averaging over the fast oscillating time scale of the system's Hamiltonian drops out this time, because as not only time is rescaled to the Markovian time scale $\xi^2 t$ but also the system's Liouvillian is, the exponentials used for the transformation into the interaction picture lose all dependence on ξ.

As it is plausible from Equation (6.3.1), the linear operator of the master equation in the singular-coupling limit is formally obtained by assuming $\Omega = 0$ in the dissipator $\mathcal{K}$ but retaining the term in the free-evolution Hamiltonian. This is achieved by adding $-\imath[H_S, \rho_S]$ to the degenerate master equation of appendix B. The splitting Ω does not appear in the dissipator and the Fermi functions coming from the trace over the bath degrees of freedom, because due to the limit $\xi \to 0$, the temperature of the bath is assumed to be too large to resolve the splitting: $\Gamma, \Omega \ll k_B T$. A straightforward perturbative expansion of the von-Neumann equation without the rotating-wave approximation would yield such a dependence and result in the Bloch–Redfield equations, which are not of Lindblad-type.

The master equation in the singular-coupling limit has several important properties. The splitting Ω only appears in the Hamiltonian part of the equation. In a pseudo-Bloch description for a two-level system, this is usually interpreted as the action of pseudo-magnetic field being directed along the z-axis. In fact, any Pauli decomposition of a two-level Hamiltonian $H_S = \sum_i \Omega_i \sigma_i$ generates the corresponding precession due to a pseudo-magnetic field,

$$-\imath[H_S, \rho] = -\imath \sum_{ij} \Omega_i S_j [\sigma_i, \sigma_j] = -\vec{\Omega} \times \vec{S}.$$

On the contrary, the pseudo-magnetic fields that naturally occur in the master equation from the bath-correlation functions are a Hamiltonian contribution to the master equation.[2] Whereas B_z is a renormalisation of the energies, B_x generates an intra-dot tunnelling term. Any perturbation-induced renormalisation of energy is, in second order perturbation theory, of order $\mathcal{O}(H_T^2)$. Thus, the *a priori* included splitting Ω and the *a posteriori* obtained renormalisation due to perturbation theory, the Lamb shift, are of the same order, namely $\mathcal{O}(H_T^2)$. In the presented theory using the singular-coupling limit, both are treated on equal footing: as a Hamiltonian term and not being resolved by the bath correlation functions. In the high-temperature regime, which we are considering here, the tunnelling-induced splitting of a degeneracy can never be resolved as steps of increasing current in the current–voltage characteristics of the quantum transport problem. In order to do so, a *low*-temperature theory has to be employed.

6.3.2 Other Approaches

After we have understood the singular-coupling limit from the formal and mathematical perspective, we turn to its incorporation into the standard techniques being used for quantum transport problems. From

[2] This is well-known and being mentioned for example in Braun *et al.* (2004) and Braig & Brouwer (2005).

the discussion of the general derivation of a Markovian master equation in the weak-coupling limit in chapter 2, it is clear that brute-force perturbation theory, the expansion of time-evolution operators in the von Neumann equation or its iterative solution, cannot produce a consistent theory like Davies's approach does. This is due to the fact that perturbation theory of the von Neumann equation has to ensure the positivity of the density matrix. In the weak-coupling limit, we have seen that the remedy is brought about by justifying reasonable approximations like the Born-approximation, the Markov-approximation, and the rotating-wave approximation. We therefore try to reason what additional assumptions and approximations have to be included in the perturbative treatment to fully reproduce the previous section's results. It will turn out that the key idea is the scaling of H_S and the proper counting of orders of ξ to obtain a true second-order equation.

Perturbation Theory

The perturbation theory for the reduced density matrix due to Rammer (1998) is similar to the real-time diagrammatic technique by König (1998) or in fact any diagrammatic technique at all. Consider for example the diagrams due to self-energy corrections by H_T:

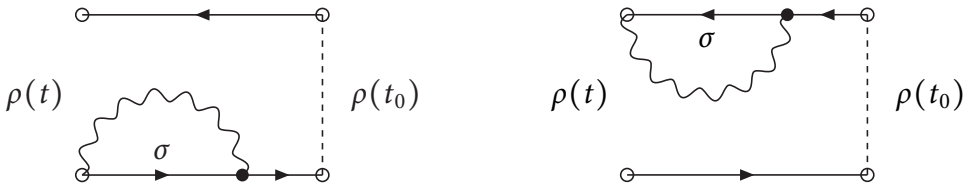

These diagrams depict the virtual tunnelling of an electron onto the nanostructure for an intermediate time τ, leaving a hole in the reservoirs and propagating in state $|\sigma\rangle$ at frequency $\pm\frac{1}{2}\Omega$. They only serve as an illustration and are therefore not labelled completely. Using a highly symbolic notation in order not to confuse the reader by unnecessary constants and formal overload, the essential parts of the integrals described by these diagrams are

$$H_T e^{\mp \imath \frac{\Omega}{2} \tau} H_T$$

with an integration over τ and being multiplied by the bath correlation functions. It is the difference of the free oscillation frequency between the two near-degenerate states that produces all complications and eventually a non-positive operator for the master equation. In the cross-over regime of small splitting, the perturbation and the free evolution with frequency $\Omega/2$ have to be treated equal. This is quite non-intuitive, because it actually demands to do perturbation theory in the system Hamiltonian, which, however, can be solved exactly. The scaling approach demonstrates that this logic is spoiled. Perturbation theory always implies that the energy scale induced by the perturbation is the smallest scale of the problem; in the weak-coupling limit, for example, we have $\Gamma \ll \Omega, k_B T$. The symbol "$\ll$" means a relation obtained by some scaling $\xi \to 0$: both quantities are infinitely far away from each other. There is no numerical trick to overcome the barrier imposed by the relation "$\ll$". Equivalently, we can understand the relation $a \ll b$ such that for all $c \in \mathbb{R}^+$, $ac \ll b$. Hence, in order to discuss the regime $\Omega \sim \Gamma$, also the system Hamiltonian has to be regarded a perturbation.

In the diagrammatic language this reads as follows: We assume the perturbation due to electronic tunnelling to be instantaneous, a quantum jump process. This is a simplification, of course: *natura non facit salti*. It always depends on the time resolution with which the problem is scrutinized. Rabi oscillations in

the problem of a two-level system interacting with a resonant light field are an example where the transition between the two levels is continuous in time. On the Markovian time scale considered here, the tunnelling is seen as an instantaneous process. But if H_S is comparable to H_T, the free time evolution with frequency Ω has to be on the same time scale and hence proceed instantaneously. To account for this, the symbolic self-energy diagrams from before should therefore rather be drawn as

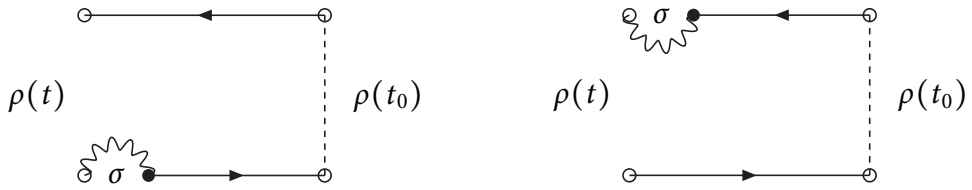

There is no trace of the free system's time evolution present in the self-energy corrections. This is in accordance with the form of Davies's dissipator, where in contrast to the weak-coupling limit all effect of $\mathcal{L}_\mathrm{S}$ is lost in the singular-coupling limit. More formally, one could keep the scaling variables and rewrite the self energy

$$\xi H_\mathrm{T} e^{\mp \imath \xi^2 \frac{\Omega}{2} \tau} \xi H_\mathrm{T} = \xi H_\mathrm{T} \left(\sum_n \frac{\left(\mp \imath \xi^2 \frac{\Omega}{2} \right)^n}{n!} \right) \xi H_\mathrm{T} = \xi H_\mathrm{T} \xi H_\mathrm{T} + \mathcal{O}(\xi^4),$$

without the free propagator appearing at all. By including the scaling and consistently counting all orders of it, the singular-coupling limit is thus recovered by the standard perturbative methods.

Remedy of the Bloch–Redfield Equation

A similar argument suffices to remedy the Bloch–Redfield equation for sequential tunnelling. We recall that these are obtained by a perturbative expansion of the von Neumann equation in the tunnelling Hamiltonian H_T by only applying the Born and the Markov approximation, but none else. This means that all bath correlation functions include the splitting Ω. We therefore find terms of the form

$$f(eV_\mathrm{g} \pm \frac{\Omega}{2} - \mu_\alpha) \, |t_{\alpha\sigma}|^2$$

in the full equation's dissipator. Like in the previous paragraph, we restore the scaling variable ξ and perform a Taylor expansion, as for non-zero temperature, the Fermi functions are smooth,

$$\begin{aligned} f(eV_\mathrm{g} \pm \xi^2 \frac{\Omega}{2} - \mu_\alpha) |\xi t_{\alpha\sigma}|^2 &\approx f(eV_\mathrm{g} - \mu_\alpha) |\xi t_{\alpha\sigma}|^2 \pm f'(eV_\mathrm{g} - \mu_\alpha) \xi^2 \frac{\Omega}{2} |\xi t_{\alpha\sigma}|^2 + \dots \\ &= f(eV_\mathrm{g} - \mu_\alpha) |\xi t_{\alpha\sigma}|^2 + \mathcal{O}(\xi^4). \end{aligned}$$

By counting the orders of ξ consistently, the dissipator, which itself is already of order $\mathcal{O}(\xi^2)$ loses all dependence on the splitting Ω, which is the result of section 6.3.1.

In the treatments of the problem by Braun *et al.* (2004, Sec. VI) and Darau *et al.* (2008), it is this argument, which is used to obtain a master equation for a near-degenerate system. Although the resulting equation is correct, one should always bear in mind that such an expansion of the bath correlation functions is only a *remedy* of the non-positive Bloch–Redfield equations and not an approximation that is applied to simplify the problem.

There is, however, one *caveat* for the remedy of perturbation theory. If one counted the orders of ξ properly, the first correction of the sequential-tunnelling dissipator due to non-zero splitting Ω, would appear at $\mathcal{O}(\xi^4)$, which is the co-tunnelling regime. For the derivation of a fourth-order master equation, we might want to take such contributions of the near-degeneracy into account. As it is clear from the discussion of the Bloch–Redfield equation in chapter 2.1, these terms are still not of Lindblad-type and as such would not yield a completely positive contribution to the dissipator. This comes about as, although one could view co-tunnelling as happening on a Markovian time scale, the corrections due to splitting would only describe sequential tunnelling, which need not be Markovian.

6.3.3 The "Singularity" of the Limit

The notion of the singular-coupling limit is actually rather old. Hepp & Lieb (1973) are the first to define the setting in the context of the theory of Lasers and their non-equilibrium dynamics. Although, so they write, the description of an inert reservoir and its interaction with a localised system is quite at hands, "it is quite another matter to *prove* that the effect of the reservoir is really as tame as it would appear to be. Since different reservoirs can produce different stationary states for the laser, the reservoir is of paramount importance to the laser." Hepp & Lieb classify several types of reservoirs according to their time-correlation function

$$\kappa(t) := \int_{\mathbb{R}} e^{\imath\omega t} \langle c_\omega^\dagger c_\omega \rangle_0 \, d\omega,$$

where the operator c_ω is the annihilation operator of a free particle of the bath with energy ω. For equilibrated fermions, $\langle c_\omega^\dagger c_\omega \rangle_0$ would be the Fermi function $f(\omega)$, and $\kappa(t)$ would be its Fourier transform. Hepp & Lieb distinguish two fundamental types of reservoirs: if the support of κ, which is that part of the domain of the correlation function where $\kappa \neq 0$, has a finite measure, they call the reservoir *regular*. If the support of κ has measure zero, which usually means that the correlation function is localised in a single point $\kappa(t) \propto \delta(t)$, the reservoir is called *singular*. Hepp & Lieb use this term, because the energy of a singular reservoir "has neither an upper nor a lower bound".

Palmer (1977) maps Hepp & Lieb's definition of the singular-coupling limit as a property of the *reservoir* to an equivalent limit, where the system's Hamiltonian is of the same order as the system–bath interaction squared: "singular-coupling" then becomes a property of the *system*. This latter idea is the situation we have been discussing in this chapter and is the result of our physical reasoning concerning the quantum transport problem. The details of Palmer's calculation are sketched in appendix F.

6.4 Applications

In the following two sections, we apply the singular-coupling limit to different transport problems, a two-level Anderson model and the molecular models that one can derive from it. We show that we are able to access the transport regime that lies between the description by rate equations and the description by the degenerate master equation. Both have been studied extensively in chapters 3 and 5, respectively. The reasoning that had actually led our discussion to considering the singular-coupling limit was the focus on the system Hamiltonian's energy scale and its relation to the tunnelling-induced energy scale. The discussion of all these energy scales, including the one of the bath, allows us to give physical meaning to the rate-equation description of degenerate systems, which in general would be considered wrong. The relation between the different energy scales of the system Ω, the bath $k_\mathrm{B}T$, and the system–bath interaction Γ as it

is described by the degenerate master equation is

$$\Omega \ll \Gamma \ll k_{\mathrm{B}}T.$$

Since in the degenerate master equation we actually assume $\Omega = 0$, this seems a contradiction. But in this regime there are no signatures of Ω neither in the dissipator nor in the Hamiltonian part of the master equation, and as such it is just not present, which means it is effectively zero.

In the singular-coupling limit, we have shown by the discussion so far that we are able to access the energy regime

$$\Omega, \Gamma \ll k_{\mathrm{B}}T.$$

We cannot overcome the barrier $\Omega \ll k_{\mathrm{B}}T$ by increasing the *numerical* value of the splitting Ω, as the relation is the result of a limit process. From the localised system's perspective the reservoirs are infinitely hot and by the definition of "infinity", they will stay so for every finite value of Ω. Instead for $\Omega \to \infty$, we obtain an infinite distance of the splitting to the tunnelling induced broadening Γ. As we shall demonstrate within the discussion of the first example, $\Omega \to \infty$ yields a solution of the stationary master equation with all off-diagonal elements of the reduced density matrix being zero. The master equation thus only couples the populations ρ_{ii}. The ignorant implementation of a rate equation for describing quantum transport through a degenerate nanostructure is, however, exactly the same equation. We can therefore interpret the description of a multi-level system by a *degenerate* rate equation as accessing the energy regime

$$\Gamma \ll \Omega \ll k_{\mathrm{B}}T.$$

The splitting is too large to maintain the coherent physics of the degenerate (or near-degenerate) master equation, which is the meaning of the relation $\Gamma \ll \Omega$, but it is still too small to be resolved by the bath correlation functions, for $\Omega \ll k_{\mathrm{B}}T$. Such an energetic resolution could only be achieved if

$$\Gamma \ll \Omega, k_{\mathrm{B}}T,$$

which is not reachable from the level of master equations but only by using the non-degenerate rate equation for the electronic and vibronic populations of the molecule that we have discussed in chapter 3.

6.4.1 Quantum Dots

The first example of a quantum transport problem in the singular-coupling limit is the simplest nanostructure we can think of: resonant tunnelling through two levels. The formal result of the singular-coupling limit is that the splitting Ω has to be added to the degenerate master equation only as a Hamiltonian term. In terms of a pseudo-Bloch equation, this is a pseudo-magnetic field directed along the z-axis. The equations we use in chapter 5 are therefore recast as

$$\dot{\vec{S}} = \sum_{\alpha}\Big[f_{\alpha 1}p_0 + \frac{1}{2}\big(f_{\alpha 2}-(1-f_{\alpha 1})\big)p_1 - (1-f_{\alpha 2})p_2\Big]\vec{n}_\alpha - \sum_{\alpha}\frac{\Gamma_\alpha}{2}\big[f_{\alpha 2}+(1-f_{\alpha 1})\big]\vec{S} - \big(\vec{B}+\Omega\,\hat{e}_z\big)\times\vec{S} \tag{6.4.1}$$

$$\frac{d}{dt}\begin{pmatrix}p_0\\p_1\\p_2\end{pmatrix} = \frac{1}{2}\sum_{\alpha}\Gamma_\alpha\begin{pmatrix}-2f_{\alpha 1} & (1-f_{\alpha 1}) & 0\\ 2f_{\alpha 1} & -f_{\alpha 2}-(1-f_{\alpha 1}) & 2(1-f_{\alpha 2})\\ 0 & f_{\alpha 2} & -2(1-f_{\alpha 2})\end{pmatrix}\begin{pmatrix}p_0\\p_1\\p_2\end{pmatrix} + \frac{1}{2}\sum_{\alpha}\begin{pmatrix}1-f_{\alpha 1}\\ f_{\alpha 2}-(1-f_{\alpha 1})\\ -f_{\alpha 2}\end{pmatrix}\vec{n}_\alpha\cdot\vec{S} \tag{6.4.2}$$

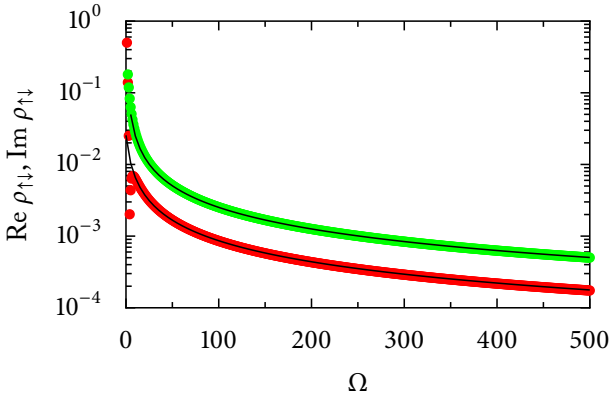

Figure 6.1: Fit of the reduced density matrix's off-diagonal element $\mathrm{Re}\rho_{\uparrow\downarrow}$ (red) and $\mathrm{Im}\rho_{\uparrow\downarrow}$ (green) as a function of the splitting Ω by the function $f(\Omega) = \frac{a}{b+\Omega}$ (solid line each). The hyperbolic relaxation of the coherence effects is very clear for larger splitting. For small Ω, there are deviations from the fit, as the terms due to $\tilde{\Gamma}$ do still play a significant role. The model has been evaluated as $U = 2.35\hbar\omega$, $eV_{\mathrm{sd}} = -2.35\hbar\omega$, such that the pseudo-magnetic field vanishes and only the influence of the splitting is observed. The couplings are $\mathbf{\Gamma} = (1,1,0,1)$, and $\Omega \in [0,500]$.

The off-diagonal element of the reduced density matrix $\rho_{\uparrow\downarrow} = \frac{1}{2}(S_x + \imath S_y)$ is determined by the equation

$$\dot{\rho}_{\uparrow\downarrow} = \sum_\alpha \left[f_{\alpha 1} p_0 + \frac{1}{2}\big(f_{\alpha 2} - (1 - f_{\alpha 1})\big) p_1 - (1 - f_{\alpha 2}) p_2 \right] \gamma_\alpha - \left(\frac{1}{2}\tilde{\Gamma} + \imath(B_z + \Omega) \right) \rho_{\uparrow\downarrow} + \frac{1}{2}\imath B_x S_z,$$

where $\tilde{\Gamma} := \sum_\alpha \Gamma_\alpha \big(f_{\alpha 2} + (1 - f_{\alpha 1}) \big)$ has been abbreviated. In steady-state, $\dot{\rho}_{\uparrow\downarrow} = 0$, and we can solve the above equation for

$$\rho_{\uparrow\downarrow} = \frac{1}{\frac{1}{2}\tilde{\Gamma} + \imath(B_z + \Omega)} \left\{ \sum_\alpha \left[f_{\alpha 1} p_0 + \frac{1}{2}\big(f_{\alpha 2} - (1 - f_{\alpha 1})\big) p_1 - (1 - f_{\alpha 2}) p_2 \right] \gamma_\alpha + \frac{1}{2}\imath B_x S_z \right\}.$$

In the limit $\Omega \to 0$, the equation tends to the result already known from the treatment of degenerate systems; the singular-coupling limit is a theory, which is continuous at $\Omega = 0$ by construction. Although this seems to be a trivial observation, it has to be noted since the description by rate equations and degenerate master equations alone constitutes a theory that is *not* continuous at $\Omega = 0$. The singular-coupling limit thus meets expectations on this side. On the other hand, since all terms in the equation for $\rho_{\uparrow\downarrow}$ are either constant or bounded by a finite number like for example $|\rho_{ii}| \leq 1$ by definition, we can estimate

$$|\rho_{\uparrow\downarrow}| \leq C \left| \frac{1}{\frac{1}{2}\tilde{\Gamma} + \imath(B_z + \Omega)} \right| \leq C' \left| \frac{1}{\Omega} \right| \tag{6.4.3}$$

for some positive constants $C, C' < \infty$. Hence $\rho_{\uparrow\downarrow} \to 0$ as $\Omega \to \infty$. The precession induced by $\Omega \hat{e}_z$ is so fast that the master-equation dynamics due to tunnelling can only resolve the averaged dynamics of the pseudo-spin, which is its projection onto the z-axis. The asymptotic master equation in steady-state, $\dot{\rho} = 0$, is solved by a diagonal density matrix and hence is only a rate equation for the populations. In the singular-coupling limit, the Hamiltonian term given by Ω does not couple to the diagonal elements of ρ, and as such the asymptotic equation is the very equation that one would have formulated for a degenerate system, if one had used a rate equation instead of a degenerate master equation. As we have pointed out in the introduction to this section, this is consistent with the description one would expect in the energy regime $\Gamma \ll \Omega \ll k_{\mathrm{B}} T$. The master equation in the singular-coupling limit therefore also meets the requirements at the border to rate equations and thus is the desired interpolating theory between both rate equation and degenerate master equation. We show the evolution of $\rho_{\uparrow\downarrow}$, the real part of which being the quantity that

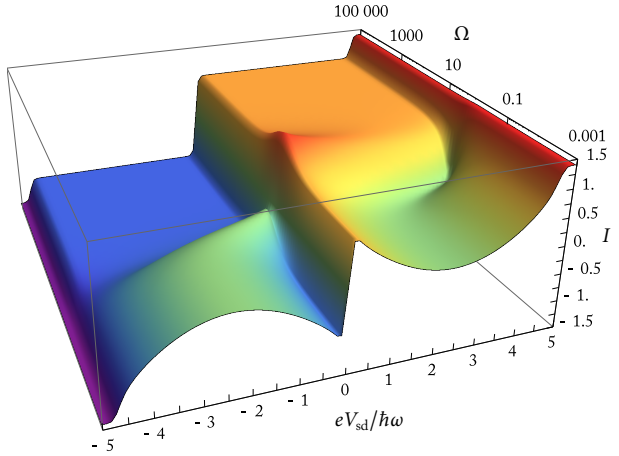

Figure 6.2: Plot of the stationary current of an interacting two-level quantum dot $\Gamma = (1, 1.5^2, 1.5^2, 1)$ at $eV_g = 0$ as a function of the splitting Ω computed with the master equation in the singular-coupling limit. The Coulomb energy is $U = 2.35\hbar\omega$. The splitting $\Omega \sim \Gamma$ is measured in units of $\frac{2\pi}{\hbar}\nu$.

determines the coherent contribution to the stationary current, as a function of Ω in Figure 6.1. Although the estimate (6.4.3) only provides an upper bound, the asymptotes do well fit against a hyperbola. In Figure 6.2, we plot the current–voltage characteristics of the two-level interacting Anderson model. We use the master equation in the singular-coupling limit and increase the numerical value of the splitting Ω from zero onwards. The signatures of the coherent on-site dynamics, the suppression due to the decoupling of one level from the drain electrode and its smoothing out by the influence of the pseudo-magnetic fields vanish as Ω becomes larger. The tip of the current suppression curve, which for $\Omega = 0$ lies at $|eV_{sd}| = U$, moves, because the zero of $B_S + \Omega$, which determines the tip's position, is being shifted as a function of Ω. Although the strong current suppression is lost within one order of magnitude of Ω, the actual recovery of the flat current profile is algebraically slow in the splitting. Such effects should be observable experimentally as even the master equation in the singular-coupling limit features a generic negative differential conductance for very larger energy differences Ω.

We want to note that since there are two points of exact current suppression, one for positive and one for negative bias, which for $\Omega = 0$ are at $|eV_{sd}| = U$, as the splitting Ω is increased both move into the same direction in Figure 6.2. The pseudo-spin description provides an intuitive graphical framework to explain this fact and relates the direction of the tip's motion to the orientation of the pseudo-magnetisations $\vec{n}_\alpha$.

We consider the configuration shown in Figure 6.3 (a) and (b). For negative bias (a), the dynamics is understood easiest in the drain-decoupled basis with $\hat{e}_{z'} \uparrow \uparrow \vec{n}_L$. The residual pseudo-magnetic field induced by electronic tunnelling is directed along $\vec{n}_R$; for positive bias (b), the situation is reversed. The tip of the current suppression curve is found at the very voltage[3] $eV_{sd}^{tip,\pm}$ where the full pseudo-magnetic field

$$\left(\vec{B}_S(eV_{sd}^{tip,\pm},) + \Omega\hat{e}_z\right) || \vec{n}_D. \tag{6.4.4}$$

In the regime where the current suppression is active, that is below the double-charging threshold, the source's pseudo-magnetic field itself is an increasing function of the bias voltage,[4] Figure 6.3 (c). To decide whether $eV_{sd}^{tip,\pm}(\Omega)$ is an increasing or decreasing function of Ω, which defines the direction of the tip's motion in the Figure, we have to understand the alignment of $\vec{B}_S$ with respect to $\vec{n}_S$.

[3] With the additional superscript $\pm$, we indicate whether we refer to the tip at positive or negative bias voltage.

[4] For this discussion, we assume $eV_g = 0$. The generalisation of the argument to finite gate voltage is straightforward.

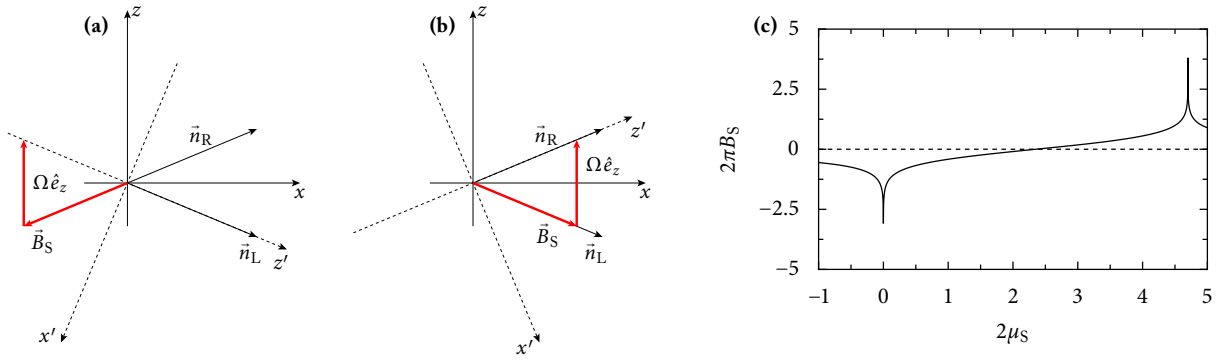

Figure 6.3: Relations of the pseudo-magnetic fields and the splitting Ω for negative (a) and positive (b) source–drain voltage. The coupling parameters are $\mathbf{\Gamma} = (1,1.5^2,1.5^2,1)$. Depending on the sign of $(\vec{n}_L)_z - (\vec{n}_R)_z$, the point of exact current suppression moves either to positive or to negative bias for increasing Ω. (c) Qualitative behaviour of the source electrode's pseudo-magnetic field B_S with $U = 2.35\hbar\omega$ for $k_B T = 0$, when the principal-value integral can be evaluated as a logarithm.

The value of the principal-value integrals that multiply the pseudo-magnetisation $\vec{n}_S$ to form the source's pseudo-magnetic field $\vec{B}_S$ is

$$2\pi B_S(\mu_S) = \mathcal{P}\int \frac{f_S(\varepsilon)}{U-\varepsilon}d\varepsilon + \mathcal{P}\int \frac{\big(1-f_S(\varepsilon)\big)}{\varepsilon}d\varepsilon, \tag{6.4.5}$$

with $\mu_S = \frac{1}{2}|eV_{sd}|$. In Figure 6.3 (c), we show the qualitative behaviour of the pseudo-magnetic fields: for $eV_{sd} < U$, the integral is negative, and for $eV_{sd} > U$ it is positive. From the geometric construction in Figure 6.3, we see that $|\vec{B}_S(eV_{sd}^{tip,\pm})|$ is an increasing function of Ω. But since for negative bias the pseudo-magnetic field has to be anti-parallel to $\vec{n}_R$, the integral (6.4.5) has to be negative with increasing modulus. From Figure 6.3 (c), we see that in order to become more negative, the voltage has to tend to zero. Hence $eV_{sd}^{tip,-} \to 0$ as $\Omega \to \infty$. For positive bias, condition (6.4.4) requires $\vec{B}_S \uparrow\uparrow \vec{n}_L$, which by the same argument amounts to $eV_{sd}^{tip,+} \to 2U$ for $\Omega \to \infty$. Therefore, as Ω is increased, both tips move from $eV_{sd}^{tip,\pm} = \pm U$ towards positive bias. If $(\vec{n}_L)_z - (\vec{n}_R)_z > 0$ that is the opposite case of the just discussed scenario, the geometric construction shows that both tips would move towards negative bias. Due to this argument, we understand that the motion of the current suppression curve's tip as a function of the splitting Ω has to be unidirectional. The direction is defined by the sign of the difference of the pseudo-magnetisations' z-components.

6.4.2 Molecules

The second application of the singular-coupling limit to the quantum transport theory are the molecular models, whose degenerate formulation we have discussed in chapter 5, the Anderson–Holstein molecule and the $E\otimes b$ Jahn–Teller molecule. To conclude the section, we also show that we can treat molecules with general linear electron–phonon coupling, which, due to the asymmetric polaron shift is only possible in the singular-coupling limit.

Anderson–Holstein Molecules

The Anderson–Holstein molecule is the simplest extension of the two-level Anderson model to single-molecule junctions. Both electronic levels are linearly coupled to the vibrational mode, and most importantly,

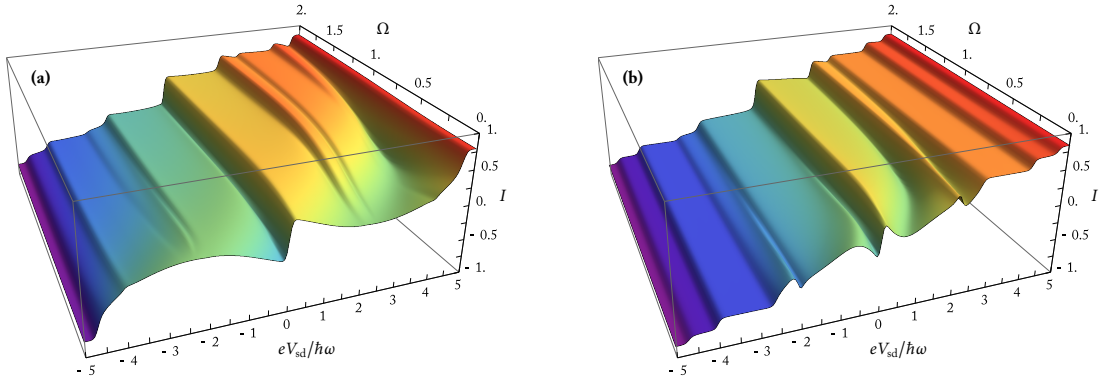

Figure 6.4: Scan of Ω at $eV_g = 0$, $eV_{sd} \in [-5\hbar\omega, 5\hbar\omega]$, $U = 2.35\hbar\omega$, (a) Anderson–Holstein molecule with $\lambda = 1.1$, $\mathbf{\Gamma} = (1, 1.5^2, 1.5^2, 1)$. The splitting is not measured in units of $\hbar\omega$ but, due to the singular-coupling limit $\Omega \sim \Gamma$ in units of $\frac{2\pi}{\hbar}\nu_0$. (b) $E\otimes b$ Jahn–Teller molecule for the same parameters.

by the same coupling constant. The phenomenology of the degenerate, $\Omega = 0$, model shows the coherent current suppression with steps and peaks at the positions of the vibronic excitations. As we have discussed in chapter 5.3, for intermediate electron–phonon coupling, the model's behaviour is a superposition of the phenomenology of the electronic levels and the vibronic sideband structure.

In the numerical evaluation of $I(eV_{sd})$ as a function of Ω in Figure 6.4 (a), the current suppression is lifted for larger splitting Ω, and the small vibronic peaks develop into well-defined steps of the current profile, which are typical for the rate-equation treatment. Due to different tunnelling-induced pseudo-magnetic fields $\vec{B}^q$, for each vibronic excitation but constant splitting Ω, the lifting of the coherent structure and the recovery of the flat profile is different for each sideband. In Figure 6.4 (a), the various vibronic sidebands emerge at different values of Ω.

Jahn–Teller Molecules

For molecules with the $E\otimes b$ Jahn–Teller effect, the linear electron–phonon coupling is defined by $\lambda_\uparrow = -\lambda_\downarrow$. We have discussed the consequences of the thus broken symmetry of the Hamiltonian in the electronic Hilbert space $\mathcal{H}_{el}$ for the degenerate transport characteristics in chapter 5.4. Due to the inability to decouple all vibronic excitations of a single electronic level from the drain electrode, the coherent current blockade being the generic phenomenology of Anderson–Holstein molecules is in general only visible if the zero of the source's pseudo-magnetic field is at a voltage below the first vibronic sideband. In Figure 6.4 (b), we show the Ω-dependent stationary current at zero gate voltage for intermediate charging energy. As we have claimed, the current blockade is localised close to zero bias and vanishes quickly as the splitting Ω is increased. Since the zero of $\vec{B}_S$, where the current blockade is fully developed, is shifted towards higher voltages for large charging energy and therefore far beyond the first vibronic sideband, systems with larger Coulomb repulsion will not show any suppression at all.

For finite Ω, however, we can shift the zero of $\vec{B}_S$ so far that it enters a voltage regime below the first vibronic sideband. Then the vibronic ground state of the system can become dark and a coherent current blockade for finite Ω can be observed. We show our findings in Figure 6.5, where we plot the current suppression due to *finite* Ω. Figure 6.5 (a) shows the current profile for $eV_g = -\hbar\omega$ and varying splitting Ω. The dip in the stationary current for $\Omega \approx 0.6$ is due to the mentioned effect. Diagrams (b) and (c)

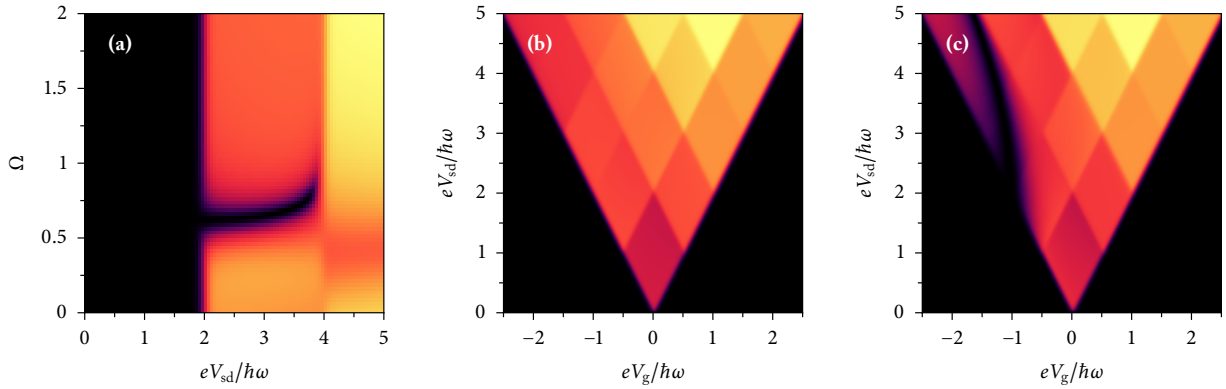

Figure 6.5: (a) Scan of Ω for the Jahn–Teller molecule at $eV_g = -\hbar\omega$, $\Gamma = (1.7^2, 1, 1.4^2, 1)$, $U = 10\hbar\omega$, $\lambda = 1.1$, and $k_B T = 0.02\hbar\omega$. (b) stationary current for $\Omega = 0$, $eV_{sd} \in [0, 5\hbar\omega]$, $eV_g \in [-2.5\hbar\omega, 2.5\hbar\omega]$. (c) same plot, however, with $\Omega = 0.6$, where similarly to the Anderson–Holstein molecule, a trough in the stationary current due to the coherent blockade effect is visible.

show a complete current–voltage profile in the (eV_g, eV_{sd})-plane. For $\Omega = 0$ (b), the current suppression is absent for all voltages. For $\Omega = 0.6$ (c), on the contrary, there is a deep trough of suppressed current, slightly reminiscent of the phenomenology of the Anderson–Holstein molecule, but only for the first vibronic sideband and negative gate voltage.

General Electron–Phonon Coupling

In the introduction to the degenerate master equation in chapter 5, we have considered the general situation of linear electron–phonon couplings. For degenerate electronic systems, these can be always diagonalised leaving only the identity and the σ_z component of the electron–phonon coupling matrix in the electronic Hilbert space $\mathcal{H}_{el}$

$$\Lambda = \lambda_0 \mathrm{Id} + \lambda_z \sigma_z.$$

Due to the polaron transformation, after which we are in the position to actually derive the master equation, because all vibronic structure has been transferred to the tunnelling matrix elements, the system's electronic levels will acquire an energy difference

$$\lambda_\uparrow^2 - \lambda_\downarrow^2 = (\lambda_0 + \lambda_z)^2 - (\lambda_0 - \lambda_z)^2 = 4\lambda_0\lambda_z.$$

For the degenerate theory, $\Omega = 0$, we have to choose either the Anderson–Holstein model, $\lambda_z = 0$, or the $E \otimes b$ Jahn–Teller model, $\lambda_0 = 0$. Using the theory of this chapter, however, we can go beyond this sharp distinction and consider molecules with both λ_0 and λ_z being non-zero to form hybrids between both models. Such models are interesting, because the different electron–phonon coupling of the system's levels amount to different Franck–Condon matrices. In chapter 3, we have discussed the influence of the Franck–Condon matrix on the transport properties at the level of rate equations and we have found a remarkably strong dependence of the phenomenology on the details of the model. For general two-level systems, the singular-coupling limit allows us to study molecules where one level is only weakly coupled but the other is already in the Franck–Condon blockade regime. The current suppression then competes with the coherent physics due to the polaron shift $\Omega = 4\lambda_0\lambda_z$, which allows for a precession of the pseudo-spin between the Franck–Condon blockaded state and the state with intermediate electron–phonon coupling.

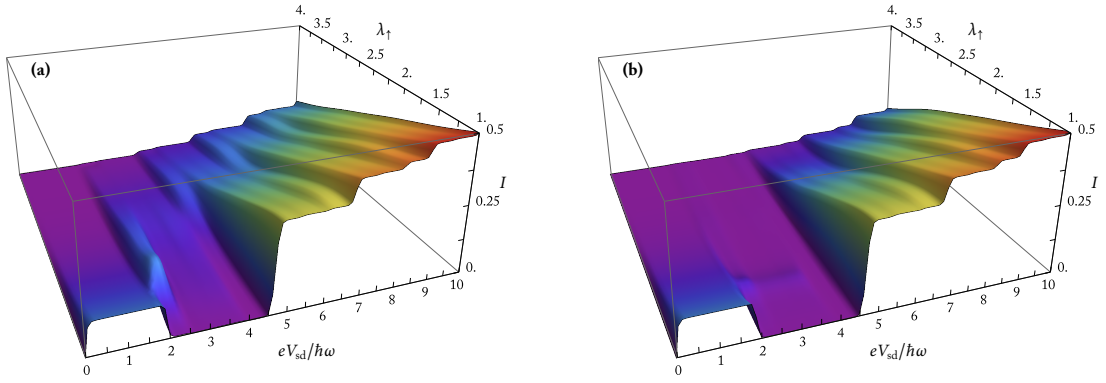

Figure 6.6: Stationary current of a single-molecule junction with general electron–phonon coupling. We set $\lambda_\downarrow = 4$ while $\lambda_\uparrow \in [1,4]$; $U = 2.35\hbar\omega$, $\mathbf{\Gamma} = (1,1,1,1.1^2)$, $k_B T = 0.02\hbar\omega$, $eV_g = 0$, and $eV_{sd} \in [0,10\hbar\omega]$. (a) scan *without* taking into account the different polaron shifts of the levels, (b) scan *with* the polaron shifts. One can clearly see that assuming always a degeneracy produces more structure in the cross-over regime than modelling the asymmetric polaron shift as a near-degeneracy.

In Figure 6.6, we show the numerically computed stationary current for zero gate voltage as a function of the bias and $\lambda_\uparrow$, where $\lambda_\downarrow = 4$, such that the respective level is Franck–Condon blockaded for low bias. In Figure (a), we ignore the asymmetric polaron shift: in Figure (b), we incorporate it via the singular-coupling limit $\Omega = 4\lambda_0\lambda_z = \lambda_\uparrow^2 - \lambda_\downarrow^2$.

For $\lambda_\uparrow = \lambda_\downarrow$, the system is fully Franck–Condon blockaded in the low-bias regime, where both diagrams show the known suppressed current profile. In the opposite case with $\lambda_\downarrow = 4$ and $\lambda_\uparrow = 1$, only one of the states is in the Franck–Condon blockade, while the other ought to have a finite conductance. This is, however, only the case for source–drain voltages before the first vibronic sideband. In this regime, the Franck–Condon blockaded state seems to be almost decoupled from both electrodes compared to the couplings of $|\uparrow\rangle$. This is due to the exponentially suppressed elastic rate $\Gamma_\downarrow^{00}$. Due to be defined by virtual transitions, the x-component of the pseudo-magnetic field B_x is, however, quite large. Following the arguments given in chapter 5.4.1, the pseudo-spin $\vec{S}^0$ of the vibronic ground state vanishes as a whole, and the stationary current is determined by the conductance of the $|\uparrow\rangle$ state alone, $I \approx \frac{1}{3}\Gamma_\uparrow^{00}$, which is of order unity. After the bias voltage has been raised beyond the first vibronic sideband $eV_{sd} > 2\hbar\omega$, this picture breaks down, and the stationary current vanishes almost completely.

In principle, a suppression of the stationary current for finite bias needs an absorbing state. In the master-equation dynamics, such a state is usually generated by a unitary transformation, which removes one of the tunnel couplings to the drain electrode. A Franck–Condon blockaded state like $|\downarrow\rangle$ in this example already has an almost vanishing tunnel coupling, although with respect to both electrodes, such that also the process for populating the state is suppressed. The difference of the Franck–Condon matrices for different electron–phonon couplings and the availability of the first vibronic sideband do, however, provide a mechanism to overcome this restriction and populate the Franck–Condon blockaded state, lock the electron on the molecule, and suppress the stationary current until the double-charging threshold, where a finite current can be transported by the second electron on the molecule.

The Franck–Condon matrix of a molecule with intermediate electron–phonon interaction $\lambda \approx 1$, Figure 3.3 (b), is quite centred at the elastic $|0;q\rangle \mapsto |1;q\rangle$ transitions and allows inelastic transitions $|0;q\rangle \mapsto |1;q+k\rangle$ with small $k \approx 1,2$ to proceed at similar rates. The Franck–Condon blockaded molecule on the contrary allows $|0;0\rangle \mapsto |1;q\rangle$ for larger q only. Due to the asymmetric electron–phonon coupling treated

here, the molecule can use the $|\uparrow\rangle$-state to climb the vibronic ladder from the ground state via several inelastic tunnel processes and then exploit the finite overlap of a highly excited vibronic state with the ground state of the Franck–Condon blockaded state $|\downarrow\rangle$ to populate $|\downarrow;0\rangle$, from which it cannot escape to the drain electrode due to the Franck–Condon blockade. The probability to climb the vibronic ladder with rates of order $\mathcal{O}(10^{-1})$ is large compared to the exponentially suppressed $\Gamma_{\downarrow}^{00}$, such that $|\downarrow;0\rangle$ becomes absorbing with an entry channel that, similarly to the $E\otimes e$ Jahn–Teller molecule discussed in chapter 3.5 is a tunnel cascade involving highly excited vibronic states.

Between the first vibronic sideband and the double-charging threshold, we therefore expect a suppression of the stationary current, which is verified in the numerical data of Figure 6.6 (a) and (b). In the cross-over regime $\lambda_{\uparrow} \to \lambda_{\downarrow}$, the fully degenerate treatment shows a regime where neither suppression mechanism, the Franck–Condon blockade and the climbing of the vibronic ladder, is fully applicable. There, we expect a finite current due comparable Franck–Condon matrix elements and non-zero pseudo-magnetic fields. Such a structure is indeed observed in Figure 6.6 (a).

If we treat the system consistently and start with degenerate states *before* the polaron transformation, and incorporate only the energy difference due to the polaron shift, the finite current for intermediate electron–phonon couplings is damped by the additional action of the pseudo-spins' precession due to $\Omega\hat{e}_z$. There is no cross-over effect.

Chapter 7

Conclusion

If we shadows have offended,
Think but this, and all is mended,
That you have but slumber'd here
While these visions did appear.

Shakespeare, *A Midsummer Night's Dream*

In the course of the research that has led to this thesis, we realised that in the model approach to molecular electronics—being opposed to any *ab-initio* treatment—there were two descriptive concepts for the weak-coupling physics being used in the literature: rate equations, which are an intuitive implementation of the sequential electronic hopping picture by Fermi's Golden Rule, and master equations for the full reduced density matrix, which are applied to more complex nanostructures featuring orbital degeneracies. In the first part, we presented a derivation of these equations from the full von Neumann equation, which is due to Davies, where the distinction in rate and master equations is only determined by the spectral structure of the system Hamiltonian. Davies's approach rests on astonishingly few assumptions, as for example the Markov property is a result of the choice of an asymptotic time scale, which at the same time causes the collapse of the master equation into a rate equation for non-degenerate systems. We were thus able to distinguish between phenomenology due to the coherences in the reduced density matrix and physics being intrinsic to the rate-equation part of the master equation.

In the following, we gave a thorough account on the phenomenology of the thus obtained rate equations when being applied to common models of molecular electronics. Although the equation describes the sequential tunnelling of electrons between well-defined states, we emphasised the importance of first computing the stationary probability distribution, which is dynamically balancing all probability flow, before modelling the current–voltage characteristics using the dynamical picture of electrons hopping onto and off the quantum nanostructure. As a result, we were able to understand various phenomena due to strong electron–phonon coupling, asymmetric coupling to the electrodes, and strong vibronic relaxation. Some of these were related to experimental observations, and we succeeded in isolating their essential physical mechanisms in effective two-state models. In the example of electronic transport through an $E\otimes e$ Jahn–Teller molecule, we could thus model the interplay of two time scales in the dynamics and reproduce the relaxation-induced deformation of differential-conductance peaks very accurately. Furthermore, we understood the Berry-phase induced current blockade also as a consequence of the two-dimensional structure of both the electronic and the vibronic Hilbert space.

Although, as we showed in chapter 3, the current blockade effect in the $E\otimes e$ Jahn–Teller molecule is independent of the basis of the electronic Hilbert space, due to the degeneracy, the problem would have had to be dealt with by a master equation for the full reduced density matrix and not by rate equations for the electronic populations alone. Being well aware of the resulting loss of the intuitive electron-hopping picture in a description by master equations, we first embarked on a discussion of a non-interacting two-level quantum dot. The absence of Coulomb interaction and the availability of a closed solution for the transport problem makes this system a controlled environment in which the dynamics of the master equation can be contrasted with the exact results of a Keldysh analysis. We found that the only effect of the coherences so far, is to rotate the eigenstates of the free system in the electronic Hilbert space by an angle that is defined by the tunnel amplitudes. A description in terms of the pseudo-spin defined by the degenerate two-level system partially restores intuition as the master equation being recast as a pseudo-Bloch equation predicts the spin's stationary orientation according to the pseudo-magnetisations of the electrodes, which are defined by the very tunnel amplitudes

Leaving the protected sandbox and turning to molecular models in chapter 5, we had to include both electron-electron interactions and electron–phonon interactions in the theory. The pseudo-spin description proved to be useful as we found that the free choice of basis in the electronic Hilbert space leads to a generic form of the tunnelling Hamiltonian, in which one of the electronic levels is disconnected from one electrode. Along with finite charging energy, this causes a suppression of the stationary current over a wide range of voltages. The generic suppression of the current and its partial restoration by the pseudo-spin's precession due to virtual intermediate states in the electronic reservoirs is the paradigm of all master-equation phenomenology in the present context. Understanding its physics allows us to explain the steady-state behaviour of multi-level single-molecule junctions in a wide range of parameter regimes with complicated electron–phonon coupling like the $E\otimes b$ Jahn–Teller effect and also persists when the number of electronic modes in the reservoirs is increased. The latter, which leads to a generalisation of the decoupling paradigm in terms of the rank of the non-interacting self energy with respect to tunnelling at a single electrode, is a first step towards modelling real-life systems such as suspended carbon nanotubes, which enjoy a growing interest in transport experiments.

With the phenomenology of the two types of equations being so different, although they have been derived by the same method, we sought to find a way to connect both descriptions. Having such a description is also justified from a practical, non-methodological point of view, as one could imagine an external field, a magnetic field, say, which allowed to tune a two-level system's energies from the degenerate master-equation regime to the non-degenerate rate-equation regime. Using again the controlled environment of the non-interacting two-level system, we realised that the cross-over regime could be accessed by not only letting the tunnelling-induced broadening tend to zero in the derivation, but also the induced energy difference thus keeping their ratio fixed in perturbation theory. By using Davies's method again, we did not correct the unusable Bloch–Redfield equations by a suitable approximation but rather derived the results consistently from beginning to end.

With our previously sharpened intuition of master equation dynamics, we could understand the additional contributions due to near-degeneracies to the precession dynamics of the molecular pseudo-spin in steady-state. The connection to rate equations was then achieved by letting the numerical value of the energy differences tend to infinity, which means we let the near-degeneracy become very large with respect to the tunnelling-induced broadening. This reproduces the rate equation description of a degenerate nanostructure and thereby closes the circle from rate equations to master equations—there and back again.

Having laid the conceptual basis with a profound understanding of the transport properties of simple model systems, we can extend the work into several directions. The two most immediate generalisations are to give up the restriction on the number of electronic levels and to consider the coherent dynamics in a degenerate electronic Hilbert space of dimension larger than two, or to consider different asymptotic time scales and hence go beyond the sequential-tunnelling regime.

Systems with more than two degenerate levels might show different transport phenomena than the one's found in this work. Although we have accounted for the situation of an arbitrary number of levels and reservoir modes from the point of view of the decoupling mechanism in chapter 5.5, a quantum nanostructure with three degenerate electronic levels can for example model the adiabatic potential of the quadratic $E\otimes e$ Jahn–Teller effect (Bersuker & Polinger, 1989, chap. 3.1.1) and enter the regime of strong electron–phonon interactions with physics beyond the Franck–Condon blockade. Braig & Brouwer (2005) formulate the general master equation and give numerical results for a number of examples, but the precise interplay and the role of the individual off-diagonal elements of the reduced density matrix remains unclear. The extension to three or more levels not only enlarges the number of independent elements of ρ but due to Coulomb repulsion also reshuffles the structure of the different energy manifolds, because the dimension of the degenerate Hilbert space depends on the number of excess charges by a binomial factor. It is therefore not clear whether density matrix theory, which relies on wave functions, or general many-body methods like Green function analysis, which deal with the particle number instead, are more appropriate to cope with the growing complexity of the molecular Hilbert space.

Considering the master-equation description beyond the sequential-tunnelling regime, is experimentally relevant as, for instance, co-tunnelling generates vibronic sidebands inside the Coulomb blockade (Lueffe *et al.*, 2008), which can be measured experimentally (Huettel *et al.*, 2008). The rate-equation formalism can be generalised by a further expansion of the von Neumann equation in terms of the tunnelling Hamiltonian. Leijnse & Wegewijs (2008) even keep the formal coherences between different oscillator states in their master equation. As we have shown in this work, such expansions have to be treated very carefully when dealing with degenerate or near-degenerate systems. Although, for example, a consistent expansion of the propagator in terms of the tunnelling Hamiltonian to fourth order would yield a contribution of a sequential-tunnelling process $\propto \xi^2 H_{\mathrm{T}}^2$ combined with one from the near-degeneracy $\xi^2\Omega$, such terms are not of Lindblad form thus posing a potential threat to positivity. In the sense of Davies's derivation of the master equation, only the slowest asymptotic time scale defines the Markov regime. And so a consistent treatment of higher-order tunnelling necessarily amounts to allow for non-Markovian contributions, where Lindblad's theorem is not valid.

From a mathematical perspective, the discussion of non-Markovian contributions is necessary to obtain a consistent picture of the system–bath interactions. In the application of effective and *ad-hoc* theories to experiments one cannot but help to acknowledge the power of these, mathematically incomplete, theories. We have shown how even a sequential-tunnelling rate-equation description suffices to account for the asymmetries in the transport characteristics of suspended carbon nanotubes although these systems feature many degenerate levels and a complex electronic structure. It is thus important to not only ask for a complete and rigorous description but also to ask why the *ad-hoc* expansions yield so astonishingly good results. Posed differently, although the perturbative approach is missing terms, why are these of no importance and can we devise situations, where they do become important and determine the transport properties?

For this endeavour, we need more sensitive probes for the non-equilibrium reduced density matrix than just the stationary current. Already in this work, we have seen that current–voltage profiles can mimic

the rate-equation behaviour although the coherences are non-zero. Thus a consequent next step in an investigation of the non-equilibrium dynamics would be to consider the higher-order cumulants of the stationary current, that is shot noise and skewness. From the microscopic and theoretical approach, one could also simulate the time evolution of a single pure state under the master equation. For rate equations, the Metropolis–Hastings algorithm proved a useful tool in unravelling the tunnelling cascades that lead to certain features in the steady-state transport characteristics. Simulating the time evolution under the fully coherent master equation with a quantum-jump technique or quantum-state diffusion might provide a similar useful insight into the pure-state dynamics.

The theory that we have presented in this work is an effective high-temperature theory. This is seen at two stages. First, by performing perturbation theory, and especially using the scaling approach, we always stick to the regime $\Gamma \ll k_\mathrm{B}T$. For the master equation, this has the effect that neither a near-degeneracy nor the tunnelling-induced energy renormalisations can be resolved energetically by the bath. Second, once the master equation in the weak- or singular-coupling limit has been obtained, the low-temperature regime cannot be accessed by simply letting $k_\mathrm{B}T \to 0$. The most obvious argument, why the two limits—except for single-level models—do not commute, although one could formally set $k_\mathrm{B}T = 0$ in the Fermi functions, is the divergence of the principal-value integrals that exactly describe the tunnelling-induced renormalisations, we wish to resolve energetically. In order to access the low-temperature regime, were $k_\mathrm{B}T \ll \Gamma$ or $k_\mathrm{B}T \sim \Gamma$, by Markovian master equations, we would have to employ a scaling strategy similar to the idea underlying the singular-coupling limit.

Appendix A

Convergence Properties

In this first appendix, we give some further details on the convergence of the operator $K^\xi(\tau) \to K$, which is required in the derivation of the master equation in chapter 2.3. We first calculate the limit by hands like it is usually done in condensed matter physics. We then discuss the role of the convergence-generating factor η, which is commonly used in the calculation of typical integrals. In the last part, we then give the precise criteria for the convergence of the operator as they are posed by Davies (1974).

The Non-Rigorous Calculation

We assume for the time being that as $\tau/\xi^2 \to \infty$, we can approximate $e^{-\imath\mathcal{L}^\xi t}$ by $e^{-\imath(\mathcal{L}_\mathrm{S}+\mathcal{L}_\mathrm{E})t}$. We thus only need to consider the convergence of

$$\tilde{K}^\xi(\tau)(\rho_\mathrm{S}\otimes\rho_\mathrm{E}) := \int_0^{\tau/\xi^2} e^{\imath\mathcal{L}_\mathrm{S}u}\,\mathrm{Tr}_\mathrm{E}\left(\mathcal{L}_{\mathrm{S}\text{–}\mathrm{E}}e^{-\imath(\mathcal{L}_\mathrm{S}+\mathcal{L}_\mathrm{E})u}\mathcal{L}_{\mathrm{S}\text{–}\mathrm{E}}\rho_\mathrm{S}\otimes\rho_\mathrm{E}\right)du.$$

Replacing the Liouville operator $\mathcal{L}_{\mathrm{S}\text{–}\mathrm{E}}$ by the commutator with $H_{\mathrm{S}\text{–}\mathrm{E}}$, we find the explicit action of $\tilde{K}$ on a reduced density matrix ρ_S

$$\tilde{K}^\xi(\tau)(\rho_\mathrm{S}\otimes\rho_\mathrm{E}) = \int_0^{\tau/\xi^2} e^{\imath\mathcal{L}_\mathrm{S}u}\,\mathrm{Tr}_\mathrm{E}\left[H_{\mathrm{S}\text{–}\mathrm{E}}, e^{-\imath(\mathcal{L}_\mathrm{S}+\mathcal{L}_\mathrm{E})u}\left[H_{\mathrm{S}\text{–}\mathrm{E}},\rho_\mathrm{S}\otimes\rho_\mathrm{E}\right]\right]du.$$

By the definition of the Liouville operator, we have the operator identity

$$e^{-\imath(\mathcal{L}_\mathrm{S}+\mathcal{L}_\mathrm{E})t}A = U_0(t)AU_0(-t),$$

with the unperturbed propagators $U_\mathrm{S}(t) := e^{-\imath H_\mathrm{S}t}$ and $U_0(t) := e^{-\imath(H_\mathrm{S}+H_\mathrm{E})t}$. With all these preparations, we can state the operator $\tilde{K}$ in full detail:

$$\begin{aligned}\tilde{K}^\xi(\tau)(\rho_\mathrm{S}\otimes\rho_\mathrm{E}) = \int_0^{\tau/\xi^2}\Big\{&\mathrm{Tr}_\mathrm{E}\big(U_\mathrm{S}(-u)H_{\mathrm{S}\text{–}\mathrm{E}}U_0(u)H_{\mathrm{S}\text{–}\mathrm{E}}(\rho_\mathrm{S}\otimes\rho_\mathrm{E})U_0(-u)U_\mathrm{S}(u)\big)\\ &-\mathrm{Tr}_\mathrm{E}\big(U_\mathrm{S}(-u)H_{\mathrm{S}\text{–}\mathrm{E}}U_0(u)(\rho_\mathrm{S}\otimes\rho_\mathrm{E})H_{\mathrm{S}\text{–}\mathrm{E}}U_0(-u)U_\mathrm{S}(u)\big)\\ &-\mathrm{Tr}_\mathrm{E}\big(U_\mathrm{S}(-u)U_0(u)H_{\mathrm{S}\text{–}\mathrm{E}}(\rho_\mathrm{S}\otimes\rho_\mathrm{E})U_0(-u)H_{\mathrm{S}\text{–}\mathrm{E}}U_\mathrm{S}(u)\big)\\ &+\mathrm{Tr}_\mathrm{E}\big(U_\mathrm{S}(-u)U_0(u)(\rho_\mathrm{S}\otimes\rho_\mathrm{E})H_{\mathrm{S}\text{–}\mathrm{E}}U_0(-u)H_{\mathrm{S}\text{–}\mathrm{E}}U_\mathrm{S}(u)\big)\Big\}du.\end{aligned}$$

The cyclic property of the trace allows us to insert the free propagator of the bath and thereby extend the free system's time-evolution operator U_S to the free time-evolution operator U_0 of the unperturbed Hamiltonian,

$$\begin{aligned}\tilde{K}^{\xi}(\tau)(\rho_S\otimes\rho_E) = \int_0^{\tau/\xi^2} \Big\{ &\mathrm{Tr}_E\big(U_0(-u)H_{S\text{–}E}U_0(u)H_{S\text{–}E}(\rho_S\otimes\rho_E)U_0(-u)U_0(u)\big)\\ &-\mathrm{Tr}_E\big(U_0(-u)H_{S\text{–}E}U_0(u)(\rho_S\otimes\rho_E)H_{S\text{–}E}U_0(-u)U_0(u)\big)\\ &-\mathrm{Tr}_E\big(U_0(-u)U_0(u)H_{S\text{–}E}(\rho_S\otimes\rho_E)U_0(-u)H_{S\text{–}E}U_0(u)\big)\\ &+\mathrm{Tr}_E\big(U_0(-u)U_0(u)(\rho_S\otimes\rho_E)H_{S\text{–}E}U_0(-u)H_{S\text{–}E}U_0(u)\big)\Big\}\,du.\end{aligned}$$

We replace the time-evolution operator U_0 by an explicit time dependence of the system–bath Hamiltonian,

$$\tilde{K}^{\xi}(\tau)(\rho_S\otimes\rho_E) = \int_0^{\tau/\xi^2} \mathrm{Tr}_E\big(H_{S\text{–}E}(u)H_{S\text{–}E}(\rho_S\otimes\rho_E) - H_{S\text{–}E}(\rho_S\otimes\rho_E)H_{S\text{–}E}(u)\big)\,du + \text{h.c.}$$

In our choice of system–bath interaction, we completely ignore the electronic spin, for it only complicates notations and does not add qualitatively different physics. The quantum number σ only labels an internal electronic degree of freedom of the system, such that we have

$$H_{S\text{–}E} = \sum_{k\alpha\sigma} t_{k\alpha\sigma} c^\dagger_{k\alpha} d_\sigma + \text{h.c.}.$$

Here we assume a non-interacting system Hamiltonian H_S. In the presence of Coulomb repulsion, the propagation frequency of the operators depends on the number of particles in the wave function it is acting on, like it is shown in chapter 2.1. Then the time dependence of the operators is

$$c^\dagger_{k\alpha}(u) = e^{-\imath\varepsilon_k u} c^\dagger_{k\alpha} \quad \text{and} \quad d^\dagger_\sigma(u) = e^{-\imath\varepsilon_\sigma u} d^\dagger_\sigma.$$

The terms appearing in the integral have for instance the form

$$\int_0^{\tau/\xi^2} \sum_{k\alpha\sigma} |t_{k\alpha\sigma}|^2 \,\mathrm{Tr}_E\left(c^\dagger_{k\alpha}(u) d_\sigma(u) d^\dagger_\sigma c_{k\alpha}(\rho_S\otimes\rho_E)\right) du.$$

After converting the sum over k into an integral $\int_{\mathbb{R}} d\varepsilon\, \nu(\varepsilon)$ with the density of states $\nu(\varepsilon)$, we consider the individual addends with respect to σ and, because it is the integral we are interested in, ignore the tunnel amplitudes $|t_{k\alpha\sigma}|^2$

$$I^{\xi}_\sigma(\tau) = \int_0^{\tau/\xi^2} \int_{\mathbb{R}} e^{-\imath(\varepsilon-\varepsilon_\sigma)u} \nu(\varepsilon) f_\alpha(\varepsilon)\, d\varepsilon\, du.$$

This integral is to be understood as an operator acting on $d_\sigma d^\dagger_\sigma \rho_S$. The trace over the bath results in the equal-time two-point function, which for fermions is the Fermi function $f_\alpha(\varepsilon) = f(\varepsilon-\mu_\alpha)$. In order to be able to evaluate the integral, we need to pose some conditions on the density of states $\nu(\varepsilon)$. Let ν be square integrable, bounded, and piecewise continuous. Square integrability is a sufficient condition for the existence of the Fourier transform. Boundedness in addition guarantees integrability, which we need to state the final result. By assuming a bounded density of states, we explicitly exclude exotic reservoirs with van-Hove singularities. Since we usually adopt the wide-band limit, such systems are excluded from the

discussion anyway. The piecewise continuity allows us to evaluate the function at every point of its domain. The Fermi function is bounded and for non-zero temperature also continuous everywhere, and hence $h := vf$ has the same properties as v itself. The Fourier transform of h is called $\tilde{h}$ and exists by definition of h. The integral thus becomes

$$I_\sigma^\xi(\tau) = \int_0^{\tau/\xi^2} e^{\imath\varepsilon_\sigma u} \int_{\mathbb{R}} e^{\imath\varepsilon u} h(\varepsilon)\, d\varepsilon\, du = \int_0^{\tau/\xi^2} e^{\imath\varepsilon_\sigma u} \tilde{h}(u)\, du$$
$$\overset{\xi\to 0}{\to} \int_{\mathbb{R}^+} e^{\imath\varepsilon_\sigma u} \tilde{h}(u)\, du = \tilde{h}_+(\varepsilon_\sigma),$$

where $\tilde{h}_+$ is the half-sided Fourier transform. We conclude that the operator

$$\tilde{K} := \lim_{\tau\to\infty} \tilde{K}^\xi(\tau) = \lim_{\xi\to 0} \tilde{K}^\xi(\tau) \tag{A.0.1}$$

does in fact exist.

The Convergence-generating Factor

The actual computation of the half-sided Fourier transform $\tilde{h}_+$ can be tedious if not impossible. We would rather like to exchange the order of integration and instead compute the integral

$$\tilde{I}_\sigma = \int_{\mathbb{R}} v(\varepsilon) f(\varepsilon) \int_{\mathbb{R}^+} e^{-\imath(\varepsilon-\varepsilon_\sigma)t}\, dt\, d\varepsilon.$$

This is, however, not possible as due to the non-existence of the integral over time, the exchanging of integrals is forbidden. By rewriting the integrals as the limits of well-behaved functions, we can achieve the existence of a related integral, which will be helpful for the actual calculations,

$$\begin{aligned}
\int_{\mathbb{R}^+}\int_{\mathbb{R}} e^{-\imath(\varepsilon-\varepsilon_\sigma)t} v(\varepsilon) f(\varepsilon)\, d\varepsilon\, dt &= \int_{\mathbb{R}^+}\int_{\mathbb{R}} \lim_{\eta\to 0} e^{-\imath(\varepsilon-\varepsilon_\sigma-\imath\eta)t} v(\varepsilon) f(\varepsilon)\, d\varepsilon\, dt \\
&= \lim_{\eta\to 0} \int_{\mathbb{R}^+}\int_{\mathbb{R}} e^{-\imath(\varepsilon-\varepsilon_\sigma-\imath\eta)t} v(\varepsilon) f(\varepsilon)\, d\varepsilon\, dt \\
&= \lim_{\eta\to 0} \int_{\mathbb{R}} v(\varepsilon) f(\varepsilon) \int_{\mathbb{R}^+} e^{-\imath(\varepsilon-\varepsilon_\sigma-\imath\eta)t}\, dt\, d\varepsilon \\
&= -\imath \lim_{\eta\to 0} \int_{\mathbb{R}} v(\varepsilon) f(\varepsilon) \frac{1}{\varepsilon-\varepsilon_\sigma-\imath\eta}\, d\varepsilon.
\end{aligned}$$

Due to the existence of the smoothed integral over time, the limit can be taken out of the integral and both integrations can be interchanged. The solution to the integral is then achieved by using a well-known theorem, for which an intuitive proof is given in Merzbacher (1998, appendix A, Equation (A.19)). For any integrable, piecewise continuous function g

$$\lim_{\eta\to 0} \int_{\mathbb{R}} \frac{g(\varepsilon)}{\varepsilon - \imath\eta} = \mathcal{P}\int \frac{g(\varepsilon)}{\varepsilon} d\varepsilon - \imath\pi g(0). \tag{A.0.2}$$

The convergence-generating factor $e^{-\eta t}$ is therefore not an artificial construct just to make the integrals converge, but rather the proper description of the interchange of integrals over energy and time. The general assumption of being able to model the electronic reservoirs in the wide-band limit and thus approximate

$\nu(\varepsilon)$ by a constant is no contradiction to the required assumption of integrability. If we set $g = \nu f$ in Equation (A.0.2) and let $\nu(\varepsilon) \equiv \nu = \text{const.}$, the principal-value integral would not converge. In the numerical treatment, we thus impose a large but finite bandwidth D, within which $\nu(\varepsilon) = \nu$ and tacitly assume this in every calculation involving the principal-value integrals.

The Mathematical Theorem

Davies (1974, Theorem 2.1) gives the precise conditions on the convergence of the operator $K^{\xi}(\tau)$ that have to be met in order that the weak-coupling limit is well-defined.

1. For all $\tau_1 > 0$ there is a constant C such that for $\xi \leq 1$ and $0 \leq \tau \leq \tau_1$

$$\left\| K^{\xi}(\tau) \right\| \leq C.$$

2. The convergence to K has to be such that for $0 < \tau_0 \leq \tau_1 \leq \tau$

$$\lim_{\xi \to 0} \left\| K^{\xi}(\tau) - K \right\| = 0$$

uniformly with respect to $\tau \in [\tau_0, \tau_1]$.

Davies shows that these conditions can be replaced by only requiring the bath correlation functions to be integrable (Davies, 1974, Theorem 3.1), which in the wide-band limit with finite bandwidth D can in general be assumed to hold true.

Appendix B

Explicit Form of the Master Equation

B.1 Master Equation

In this appendix, we give an explicit representation of the master equation derived in chapter 2.3 for a degenerate two-level molecule with arbitrary Coulomb interaction U. For treating the effect due to Coulomb repulsion, we use the fact that the master equation is diagonal in charge states and thus need not to take into account any superpositions of states with a different number of electrons on the device. With this restriction, which for sequential tunnelling is exact, the action of the system's free Hamiltonian is

$$H_\mathrm{S}|\sigma\rangle = \varepsilon_1|\sigma\rangle = (\varepsilon_\mathrm{d} + eV_\mathrm{g})|\sigma\rangle$$
$$H_\mathrm{S}|\sigma\bar{\sigma}\rangle = \varepsilon_2|\sigma\bar{\sigma}\rangle = (2\varepsilon_1 + U)|\sigma\bar{\sigma}\rangle\,.$$

As we have shown in chapter 2.1, one therefore has to be careful when evaluating the self-energy corrections to the unperturbed propagator as the free evolution frequency between two interaction vertices depends on the state the system is in. Since the master equation only accounts for perturbation theory up to second order in the tunnelling Hamiltonian, the failure of Wick's theorem is no problem; there are no contractions to be computed.

The symbols we are using are defined by

$$p_0^q := |0;q\rangle\langle 0;q|, \quad \rho_\sigma^q := |\sigma;q\rangle\langle\sigma;q|, \quad p_1^q := \rho_\sigma^q + \rho_{\bar{\sigma}}^q, \quad p_2^q := |{\uparrow\downarrow};q\rangle\langle{\uparrow\downarrow};q|.$$

The first entry of the ket specifies the charge state of the molecule and the second the number of excited quanta of the harmonic oscillator in the polaron picture. For the electronic two-level system, we use the pseudo-spin notation $\sigma \in \{\uparrow,\downarrow\}$, where $\bar{\sigma}$ denotes the opposite state of σ. A similar notation is used for the electrode index α. The electrons are fermions, which requires to choose a definition of the wave function of the doubly occupied state: $|2\rangle := |{\uparrow\downarrow}\rangle = d_\downarrow^\dagger d_\uparrow^\dagger|0\rangle$. The matrix elements of the molecular terms in the tunnelling Hamiltonian for having a neutral or a doubly occupied state therefore differ by a sign

$$\langle{\uparrow\downarrow}|\, t_{\alpha\downarrow}^* d_\downarrow^\dagger \,|\uparrow\rangle = t_{\alpha\downarrow}^* = \langle\downarrow|\, t_{\alpha\downarrow}^* d_\downarrow^\dagger \,|0\rangle \qquad \langle{\uparrow\downarrow}|\, t_{\alpha\uparrow}^* d_\uparrow^\dagger \,|\downarrow\rangle = -t_{\alpha\uparrow}^* = -\langle\uparrow|\, t_{\alpha\uparrow}^* d_\uparrow^\dagger \,|0\rangle\,.$$

We also assume real tunnel matrix elements and the wide-band limit for the electronic reservoirs, that is the density of states is independent of energy and then set to unity for convenience. We define several

short-hands for the transition rates and cast them into the form of Golden-Rule rates:[1]

$$\Gamma^{pq}_{\alpha\sigma} := \frac{2\pi}{\hbar}\nu\left|t^{pq}_{\alpha\sigma}\right|^2, \quad \gamma^{pq}_{\alpha} := \frac{2\pi}{\hbar}\nu t^{qp}_{\alpha\uparrow} t^{\dagger pq}_{\alpha\downarrow} = \frac{2\pi}{\hbar}\nu t^{qp}_{\alpha\downarrow} t^{\dagger pq}_{\alpha\uparrow}.$$

The matrix $t^{qp}_{\alpha\sigma}$ is an element of the matrix-valued tunnel amplitude generated by the polaron transformation $t^{qp}_{\alpha\sigma} = t_{\alpha\sigma}\langle p|e^{-\lambda_\sigma(b^\dagger - b)}q\rangle$. A missing index on Γ or γ indicates that the sum over the respective index is implied. The symbol $\mathcal{P}\int$ stands for the principal-value integral.

$$\begin{aligned}
\dot{p}^q_0 =& -\sum_{\alpha p} f_\alpha(\varepsilon^p_1 - \varepsilon^q_0)\Gamma^{pq}_\alpha p^q_0 + \sum_{\alpha\sigma p}\big(1 - f_\alpha(\varepsilon^p_1 - \varepsilon^q_0)\big)\Gamma^{pq}_{\alpha\sigma}\rho^p_\sigma \\
&+ \sum_{\alpha p}\big(1 - f_\alpha(\varepsilon^p_1 - \varepsilon^q_0)\big)\gamma^{pq}_\alpha 2\mathrm{Re}\,\rho^p_{\sigma\bar\sigma} && \text{(B.1.1a)} \\
\dot{p}^q_2 =& -\sum_{\alpha p}\big(1 - f_\alpha(\varepsilon^q_2 - \varepsilon^p_1)\big)\Gamma^{qp}_\alpha p^q_2 + \sum_{\alpha\sigma p} f_\alpha(\varepsilon^q_2 - \varepsilon^p_1)\Gamma^{qp}_{\alpha\bar\sigma}\rho^p_\sigma \\
&- \sum_{\alpha p} f_\alpha(\varepsilon^q_2 - \varepsilon^p_1)\gamma^{qp}_\alpha 2\mathrm{Re}\,\rho^p_{\sigma\bar\sigma} && \text{(B.1.1b)} \\
\dot{\rho}^q_\sigma =& -\sum_{\alpha p}\Big[f_\alpha(\varepsilon^p_2 - \varepsilon^q_1)\Gamma^{pq}_{\alpha\bar\sigma} + \big(1 - f_\alpha(\varepsilon^q_1 - \varepsilon^p_0)\big)\Gamma^{qp}_{\alpha\sigma}\Big]\rho^q_\sigma \\
&- \sum_{\alpha p}\Big[-f_\alpha(\varepsilon^p_2 - \varepsilon^q_1)\gamma^{pq}_\alpha + \big(1 - f_\alpha(\varepsilon^q_1 - \varepsilon^p_0)\big)\gamma^{qp}_\alpha\Big]\mathrm{Re}\,\rho^q_{\sigma\bar\sigma} \\
&+ \sum_{\alpha p}\Big[f_\alpha(\varepsilon^q_1 - \varepsilon^p_0)\Gamma^{qp}_{\alpha\sigma} p^p_0 + \big(1 - f_\alpha(\varepsilon^p_2 - \varepsilon^q_1)\big)\Gamma^{pq}_{\alpha\bar\sigma} p^p_2\big)\Big] \\
&- \frac{1}{\pi}\sum_{\alpha p}\mathcal{P}\int d\varepsilon\left\{\frac{f_\alpha(\varepsilon)}{\varepsilon^p_2 - \varepsilon^q_1 - \varepsilon}\gamma^{pq}_\alpha + \frac{1 - f_\alpha(\varepsilon)}{\varepsilon^q_1 - \varepsilon^p_0 - \varepsilon}\gamma^{qp}_\alpha\right\}\mathrm{Im}\,\rho^q_{\sigma\bar\sigma} && \text{(B.1.1c)} \\
\dot{\rho}^q_{\sigma\bar\sigma} =& \sum_{\alpha p}\Big[f_\alpha(\varepsilon^q_1 - \varepsilon^p_0)\gamma^{qp}_\alpha p^p_0 - \big(1 - f_\alpha(\varepsilon^p_2 - \varepsilon^q_1)\big)\gamma^{pq}_\alpha p^p_2\Big] \\
&- \frac{1}{2}\sum_{\alpha p}\Big[-f_\alpha(\varepsilon^p_2 - \varepsilon^q_1)\gamma^{pq}_\alpha + \big(1 - f_\alpha(\varepsilon^q_1 - \varepsilon^p_0)\big)\gamma^{qp}_\alpha\Big](\rho^q_\sigma + \rho^q_{\bar\sigma}) \\
&- \frac{1}{2}\sum_{\alpha p}\Big[f_\alpha(\varepsilon^p_2 - \varepsilon^q_1)\Gamma^{pq}_\alpha + \big(1 - f_\alpha(\varepsilon^q_1 - \varepsilon^p_0)\big)\Gamma^{qp}_\alpha\Big]\rho^q_{\sigma\bar\sigma} \\
&- \frac{1}{2\pi}\imath\sum_{\alpha p}\mathcal{P}\int d\varepsilon\left\{\frac{f_\alpha(\varepsilon)}{\varepsilon^p_2 - \varepsilon^q_1 - \varepsilon}(\Gamma^{pq}_{\alpha\sigma} - \Gamma^{pq}_{\alpha\bar\sigma}) + \frac{1 - f_\alpha(\varepsilon)}{\varepsilon^q_1 - \varepsilon^p_0 - \varepsilon}(\Gamma^{qp}_{\alpha\sigma} - \Gamma^{qp}_{\alpha\bar\sigma})\right\}\rho^q_{\sigma\bar\sigma} \\
&- \frac{1}{2\pi}\imath\sum_{\alpha p}\mathcal{P}\int d\varepsilon\left\{\frac{f_\alpha(\varepsilon)}{\varepsilon^p_2 - \varepsilon^q_1 - \varepsilon}\gamma^{pq}_\alpha + \frac{1 - f_\alpha(\varepsilon)}{\varepsilon^q_1 - \varepsilon^p_0 - \varepsilon}\gamma^{qp}_\alpha\right\}(\rho^q_{\bar\sigma} - \rho^q_\sigma). && \text{(B.1.1d)}
\end{aligned}$$

Some cosmetic simplifications can be applied by noting that $\Gamma^{pq} = \Gamma^{qp}$ and abbreviating the Fermi factors $f^{pq}_{\alpha 1} := f(\varepsilon^p_1 - \varepsilon^q_0 - \mu_\alpha)$ and $f^{pq}_{\alpha 2} := f(\varepsilon^p_2 - \varepsilon^q_1 - \mu_\alpha) = f(\varepsilon^q_1 + U - \varepsilon^p_0 - \mu_\alpha)$. In the Anderson–Holstein case, $\lambda_\sigma = \lambda_{\bar\sigma}$, also $\gamma^{pq} = \gamma^{qp}$. The stationary current through lead α can either be computed using the formulae given in section 2.4 or be derived from the above equations of motion by noting that this current is given by the α-contribution of the expression $-\sum_p(\dot{p}^p_0 - \dot{p}^p_2)$. This is due to the Ramo–Shockley theorem (Blanter & Büttiker, 2000, chaps. 3.1 and 5.2). Given the capacitances of the tunnel junctions, c_L and c_R, the total

[1] Although we mention the density of states ν and Planck's constant $\hbar$ explicitly, we tacitly assume their values to be unity, as they will not play any role in the theory.

current through the device is

$$I = \frac{c_{\mathrm{L}}\dot{Q}_{\mathrm{R}} + c_{\mathrm{R}}\dot{Q}_{\mathrm{L}}}{c_{\mathrm{R}} + c_{\mathrm{L}}},$$

with $\dot{Q}_\alpha$ being the number of charges leaving reservoir α per unit time. For equal capacitances $c_{\mathrm{R}} = c_{\mathrm{L}}$, the steady-state particle currents through both junctions are equal and exactly described by the change of probability of the neutral and charged state of the system. Either way we find[2]

$$\begin{aligned} I_\alpha = &\sum_{pq} f_{\alpha 1}^{pq}\Gamma_\alpha^{pq} p_0^q - \sum_{pq}(1-f_{\alpha 2}^{qp})\Gamma_\alpha^{qp} p_2^q - \sum_{\sigma pq}\Big[(1-f_{\alpha 1}^{pq})\Gamma_{\alpha\sigma}^{pq} - f_{\alpha 2}^{qp}\Gamma_{\alpha\bar{\sigma}}^{qp}\Big]\rho_\sigma^p \\ &- \sum_{pq}\Big[(1-f_{\alpha 1}^{pq})\gamma_\alpha^{pq} + f_{\alpha 2}^{qp}\gamma_\alpha^{qp}\Big] 2\mathrm{Re}\,\rho_{\uparrow\downarrow}^p. \end{aligned} \tag{B.1.2}$$

The current is assumed to be positive, when it is flowing *out* of the respective electrode. For positive bias, one therefore finds $I_{\mathrm{L}} = -I_{\mathrm{R}}$.

B.2 Pseudo-Bloch Representation

The only non-diagonal elements of the density matrix that remain non-zero in our treatment of the molecular-electronics devices are those between degenerate (or near-degenerate) states. We only discuss electronic two-level systems, which define a pseudo-spin on and inside the Bloch-sphere. As the Hilbert space of the singly charged molecule is the product $\mathcal{H}_{\mathrm{vib}} \otimes \mathbb{C}^2$, the pseudo-spin also acquires a vibronic index. We define $\vec{S}$ for every vibronic level q obtaining $\vec{S}^q$ with

$$S_x^q := 2\,\mathrm{Re}\,\rho_{\uparrow\downarrow}^q, \quad S_y := 2\,\mathrm{Im}\,\rho_{\uparrow\downarrow}^q, \quad S_z^q := \rho_\uparrow^q - \rho_\downarrow^q.$$

The explicit representation of the master equation in terms of the pseudo-spin $\vec{S}^q$ and the populations of the three charge states p_i is

$$\begin{aligned} \dot{\vec{S}}^q = &\frac{1}{2}\sum_{\alpha p}\Big[2f_{\alpha 1}^{qp}\vec{n}_\alpha^{qp} p_0^p + \big(f_{\alpha 2}^{pq}\vec{n}_\alpha^{pq} - (1-f_{\alpha 1}^{qp})\vec{n}_\alpha^{qp}\big)p_1^q - 2(1-f_{\alpha 2}^{pq})\vec{n}_\alpha^{pq} p_2^p\Big] \\ &- \frac{1}{2}\sum_\alpha\Big[f_{\alpha 2}^{pq} + (1-f_{\alpha 1}^{qp})\Big]\Gamma_\alpha^{qp}\vec{S}^q - (\vec{B}_2^{pq} + \vec{B}_0^{qp}) \times \vec{S}^q \end{aligned}$$

The pseudo-magnetisation $\vec{n}_\alpha^{pq}$ is defined by the tunnel couplings,

$$\vec{n}_\alpha^{pq} := \begin{pmatrix} 2\gamma_\alpha^{pq} \\ 0 \\ \Gamma_{\alpha\uparrow}^{pq} - \Gamma_{\alpha\downarrow}^{pq} \end{pmatrix}$$

The pseudo-magnetic fields are defined by the principal-value terms and are parallel to the pseudo-magnetisations $\vec{n}_\alpha$

$$\vec{B}_2^{pq} := \frac{1}{2\pi}\sum_\alpha \mathcal{P}\!\int \frac{f_\alpha(\varepsilon)}{\varepsilon_2^p - \varepsilon_1^q - \varepsilon} d\varepsilon\, \vec{n}_\alpha^{pq} \quad \text{and} \quad \vec{B}_0^{qp} := \frac{1}{2\pi}\sum_\alpha \mathcal{P}\!\int \frac{1-f_\alpha(\varepsilon)}{\varepsilon_1^q - \varepsilon_0^p - \varepsilon} d\varepsilon\, \vec{n}_\alpha^{qp}.$$

[2] For notational convenience we usually drop the angular brackets denoting the expectation value.

The index indicates the excess charge of the virtual intermediate state. For the numerical implementation, these integrals imply a large but finite bandwidth D, since in the wide-band limit, the integral over the full real line diverges logarithmically. The equation for the populations is

$$\begin{aligned}\frac{d}{dt}\begin{pmatrix}p_0^q\\ p_1^q\\ p_2^q\end{pmatrix} &= \frac{1}{2}\sum_{\alpha p}\begin{pmatrix}-2f_{\alpha 1}^{pq}\Gamma_\alpha^{pq} & (1-f_{\alpha 1}^{pq})\Gamma_\alpha^{pq} & 0\\ 2f_{\alpha 1}^{qp}\Gamma_\alpha^{qp} & -f_{\alpha 2}^{pq}\Gamma_\alpha^{pq}-(1-f_{\alpha 1}^{qp})\Gamma_\alpha^{qp} & 2(1-f_{\alpha 2}^{pq})\Gamma_\alpha^{pq}\\ 0 & f_{\alpha 2}^{qp}\Gamma_\alpha^{qp} & -2(1-f_{\alpha 2}^{qp})\Gamma_\alpha^{qp}\end{pmatrix}\begin{pmatrix}p_0^q\\ p_1^q\\ p_2^q\end{pmatrix}\\ &+\frac{1}{2}\sum_{\alpha p}\left\{\begin{pmatrix}1-f_{\alpha 1}^{pq}\\ 0\\ 0\end{pmatrix}\vec{n}_\alpha^{pq}\cdot\vec{S}^p+\begin{pmatrix}0\\ f_{\alpha 2}^{pq}\\ 0\end{pmatrix}\vec{n}_\alpha^{pq}\cdot\vec{S}^q\right\}\\ &+\frac{1}{2}\sum_{\alpha p}\left\{\begin{pmatrix}0\\ -(1-f_{\alpha 1}^{qp})\\ 0\end{pmatrix}\vec{n}_\alpha^{qp}\cdot\vec{S}^q+\begin{pmatrix}0\\ 0\\ -f_{\alpha 2}^{qp}\end{pmatrix}\vec{n}_\alpha^{qp}\cdot\vec{S}^p\right\}.\end{aligned}$$

B.3 Equations for Systems without Phonons

We can often understand the fundamental physics of a molecular electronics device by first discussing the dynamics with the bare electronic levels and then adding the vibronic structure on top. We therefore formulate the above master equation in terms of the electronic state alone. Formally, this is achieved by removing all vibronic indices.

B.3.1 Master Equation

The master equation without the vibronic indices simplifies as several of the coupling constants become equal and can be taken outside the brackets.

$$\dot{p}_0 = -\sum_\alpha f_{\alpha 1}\Gamma_\alpha p_0 + \sum_{\alpha\sigma}(1-f_{\alpha 1})\Gamma_{\alpha\sigma}\rho_\sigma + \sum_\alpha (1-f_{\alpha 1})\gamma_\alpha 2\mathrm{Re}\rho_{\sigma\bar{\sigma}} \tag{B.3.1a}$$

$$\dot{p}_2 = -\sum_\alpha (1-f_{\alpha 2})\Gamma_\alpha p_2 + \sum_{\alpha\sigma} f_{\alpha 2}\Gamma_{\alpha\bar{\sigma}}\rho_\sigma - \sum_\alpha f_{\alpha 2}\gamma_\alpha 2\mathrm{Re}\rho_{\sigma\bar{\sigma}} \tag{B.3.1b}$$

$$\begin{aligned}\dot{\rho}_\sigma = &-\sum_\alpha\Big[f_{\alpha 2}\Gamma_{\alpha\bar{\sigma}}+(1-f_{\alpha 1})\Gamma_{\alpha\sigma}\Big]\rho_\sigma - \sum_\alpha\Big[-f_{\alpha 2}+(1-f_{\alpha 1})\Big]\gamma_\alpha\mathrm{Re}\rho_{\sigma\bar{\sigma}}\\ &+\sum_\alpha\Big[f_{\alpha 1}\Gamma_{\alpha\sigma}p_0+(1-f_{\alpha 2})\Gamma_{\alpha\bar{\sigma}}p_2\Big] - \frac{1}{\pi}\sum_\alpha\mathcal{P}\int d\varepsilon\left\{\frac{f_\alpha(\varepsilon)}{\varepsilon_2-\varepsilon_1-\varepsilon}+\frac{1-f_\alpha(\varepsilon)}{\varepsilon_1-\varepsilon_0-\varepsilon}\right\}\gamma_\alpha\mathrm{Im}\rho_{\sigma\bar{\sigma}}\end{aligned} \tag{B.3.1c}$$

$$\begin{aligned}\dot{\rho}_{\sigma\bar{\sigma}} = &\sum_\alpha\Big[f_{\alpha 1}p_0-(1-f_{\alpha 2})p_2\Big]\gamma_\alpha - \frac{1}{2}\sum_\alpha\Big[-f_{\alpha 2}+(1-f_{\alpha 1})\Big]\gamma_\alpha(\rho_\sigma+\rho_{\bar{\sigma}}) - \frac{1}{2}\sum_\alpha\Big[f_{\alpha 2}+(1-f_{\alpha 1})\Big]\Gamma_\alpha\rho_{\sigma\bar{\sigma}}\\ &-\frac{1}{2\pi}\imath\sum_\alpha\mathcal{P}\int d\varepsilon\left\{\frac{f_\alpha(\varepsilon)}{\varepsilon_2-\varepsilon_1-\varepsilon}+\frac{1-f_\alpha(\varepsilon)}{\varepsilon_1-\varepsilon_0-\varepsilon}\right\}(\Gamma_{\alpha\sigma}-\Gamma_{\alpha\bar{\sigma}})\rho_{\sigma\bar{\sigma}}\\ &-\frac{1}{2\pi}\imath\sum_\alpha\mathcal{P}\int d\varepsilon\left\{\frac{f_\alpha(\varepsilon)}{\varepsilon_2-\varepsilon_1-\varepsilon}+\frac{1-f_\alpha(\varepsilon)}{\varepsilon_1-\varepsilon_0-\varepsilon}\right\}\gamma_\alpha(\rho_{\bar{\sigma}}-\rho_\sigma).\end{aligned} \tag{B.3.1d}$$

The stationary current through the tunnel junction at electrode α is obtained by contracting Equation (B.1.2)

$$I_\alpha = f_{\alpha 1}\Gamma_\alpha p_0 - (1-f_{\alpha 2})\Gamma_\alpha p_2 - \sum_\sigma\Big[(1-f_{\alpha 1})\Gamma_{\alpha\sigma} - f_{\alpha 2}\Gamma_{\alpha\bar{\sigma}}\Big]\rho_\sigma - \Big[(1-f_{\alpha 1})\gamma_\alpha + f_{\alpha 2}\gamma_\alpha\Big]2\,\mathrm{Re}\,\rho_{\uparrow\downarrow}.$$

B.3.2 Pseudo-Bloch Representation

Just like for the master equation for the molecule, the system without phonons can be described by an equation for the pseudo-spin and the populations

$$\dot{\vec{S}} = \frac{1}{2}\sum_\alpha \Big[2f_{\alpha1}p_0 + \big(f_{\alpha2}-(1-f_{\alpha1})\big)p_1 - 2(1-f_{\alpha2})p_2\Big]\vec{n}_\alpha - \frac{1}{2}\sum_\alpha \Big[f_{\alpha2}+(1-f_{\alpha1})\Big]\Gamma_\alpha\vec{S} - \vec{B}\times\vec{S}, \tag{B.3.2a}$$

$$\frac{d}{dt}\begin{pmatrix}p_0\\p_1\\p_2\end{pmatrix} = \frac{1}{2}\sum_\alpha \Gamma_\alpha \begin{pmatrix}-2f_{\alpha1} & (1-f_{\alpha1}) & 0\\ 2f_{\alpha1} & -f_{\alpha2}-(1-f_{\alpha1}) & 2(1-f_{\alpha2})\\ 0 & f_{\alpha2} & -2(1-f_{\alpha2})\end{pmatrix}\begin{pmatrix}p_0\\p_1\\p_2\end{pmatrix} + \frac{1}{2}\sum_\alpha \begin{pmatrix}1-f_{\alpha1}\\ f_{\alpha2}-(1-f_{\alpha1})\\ -f_{\alpha2}\end{pmatrix}\vec{n}_\alpha\cdot\vec{S}, \tag{B.3.2b}$$

$$\vec{B} := \frac{1}{2\pi}\sum_\alpha \mathcal{P}\!\int f_\alpha(\varepsilon)\left(\frac{1}{U-\varepsilon}+\frac{1}{\varepsilon}\right)d\varepsilon\,\vec{n}_\alpha. \tag{B.3.2c}$$

The stationary current in this notation is

$$I_\alpha = \Gamma_\alpha\left[f_\alpha p_0 - \frac{1}{2}\Big((1-f_\alpha)-f_{\alpha2}\Big)p_1 - (1-f_{\alpha2})p_2\right] - \frac{1}{2}\Big((1-f_\alpha)+f_{\alpha2}\Big)\vec{n}_\alpha\cdot\vec{S}.$$

By considering the dynamics of the electronic levels only and neglecting any oscillator excitations, our equations acquire a form similar to those of Braun *et al.* (2004). There, however, the pseudo-magnetisations are the actual magnetisations of ferromagnetic reservoirs, whereas in our context they are defined by the tunnel amplitudes.

B.4 Numerical Implementation

The numerical implementation of the above equations is straightforward. The density matrix is mapped to a vector

$$\begin{pmatrix}p_0 & 0 & 0 & 0\\ 0 & \rho_\uparrow & \rho_{\uparrow\downarrow} & 0\\ 0 & \rho^*_{\uparrow\downarrow} & \rho_\downarrow & 0\\ 0 & 0 & 0 & p_2\end{pmatrix} \mapsto \begin{pmatrix}p_0\\ \rho_\uparrow\\ \rho_\downarrow\\ p_2\\ \mathrm{Re}\,\rho_{\uparrow\downarrow}\\ \mathrm{Im}\,\rho_{\uparrow\downarrow}\end{pmatrix}.$$

The extension to the system with phonons is done by defining a cut-off N of the phonon number and enumerating the individual states by the vibronic index: for example

$$p_0 \mapsto \begin{pmatrix}p_0^0\\ p_0^1\\ \vdots\\ p_0^N\end{pmatrix}.$$

Splitting the off-diagonal element of ρ into its real and imaginary part has the advantage that the master equation becomes a linear equation in a *real* vector space. The numerical algorithms available for real-valued problems are much faster than those involving complex numbers, although the possibility of operator-overloading of C++ simplifies the treatment of complex variables drastically. The master equation can thus

be written—not just symbolically or with superoperators but actually—

$$\dot{\rho} = \mathcal{M}\rho,$$

where $\mathcal{M}$ is a suitable matrix implementing the above linear equation. Its unique steady-state solution is found by computing the kernel of the matrix $\mathcal{M}$ and normalising the result with respect to the populations.[3] The kernel of $\mathcal{M}$ is the solution of the linear equation $\mathcal{M}\rho = 0$. To find this, one replaces one, say the ith, of the equations with the normalisation condition $\|\rho\| = 1$. The thus obtained matrix $\mathcal{M}'$ for the linear system has empty kernel and the solution to the linear system

$$\mathcal{M}'\rho = \vec{e}_i, \tag{B.4.1}$$

where $\vec{e}_i$ is the vector with the ith element being one and all others zero, is the normalised stationary density matrix in vector form. If the solution to Equation (B.4.1) is not unique, this is an indicator that the master equation splits into two or more independent sub-systems. This behaviour is seen for instance in the decoupling regime for the master equation, chapter 5.1 or in the non-equilibrium treatment of the $E\otimes e$ Jahn–Teller problem, chapter 3.5, where the appearance of many dark states renders the solution non-unique.

[3] Obviously, if $\rho = (p_0, \rho_\uparrow, \rho_\downarrow, p_2, \mathrm{Re}\rho_{\uparrow\downarrow}, \mathrm{Im}\rho_{\uparrow\downarrow})$, the trace norm is $\|\rho\| = p_0 + \rho_\uparrow + \rho_\downarrow + p_2$.

Appendix C

The Metropolis–Hastings Algorithm

The Monte-Carlo technique is a powerful and widely used stochastic method for approximating integrals numerically. For example, the area enclosed by an arbitrary curve C in the plane might be difficult to compute by implementing Riemann's method by further and further subdividing geometric partitions of area to be computed. Using a huge number of randomly chosen points of the plane and dividing them into two sets: inside and outside the closed curve, the number

$$A_C(N) = \frac{N_{\text{in}}}{N_{\text{in}} + N_{\text{out}}}$$

approximates the area enclosed by the curve as the total number of chosen points $N = N_{\text{in}} + N_{\text{out}} \to \infty$.

The Monte-Carlo technique can also be used to solve the master equation of the weak-coupling transport problem. At first sight, such an approach is unnecessary as the master equation is a linear system of equations and can be easily solved numerically. Also the time evolution of the density matrix can be computed by exponentiating the Liouvillian, which is only a finite-dimensional matrix. What a Monte-Carlo simulation, however, produces in addition is a time-evolution of the system in terms of *quantum jumps*. This corresponds to the intuitive picture of single particles *hopping* from the electrodes onto the molecule and back again. One thus simulates a single quantum trajectory of a pure state under the Schrödinger equation. By summing over many realisations of a trajectory, one obtains the mixed ensemble that is given by the time evolution of the density matrix due to the master equation. We thus get a very good picture of what the system actually does in a single realisation of the stochastic time evolution defined by the von Neumann equation. We can trace the trajectory into dark or almost absorbing states like in chapter 3.5 and thus not only understand the actual mechanism of a current suppression but follow the time evolution of the system through tunnel cascades, which in turn helps to understand the conditions to actually observe such a current suppression. By simulating the time-dependent current through the device, one also obtains an intuitive feeling of the different time scales that are present in the system's dynamics. We used such a technique to understand the relaxation-induced modifications of the differential conductance peaks in chapter 3.5. Koch & von Oppen (2005b), for example, use Monte-Carlo simulations to show that the time-dependent transport of charges through a Franck–Condon blockaded Anderson–Holstein molecule proceeds in self-similar charge avalanches. The Metropolis–Hastings algorithm, which is due to Metropolis *et al.* (1953) and Hastings (1970), used for the simulation of rate-equation dynamics is very simple and intuitive:[1]

[1] See for instance Koch (2006, appendix F).

Given a state $|i\rangle$ with exit channels $|f\rangle$ and associated transition probabilities $\Gamma^{i\to f}$, the probability of a hopping event between time t and $t+dt$ is given by the exponential distribution

$$p_{exit}(t)dt = \sum_f \Gamma^{i\to f} e^{-(\sum_f \Gamma^{i\to f})t} dt.$$

If an event occurs, the target channel is chosen according to the distribution

$$p_{target}(f) = \frac{\Gamma^{i\to f}}{\sum_{f'} \Gamma^{i\to f'}}.$$

There are two widely used methods available to port this concept to general master equations, which actually provide a rigorous derivation of the Metropolis–Hastings algorithm from the equations themselves: quantum-state diffusion (Gisin & Percival, 1992), which is a purely stochastic interpretation of the Schrödinger equation, and the quantum-jump approach (Dalibard *et al.*, 1992; Dum *et al.*, 1992). Gisin *et al.* (1993) show numerically that quantum-state diffusion implies the quantum-jump technique and since the latter is technically less involved and more intuitive, we shall focus thereon.

The quantum-jump approach to open systems has first been used in the field of quantum optics, but it is equally well applicable to electronic transport problems. Plenio & Knight (1998) review the history and the conceptual background of the technique and give a broad overview over possible applications. The approach divides the Markovian dynamics of the master equation in two sets of processes: a coherent evolution due to an effective Hamiltonian and discontinuous jump processes. Assume a quantum-optical two-level system $|g\rangle$ and $|e\rangle$ with an externally applied laser field. The field will drive Rabi oscillations of the two-level system, mixing $|g\rangle$ and $|e\rangle$. Once in while, a photon will be emitted spontaneously in the surrounding radiation field, which acts as a dissipative environment, and the system will be reset to the ground state $|g\rangle$. This process is interpreted as a measurement on the quantum mechanical two-level system that projects the superpositions $\alpha|g\rangle+\beta|e\rangle$ onto $|g\rangle$; it induces the collapse of the wave function. The theoretical description relies on the Lindblad form of the Markovian master equation for the reduced density matrix ρ,

$$\begin{aligned}\dot\rho &= -\imath[H_S,\rho]+\frac{\gamma}{2}\left(2a\rho a^\dagger - a^\dagger a\rho - \rho a^\dagger a\right)\\ &= -\imath\left[H_S - \imath\frac{\gamma}{2}a^\dagger a,\rho\right]+\gamma a\rho a^\dagger\\ &= -\imath[H_{\text{eff}},\rho]+\gamma a\rho a^\dagger,\end{aligned}$$

with a coupling constant γ and bosonic bath operators a, $a^\dagger$. By rewriting the master equation in this way, part of the dissipative Lindblad dynamics has been absorbed into an effective, non-self-adjoint operator $H_{\text{eff}} := H_S - \imath\frac{\gamma}{2}a^\dagger a$. The second operator on the right-hand-side of the master equation is interpreted as the jump operator S, acting on a pure state $|\psi\rangle\langle\psi|$ by

$$S\,|\psi\rangle\,\langle\psi| := \gamma a\,|\psi\rangle\,\langle\psi|a^\dagger,$$

which on the wave-function level of quantum mechanics corresponds to the map $|\psi\rangle \mapsto \sqrt{\gamma}a|\psi\rangle$. In an infinitesimal time step, the operator S removes a photon from the combined atom–field system, and we can

count this photon as having been emitted spontaneously. The probability that a quantum jump occurs in the time interval $[t, t+dt]$ is given by (Carmichael, 1993, chap. 7.4)

$$p_{\text{jump}}(t)dt = \text{Tr}\big(S\rho(t)\big)dt$$

Dalibard *et al.* (1992) and Dum *et al.* (1992) provide a numerical algorithm, which implements this interpretation of the master equation

1. If the system is in state $|\psi\rangle$, determine the jump probability $p_{\text{jump}}(t)$.
2. Draw a random number and decide whether a jump has occurred or not.
3. If the system jumps, map $|\psi\rangle \mapsto a|\psi\rangle$ and renormalise the wave function. If the system does not jump, continue the non-unitary time evolution generated by the effective Hamiltonian $|\psi\rangle \mapsto e^{-\imath H_{\text{eff}} t}|\psi\rangle$ and renormalise.
4. Repeat the above procedure for many time steps.
5. Repeat the computation of the single trajectory such that an ensemble average for the time-dependent evolution of observables is obtained.

The connection to the implementation of the Metropolis–Hastings algorithm for rate equations is made by an explicit application of the quantum-jump technique to the rate equation. For simplicity, we only consider a two-state system, a quantum dot, whose reduced dynamics is given by an explicit evaluation of the Lindblad equation

$$\begin{aligned}\dot{p}_0 &= -W^{0\to1} dd^\dagger \langle c^\dagger c\rangle p_0 - W^{0\to1} p_0 dd^\dagger \langle c^\dagger c\rangle + 2W^{1\to0}\langle cc^\dagger\rangle dp_1 d^\dagger \\ \dot{p}_1 &= -W^{1\to0} d^\dagger d\langle cc^\dagger\rangle p_1 - W^{1\to0} p_1 d^\dagger d\langle cc^\dagger\rangle + 2W^{0\to1}\langle c^\dagger c\rangle d^\dagger p_0 d.\end{aligned}$$

The equations assume the familiar form

$$\begin{aligned}\dot{p}_0 &= -\Gamma^{0\to1} p_0 + \Gamma^{1\to0} p_1 \\ \dot{p}_1 &= -\Gamma^{1\to0} p_1 + \Gamma^{0\to1} p_0,\end{aligned}$$

for the suitably redefined rates

$$\Gamma^{0\to1} := 2W^{0\to1}\langle c^\dagger c\rangle \quad \text{and} \quad \Gamma^{1\to0} := 2W^{1\to0}\langle cc^\dagger\rangle.$$

The notation is self-explanatory: the index indicates the charge state of the system and $W^{i\to j}$ is the wave-function overlap of the transition $|i\rangle \mapsto |j\rangle$, which together with the factor of two and the bath correlation function constitutes the transition rate. Normalisation of the probability distribution $p_0 + p_1 = 1$ is implied. The operators d are dot operators, c abstractly describes the bath particles, and $\langle\cdot\rangle$ denotes averaging with respect to the equilibrium bath distribution. Using the fact that there are only two states, we have

$$dp_0 = 0 = d^\dagger p_1.$$

As such the dot operators correspond to the projection operators $d^\dagger d \cong |1\rangle\langle 1|$ and $dd^\dagger \cong |0\rangle\langle 0|$. Since there

is no coherent internal dynamics, $H_S = 0$, the effective Hamiltonian in matrix form[2] is

$$H_{\text{eff}} = -\imath \begin{pmatrix} W^{0\to1}\langle c^\dagger c\rangle & 0 \\ 0 & W^{1\to0}\langle cc^\dagger\rangle \end{pmatrix}.$$

The vanishing of H_S is a consequence of assuming zero gate voltage. For finite gate or, for instance, a molecule with an internal harmonic oscillator dynamics, H_S is diagonal in the chosen basis. The time evolution generated by H_S only amounts to a dynamic phase. This is different from the quantum optics problem, where the external field couples the atomic states, in which case H_S would be non-diagonal. The coherent evolution between two quantum jumps is, due to H_{eff} being non-hermitian, an exponentially damped evolution of the two charge states. The jump operator is given by its action on the density matrix

$$S\rho = 2W^{0\to1}\langle c^\dagger c\rangle d^\dagger p_0 d + 2W^{1\to0}\langle cc^\dagger\rangle d p_0 d^\dagger.$$

The induced "collapse operator" that projects onto the respective charge state is[3]

$$C = \sqrt{2W^{0\to1}\langle c^\dagger c\rangle}\, d^\dagger + \sqrt{2W^{1\to0}\langle cc^\dagger\rangle}\, d.$$

Combining all of the above, we see how the quantum-jump approach being applied to a rate equation realises the Metropolis–Hastings algorithm. The time evolution of a wave function $|i\rangle$ between two jumps is

$$|i(t)\rangle = e^{-\imath H_{\text{eff}} t}\,|i(0)\rangle = e^{-\frac{1}{2}\Gamma^{i\to j}t}\,|i(0)\rangle\,.$$

Then the probabilities decay according to

$$p_i(t) = |i(t)\rangle\,\langle i(t)| = e^{-\Gamma^{i\to j}t} p_i(0)$$

and the probability for a quantum jump in time $[t, t+dt]$ is

$$p_{\text{jump}}(t)dt = \text{Tr}\big(S\rho(t)\big)dt = \Gamma^{i\to j} e^{-\Gamma^{i\to j}} dt,$$

which is the result obtained by direct application of the Metropolis–Hastings algorithm. The rate equation for a single molecule between two electronic leads is treated the same way. Additional vibronic degrees of freedom do not add new internal dynamics; since there are no coherences between states with different phonon number considered in the rate equation, the effective Hamiltonian is also diagonal in the phonon number.

[2] We set $\hat{e}_0 := |0\rangle$ and $\hat{e}_1 := |1\rangle$.

[3] Note that we do not sum over the states $|j\rangle$ as there is only one of them, namely the other charge state.

Appendix D

The Jahn–Teller Effect

In molecular physics, where one uses the Born–Oppenheimer approximation[1] to separate the fast electronic motion from the slow dynamics of the nuclei, there is a connection between orbital degeneracy, that is degeneracy of electronic states, and the spatial symmetry of the molecular geometry. Jahn & Teller (1937) discuss the stability of nuclear geometries that have the same symmetry as the degenerate electronic orbitals. By an exhaustive investigation for an enormous number of point groups they are able to prove a theorem[2]

> "All non-linear nuclear configurations are … unstable for an orbitally degenerate electronic state."

As the striking consequence for the equilibrium configuration of the molecule, they infer

> "… if we know of a polyatomic molecule that the nuclei in the equilibrium configuration do not all lie on a straight line, then we know at the same time that its ground electronic state does not possess orbital degeneracy."

They construct perturbations of the potential energy of the molecule from the symmetric configuration in terms of the normal modes[3] $\{Q_i\}$ of the molecule that do respect the invariance under the respective point group and show that none of these perturbed potential energies has a minimum at the origin. Ruch & Schönhofer (1965) and Blount (1971) give a rigorous proof of the Jahn–Teller theorem in terms of group theory.

The Jahn–Teller theorem has severe implications for the kinematics of the molecule: the potential energy term of the nuclear part of the Hamiltonian has no local minimum at the symmetric configuration $\{Q_i = 0\}$. There is at least one normal coordinate along which the potential energy is lowered. Such a mode is said to be *Jahn–Teller active*. The geometry of the molecule in equilibrium is therefore *not* invariant under symmetry group that produces the orbital degeneracy, but it appears to be distorted. These distortions are so-called *Jahn–Teller distortions*.

In their extensive textbooks on the Jahn–Teller effect, Bersuker & Polinger (1989) and Bersuker (2006) clarify two widespread misunderstandings of the Jahn–Teller effect. First, the Jahn–Teller distortion does

[1] See for instance Baym (1990, pp. 471).

[2] A proof by example is, of course, no proof at all. Jahn & Teller check the theorem for a great number of cases and hereby, since they are unable to construct a counter example, suggest the validity of their theorem.

[3] The quantities Q_i are measured with respect to the symmetric configuration; they denote the displacement of the respective normal coordinate of the molecular vibration from the symmetric geometry.

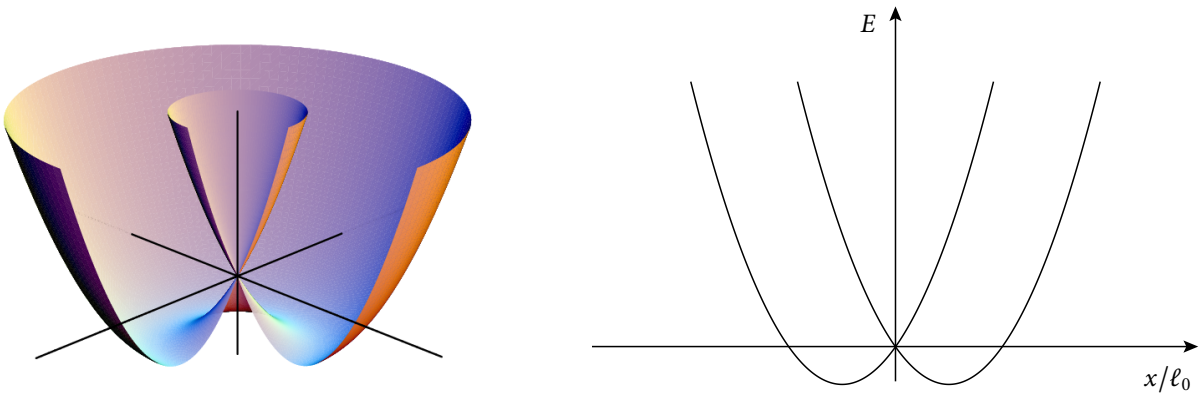

Figure D.1: Illustration of the adiabatic potential energy surfaces of the $E\otimes e$ (left) and the $E\otimes b$ (right) Jahn–Teller effect. Whereas the $E\otimes b$ Jahn–Teller effect only has the harmonic oscillators shifted with respect to each other, the $E\otimes e$ Jahn–Teller effect's adiabatic potential is obtained from the $E\otimes b$ effect's by a rotation about a vertical axis from where it acquires its two-dimensional structure.

not remove the degeneracy. Although for a specific set of normal coordinates $\{Q_i\}$, the electronic energies of the previously degenerate orbitals differ, there are still other points $\{Q_i'\}$ in configuration space with exactly the same energy. This is due to the fact that by the invariance also of the perturbed potential energy under the symmetry group G, any element g of that group can generate another configuration from any given solution without changing the energy. The breaking of the symmetry is spontaneous. The symmetric solution of the problem at $\{Q_i = 0\}$ is itself invariant under G, but the energetic ground states are not. The graphical representation of the potential energy terms for the Jahn–Teller effects treated in this thesis illustrate this property in Figure D.1.

Bersuker's second remark concerns the Born–Oppenheimer approximation. The picture of separable electronic and nuclear degrees of freedom is void in Jahn–Teller problems. Close to the point of degeneracy $\{Q_i = 0\}$, the different sheets of the adiabatic potential energy surfaces, which actually intersect in that very point, come very close to each other. One of the basic assumptions for using the Born–Oppenheimer approximation is that the energetic difference of two such sheets is large compared with the energy $\hbar\omega$ of the nuclear vibrations. Under this assumption, it is guaranteed that excitations of normal modes cannot change the electronic state of the molecule and therefore do not mix the electronic and vibronic degrees of freedom that the Born–Oppenheimer approximation pursues to separate. In the Jahn–Teller problem, such a situation is not given as the potential energy surfaces intersect. A separate discussion of electronic and nuclear dynamics is not possible, and the Schrödinger equation of the *full* problem has to be solved instead.

We sketch the mathematics and the group theory that are necessary to acquire some understanding of the Jahn–Teller effect. The material is compiled from Jahn & Teller (1937) and Bersuker (2006) for the physics and Cornwell (1997) for the group theory.

Given a group G with elements g, we denote their representations[4] by $\Gamma(g)$. Representations Γ of G are linear transformations—matrices—on a vector space X. A representation Γ of G is called *irreducible* if the only Γ-invariant subspaces of X are the empty set and X itself. The different irreducible representations are given symbols according to their dimensionality: $\dim(A) = 1$, $\dim(B) = 1$ (this representation is antisymmetric under rotations), $\dim(E) = 2$, $\dim(T) = 3$, $\dim(G) = 4$ (this representation is sometimes

[4] Although we use the same symbol as for the Golden-Rule rates, there ought to be no confusion between the two concepts.

also denoted by Γ), and $\dim(H) = 5$. A subscript *g* or *u* refers to the behaviour—*gerade* (even) or *ungerade* (odd)—under parity transformations. A number as a subscript is used to distinguish different irreducible representations of the same dimension and parity.

The nomenclature of different Jahn–Teller effects is a tensor product of the representation of the electronic states (in capital letters) and the representation of the vibrational states (in lower-case letters). The $E\otimes b$ Jahn–Teller effect is due to a two-fold electronic degeneracy coupled to a single vibrational mode, the $T\otimes h$ problem is due to a three-fold electronic degeneracy coupled to a five-fold vibrational degeneracy.

The proof of the Jahn–Teller theorem amounts to computing perturbations of the potential energy V around a configuration that is invariant under some group G. Consider an irreducible representation Γ of G and the associated normal coordinate Q_Γ, which is the coordinate describing the amplitude of the Γ-symmetric deformation, for example a breathing mode; see Bersuker & Polinger (1989, pp. 16) for other concrete examples. Then if φ_σ and φ_ρ are nuclear wave functions of the irreducible representation Γ, the matrix element

$$F_{\sigma\rho}^{\Gamma'} := \langle \varphi_\sigma \,|\, \frac{\partial V}{\partial Q_{\Gamma'}} \,|\, \varphi_\rho \rangle$$

defines the linear electrostatic force driving the system out of the symmetric configuration. If $F_{\sigma\rho}^{\Gamma'}$ vanishes, the $Q_{\Gamma'}$ mode will be stable. The Jahn–Teller theorem states that for non-linear molecules, there is always a set of indices such that $F_{\sigma\rho}^{\Gamma'}$ is non-zero and therefore that there is always one mode along which distortions are unstable. Due to time-reversal symmetry $F_{\sigma\rho}^{\Gamma'}$ is real and symmetric. Due to the orthogonality relations of irreducible representations,[5] it will vanish as long as Γ' is not an element of the symmetrised product representation $[\Gamma^2]$ (Bersuker, 2006). Equivalently, $F_{\sigma\rho}^{\Gamma'} = 0$ if the identity representation is not present in the product $\Gamma'[\Gamma^2]$ (Jahn & Teller, 1937). A simple example is the electronic basis of both the $E\otimes b$ and the $E\otimes e$ Jahn–Teller effect. Molecules exhibiting these Jahn–Teller effects are for example octahedral complexes. Due to the presence of a rotational symmetry C_n of order $n > 2$ in their symmetry group, there are two-dimensional irreducible representations E_k with $k \leq n$. The symmetrised square is

$$[E_k^2] = \begin{cases} A_1 + B_1 + B_2 & \text{for } 2k = \frac{n}{2} \\ A_1 + E_{2k} & \text{else.} \end{cases}$$

By the interaction of single-level molecular vibrations of type B_1 or B_2 with an electronic doublet of type E_k, the first case produces the $E\otimes(b_1 + b_2)$ Jahn–Teller effect. Similarly, doubly degenerate vibrations of type E_{2k} cause the instability in $E\otimes e$ systems, when interacting with electronic orbitals of E_k-type. For a derivation of the Hamiltonians in terms of wave functions we refer to Bersuker & Polinger (1989, chap. 3.1.1).

[5] The Wigner–Eckart theorem is one example of a well-known application of these orthogonality theorems to physics.

Appendix E

Franck–Condon Matrix Elements of the $E\otimes e$ Jahn–Teller Molecule

In this appendix, we discuss the quantum mechanics of the two charge states of the $E\otimes e$ Jahn–Teller molecule, whose transport properties are analysed in chapter 3.5, and their connection by the tunnelling Hamiltonian. In the neutral state, we assume the molecular coordinates to behave like an isotropic two-dimensional harmonic oscillator; in the singly charged state, the molecule is supposed to be $E\otimes e$ Jahn–Teller active. We assume the charging energy so large that there is at most one electron on the molecule. The potential energy terms of both charge states are $U(1)$-symmetric in the plane spanned by the degenerate distortions such that a natural description of their quantum mechanics uses polar coordinates. In the first section, we discuss the quantum mechanics of the two-dimensional harmonic oscillator in polar coordinates. The results will serve as a basis for the numerical diagonalisation of the $E\otimes e$ Jahn–Teller Hamiltonian in section E.2. In the third section of this appendix, we show how the numerically computed eigenstates of the neutral and the charged configuration are used to compute the Franck–Condon matrix in the $E\otimes e$ Jahn–Teller transport problem.

E.1 The Two-Dimensional Isotropic Harmonic Oscillator

The two-dimensional isotropic harmonic oscillator is a standard problem that is given to students in the introductory course on quantum mechanics. Once the solution for the one-dimensional problem is known, it can be generalised to higher dimensions with ease. The cartesian representation, which makes the problem so simple, is, however, of no use to us, because due to the rotational symmetry of the $E\otimes e$ Jahn–Teller Hamiltonian, the harmonic oscillator has to be solved in *polar* coordinates. Pauling & Wilson (1935, chapter IV-17) give a thorough and comprehensible solution to the problem.

The stationary Schrödinger equation for the harmonic oscillator of unit mass[1] in dimensionless polar coordinates is

$$\left[-\partial_r^2 - \frac{1}{r}\partial_r - \frac{1}{r^2}\partial_\varphi^2 + \omega^2 r^2\right]\psi(r,\varphi) = 2E\psi(r,\varphi).$$

Due to the $U(1)$-symmetry of the potential energy, there is an associated angular-momentum quantum

[1] For reasons of readability, we also set $\hbar = 1$. Planck's constant can be reintroduced at any stage of the calculation by the mapping $\omega \mapsto \frac{\omega}{\hbar}$ and $E \mapsto \frac{E}{\hbar^2}$.

number, which is conserved, and we can use the separation ansatz

$$\psi(r,\varphi) = \chi(r)e^{\imath m\varphi},$$

which provides an ordinary differential equation for the radial wave function $\chi(r)$,

$$-\chi'' - \frac{1}{r}\chi' + \left(\frac{m^2}{r^2} + \omega^2 r^2\right)\chi = 2E\chi. \tag{E.1.1}$$

We let $\frac{1}{r} \to 0$, approximate $\omega^2 r^2 - 2E \approx \omega^2 r^2$, and find as the asymptotic equation for $r \to \infty$

$$-\chi'' + \omega^2 r^2 \chi = 0,$$

which, by the same approximation, is the asymptotic form of the differential equation $-\chi'' + (\omega^2 r^2 - \omega)\chi = 0$, whose bounded solution is $\chi_{\text{asymp}}(r) = e^{-\frac{\omega}{2}r^2}$. This suggests to further separate the asymptotic solution from χ such that with the ansatz $\chi(r) = e^{-\frac{\omega}{2}r^2}P(r)$, we find

$$-P'' + \left(2\omega r - \frac{1}{r}\right)P' + \left(\frac{m^2}{r^2} + 2\omega - 2E\right)P = 0. \tag{E.1.2}$$

This equation can be solved in closed form using confluent hypergeometric functions of the first kind ${}_1F_1(a,b,z)$,

$$P(r) = C_1 r^{-m}\omega^{-\frac{m}{2}}{}_1F_1\left(\frac{1-m-\frac{E}{\omega}}{2}, 1-m, r^2\omega\right) + C_2(-r)^m\omega^{\frac{m}{2}}{}_1F_1\left(\frac{1+m-\frac{E}{\omega}}{2}, 1+m, r^2\omega\right). \tag{E.1.3}$$

The constants C_1 and C_2 are constants of integration and are determined by the initial conditions of the problem. The functions ${}_1F_1$ have special properties that characterise the solution (Abramowitz & Stegun, 1970, chapter 13),

1. The confluent hypergeometric function ${}_1F_1(a,-b,z)$ is undefined for all non-negative integers $b \in \mathbb{N}_0$. In that case, the respective part of the solution (E.1.3) is set to zero. Without loss of generality, we set $m > 0$ in Equation (E.1.3), since Equation (E.1.1) is invariant under the change of sign $m \mapsto -m$. We therefore only have to care about the second addend in Equation E.1.3. In the case $m = 0$, both hypergeometric functions are equal.

2. For positive integers n and k, the confluent hypergeometric function of the first kind is related to the generalised Laguerre polynomial L_k^m by

$${}_1F_1(-k, n+1, z) = \frac{n!k!}{(n+k)!}L_k^m(z).$$

3. There is a series expansion

$${}_1F_1(a,b,z) = \sum_{n\in\mathbb{N}_0}\frac{(a)_n}{(b)_n}\frac{z^n}{n!}$$

in terms of the Pochhammer symbol $(x)_n := \prod_{k=0}^{n-1}(x+k)$.

Due to the existence of a series expansion of ${}_1F_1$, we can rewrite $P(r) = \sum_{n\in\mathbb{N}_0} a_n r^{2n+m}$ and neglect all unnecessary pre-factors. With the knowledge of $P'(r)$ and $P''(r)$, we use the differential equation (E.1.2) to derive a recursion relation for the coefficients a_n. Let $k := E/\omega$, then

$$\frac{a_{n+1}}{a_n} = \frac{2\omega\,(2+n+1+m-k)}{(2n+2+m)^2+m^2}.$$

For large n, the ratio $\frac{a_{n+1}}{a_n}$ behaves like $\frac{\omega}{2n}$, and hence $a_n \approx \left(\frac{\omega}{2}\right)^n \frac{1}{n!}$. For large r, it is the higher-order monomials that contribute most to the value of the series, which means that for large r the radial wave function will approximately[2] behave like $P(r) \approx r^m e^{\frac{\omega}{2}r^2}$. The asymptote of the radial wave function

$$\chi(r) \approx e^{-\frac{\omega}{2}r^2} r^m e^{\frac{\omega}{2}r^2} = r^m$$

would therefore not yield a square-integrable function, since $\lim_{r\to\infty} r^m = \infty$. If, however, $2n+1+m = k$, the series terminates and due to P being a polynomial of degree $k-1$, $\chi(r) \in L^2(\mathbb{R}^+)$ can be ensured. Considering the exact series expansion of ${}_1F_1$ in terms of Pochhammer symbols, the finite polynomial degree of P translates into the condition that there exists some $n \in \mathbb{N}_0$, which enumerates the radial wave functions, such that

$$2n+1+m = k \quad \Leftrightarrow \quad (a)_n = 0 \quad \Leftrightarrow \quad a = -n.$$

This means that a has to be a negative integer. Since $a = \frac{1}{2}(1+m-\frac{E}{\omega})$, this puts the condition on the eigenvalues of the Hamiltonian to be integer multiples of the oscillator quantum, which is well-known from the discussion of the problem in cartesian coordinates. Collecting all of the above results, we finally state:

1. Due to $a \in -\mathbb{N}$, $\frac{m+1-k}{2} = -n$ and thus $|m-k| \in 2\mathbb{N}+1$. This condition in turn implies that also the difference between n and m has to be odd.

2. The angular momenta are bounded by the energy $m < k$. Because $m \in \mathbb{N}$, $k \in \mathbb{N}$, too, and $k-1$ can be the maximal value of m. Put differently, m is a lower bound for all possible values of k.

3. Since $a = -n \in -\mathbb{N}$ and $m \geq 0$, the solution permits a representation in terms of generalised Laguerre polynomials.

The radial solution of the two-dimensional isotropic harmonic oscillator is

$$P(r) = C(-r)^m \omega^{\frac{m}{2}} \frac{\left(\frac{k-(m+1)}{2}\right)! m!}{\left(\frac{k+m-1}{2}\right)!} L^m_{\frac{k-(m+1)}{2}}(r^2\omega).$$

The energy eigenvalues of the Hamiltonian in terms of angular momenta and radial excitation number are

$$E = \omega(m+2n+1) \quad \text{with } n \in \mathbb{N}.$$

The graphical representation of these eigenvalues in terms of m and k is shown in the left diagram of Figure E.1.

[2] Using Formula 13.5.17 in Abramowitz & Stegun (1970), this approximation is recovered from the leading terms.

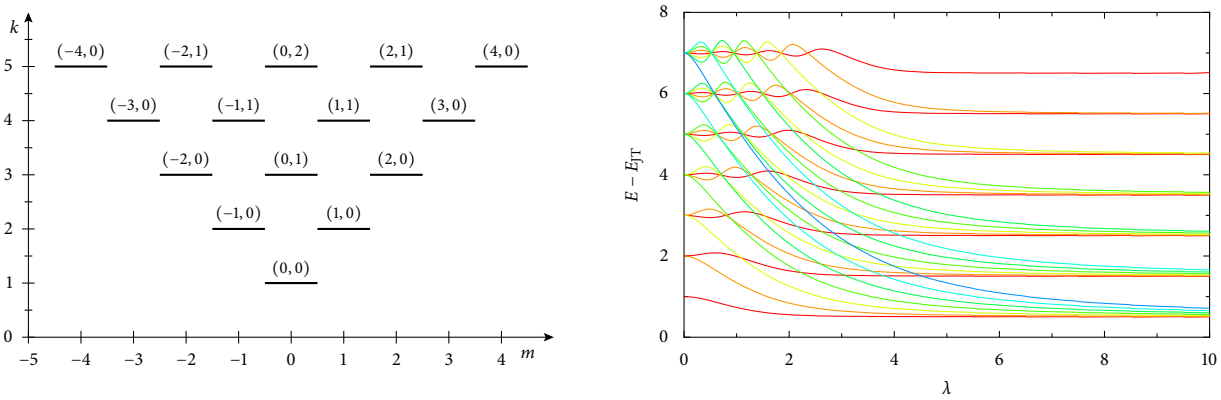

Figure E.1: Left: Location of the energy eigenstates with respect to angular momentum and radial excitation (m,n). Right: Spectrum of the $E\otimes e$ Jahn–Teller problem for the lowest excited states as a function of the electron–phonon coupling λ. Curves with the same colour are radial excitations of the system with the same angular momentum j. The Jahn–Teller energy is defined as $E_{\mathrm{JT}} := \frac{\lambda^2}{2}\hbar\omega$.

E.2 The $E\otimes e$ Jahn–Teller Hamiltonian

Similar to the two-dimensional harmonic oscillator, the $E\otimes e$ Jahn–Teller Hamiltonian (Bersuker & Polinger, 1989, chap. 3.1) comprises two degenerate oscillators whose coordinates Q_θ and Q_ε are coupled to two degenerate electronic levels $|+\rangle$ and $|-\rangle$. The adiabatic potential, which, due to the invalidity of the Born–Oppenheimer approximation, can only serve as an idea of this problem's quantum mechanics, is the well-known "mexican-hat potential" (Figure D.1). We use Pauli matrices as operators in the pseudo-spin space spanned by the degenerate electronic levels[3] and neglect all references to the electronic spin. The linear[4] $E\otimes e$ Jahn–Teller Hamiltonian is

$$H_{E\otimes e} = eV_{\mathrm{g}} + \frac{1}{2}\left(P_\theta^2 + \omega^2 Q_\theta^2\right) + \frac{1}{2}\left(P_\varepsilon^2 + \omega^2 Q_\varepsilon^2\right) + \lambda\frac{\hbar\omega}{\ell_0}\left(Q_\theta\sigma_x + Q_\varepsilon\sigma_y\right).$$

The strength of the electron–phonon interaction is characterised by the dimensionless constant[5] λ; the quantity $\ell_0 = \sqrt{\hbar/\omega}$ is the oscillator length for unit mass. The electron–phonon interaction can be recast in polar coordinates (r,φ) of the coordinate space spanned by the degenerate oscillator modes

$$\left(Q_\theta\sigma_x + Q_\varepsilon\sigma_y\right) = r\begin{pmatrix} 0 & e^{-i\varphi} \\ e^{i\varphi} & 0 \end{pmatrix}.$$

A technique to diagonalise the Jahn–Teller Hamiltonian has first been proposed by Longuet-Higgins *et al.* (1958). They consider the Jahn–Teller problem in terms of the eigenbasis of the two-dimensional isotropic harmonic oscillator. This is a natural treatment as for $\lambda = 0$, the Jahn–Teller problem reduces to the harmonic oscillator being decoupled from the electronic modes. The basis in which we shall work

[3] To be precise, we set $\hat{e}_1 = |+\rangle$ and $\hat{e}_2 = |-\rangle$.

[4] The symmetry-preserving expansion of the electron–phonon coupling can, in principle, be performed up to arbitrary order. Bersuker & Polinger (1989) also discuss the physics of the quadratic terms. Here, we restrict ourselves to the linear terms in the expansion: the linear Jahn–Teller effect.

[5] Bersuker & Polinger (1989) use a different coupling constant, $V_{\mathrm{E}} := \lambda\sqrt{\hbar\omega^3}$, with which the $E\otimes e$ electron–phonon coupling is $V_{\mathrm{E}}\left(Q_\theta\sigma_x + Q_\varepsilon\sigma_y\right)$.

is the electronic basis $|+\rangle,|-\rangle$ multiplied with the eigenbasis of the two-dimensional isotropic harmonic oscillator in polar coordinates. With the results of the previous section and the diagram in Figure E.1, it is more convenient to use the energy k instead of the radial excitation number n as the second quantum number besides the angular momentum m. We label the states of the problem $|\pm;k,m\rangle$ with $k\in\mathbb{N}$ and $m\in[-k+1,-k+3,\ldots,k-1]$. For given m, the possible radial excitations are determined by the condition $n=\frac{1}{2}\big(k-(m+1)\big)$, which in the previous section was the condition for the radial wave function to be square integrable. As we show in chapter 3.5, the Jahn–Teller Hamiltonian conserves the total momentum $j:=m\pm\frac{1}{2}$ of the vibronic angular momentum m and the z-component of the electronic pseudo-spin. The fact that, in contrast to the harmonic oscillator and the obvious symmetry of the adiabatic potential in Figure D.1, the conserved momentum is *half-integer* can also be attributed to the Berry phase of π that is present due to the conical intersection of the two sheets in the adiabatic potential. Indeed, the $E\otimes e$ Jahn–Teller Hamiltonian was one of the first systems where the existence of a geometric phase was actually shown (Berry, 1984). Due to the conservation of j, the Hamiltonian separates into blocks with fixed j. By the definition of the total angular momentum, the symmetry restricts m to be in the range $[j-\frac{1}{2},j+\frac{1}{2}]$. In the following, we neglect the explicit mentioning of j in all quantities as we focus only on one j-subspace of the Hilbert space. The conservation of angular momentum induces not only a mixing between the two electronic states and but also a mixing between electronic and vibronic states. As such, the Born–Oppenheimer approximation breaks down and the full Schrödinger equation has to be solved.

Given j, the $|+\rangle$-state has angular momentum $m^+:=j-\frac{1}{2}=:m$ and the $|-\rangle$-state has $m^-:=j+\frac{1}{2}=m+1$. The energy quantum numbers are an odd integer larger than the respective m^+ or m^-. Thus the possible quantum numbers k in the $|+\rangle$-state are $m+(2n+1)$, and $m^-+(2n+1)=m+(2n+2)$ in the $|-\rangle$-state. In terms of n and m, that subset of the basis of the Hilbert space with fixed j comprises the states

$$|+;m+(2n+1),m\rangle \quad \text{and} \quad |-;m+1+(2n+1),m+1\rangle\,.$$

These can be ordered according to the energy quantum number $m+l$ with $l\in\mathbb{N}_0$. The basis, in which the Jahn–Teller Hamiltonian factorises into block matrices with fixed total angular momentum j, is

$$\begin{aligned}
e_1 &:= |+;m+1,m\rangle\\
e_2 &:= |-;m+2,m+1\rangle\\
e_3 &:= |+;m+3,m\rangle\\
e_4 &:= |-;m+4,m+1\rangle\\
&\vdots\\
e_{2l+1} &:= |+;m+l,m\rangle\\
e_{2l+2} &:= |-;m+l+1,m+1\rangle
\end{aligned}$$

The only non-vanishing matrix elements of the Jahn–Teller electron–phonon interaction are (Longuet-Higgins *et al.*, 1958)

$$\begin{aligned}
A_{km} &:= \langle k,m|Q_\theta-\imath Q_\varepsilon|k+1,m+1\rangle = \langle k+1,m+1|Q_\theta+\imath Q_\varepsilon|k,m\rangle,\\
B_{km} &:= \langle k,m|Q_\theta-\imath Q_\varepsilon|k-1,m+1\rangle = \langle k-1,m+1|Q_\theta+\imath Q_\varepsilon|k,m\rangle,
\end{aligned}$$

which are evaluated as

$$A_{km} = \sqrt{\frac{1}{2}(k+m+1)} \quad \text{and} \quad B_{km} = \sqrt{\frac{1}{2}(k-m-1)}.$$

Gathering all of the above results, the $E\otimes e$ Hamiltonian being restricted to total angular momentum j turns out to be

$$H^j_{E\otimes e} = \begin{pmatrix} m+1 & \lambda\frac{\hbar\omega}{\ell_0}\sqrt{m+1} & 0 & 0 & 0 & \dots \\ \lambda\frac{\hbar\omega}{\ell_0}\sqrt{m+1} & m+2 & \lambda\frac{\hbar\omega}{\ell_0}\sqrt{1} & 0 & 0 & \dots \\ 0 & \lambda\frac{\hbar\omega}{\ell_0}\sqrt{1} & m+3 & \lambda\frac{\hbar\omega}{\ell_0}\sqrt{m+2} & 0 & \dots \\ 0 & 0 & \lambda\frac{\hbar\omega}{\ell_0}\sqrt{m+2} & m+4 & \lambda\frac{\hbar\omega}{\ell_0}\sqrt{2} & \dots \\ 0 & 0 & 0 & \lambda\frac{\hbar\omega}{\ell_0}\sqrt{2} & m+5 & \dots \\ \vdots & \vdots & \vdots & \vdots & \vdots & \ddots \end{pmatrix}.$$

With a large but finite cut-off, this matrix is easily diagonalised with the help of standard numerical methods. If the above treatment is repeated for each value of the total angular momentum j, the coupling-dependent behaviour of the Jahn–Teller spectrum of Figure E.1 is obtained. From the Figure, it is obvious that in the regimes of small and large electron–phonon coupling respectively, the system is characterised by a completely different set of quantum numbers. For weak coupling, the quantum states are those of the two-dimensional harmonic oscillator in polar coordinates, and the energies are found by perturbation theory (Bersuker & Polinger, 1989, chap. 4.1.2). For strong couplings, the behaviour is different. We define the Jahn–Teller energy $E_{\mathrm{JT}} := \frac{\lambda^2}{2}\hbar\omega$ and compute the approximate minimum of the lower sheet of the potential energy surface in Figure D.1 in the radial direction (Bersuker & Polinger, 1989, chap. 4.2.1)

$$r_0 \approx \lambda\ell_0\left(1+\frac{j^2}{\lambda^4}\right).$$

The excitation energies for the dynamics of the lower sheet are well approximated by

$$E_{\tilde{n}j} \approx \hbar\omega_E\left(\tilde{n}+\frac{1}{2}\right) + \frac{\hbar^2 j^2}{2r_0^2} - E_{\mathrm{JT}}.$$

The strong-coupling spectrum is that of a quantum mechanical rigid rotor of unit mass with angular momentum j and moment of inertia r_0^2 plus harmonic oscillations in the radial directions, which are enumerated by some quantum number $\tilde{n} \in \mathbb{N}_0$. Due to the strong-coupling assumption, the energy is dominated by the oscillator, and the rotor spectrum appears as a rotational sideband structure in Figure E.1. In contrast to the weak-coupling regime, where due to the two-dimensional harmonic oscillator structure, the angular momentum defines the minimal energy of the respective irreducible component of the Hamiltonian, the strong-coupling regime has no such lower bound. The qualitatively different asymptotes for weak and strong coupling of states with fixed j, shine some light onto the cross-over behaviour of the energies, the rapid fall-off, when sweeping the electron–phonon coupling. For fixed electron–phonon coupling λ, this fall-off produces very pronounced distortions in the spectrum of the system and by that property has a significant effect on the transport properties of $E\otimes e$ Jahn–Teller molecules as the discussion in chapter 3.5 shows. Judd (1977) tries to give an explanation of the oscillatory behaviour of the eigenvalues and the

accidental pseudo-degeneracy of states with the same n. His approach does not explain the underlying physics but succeeds in computing the position of these pseudo-degeneracies rather accurately. He observes that the Hamiltonian of the linear $\gamma_8 \otimes \tau_{2g}$ (and similarly the linear $E \otimes e$) Jahn–Teller effect with angular momentum $j = -\frac{1}{2}$ is exactly that of a displaced harmonic oscillator. Since the solutions of the latter are well known, perturbation theory in $j + \frac{1}{2}$ up to third (and even sixth) order results in corrections of the energies in terms of Bessel-functions of the first kind.

E.3 Calculation of the Franck–Condon Matrix

The Franck–Condon matrix is the heart of the tunnelling dynamics. It describes the wave-function overlap between the vibronic states in the charged and in the neutral state of the molecule and is thus the correction of the electronic Golden-Rule rate due to the electron–phonon coupling. In the Anderson–Holstein model, where only one phonon is coupled to a single electronic state, the electron–phonon interaction is

$$H_{\text{el–ph}} = \lambda \hbar \omega (b^\dagger + b) d^\dagger d.$$

The matrix elements of H_T enter the tunnel rates as the square moduli

$$M^{qq'} := \left| \langle 1; q \,|\, d^\dagger \,|\, 0; q' \rangle \right|^2,$$

where the first quantum number labels the number of electrons on the molecule and the second the vibronic state. This model can be diagonalised analytically by a canonical transformation (Mahan, 2000, chap. 4.2), which results, among energy renormalisations, in the mapping

$$d \mapsto e^{-\lambda(b^\dagger - b)} d.$$

This operator is the displacement-operator, which shifts the potential energy by $\sqrt{2}\lambda\ell_0$ into the direction of the positive axis. The thus generated states are coherent states of the harmonic oscillator, and the distribution of the displaced states in terms of the original Fock states are described by generalised Laguerre polynomials. The Franck–Condon matrix of this model has elements[6] (Koch, 2006)

$$\begin{aligned} M^{qq'} &= \left| \langle 1; q | d^\dagger | 0; q' \rangle \right|^2 = \left| \langle 1; q | \left(e^{\lambda(b^\dagger - b)} | 1; q' \rangle \right) \right|^2 \\ &= \left| \langle 0; e^{-\lambda(b^\dagger - b)} q | 0; q' \rangle \right|^2 \\ &= \left(\lambda^{Q-q} e^{-\frac{\lambda^2}{2}} \sqrt{\frac{q!}{Q!}} L_q^{Q-q}(\lambda^2) \right)^2, \end{aligned}$$

where we have abbreviated $q := \min\{q, q'\}$ and $Q := \max\{q, q'\}$. The second line is due to our freedom to shift the origin of the integration in the spatial basis or, equivalently, the definition of the adjoint. Adding more electronic states to the system without additional interactions would not change this form of the Franck–Condon matrix.

[6] One has to bear in mind that the displacement operator is unitary but not hermitian. In a scalar product, it cannot be operated to both the bra and the ket. In general, the operators are assumed to operate to the right.

For the case of an $E\otimes e$ Jahn–Teller molecule things are more difficult, but the general scheme persists. We have already obtained a first part of the transformation $|\pm;n,m\rangle \mapsto |0;n,m\rangle$ by diagonalising the molecular Hamiltonian. In the diagonal basis, there are pseudo-spin degrees of freedom, which have no meaning in the unoccupied state. We have to represent both the eigenbasis of the Jahn–Teller effect and the tunnel Hamiltonian H_T as matrices in the electronic Hilbert space and transform H_T according to the map induced by the eigenbasis.

In the following, we consider block-matrices of electronic states and do not explicitly mention the vibrational degrees of freedom. It is convenient to consider the full electronic system as a fictitious spin-1 system. The zero component of its z-component then describes the neutral state, whereas the ±1 components correspond to the z-component of the Jahn–Teller pseudo-spin. Using the order

$$\hat{e}_1 := |+\rangle\,, \quad \hat{e}_2 := |0\rangle\,, \quad \hat{e}_3 := |-\rangle\,,$$

the creation and annihilation operators are identified with the respective entries in the matrix[7]

$$\begin{pmatrix} d_+^\dagger d_+ & d_+^\dagger & d_+^\dagger d_- \\ d_+ & 1 & d_- \\ d_-^\dagger d_+ & d_-^\dagger & d_-^\dagger d_- \end{pmatrix}$$

The full set of quantum numbers is $|s;q\rangle = |s\rangle\otimes|q\rangle$, such that the above matrix is block-diagonal in the vibrational degrees of freedom. The matrix of the eigenvectors of the $E\otimes e$ Jahn–Teller Hamiltonian can be decomposed into four blocks, which are only acting in the Jahn–Teller pseudo-spin space spanned by $\hat{e}_1$ and $\hat{e}_3$,

$$U = \begin{pmatrix} A & B \\ C & D \end{pmatrix},$$

which after including the neutral states and using the above defined matrix representation of second quantisation reads

$$U_{\text{2nd quant}} = \begin{pmatrix} A & 0 & B \\ 0 & 1 & 0 \\ C & 0 & D \end{pmatrix}.$$

For the representation of the tunnelling Hamiltonian $H_\mathrm{T} = \sum_{k\alpha} t_{\alpha\pm} c_{k\alpha}^\dagger d_\pm + \text{h.c.}$ in this Hilbert space, we only consider one addend of the sum over the electrode index α

$$H_{\mathrm{T}\alpha} = \begin{pmatrix} 0 & t_{\alpha+} & 0 \\ t_{\alpha+}^* & 0 & t_{\alpha-}^* \\ 0 & t_{\alpha-} & 0 \end{pmatrix},$$

The diagonalisation of the molecular Hamiltonian implies a transformation of $H_{\mathrm{T}\alpha}$. For the Anderson–Holstein model, this results in the polaron transformation and the matrix-valued renormalisation of the

[7] The notation means that for instance the matrix representation of the operator $d_+^\dagger d_+$

$$d_+^\dagger d_+ \cong \begin{pmatrix} 1 & 0 & 0 \\ 0 & 0 & 0 \\ 0 & 0 & 0 \end{pmatrix}.$$

bare tunnelling rates. In the Jahn–Teller case, the Franck–Condon matrix is

$$\tilde{M}_\alpha = U^\dagger H_{\mathrm{T}\alpha} U = \begin{pmatrix} 0 & A^\dagger t_{\alpha+} + C^\dagger t_{\alpha-} & 0 \\ A t^*_{\alpha+} + C t^*_{\alpha-} & 0 & B t^*_{\alpha+} + D t^*_{\alpha-} \\ 0 & B^\dagger t_{\alpha+} + D^\dagger t_{\alpha-} & 0 \end{pmatrix},$$

and finally $M_\alpha^{qq'} := |\tilde{M}_\alpha^{qq'}|^2$. The renormalisation of the tunnelling Hamiltonian and thus the rates for changing the internal state of the molecule by an electron jumping onto or off the molecule is given by the block-matrices

$$\langle - \,|\, \tilde{M}_\alpha \,|\, 0 \rangle = (B^\dagger t_{\alpha+} + D^\dagger t_{\alpha-}) \quad \text{and} \quad \langle + \,|\, \tilde{M}_\alpha \,|\, 0 \rangle = (A^\dagger t_{\alpha+} + C^\dagger t_{\alpha-})$$

and their hermitian conjugates.

The $E \otimes e$ Jahn–Teller Hamiltonian has a conserved quantity: the total angular momentum $j := m \pm \frac{1}{2}$. The tunnelling between the leads and the Jahn–Teller molecule will therefore be restricted by selection rules in the angular momentum m. The above developed scheme helps to find these without tedious calculations. We recall that each state of the singly charged sector, $|j,n\rangle$, can be written as $|s;m,n\rangle$ with $s \in \{+,-\}$. Putting the pseudo-spin state as a superscript to the m variable, one has $|m^-,n\rangle$ and $|m^+,n\rangle$, respectively. We are only interested in the behaviour of the angular-momentum quantum numbers, which justifies to ignore the n-part of the matrices by implying a suitable block-matrix structure. After the diagonalisation of the Jahn–Teller Hamiltonian with the scheme presented in the previous section, each j-block of the eigenbasis has the pseudo-spin structure[8]

$$\begin{pmatrix} \langle m^+ | m^+ \rangle & \langle m^+ | m^- \rangle \\ \langle m^- | m^+ \rangle & \langle m^- | m^- \rangle \end{pmatrix}.$$

From this, we construct the block matrices A, B, C, and D:

$$A = \langle m^+ \,|\, m^+ \rangle, \quad B = \langle m^+ \,|\, m^- \rangle, \quad C = \langle m^- \,|\, m^+ \rangle, \quad D = \langle m^- \,|\, m^- \rangle.$$

The Franck–Condon block matrices are accordingly

$$\begin{aligned} (A t^*_{\alpha+} + C t^*_{\alpha-}) &= \left[\langle m^+ | t^*_{\alpha+} + \langle m^- | t^*_{\alpha-} \right] | m^+ \rangle \\ (B t^*_{\alpha+} + D t^*_{\alpha-}) &= \left[\langle m^+ | t^*_{\alpha+} + \langle m^- | t^*_{\alpha-} \right] | m^- \rangle \end{aligned}$$

for jumping off the molecule. We recall the relation $m^- = m^+ + 1$ for constant j from the previous section and find the possible tunnel events, which amounts to identifying a selection rule,[9]

$$\begin{aligned} |+;m\rangle &\mapsto |0;m\rangle + |0;m-1\rangle \\ |-;m\rangle &\mapsto |0;m\rangle + |0;m+1\rangle \\ |0;m\rangle &\mapsto |+;m+1\rangle + |+;m\rangle + |-;m-1\rangle + |-;m\rangle \end{aligned}$$

[8] The notation of the scalar product, $\langle m^+ | m^- \rangle$, say, represents that sub-matrix of the eigenbasis that, in the example, maps the m^- components onto the m^+ components.

[9] The notation of this selection rule is only valid as an indication of which states are mapped onto which. It is *not* the actual map itself.

These rules state that by tunnelling off the molecule the angular momentum in the $|-\rangle$-state is never lowered, while in the $|+\rangle$-state it is never raised. By tunnelling onto the molecule, the rule is reversed. In addition to the prescription of a certain direction of the tunnelling event in angular momentum space, the step-size is restricted to one. In the language of the total angular momentum j, the effect of the selection rule is that a tunnelling event can change the angular momentum or total angular momentum only by one-half,[10]

$$|0;m\rangle \mapsto |1;m\pm\frac{1}{2}\rangle \mapsto \begin{Bmatrix} |0;m\pm1\rangle \\ |0;m\rangle \end{Bmatrix} \mapsto \begin{Bmatrix} |1;m\pm\frac{3}{2}\rangle \\ |1;m\pm\frac{1}{2}\rangle \end{Bmatrix} \dots$$

[10] Again, we refrain from denoting the radial excitations and only mention the charge and angular momentum quantum numbers; $|0;m\rangle$ are neutral, and $|1;j\rangle$ are the charged states with m being integer and j being half-integer.

Appendix F

The Mathematical Theory of the Singular-Coupling Limit

In order to understand that the formulation of the singular-coupling limit by Palmer (1977) is equivalent to the original definition by Hepp & Lieb (1973), we need to introduce a mathematical formulation of second quantisation. For references regarding the material covered in this appendix, see Davies (1976b, chap. 8) and Bratteli & Robinson (1996, chap. 5.2.1). An application of the formalism to physics is given by Salmhofer (1999).

Palmer formulates a Hamiltonian H_ξ^{sc} that by a suitable rescaling of the basis of the underlying Hilbert space shows the singular bath correlation function that Hepp & Lieb (1973) use to define the notion of singular reservoirs. He also states a weak-coupling problem H_ξ^{wc}, which is the Hamiltonian used in chapter 6, and proves that H_ξ^{wc} can be mapped onto H_ξ^{sc} proving that both formulations are equivalent. We give a formulation of his proof, which without referring to Palmer's mathematical rigour, elucidates the equivalence of the two models and thus explains the terminology of the "singular-coupling limit".

F.1 Second Quantisation and Canonical Anticommutation Relations

In the mathematical-physics literature, second quantisation of quantum mechanics is formulated using C^*-algebras. From a single-particle Hilbert space $\mathcal{H}$, for instance[1] $\mathcal{H} = L^2(\mathbb{R}, d\omega)$, one constructs a fermionic Fock space (Bratteli & Robinson, 1996) by directly adding n-fold direct products of $\mathcal{H}$

$$\mathcal{F} := \bigoplus_{n\geq 0} \left(\bigotimes_{\mathrm{asym}}^{n} \mathcal{H} \right).$$

The space $\bigotimes_{\mathrm{asym}}^{n} \mathcal{H}$ is the n-fold antisymmetric direct product of the single-particle Hilbert space: it is a space that describes n fermions. The direct sum in the definition of the Fock space accounts for the varying particle number in second quantisation. For $n = 0$, $\mathcal{H}^0 = \mathbb{C}$ is the vacuum space. We also denote by $\psi^{(n)}$ a vector in the n-particle Hilbert space, that is an n-particle wave function.

Creation and annihilation operators are defined as elements of a C^*-algebra over the Fock space, which puts the whole machinery of functional analysis at our hands. For every $f \in \mathcal{H}$, one can define operators

[1] This is the space of functions $f : \mathbb{R} \to \mathbb{R}$ that are square-integrable with respect to the Lebesgue measure $d\omega$.

$a(f)$ and $a^\dagger(f)$ acting on the Fock space by their action on the vacuum

$$a(f)\psi^{(0)} = 0 \quad \text{and} \quad a^\dagger(f)\psi^{(0)} = f.$$

Similarly, without denoting the antisymmetrisation explicitly, their action on n-particle states is given by

$$a(f)(f_1\otimes\cdots\otimes f_n) = \sqrt{n}\langle f, f_1\rangle f_2\otimes\cdots\otimes f_n$$
$$a^\dagger(f)(f_1\otimes\cdots\otimes f_n) = \sqrt{n+1}f\otimes f_1\otimes\cdots\otimes f_n.$$

The scalar product $\langle\cdot,\cdot\rangle$ is the one defined in the single-particle Hilbert space $\mathcal{H}$. The elements of the n-particle Hilbert space are antisymmetric combinations, and as such the Pauli principle

$$a^\dagger(f)a^\dagger(f) = 0$$

is effective. By this property, the canonical anticommutation relations take the form

$$\{a(f), a^\dagger(g)\} = \langle f, g\rangle\mathrm{Id}. \tag{F.1.1}$$

Notice that they assume the form generally used in physics for f and g being elements of the orthonormal basis of $\mathcal{H}$. This formulation, in contrast to the standard physics method, allows us to redefine the creation and annihilation operators under invariance of the canonical anticommutation relations if we modify the single-particle Hilbert space accordingly. This property is the key to Palmer's proof.

F.2 The Singular-Coupling Limit

Hepp & Lieb (1973) define singular reservoirs as being those with singular, that is δ-like, time correlation function. A very simple construction of such a singular reservoir is a Fermi gas with infinite temperature. Then

$$\kappa(t) = \int_{\mathbb{R}} e^{\imath\omega t}\langle c_\omega^\dagger c_\omega\rangle_0 d\omega,$$

where the $c_\omega^\dagger$ creates a fermion with energy ω and $\langle\cdot\rangle_0$ is the trace with respect to the Fermi distribution, becomes the Fourier transform of a constant. Another construction, which is given by Palmer (1977), Spohn (1980, chap. V. C 2), and Friegerio & Gorini (1976), is comprehensibly reviewed in Accardi *et al.* (1992). Let $\mathcal{H}^{\mathrm{sc}} = L^2(\mathbb{R}, d\omega)$. Define the time evolution of a single-particle wave function $f\in\mathcal{H}^{\mathrm{sc}}$ by $f_\tau(\omega) := e^{\imath\omega\tau}f(\omega)$. Also define a single-parameter family $f^\xi(\omega) := f(\xi^2\omega)$ of functions with time evolution[2]

$$f_\tau^\xi(\omega) = e^{-\imath\omega\tau}f^\xi(\omega) = e^{-\imath\omega\tau}f(\xi^2\omega).$$

Then a scaled Hamiltonian of the open quantum system is defined by

$$H_\xi^{\mathrm{sc}} = H_{\mathrm{S}}^{\mathrm{sc}}\otimes\mathrm{Id} + \mathrm{Id}\otimes H_{\mathrm{E}}^{\mathrm{sc}} + H_{\mathrm{S-E}}^{\mathrm{sc}},$$

with $H_{\mathrm{S-E}}^{\mathrm{sc}} := Q\otimes a^{\mathrm{sc}}(f^\xi) + \mathrm{h.c.}$ The operator Q is an arbitrary bounded operator acting on the system, and the creation and annihilation operators of the reservoir particles are labelled by a superscript to indicate the

[2] Friegerio & Gorini (1976) for example use Gaussian representations of the wave functions with $f_\tau^\xi(\omega) = e^{-(\xi\omega)^2/8+\imath\omega\tau}$.

picture they belong to. The bath operator is assumed to be quasi-free in the sense that it operates on $\otimes\mathcal{H}$ by operating on the single-particle Hilbert spaces only

$$H_{\mathrm{E}}^{\mathrm{sc}}\left(f_1 \otimes f_2 \otimes \cdots \otimes f_n\right) = \sum_{i=1}^{n} \left(f_1 \otimes f_2 \otimes \cdots \otimes H_{\mathrm{E}}^{\mathrm{sc}} f_i \otimes \cdots \otimes f_n\right).$$

The action on the single-particle spaces is then assumed to generate the previously defined time evolution. The time correlation function of the reservoir is

$$\begin{aligned}\kappa(\tau) &= \langle a^{\mathrm{sc},\dagger}(f_\tau^\xi) a^{\mathrm{sc}}(f^\xi)\rangle_0 \\ &= \langle a^{\mathrm{sc},\dagger}(e^{-\imath\omega\tau} f^\xi) a^{\mathrm{sc}}(f^\xi)\rangle_0 \\ &= \langle e^{\imath\omega\tau} f^*(\xi^2\omega) f(\xi^2\omega)\rangle_0 \\ &= \int_{\mathbb{R}} e^{\imath\omega\tau} \left|f(\xi^2\omega)\right|^2 \frac{1}{e^{(\xi^2\omega-\mu)\beta}+1}\, d\omega,\end{aligned}$$

which for $\xi \to 0$ converges to a δ-function at $\tau = 0$, since it is the Fourier transform of a function $G(\xi^2\omega)$. For the proof, see for instance Accardi *et al.* (1992, Example 2).

F.3 The Mapping by Palmer

We discuss the integrated von Neumann equation (2.3.4) for the construction of the singular-coupling limit of the previous section and then apply the transformation of Palmer in order to obtain the equation for the singular-coupling limit (6.3.2), which we use in this thesis. Consider Equation (2.3.4) being applied to H_ξ^{sc}

$$\rho_{\mathrm{S}}^{\mathrm{I}}(\tau) - \rho_{\mathrm{S}}^{\mathrm{I}}(0) = -\int_0^\tau e^{\imath\mathcal{L}_{\mathrm{S}}^{\mathrm{sc}}\sigma} \left\{ \int_0^{\tau-\sigma} e^{\imath\mathcal{L}_{\mathrm{S}}^{\mathrm{sc}}\nu} \mathrm{Tr}_{\mathrm{E}}\left(\mathcal{L}_{\mathrm{S-E}}^{\mathrm{sc}} e^{-\imath\mathcal{L}^{\mathrm{sc}}\nu} \mathcal{L}_{\mathrm{S-E}}^{\mathrm{sc}} \rho_{\mathrm{E}}\right) d\nu \right\} e^{-\imath\mathcal{L}_{\mathrm{S}}^{\mathrm{sc}}\sigma} \rho_{\mathrm{S}}^{\mathrm{I}}(\sigma) d\sigma,$$

where all operators superscripted with "sc" are scaled by ξ. The key mappings from Hepp and Lieb's formulation of the singular-coupling limit to Palmer's are a rescaling of time $\tau = \xi^2 t$ and of frequency $w = \xi^2\omega$, which induces a dilation of the single-particle Hilbert space. The singular-coupling limit uses ω, whereas the equivalent weak-coupling formulation relies on w. The consequences of the second transformation are most important. First the reservoir Hamiltonian is transformed $H_{\mathrm{E}}^{\mathrm{wc}} = \xi^2 H_{\mathrm{E}}^{\mathrm{sc}}$, as the dilation only affects the eigenvalues of the Hamiltonian. In order to keep the reservoir's equilibrium distribution invariant,

$$\beta^{\mathrm{wc}}(H_{\mathrm{E}}^{\mathrm{wc}} - \mu^{\mathrm{wc}}) = \beta^{\mathrm{sc}}(H_{\mathrm{E}}^{\mathrm{sc}} - \mu^{\mathrm{sc}}),$$

we also have to rescale temperature and the chemical potential

$$\xi^2\beta^{\mathrm{wc}} = \beta^{\mathrm{sc}} \quad \text{and} \quad \mu^{\mathrm{wc}} = \xi^2\mu^{\mathrm{sc}}.$$

By performing the transformation from the weak-coupling limit to Hepp and Lieb's formulation, a finite weak-coupling temperature β^{wc} will become infinitely large, which substantiates the physical interpretation of the singular-coupling limit and its quantum transport phenomenology we have given in chapter 6: from the perspective of the isolated system, the bath appears to have infinite temperature and is not able to resolve any of the system's quantum mechanics energetically.

By rescaling not only temperature and chemical potential but also the times $\sigma = \xi^2 s$, $\tau = \xi^2 t$, and $\nu = \xi^2 u$, the von Neumann equation eventually assumes the form

$$\rho_{\mathrm{S}}^{\mathrm{I}}(t) - \rho_{\mathrm{S}}^{\mathrm{I}}(0) = -\xi^4 \int_0^t e^{\imath \mathcal{L}_{\mathrm{S}}^{\mathrm{sc}} \xi^2 s} \left\{ \int_0^{t-s} e^{\imath \mathcal{L}_{\mathrm{S}}^{\mathrm{sc}} \xi^2 u} \operatorname{Tr}_{\mathrm{E}} \left(\mathcal{L}_{\mathrm{S-E}}^{\mathrm{sc}} e^{-\imath \mathcal{L}^{\mathrm{sc}} \xi^2 u} \mathcal{L}_{\mathrm{S-E}}^{\mathrm{sc}} \rho_{\mathrm{E}} \right) du \right\} e^{-\imath \mathcal{L}_{\mathrm{S}}^{\mathrm{sc}} \xi^2 s} \rho_{\mathrm{S}}^{\mathrm{I}}(s) ds. \quad \text{(F.3.1)}$$

The mapping of the Liouvillians is actually a mapping of the Hamiltonian

$$\xi^2 H^{\mathrm{sc}} = \xi^2 H_{\mathrm{S}}^{\mathrm{sc}} + \xi^2 H_{\mathrm{E}}^{\mathrm{sc}} + \xi^2 Q \otimes a^{\mathrm{sc}}(f^\xi) + \mathrm{h.c.}$$

into

$$H^{\mathrm{wc}} = \xi^2 H_{\mathrm{S}}^{\mathrm{wc}} + H_{\mathrm{E}}^{\mathrm{wc}} + \xi Q \otimes a^{\mathrm{wc}}(f) + \mathrm{h.c.}$$

The system Hamiltonian H_{S} is untouched $H_{\mathrm{S}}^{\mathrm{wc}} = H_{\mathrm{S}}^{\mathrm{sc}}$ and the reservoirs are transformed by $H_{\mathrm{E}}^{\mathrm{wc}} = \xi^2 H_{\mathrm{E}}^{\mathrm{sc}}$. The final task for proving the equivalence of the two notions is to adjust the factors of ξ in the system–bath interaction in Equation (F.3.1), for which we use the machinery introduced in the first section of this appendix.

By defining new wave functions $f := \xi f^\xi$ with now[3] $f \in \mathcal{H}^{\mathrm{wc}} = L^2(\mathbb{R}, dw)$, we need to modify the creation and annihilation operators such that the canonical anticommutation relations remain invariant. We remember the general relation

$$\{a(f), a^\dagger(g)\} = \langle f, g \rangle \mathrm{Id},$$

where the inner product is taken in the single-particle Hilbert space $\mathcal{H}$. Consider two wave functions $f^\xi, g^\xi \in \mathcal{H}^{\mathrm{sc}}$. Then

$$\langle f^\xi, g^\xi \rangle_{\mathrm{sc}} = \int_{\mathbb{R}} f(\xi^2 \omega)^* g(\xi^2 \omega)\, d\omega = \frac{1}{\xi^2} \int_{\mathbb{R}} f(w)^* g(w)\, dw = \frac{1}{\xi^2} \langle f, g \rangle_{\mathrm{wc}}.$$

Hence if we map $a^{\mathrm{wc}}(f) := \xi a^{\mathrm{sc}}(f^\xi)$, and for the creation operator accordingly,

$$\{a^{\mathrm{sc}}(f^\xi), a^{\dagger,\mathrm{sc}}(g^\xi)\} = \{a^{\mathrm{wc}}(f), a^{\dagger,\mathrm{wc}}(g)\}.$$

With this result, the transformation of the system–bath interaction is

$$Q \otimes a^{\mathrm{sc}}(f^\xi) = \frac{1}{\xi} Q \otimes a^{\mathrm{wc}}(f),$$

such that finally $\xi^2 \mathcal{L}_{\mathrm{S-E}}^{\mathrm{sc}} = \xi \mathcal{L}_{\mathrm{S-E}}^{\mathrm{wc}}$ and Equation (F.3.1) becomes Equation (6.3.2) thus proving the claimed equivalence of the two formulations of the singular-coupling limit.

[3] Note the different Lebesgue measure.

Danksagung

Il dit : « Tiens! Tu travailles? »
Je répondis : « J'écris Paludes. »

Gide, *Paludes*

Eine Doktorarbeit zu schreiben ist ein schwieriges Unterfangen. Muß man sich doch durch Berge von Fachliteratur in seit langem wohl etablierte Terminologie und Begrifflichkeiten einlesen, muß die gelösten von den ungelösten Problemen unterscheiden und mit der wenigen Erfahrung, die man am Anfang einer wissenschaftlichen Karriere noch hat, auch noch ein ungelöstes lösbares Problem finden, mit dessen Bearbeitung der eigene wissenschaftliche Beitrag die Aufnahme und Initiation in die akademische Ränge rechtfertigt. Nur wenige, zu denen ich mich nicht zählen möchte, können dies alleine und ohne jegliche Unterstützung anderer. Von den vielen meiner Kollegen und Freunden, die direkt oder indirekt einen Anteil am Gelingen dieser Arbeit hatten, möchte ich einigen besonders danken.

Ich danke Felix von Oppen, meinem Doktorvater, der mir mit der Aufnahme in seine Arbeitsgruppe und der Initiative eines Forschungsprojekts half, meinen mäandernden Weg durch die Wissenschaften endlich in konkrete Bahnen zu lenken, um mein „Paludes" zu schreiben. Sein Vertrauen in mich und in meine Fähigkeiten erlaubte mir die eigenverantwortliche Bearbeitung meines Promotionsthemas und gab mir die Möglichkeit, mich selbständig wissenschaftlich zu orientieren und zu positionieren ohne jedoch Gefahr zu laufen, mich in den unendlichen Weiten der theoretischen Physik zu verirren oder am Ende zu verlieren. Ich danke Tobias Brandes für seine Bereitschaft, meine Arbeit als Zweitgutachter zu bewerten, und mir sowohl bei wissenschaftlichen als auch beruflichen Fragen und Problemen jederzeit unkompliziert zur Seite zu stehen.

Meinem Mitbewohner im Büro 1.4.01, Guillaume Weick, danke ich für die Antworten auf die vielen „dummen Fragen" meinerseits und der Ehrlichkeit auch ein paar derartige Fragen an mich zu richten. Niels Bode, Friedrich Gethmann, Christian Graf und Matthias Lüffe sei für die vielen gemeinsamen Tassen Kaffee und die Wertschätzung einer kleinen Espressomaschine gedankt. Ich danke Michael Schindler und Rüdiger Thul für die unschätzbare seelische Unterstützung aus den Gefilden jenseits der Disputation und ihrem kritischen Lektorat meiner Arbeit.

Eine Doktorarbeit ist nicht nur das Ergebnis dreijähriger Forschungsarbeit. Im Grunde führt ihr Abschluß die vielen kleinen und ungezählten Entscheidungen und Impulse schon während des Studiums, aber auch und vor allem des Privatlebens zu einem Punkt zusammen, von dem aus sich eine andere, neue Zukunft erstreckt. Ich danke meiner Familie, meinen Eltern, meiner Schwester und meiner Freundin Julia. Euer Vertrauen in mich, Eure Unterstützung und der Halt, den ich in den vergangenen Jahren durch Euch erfahren habe, festigte den von Zweifeln und Ängsten aufgeweichten Boden unter meinen Füßen, in dem ich manches mal zu versinken drohte, und zeigte mir dadurch den einzig sicheren Weg aus den Sümpfen: meinen.

Bibliography

Abramowitz M & Stegun IA (1970). *Handbook of Mathematical Functions* (Dover Publications, New York), 9th edition.

Accardi L, Friggerio A & Lu YG (1992), *On the Relation Between the Singular and the Weak Coupling Limits*. Acta Appl Math **26**, 197.

Alicki R (1996), *Comment on "Reduced Dynamics Need Not Be Completely Positive"*. Phys Rev Lett **75**(16), 3020.

Averin DV & Nazarov YV (1990), *Virtual Electron Diffusion during Quantum Tunneling of the electric Charge*. Phys Rev Lett **65**, 2446.

Baym G (1990). *Lectures on Quantum Mechanics* (Addison-Wesley, Reading, Massachusetts).

Begemann G, Darau D, Donarini A & Grifoni M (2008), *Symmetry fingerprints of a benzene single-electron transistor: Interplay between Coulomb interaction and orbital symmetry*. Phys Rev B **77**, 201406.

Benatti F & Floreanini R (2005), *Open Quantum Dynamics: Complete Positivity and Entanglement*. Int J Mod Phys B **19**, 3063, quant-ph/0507271.

Berkovits R, von Oppen F & Kantelhardt JW (2004), *Discrete charging of a quantum dot strongly coupled to external leads*. Europhys Lett **68**(5), 699.

Berry MV (1984), *Quantual phase factors accompanying adiabatic changes*. Proc R Soc Lond A **392**, 45.

Bersuker IB (2006). *The Jahn–Teller Effect* (Cambridge University Press, Cambridge).

Bersuker IB & Polinger VZ (1989). *Vibronic Interactions in Molecules and Crystals*, vol. 49 of *Springer Series in Chemical Physics* (Springer Verlag, Berlin).

Blanter YM & Büttiker M (2000), *Shot Noise in Mesoscopic Conductors*. Phys Rep **336**, 1.

Blount EI (1971), *The Jahn–Teller Theorem*. J Math Phys **12**(9), 1890.

Blum K (1981). *Density Matrix Theory and Applications* (Plenum Press, New York and London).

Braig S & Brouwer PW (2005), *Rate equations for Coulomb blockade with ferromagnetic leads*. Phys Rev B **71**, 195324.

Brandes T (2005), *Coherent and collective quantum optical effects in mesoscopic systems*. Phys Rep **408**, 315.

Bratteli O & Robinson DW (1996). *Operator Algebras and Quantum Statistical Mechanics 2: Equilibrium States. Models in Quantum Statistical Mechanics.* (Springer-Verlag, Berlin), 2nd edition.

Braun M, König J & Martinek J (2004), *Theory of transport thorugh quantum-dot spin valves in the weak-coupling regime*. Phys Rev B **70**, 195345.

Breuer HP & Petruccione F (2002). *The Theory of Open Quantum Systems* (Oxford University Press, Oxford).

Brouwer P (2005). *Theory of Many-Particle Systems*. http://www.ccmr.cornell.edu/~brouwer/p654/notes.pdf.

Carmichael H (1993). *An Open Systems Approach to Quantum Optics*, vol. m 18 of *Lecture Notes in Physics* (Springer-Verlag, Berlin).

Castro Neto AH, Guinea F, Peres NMR, Novoselov KS & Geim AK (2009), *The electronic properties of graphene*. Rev Mod Phys **81**, 109.

Chudnovskiy AL (2005), *SU(4) versus SU(2) Kondo effect in double quantum dot*. Europhys Lett **71**, 673, cond-mat/0502282.

Cornwell JF (1997). *Group Theory in Physics: An Introduction* (Academic Press, London).

Cuniberti G, Fargas G & Richter K (editors) (2005). *Introducing Molecular Electronics*, vol. 680 of *Lecture Notes in Physics* (Springer-Verlag, Berlin).

Dalibard J, Castin Y & Mølmer K (1992), *Wave-Function Approach to Dissipative Dynamics in Quantum Optics*. Phys Rev Lett **68**(5), 580.

Darau D, Begemann G, Donarini A & Grifoni M (2008), *A benzene interference single-electron transistor* cond-mat/0810.2461.

Davies EB (1974), *Markovian Master Equations*. Commun Math Phys **39**, 91.

—— (1976a), *Markovian Master Equations II*. Math Ann **219**, 147.

—— (1976b). *Quantum Theory of Open Systems* (Academic Press, London).

Donarini A (2005). *Dynamics of Shuttle Devices*. Ph.D. thesis, Technical University of Denmark.

Donarini A, Grifoni M & Richter K (2006), *Dynamical Symmetry Breaking in Transport through Molecules*. Phys Rev Lett **97**, 166801.

Dum R, Zoller P & Ritsch H (1992), *Monte Carlo simulation of the atomic master equation for spontaneous emission*. Phys Rev A **45**(7), 4879.

Dümcke R & Spohn H (1979), *The Proper Form of the Generator in the Weak Coupling Limit*. Z Physik B **34**, 419.

Elste F & Timm C (2005), *Theory for transport through a single magnetic molecule: endohedral $N@C_{60}$*. Phys Rev B **71**, 155403.

Elste F, Weick G, Timm C & von Oppen F (2008), *Current-induced conformational switching in single-molecule junctions*. Appl Phys A **93**, 345.

Flensberg K (2003), *Tunneling broadening of vibrational sidebands in molecular transistors*. Phys Rev B **68**, 205323.

Forster D (1975). *Hydrodynamic Fluctuations, Broken Symmetry, and Correlation Functions*, vol. 74 of *Frontiers in Physics* (W. A. Benjamin, Reading, Massachusetts).

Friegerio A & Gorini V (1976), *N-Level systems in contact with a singular reservoir. II*. J Math Phys **17**(12), 2123.

Galperin M, Ratner MA & Nitzan A (2007), *Molecular transport junctions: vibrational effects*. J Phys: Condens Matter **19**, 103201.

Gisin N, Knight PL, Percival IC, Thompson RC & Wilson DC (1993), *Quantum state diffusion theory and a quantum jump experiment*. J Mod Opt **40**(9), 1663.

Gisin N & Percival IC (1992), *The quantum-state diffusion-model applied to open systems*. J Phys A: Math Gen **25**, 5677.

Glazman LI & Raikh ME (1988), *Resonant Kondo transparency of a barrier with quasilocal impurity states*. JETP Lett **47**, 452.

Glazman LI & Shekhter RI (1988), *Inelastic resonant tunneling of electrons through a potential barrier*. Sov Phys JETP **67**(1), 162.

Goldhaber-Gordon D, Shtrikman H, Mahalu D, Abusch-Magder D, Meirav U & Kastner MA (1998), *Kondo effect in a single-electron transistor*. Nature (London) **391**, 156.

Gorini V, Kossakowski A & Sudarshan ECG (1976), *Completely Positive Dynamical Semigroups of N-Level Systems.*. J Math Phys **17**, 821.

Grabert H & Devoret MH (editors) (1992). *Single Charge Tunneling. Coulomb Blockade Phenomena In Nanostructures*, vol. 294 of *NATO ASI Series B: Physics* (Plenum Press, New York and London).

Gurvitz SA (1998), *Rate equations for quantum transport in multidot systems*. Phys Rev B **57**(11), 6602.

Hastings WK (1970), *Monte Carlo sampling methods using Markov chains and their applications*. Biometrika **57**(1), 97.

Hepp K & Lieb EH (1973), *Phase Transitions in Reservoir-Driven Open Systems with Applications to Lasers and Superconductors*. Helv Acta Phys **46**, 573.

Horodecki M, Horodecki P & Horodecki R (1996), *Separability of mixed states: necessary and sufficient conditions*. Phys Lett A **223**, 1.

Huettel AK, Witkamp B, Leijnse M, Wegewijs MR & van der Zant HSJ (2008). *Pumping of vibrational excitations in a Coulomb blockaded suspended carbon nanotube*, arXiv:0812.1769.

Jahn HA & Teller E (1937), *Stability of Polyatomic Molecules in Degenerate Electronic States I—Orbital Degeneracy*. Proc R Soc London A **161**, 220.

Judd BR (1977), *Jahn–Teller degeneracies of Thorson and Moffit*. J Chem Phys **67**(3), 1174.

Kane CL & Mele EJ (1997), *Size, Shape, and Low Energy Electronic Structure of Carbon Nanotubes*. Phys Rev Lett **78**(10), 1932.

Karrasch C, Enss T & Meden V (2006), *Functional renormalization group approach to transport through correlated quantum dots*. Phys Rev B **73**, 235337.

Kato T (1966). *Perturbation theory for linear operators*, vol. 132 of *Die Grundlehren der mathematischen Wissenschaften* (Springer-Verlag, Berlin).

Koch J (2006). *Quantum transport through single-molecule devices*. Ph.D. thesis, Fachbereich Physik, Freie Universität Berlin.

Koch J & von Oppen F (2005a), *Effects of charge-dependent vibrational frequencies and anharmonicities in transport through molecules*. Phys Rev B **72**, 113308.

—— (2005b), *Franck-Condon Blockade and Giant Fano Factors in Transport Through Single Molecules*. Phys Rev Lett **94**, 206804.

Koch J, von Oppen F & Andreev AV (2006a), *Theory of the Franck-Condon blockade regime*. Phys Rev B **74**, 205438.

Koch J, von Oppen F, Oreg Y & Sela E (2004), *Thermopower of single-molecule devices*. Phys Rev B **70**, 195107.

Koch J, Sela E, Oreg Y & von Oppen F (2007), *Nonequilibrium charge-Kondo transport through negative-U molecules*. Phys Rev B **75**, 195402.

Koch J, Semmelhack M, von Oppen F & Nitzan A (2006b), *Current-induced nonequilibrium vibrations in single-molecule devices*. Phys Rev B **73**, 155306.

König J (1998). *Quantenfluktuationen im Einzel-Elektronen-Transistor*. Ph.D. thesis, Fakultät für Physik, Universität Karlsruhe.

König J, Schoeller H & Schön G (1997), *Cotunneling at Resonance for the Single-Electron Transistor*. Phys Rev Lett **78**(23), 4482.

Kouwenhove LP & Marcus C (1998), *Quantum dots*. Physics World **11**(6), 35.

Kouwenhoven LP, Austing DG & Tarucha S (2001), *Few-electron quantum dots*. Rep Prog Phys **64**, 701.

Königsberger K (2000). *Analysis 2* (Springer-Verlag, Berlin), 3rd edition.

Leibfried D, Blatt R, Monroe C & Wineland D (2003), *Quantum dynamics of single trapped ions*. Rev Mod Phys **75**(1), 281.

Leijnse M & Wegewijs MR (2008), *Kinetic equations for transport through single-molecule transistors*. Phys Rev B **78**, 235424.

Leturcq R, Stampfer C, Durrer L, Hierold C, Mariani E, Schultz MG, von Oppen F & Ensslin K (2009), *Franck–Condon blockade in suspended carbon nanotube quantum dots*. Nature Physics **5**, 327.

Lindblad G (1976), *On the Generators of Quantum Dynamical Semigroups*. Comm Math Phys **48**, 119.

Longuet-Higgins HC, Öpik U, Pryce MHL & Sachs RA (1958), *Studies of the Jahn–Teller effect. II. The dynamical problem*. Proc R Soc Lond A **244**, 1.

Ludwig W & Falter C (1988). *Symmetries in Physics*, vol. 64 of *Springer Series in solid state sciences* (Springer-Verlag, Berlin).

Lueffe MC, Koch J & von Oppen F (2008), *Theory of vibrational absorption sidebands in the Coulomb-blockade regime of single-molecule transistors*. Phys Rev B **77**, 125306.

Mahan GD (2000). *Many-Particle Physics* (Kluwer Academic, New York), 3rd edition.

Mahaux C & Weidenmüller HA (1969). *Shell-Model Approach to Nuclear Reactions* (North-Holland Publishing Company, Amsterdam).

Mead CA (1992), *The geometric phase in molecular systems*. Rev Mod Phys **64**(1), 51.

Merzbacher E (1998). *Quantum Mechanics* (John Wiley & Sons, New York), 3rd edition.

Metropolis N, Rosenbluth AW, rosenbluth MN, Teller AH & Teller E (1953), *Equation of State Calculations by Fast Computing Machines*. J Chem Phys **21**, 1087.

Mitra A, Aleiner I & Millis AJ (2004), *Phonon effects in molecular transistors: Quantal and classical treatment*. Phys Rev B **69**, 245302.

Palmer PF (1977), *The singular coupling and weak coupling limits*. J Math Phys **18**(3), 527.

Park H, Park J, Lim AKL, Anderson EH, Alivisatos AP & McEuen PL (2000), *Nanomechanical oscillations in a single-C_{60} transistor*. Nature (London) **407**, 57.

Pauling L & Wilson EB (1935). *Introduction to Quantum Mechanics* (McGraw–Hill, New York).

Pechukas P (1994), *Reduced Dynamics Need Not Be Completely Positive*. Phys Rev Lett **73**(8), 1060.

Peres A (1996), *Separability Criterion for Density Matrices*. Phys Rev Lett **77**(8), 1413.

Plenio MB & Knight PL (1998), *The quantum-jump approach to dissipative dynamics in quantum optics*. Rev Mod Phys **70**(1), 101.

Pustilnik M & Glazman LI (2005). In H Bouchiat (editor), *Nanophysics: Coherence and Transport. Les Houches Session LXXXI*, pages 427–478 (Elsevier, Amsterdam).

Qiu XH, Nazin GV & Ho W (2003), *Vibrationally Resolved Fluorescence Excited with Submoecular Precision*. Science **299**, 542.

Rammer J (1998). *Quantum Transport Theory*, vol. 99 of *Frontiers in Physics* (Perseus Books, Reading, Massachusetts).

Reckermann F, Leijnse M, Wegewijs MR & Schoeller H (2008), *Transport signature of pseudo Jahn–Teller dynamics in a single-molecule transistor*. Europhys Lett **83**, 58001.

Reichl LE (1998). *A Modern Course in Statistical Physics* (John Wiley & Sons, New York), 2nd edition.

Ruch E & Schönhofer A (1965), *Ein Beweis des Jahn–Teller-Theorems mit Hilfe eines Satzes über die Induktion von Darstellungen endlicher Gruppen*. Theoret chim Acta (Berl) **3**, 291.

Salmhofer M (1999). *Renormalization: An Introduction* (Springer-Verlag, Berlin).

Sapmaz S, Jarillo-Herrero P, Blanter YM, Dekker C & van der Zant HSJ (2006), *Tunneling in Suspended Carbon Nanotubes Assisted by Longitudinal Phonons*. Phys Rev Lett **96**, 026801.

Schrieffer JR & Wolff PA (1966), *Relation between the Anderson and Kondo Hamiltonians*. Phys Rev **149**(2).

Schultz MG, Nunner TS & von Oppen F (2008), *Berry-phase effects in transport through single Jahn–Teller molecules*. Phys Rev B **77**(7), 075323.

Schultz MG & von Oppen F (2008). *Quantum transport through nanostructures in the singular-coupling limit*, cond-mat/0812.1491. Accepted for publication in Phys Rev B.

Shahbazyan TV & Raikh ME (1994), *Two-channel resonant tunneling*. Phys Rev B **49**(24), 17123.

Shaji A & Sudarshan ECG (2005), *Who's afraid of not completely positive maps?*. Phys Lett A **341**, 48.

Shekhter RI, Gorelik Y, Glazman LI & Jonson M (2006), *Electronic Aharonov-Bohm Effect Induced by Quantum Vibrations*. Phys Rev Lett **97**, 156801.

Spohn H (1980), *Kinetic equations from Hamiltonian dynamics: Markovian limits*. Rev Mod Phys **53**, 569.

Spohn H & Lebowitz JL (1978). *Irreversible Thermodynamics for Quantum Systems weakly coupled to Thermal Reservoirs*, In SA Rice (editor), *For Ilya Prigogine*, vol. XXXVIII of *Advances in Chemical Physics*, pages 109–142 (John Wiley & Sons, New York).

Stinespring WF (1955), *Positive Functions on C^*-Algebras*. Proc Amer Math Soc **6**, 211.

Thijssen WHA, Djukic D, Otte AF, Bremmer RH & van Ruitenbeek JM (2006), *Vibrationally Induced Two-Level Systems in Single-Molecule Junctions*. Phys Rev Lett **97**, 226806.

Timm C (2008), *Tunneling through molecules and quantum dots: Master-equation approaches*. Phys Rev B **77**, 195416.

Timm C & Elste F (2006), *Spin amplification, reading, and writing in transport through anisotropic magnetic molecules*. Phys Rev B **73**, 235304.

Wegewijs MR & Nazarov YV (1999), *Resonant tunneling through linear arrays of quantum dots*. Phys Rev B **60**(20), 14318.

Wegewijs MR & Nowack KC (2005a), *Nuclear wavefunction interference in single-molecule electron transport*. New Journal of Physics **7**, 239.

—— (2005b), *Vibration-assisted tunneling through competing molecular states.* cond-mat/0506552.

Wingreen NS, Jacobsen KW & Wilkins JW (1988), *Resonant Tunneling with Electron-Phonon Interaction: An Exactly Solvable Model*. Phys Rev Lett **61**(12), 1396.

—— (1989), *Inelastic scattering in resonant tunneling*. Phys Rev B **40**(17), 11834.

Wingreen NS & Meir Y (1992), *Landauer Formula for the Current through an Interacting Electron Region*. Phys Rev Lett **68**(16), 2512.

Yarkony DR (1996), *Diabolical conical intersections.* Rev Mod Phys **68**(4), 985.

Zusammenfassung der Ergebnisse

Bei der Modellierung realistischer physikalischer Systeme mit dem Anspruch, experimentelle Ergebnisse adäquat zu beschreiben, erfährt die theoretische Physik seit jeher ein grundsätzliches Dilemma. Effektive, generische Modelle müssen erweitert und damit komplexifiziert werden, wodurch im allgemeinen nicht nur die Möglichkeit der geschlossenen analytischen Lösbarkeit verloren geht. Vielmehr leidet oftmals auch die physikalisch intuitive Interpretation der beschreibenden Gleichungen und ihrer Lösungen.

Im Kontext der Transporttheorie einzelner Moleküle, der Molekularelektronik, manifestiert sich dieser Zwiespalt in der Spezialisierung der Markovschen Dynamik schwach mit den Elektroden wechselwirkender Nanostrukturen auf zwei vollkommen unterschiedliche Typen linearer Gleichungen. Je nach der elektronischen Struktur des molekularen Modells und seines Entartungsgrades, folgt die asymptotische Dynamik entweder einer Ratengleichungen für die Besetzungszahlen der elektronischen und vibronischen Niveaus und damit dem intuitiven Bild einzelner elektronischer Sprungprozesse, oder sie gehorcht einer Mastergleichungen für die volle reduzierte Dichtematrix, die Besetzungszahlen und Kohärenzen zwischen entarteten Zuständen koppelt.

Die Intention der vorliegenden Arbeit ist, den durch die Mastergleichungen im Vergleich zur Ratengleichung bedingten Verlust an physikalischer Intuition für das stationäre Verhalten des Systems durch eine ausführliche und an den funktionalen Strukturen der Gleichung orientierten Darstellung zu beheben. Im Zuge einer sorgfältigen Herleitung der Markovschen Gleichungen aus der von-Neumann-Gleichung mit einer der mathematischen Theorie linearer System-Bad-Wechselwirkungen entlehnten Methode wird die Unterscheidung in die zwei Gleichungstypen – im Gegensatz zur vorherrschenden Praxis – nicht als zweckdienliche Näherung, sondern als Resultat der asymptotischen Zeitskala interpretiert. Die Markovsche Dynamik komplexer molekulare Modelle separiert somit einerseits in Ratengleichungen zwischen Zuständen unterschiedlicher Energie andererseits in Mastergleichungen innerhalb entarteter Unterräume des molekularen Hilbertraums.

Bereits das stationäre Verhalten der Ratengleichungsdynamik zeigt Signaturen, die nicht mit dem intuitiven Bild sequentiell springender Elektronen zu erklären sind. In vielen experimentell relevanten Parameterbereichen wird die Phänomenologie vollständig durch das dynamische Gleichgewicht zwischen Landungs- und Entladungsprozessen, zwischen Absorption und Emission einzelner molekularer Schwingungsquanten bestimmt. Um die Strom-Spannungscharakteristik zu verstehen, reicht nicht allein die Betrachtung der einzelnen Sprungraten. Vielmehr muß zuvor die stationäre Ratengleichung vollständig gelöst werden, um die aus dem Gleichgewicht der elektronischen Sprungprozesse resultierende Wahrscheinlichkeitsverteilung zu erhalten, die den Strom bestimmt. Dies wird an mehreren prototypischen Beispielen, unter anderem einem Jahn-Teller-aktiven Molekül mit mehreren Schwingungsmoden und der Anwendung der Theorie auf ein kürzlich durchgeführtes Transportexperiment an Kohlenstoffnanoröhrchen, demonstriert.

Das einfachste Modell einer Nanostruktur, die nicht mehr allein mittels einer Ratengleichung beschrieben werden kann, besitzt zwei entartete elektronische Niveaus. Die Diskussion der Mastergleichung für die volle reduzierte Dichtematrix dieses Modells erfolgt in zwei Schritten: Die vollständige Berechnung der Transporteigenschaften eines verallgemeinerten Resonanten Tunnelmodells zeigt erste, quantitative Einflüsse der Kohärenzen auf den stationären transmittierten Strom. In der anschließenden Diskussion der Mastergleichung für das molekulare Modell entfaltet sich das grundlegende Paradigma dieser Gleichung. Die Betrachtung der vollen reduzierten Dichtematrix erlaubt durch die Wahl spezieller Basen des elektronischen Hilbertraums, einzelne Molekülniveaus von einer Elektrode zu entkoppeln. Die damit einhergehende Unterdrückung des stationären Stroms durch Coulomb-Blockade-Effekte wird durch die Wechselwirkung des lokalisierten Systems mit dem Kontinuum der Badzustände teilweise aufgehoben, stellt jedoch, wie anhand mehrer Beispiele demonstriert wird, die generische Physik dieser System dar.

Die Verbindung von Ratengleichung und Mastergleichung, deren Herleitung durch das bloße qualitative Kriterium, ob eine Entartung vorhanden ist oder nicht, eine konzeptionelle Unstetigkeit in den Modellparametern darstellt, beschließt die Arbeit. Um diese Lücke der Theorie zu schließen wird – wiederum im Rückgriff auf die mathematischen Methoden abstrakter System-Bad-Wechselwirkungen – das Konzept der Fastentartung betrachtet. Energiedifferenzen derselben Größenordnung wie die störungsinduzierten Renormierungen der molekularen Energieniveaus werden in die Störungstheorie der von-Neumann-Gleichung miteinbezogen. Mit der Herleitung einer entsprechenden Mastergleichung für fastentartete Systeme und der Diskussion ihrer Eigenschaften und ihrer generischen Dynamik, gelingt die Interpolation von Ratengleichungen und Mastergleichungen mittels eines einzelnen Parameters: des numerischen Werts der Fastentartung. Damit wird der konzeptionelle Kreis von Ratengleichungen zu Mastergleichungen konsistent geschlossen, dem die Arbeit durch das Tolkiensche Wort Rechnung trägt: „Hin und wieder zurück“.